

AD-A021 294

SPECIALISTS MEETING ON IMPACT DAMAGE
TOLERANCE OF STRUCTURES

Advisory Group for Aerospace Research and Development
Paris, France

January 1976

DISTRIBUTED BY:

NTIS

National Technical Information Service
U. S. DEPARTMENT OF COMMERCE

068114

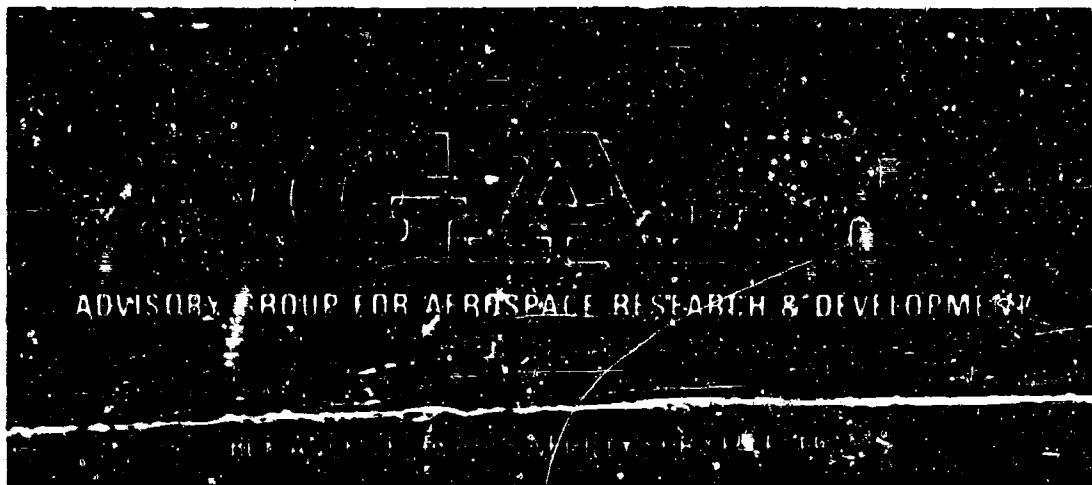
1

FG

AGARD-CP-186

AGARD-CP-186

ADA021294

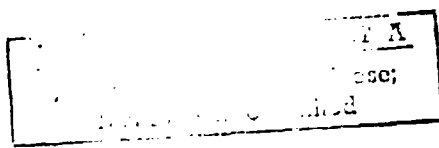


AGARD CONFERENCE PROCEEDINGS No. 186

Specialists Meeting

on

Impact Damage Tolerance of Structures



1 1976

NORTH ATLANTIC TREATY ORGANIZATION



Reproduced by
NATIONAL TECHNICAL
INFORMATION SERVICE
U S Department of Commerce
Springfield VA 22151

**DISTRIBUTION AND AVAILABILITY
ON BACK COVER**



**Papers presented at the 41st Meeting of the Structures and Materials Panel
in Ankara, Turkey, 28 September - 3 October 1975.**

THE MISSION OF AGARD

The mission of AGARD is to bring together the leading personalities of the NATO nations in the fields of science and technology relating to aerospace for the following purposes:

Exchanging of scientific and technical information;

Continuously stimulating advances in the aerospace sciences relevant to strengthening the common defence posture;

Improving the co-operation among member nations in aerospace research and development;

Providing scientific and technical advice and assistance to the North Atlantic Military Committee in the field of aerospace research and development;

Rendering scientific and technical assistance, as requested, to other NATO bodies and to member nations in connection with research and development problems in the aerospace field;

Providing assistance to member nations for the purpose of increasing their scientific and technical potential;

Recommending effective ways for the member nations to use their research and development capabilities for the common benefit of the NATO community.

The highest authority within AGARD is the National Delegates Board consisting of officially appointed senior representatives from each member nation. The mission of AGARD is carried out through the Panels which are composed of experts appointed by the National Delegates, the Consultant and Exchange Program and the Aerospace Applications Studies Program. The results of AGARD work are reported to the member nations and the NATO Authorities through the AGARD series of publications of which this is one.

Participation in AGARD activities is by invitation only and is normally limited to citizens of the NATO nations.

A large part of the content of this publication has been reproduced directly from material supplied by AGARD or the authors; the remainder has been set by Technical Editing and Reproduction Ltd.

Published January 1976

Copyright © AGARD 1976

All Rights Reserved
ISBN 92-835-0154-3

629.73.02:539.537

National Technical Information Service is authorized to reproduce and sell this report.

A

EP

Printed by Technical Editing and Reproduction Ltd
Harford House, 7-9 Charlotte St, London, W1P 1HD

PREFACE

Aircraft must maintain structural integrity relative to many types of damaging mechanisms including, for example, fatigue, non-detectable initial defects and in-flight damage such as that inflicted by military weapons or by debris from disintegration of an engine. Whilst the structural design methodology for many of these is well established, that for in-flight damage is currently in a state of rapid development and has not been widely distributed to and implemented by designers.

The resistance of the structure to the impact of projectiles is an important parameter in consideration of the vulnerability of military aircraft. Information on this subject is contained in AGARD Advisory Report AR-47 "Physical Vulnerability of Aircraft". However there is a need for considerable augmentation of this information, extending the scope to include the design methodology. The Structures and Materials Panel of AGARD, recognising this need, intends to publish a Design Manual in 1977. The Panel decided that this Manual should also embrace the clearly analogous problem, arising mainly on the longer life transport aircraft, of the impact on the structure of debris from engine disintegration, a subject of rapidly growing importance which has so far received little attention in the literature.

In order to stimulate the collection of data for the Manual, a Specialist Meeting was organised. The presentations and a summary of the subsequent discussions are published in this volume. Amongst the subjects covered are the types of damage produced by various projectiles, the failure characteristics of the structure under load and its residual strength and life after damage. The relationship between the spread of the damage and the materials used and the detail design features of the structure is considered. Where neighbouring systems or fuel tanks are vulnerable the degree of penetration of the projectile into the structure is important and this is discussed as is the hydraulic ram effect which can result in very high pressures if a projectile enters a fuel tank. Blast effects are considered. Descriptions are given of methods of overall analysis of damaged structures and their use in the vulnerability assessment of the aircraft. The likely distribution of size, velocity and direction of engine debris fragments is discussed together with information on methods of determining the effect on the structure. The possibilities are described of reducing the severity of the problem by modifying the engine design to cause blade failures to be more likely than disc failures and to contain a large proportion of the resultant debris. The effects of the overall aircraft layout, armour and deflectors on the problem are also discussed.

It is considered that the publication of these conference proceedings will be of immediate value to those concerned with the problem of impact damage tolerance. The AGARD Structures and Materials Panel would welcome any comments, suggestions, etc. which would be of help in preparing the Design Manual.

The Panel wishes to express its appreciation to the many groups and individuals who contributed to the success of the Specialists Meeting; to the Turkish National Delegates who hosted the meeting; to Mr J.G. Avery, AGARD Coordinator for the work on Impact Damage Tolerance; to the authors, session chairmen and those who contributed to the technical discussions; and to the Panel Members and Staff who so ably assisted in the planning and carrying through of the meeting.

N.E. HARPUR
Chairman, Working Group on
Impact Damage Tolerance of Structures.

CONTENTS

	Page
PREFACE by N.F.Harpur	iii
	Reference
 <u>SESSION I</u>	
STRUCTURAL INTEGRITY REQUIREMENTS FOR PROJECTILE IMPACT DAMAGE AN OVERVIEW by J.G.Avery, T.R.Porter and R.W.Lauzze	1
STRUCTURAL ANALYSIS OF IMPACT DAMAGE ON WINGS by J.Massmann	2
FLUID DYNAMIC ANALYSIS OF HYDRAULIC RAM by E.A.Lundstrom and W.K.Fung	3
CALCUL DE QUELQUES PROBLEMES D'IMPACT SUR DES STRUCTURES AERONAUTIQUES par C.Petiau	4
COMPUTER METHOD FOR AIRCRAFT VULNERABILITY ANALYSIS AND THE INFLUENCE OF STRUCTURAL DAMAGE ON TOTAL VULNERABILITY by D.Kardels	5
DAMAGE TOLERANCE OF SEMIMONOCOQUE AIRCRAFT by D.F.Haskell	6
 <u>SESSION II</u>	
DEFINITION OF ENGINE DEBRIS AND SOME PROPOSALS FOR REDUCING POTENTIAL DAMAGE TO AIRCRAFT STRUCTURE by D.McCarthy	7
PROBABILITE DE PERFORATION D'UNE STRUCTURE D'AVION PAR DES DEBRIS DE MOTEURS par Michel Huret	8
STRUCTURAL EFFECTS OF ENGINE BURST NON-CONTAINMENT by T.W.Coombe and D.F.Vowles	9
STUDIES OF ENGINE ROTOR FRAGMENT IMPACT ON PROTECTIVE STRUCTURE by G.J.Mangano	10
TENUE DES CARTERS MOTEURS LORS DES RUPTURES D'AUBES par J.Thiery	11
DISCUSSION SUMMARY by J.G.Avery	D

STRUCTURAL INTEGRITY REQUIREMENTS FOR PROJECTILE IMPACT DAMAGE-- AN OVERVIEW

by

J. G. Avery

and

T. R. Porter

BOEING AEROSPACE COMPANY
Research and Engineering Division
P. O. Box 3999
Seattle, Washington 98124

and

R. W. Lauzze

Air Force Flight Dynamics Laboratory
Wright-Patterson AFB, Ohio

SUMMARY

Aircraft can be exposed to projectile impacts from several sources, including military weapons, hailstones, pebbles, and debris from engine failures. In spite of the importance of the projectile damage threat to many types of aircraft, this category of damage is addressed in only a limited degree by existing design guidelines and specifications. There are, however, a growing body of research results becoming available, and attention must be directed toward making this information usable to designers. The only means of doing this is to integrate projectile damage tolerance considerations within the existing structural design process. This paper outlines a design methodology for projectile damage tolerance and summarizes some of the research results available for implementing the methodology.

1. INTRODUCTION

As indicated in Figure 1, aircraft must maintain structural integrity relative to many types of damaging mechanisms, including for example:

1. Fatigue
2. Non-detectable initial defects
3. In-flight damage, such as inflicted by military weapons and engine debris.

The objective in designing for fatigue considerations is to prevent wear-out during the anticipated usage of the aircraft. The objective of the second structural integrity requirement is to prevent an airplane from unexpectedly falling as a result of an undetected flaw or defect. In both cases, the benefits of successful design are improved safety and economics.

With respect to in-flight damage, the design objective is to prevent structural failure from suddenly inflicted damage during flight. For example, a substantial portion of combat aircraft attrition has been caused by structure-related failures induced by projectile damage. Weapon damage may cause loss of strength and stiffness, and these effects are often amplified by the interaction between primary structure and engine fuel storage. This interaction leads to damage mechanisms such as hydraulic ram, vapor explosions and fire.

In spite of the importance of the projectile damage threat to many types of aircraft, this category of damage is addressed in only a limited degree by existing design guidelines and military specifications. Although the vulnerability analyst has always been concerned with the effects of projectiles, this often represents unfamiliar ground for the structural designer.

Because of these consequences, effort is required to integrate battle damage tolerance considerations within the structural design process, along with related fatigue and fail-safe criteria, as indicated in Figure 2. In recognition of this need, the Air Force Flight Dynamics Laboratory has recently supported research under contract F33615-73-Q-3032 "Survivable Combat Aircraft Structures Design Guidelines and Criteria," (Reference 1), in order to formulate the required technology within a methodology that can be readily accepted by structural designers.

The remainder of this paper presents an overview of a methodology for projectile damage tolerant design and certain of the techniques and guidelines available for implementation.

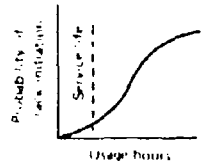
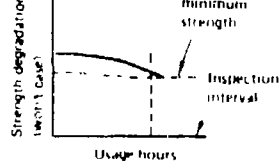
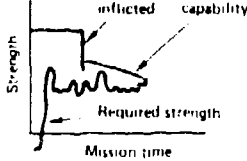
	Fatigue (crack initiation)	Non detectable initial defects	Inflicted damage
Design requirements	Related MIL specification MIL 8860	Related MIL specification MIL 8838	Related MIL specification None Guidelines: AFFDL-TR 74-50 (Battle damage)
Design objective	Prevent wear out	Prevent failure from worst case initial flaws	Prevent failure from inflicted damage
Design criteria	Design criteria based on statistical material responses	Damage criteria based on NDI capabilities	Damage criteria determined by damage size inflicted by specified threat
			

Figure 1 Aircraft Structural Integrity Requirements

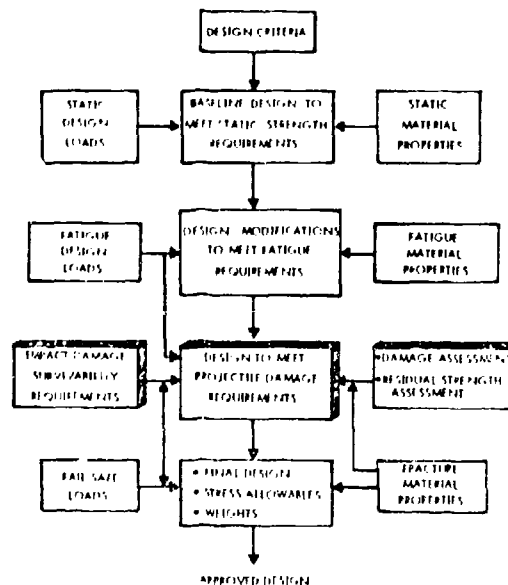


Figure 2 Inclusion of Impact Damage Tolerance in Structural Design Methodology

II. METHODOLOGY FOR IMPACT DAMAGE TOLERANT DESIGN

To achieve desired structural survivability with minimum performance degradation, a quantitative assessment of structural survivability should be included during the design phase of the aircraft. This requires implementing an assessment and design methodology that allows designers to determine the survival capability of a current design and then compare this capability with the structural performance specified by criteria. The objectives of the methodology are to evaluate the structural capability of the damaged airframe, and to compare this with structural performance requirements as dictated by mission criteria. Figure 3 is a flow diagram illustrating the steps required to evaluate the survivability level of a structural design (Reference 2).

A first step in the methodology is to determine the conceptual goals for the aircraft, including aircraft type and anticipated usage. From these, specific mission and threat requirements are defined. Non-nuclear ballistic threats can be categorized into three basic types:

- a. Non-explosive projectiles (penetrators)
- b. High explosive (HE) projectiles
- c. Warheads

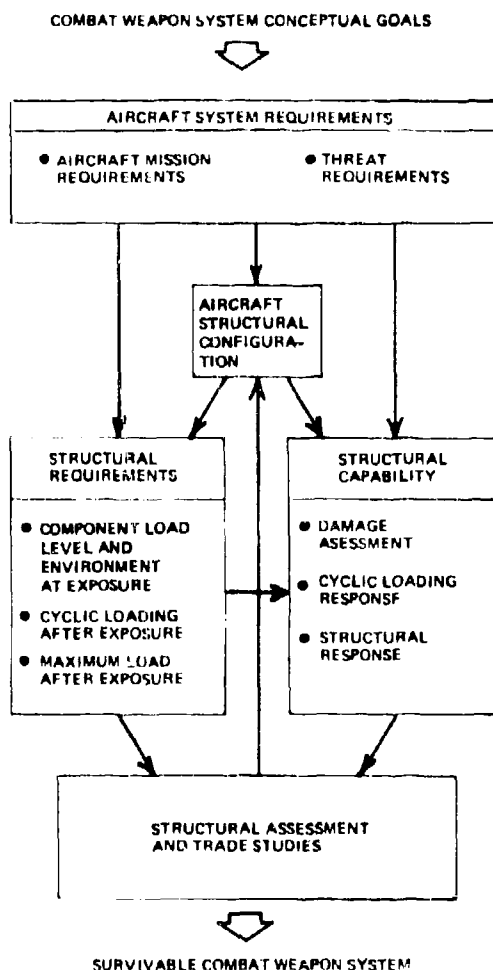


Figure 3. Structural S/V Design Methodology

Information on the projectile type, size, velocity, number, and direction must be considered when making a structural vulnerability assessment. In addition to mission and threat requirements, the conceptual structural designs are a necessary input. The structural design is not final, since the final selection of the structural configuration and materials should include the vulnerability assessment results, because structural concepts and material selection significantly influence the survivability of the total structure.

The remaining steps illustrated in Figure 3 use the above factors as input data in establishing the structural capability and requirements for the final assessment. These steps are described in the following paragraphs.

II.1 DETERMINATION OF STRUCTURAL REQUIREMENTS

Structural requirements are determined by the physical and loading environments of the aircraft. For survivability analysis, three basic types of information are required for each structural component considered. These are:

- The probable load-level and the physical environment at the time of damage occurrence;
- The cyclic loading spectrum after damage occurrence;
- The maximum load and the associated physical environment that will be encountered after damage has occurred.

This information is obtained from the anticipated operational stress/time history for the aircraft. This includes the lift loading, gust loadings, and maneuver load factors for the prescribed missions. A sample stress/time history is shown in Figure 4. From information of this type a rational stress level requirement at the time of impact can be defined.

The maximum loadings anticipated from the time of damage occurrence until mission completion or repair will define the residual strength requirements for the airplane. Likewise, the operating stresses from damage incidence until the airplane is repaired will define the cyclic loading requirements for the damaged airframe.

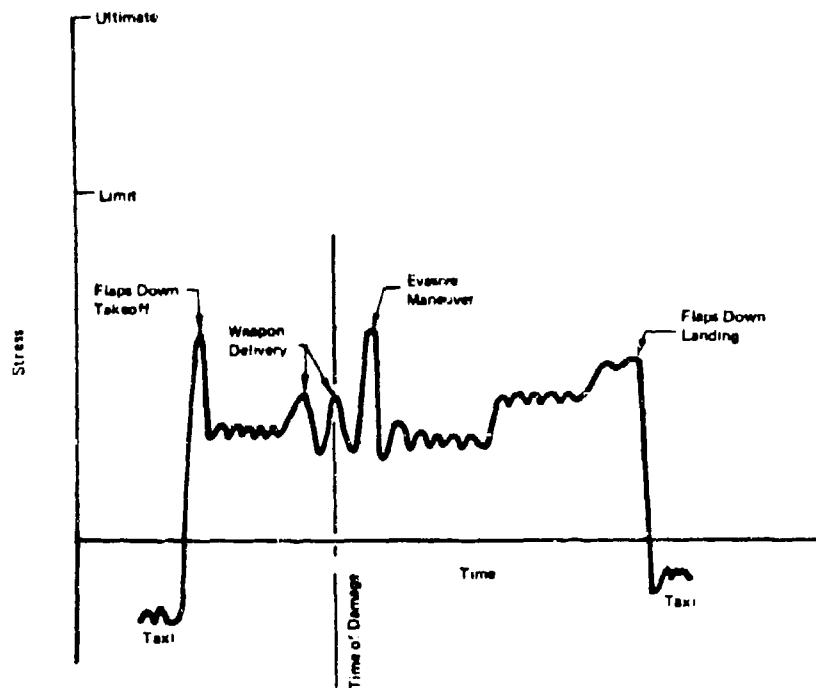


Figure 4 Stress-Time History for Structural Element

Physical environment is an important consideration. Temperature, for example, can affect the residual strength of damaged structure because it influences the fracture behavior of some aircraft materials. Other possible degrading physical environments include: humidity, moisture, cleaning fluids, hydraulic fluids, and fuel, especially during the application of cyclic loads.

II.2 DETERMINATION OF THE CAPABILITY OF DAMAGED STRUCTURE

The determination of structural capability requires an evaluation of structural degradation due to weapon damage. Several unique technical disciplines come into operation at this point in the analysis. Evaluating structural degradation due to weapon damage requires a consideration of the mechanics of damage and damage tolerance. The required analysis steps were shown on the right side of Figure 3.

The first step is to determine the type and extent of the damage inflicted by the threat. Structural damage from projectile impact is a function of the threat and engagement conditions, as well as the structural configuration including geometry and material. Consideration must be given to the environment, loads, and compounding effects such as hydraulic ram.

Damaged structure that does not fail at the time of impact is subjected to subsequent cyclic loading as a result of gust and maneuvers during continued flight. These cyclic loadings induce fatigue that can

influence the damage size and character, thereby changing the strength of the structure. In metal structure, cyclic stresses will generally increase the damage size and severity, thus reducing the strength of the ballistic-damaged structure.

The damaged airframe must sustain the maximum flight loads subsequently encountered. The residual strength of the damaged structure is related to design and damage size. The stiffness of aircraft structure that has been damaged is also altered. This stiffness degradation can produce several effects that can also lead to failure. Among these are flutter, loss of control, or extensive load redistribution within the structure.

The final results of the structural capability determination can be presented in a manner analogous to the stress/time history presented in Figure 4. This is termed the "strength-time" history (an example is shown in Figure 5). The figure shows that structural capability is the design ultimate strength before encountering damage. After projectile impact, however, the structural strength is severely degraded in this example. The initial response is characterized by the strength during the time of impact. Immediately after impact, the structural capability is determined by the residual strength. After this point, the strength degrades due to the fatigue damage caused by cyclic loadings.

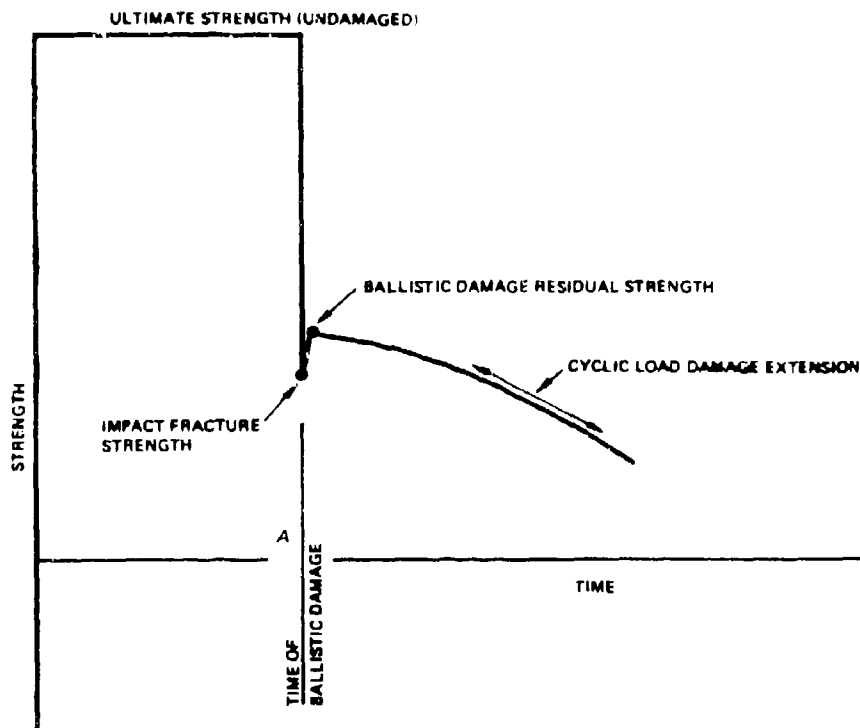


Figure 5. Strength Time History for Structural Element

II.3 STRUCTURAL VULNERABILITY ASSESSMENT

The final survivability assessment compares the stress/time and the strength/time histories; that is, the requirements and the capabilities. A typical comparison is shown in Figure 6. This figure shows the stress/time and strength/time histories for a wing structural detail. At time "A" the strength capability is reduced significantly due to damage inflicted by projectile impact; however, the structural element did not fail catastrophically. In this example, the strength requirements exceed the strength capability in the landing approach, and structural failure occurs. The final assessment depends on the impact damage tolerance criteria selected for the aircraft, and criteria selection and specification is an extremely important aspect of impact damage tolerant design.

III. DESIGN TECHNIQUES AND GUIDELINES

The structural designer can employ several techniques for improving the response of aircraft structure to projectile impact, including:

- a. Reduce the probability of hitting critical structure.
- b. Improve damage resistance of structure.
- c. Improve damage tolerance of structure.

The first approach includes reducing the size of critical elements, locating critical structural elements so that they are shielded by less critical components, or locating critical elements so that they

are removed from a probable projectile flight path. The techniques and reliability of these techniques will not be discussed further in this paper because they depend on design considerations, and examples will be given in subsequent papers.

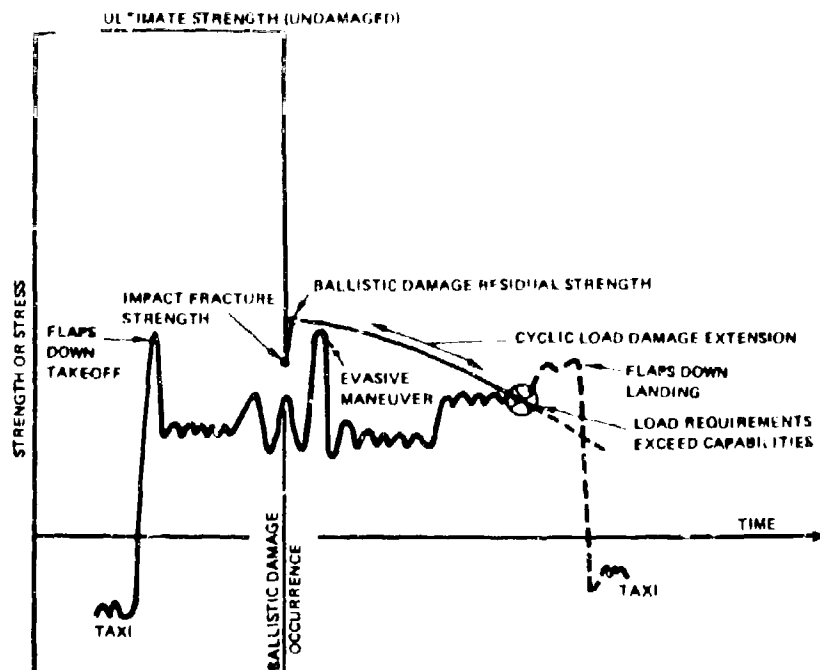


Figure 6 Comparison of Stress-Time and Strength-Time Histories

Damage resistance, as shown in Figure 7, is measured by the extent of damage inflicted by a given threat. The importance of damage size in the assessment of structural survivability cannot be over-emphasized, since failure criteria for structure depends on damage size. This is in contrast to failure criteria for many other aircraft system components that can often be rationally based solely on penetration.

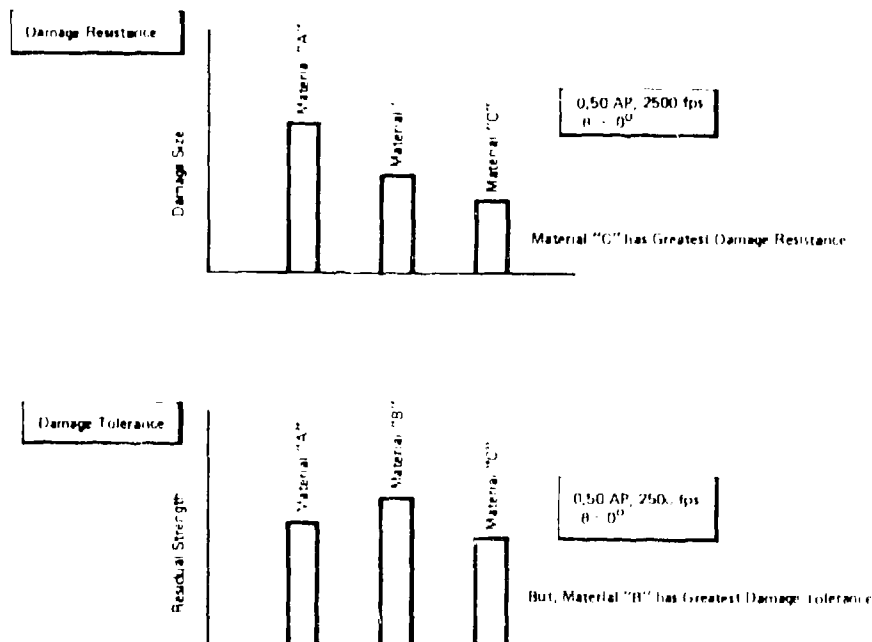


Figure 7 Damage Resistance and Tolerance

Material properties and geometric configuration determine damage resistance. For example, 2024-T3 skin is more damage resistant (less crackling) than 7075-T6 skin when exposed to projectile impact. In general, the use of high-toughness materials will provide a high level of damage resistance.

Damage tolerance, on the other hand, is measured by the ability of the structure to survive or "tolerate" damage of a given size. A damage-tolerant structure is obtained by careful attention to both detail design and material selection. Multiple load paths and structural members capable of limiting or containing damage extension should be incorporated.

In areas where both members of a dual load path could be damaged by a single impact, and where design (geometry) limitations restrict the use of redundant structure, special effort should be made to provide damage resistance. This is achieved by minimizing the exposed area and utilizing damage-resistant materials. Good damage resistance will also enhance repair capability.

Damage tolerance should be considered in the design of every major component. Multiple-load-path structure should be used and the load paths should be separated to minimize the possibility of critical damage from a single impact. Short load paths are recommended to minimize the vulnerable area. Flammable and/or explosive components should not be placed in close proximity to the primary load paths.

The above general design considerations are deceptively simple. In actuality, their application in specific circumstances is complex, and requires both design awareness and inventiveness. Although it is dangerous to generalize, design features that typically enhance structural survivability are:

- a. Extensive use of high toughness materials to provide a high level of damage resistance.
- b. Multispar wing construction.
- c. Multiple skin panel construction.
- d. Riveted skin construction with patterns selected to minimize blast effects.
- e. Multistringer, skin fuselage construction.
- f. Fuselage configuration with short primary load paths.
- g. Fuselage configuration with large volume to minimize blast effects.

However, the designer needs more specific analytical tools in order to implement the tasks defined previously in the design methodology. These analytical methods must be formulated in terms of design parameters, so that the effects of design alternatives can be evaluated. The remainder of this section presents a brief overview of impact damage effects in aircraft structure, and certain analysis methods available for use in design.

The topics addressed include:

- a. Characteristics of Projectile Impact Damage
- b. Prediction of Impact Damage
- c. Internal Load Redistribution in Damaged Structure
- d. Failure Criteria for Damaged Structure

III.1 CHARACTERISTICS OF PROJECTILE IMPACT DAMAGE

Projectile damage has diverse characteristics depending on the projectile, the configuration of the structure, and the conditions of impact. Damage can range from dents, cracks, and holes, to large petalled areas accompanied by extensive out-of-plane deformation. The diverse character of projectile damage raises questions. How can it be quantified? What should be measured?

Although there are several meaningful measures of impact damage, lateral damage is the measurement that has been found most useful for vulnerability analysis. Lateral damage, as shown in Figure 8, is defined as the diameter of an imaginary circle that just encloses the limits of fracture or material removal in the plane parallel to the original surface of the sheet. The terms "lateral damage", "damage size", and sometimes simply "damage" are used synonymously.

A second significant measurement when stressed panels are considered is the component of lateral damage transverse to the applied load. This index is referred to as transverse lateral damage, often abbreviated as TLD.

The following paragraphs describe the basic characteristics of projectile damage in metal and fiber-composite structure.

III.1.1 IMPACT DAMAGE IN METALS

The impact-damage response of metals depends upon many interrelated parameters. Because of this, there is appreciable scatter in the test data, and it is often difficult if not impossible to isolate and quantify the effect of individual parameters.

An extensive investigation of impact damage in metals is reported in Reference 3. This reference discusses types of damage and the parameters that influence damage. Some pertinent results from that study are summarized in the following paragraphs. These results have been demonstrated in the high-strength aluminum alloys, such as 2024-T3 and 7075-T6.

Damage Type

Impact damage in metal sheet and plate structure can be cracks, spallation, petals, holes, dents or

gouges. For a given target material, the damage type sustained depends on the sheet thickness and the projectile velocity and impact angle. This behavior is illustrated in Figure 9.

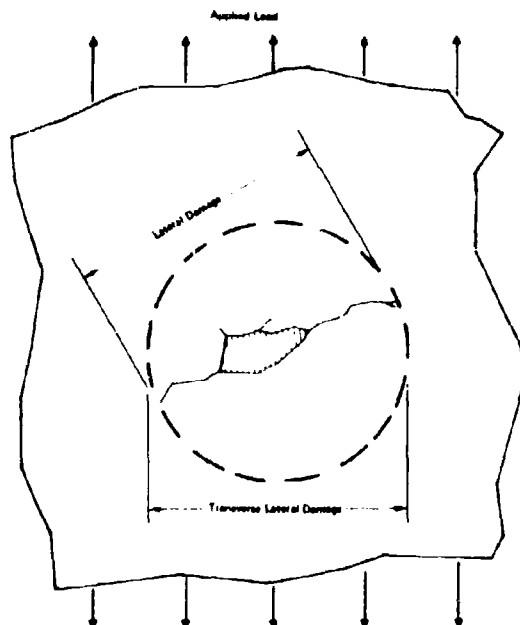


Figure 8. Lateral Damage Definition

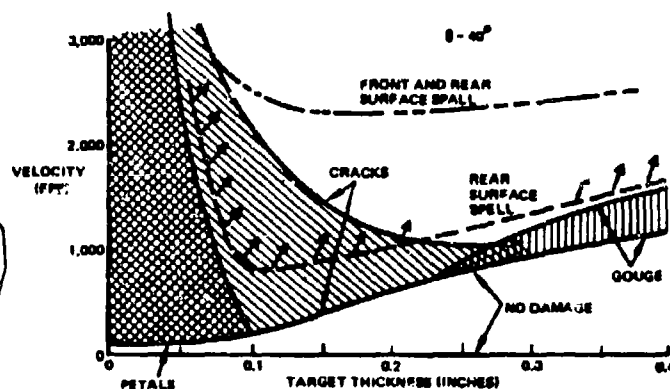


Figure 9. Damage Type Regime Diagram, 0.30 AP, 7075-T6

Effect of Projectile Velocity

For a given panel and obliquity, the variation of projectile impact velocity can result in the response shown in Figure 10 which also illustrates the concepts of incipient damage, maximum damage and high-velocity damage. This response is characterized by a maximum lateral damage size that occurs just above the penetration limit. Further increases in projectile velocity result in lesser damage, until a plateau is reached called the high-velocity lateral damage. Velocity increases beyond this limit do not produce any significant change in damage size, unless velocities can be reached that result in appreciable projectile break-up. The difference between the maximum damage and the high-velocity damage depends primarily on sheet thickness.

Figure 11 is a photograph showing the effects of projectile velocity for .30-caliber AP impacting 0.090-inch 7075-T6 sheet. The increase in damage with reduced velocity is evident.

Effect of Projectile Obliquity

The angle of obliquity (or impact angle) has a pronounced effect on damage size. The following are generally true regarding obliquity effects:

1. When impact angles are increased and other conditions held constant, the maximum lateral damage will also increase as long as penetration occurs;
2. The velocities required for incipient lateral damage, maximum lateral damage and the onset of high-velocity lateral damage increase directly with impact-angle increase.

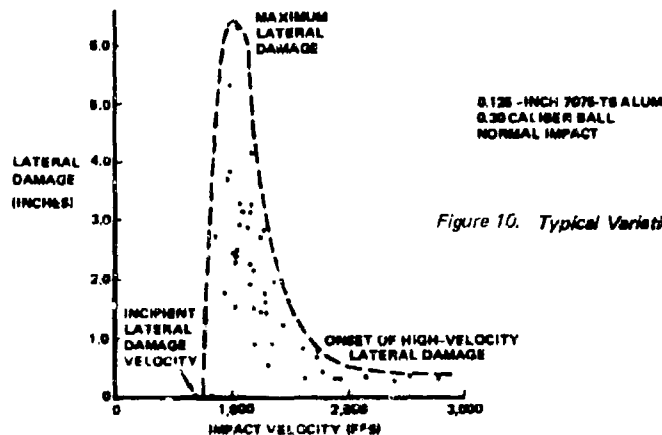


Figure 10. Typical Variation of Damage Size with Projectile Velocity

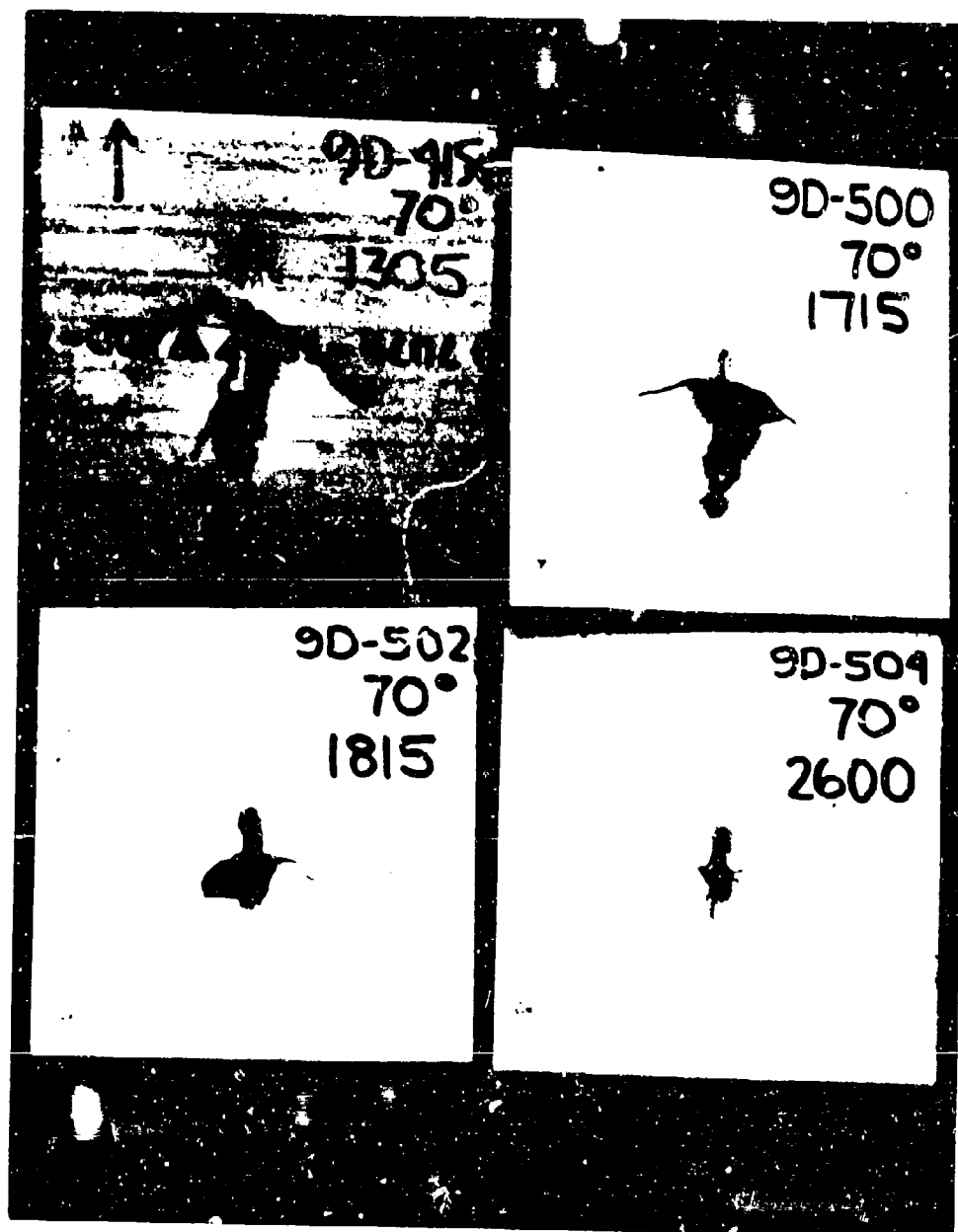


Figure 11. Effect of Projectile Velocity on Damage Size (0.090 7075-T6 Impacted by 0.30 Cal AP)

Figure 12 illustrates this response schematically, and Figure 13 is a photograph showing .090-inch 7075-T6 impacted at several obliquities with velocity held constant. There is a dramatic reduction in damage size as the impact angle increases from 60 to 70 degrees caused by projectile ricochet.

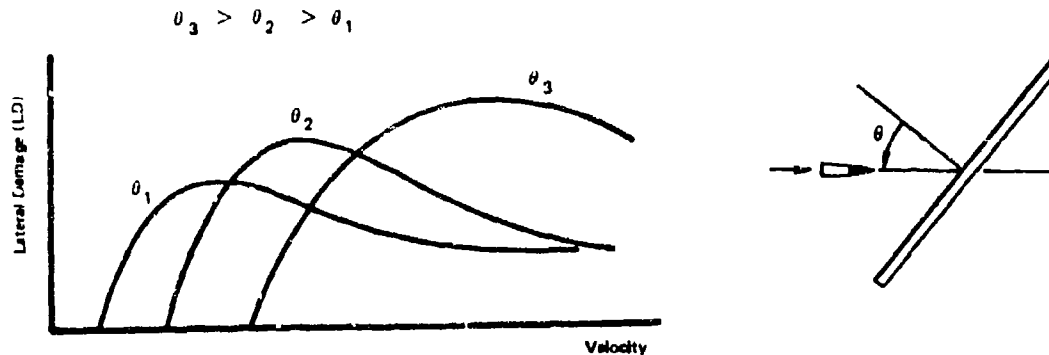


Figure 12. Typical Effect of Obliquity on Damage Size

Effect of Projectile Type

When projectiles are similar in shape and construction but differ in size, it is generally found that larger projectiles produce greater damage. When this similarity is not present, however, it is not possible to make lateral damage predictions based only on projectile size. Projectile type must also be considered.

A distinction must be made between ogive bullets and compact fragments, for example. Ogive projectiles can exert significant in-plane wedging forces that contribute to panel cracking during projectile penetration. Compact fragments tend to push through the panel, causing a different mode and size of damage.

Effect of Sheet Thickness

Damage size is highly dependent on sheet thickness. A convenient thickness parameter is the ratio of thickness to projectile diameter (t/D). Typically, as t/D ratios are increased beyond 0.1, the maximum lateral damage size increases from a projectile-sized hole to a relatively large damaged area. This principal maximum lateral damage occurs at t/D values between 0.3 and 0.4 for aluminum and titanium alloys. Increasing t/D ratios beyond 0.4 reduces the lateral damage to a projectile-sized hole that may be accompanied by significant amounts of spallation.

The typical response is shown graphically in Figure 14a. It should be kept in mind that since lateral damage is also dependent on projectile velocity, this figure shows the largest damage (i.e., the maximum lateral damage) that occurs for each given t/D ratio.

The remaining illustrations in Figure 14 demonstrate the parametric effects discussed, namely: the effect of projectile velocity, impact angle and projectile type.

Effect of Sheet Material

The choice of material will have a marked effect on the resulting size and type of damage, since materials differ in their resistance to impact damage. A comparison of damages produced under identical impact conditions, changing only target material, will show large differences in damage size. It was shown that the damage sizes for 2024-T3, 2024-T81 and 7075-T6 aluminums have the ratios 1/2.2/5.1, respectively. On the same basis, the ratio for 6Al-4V titanium was found to be 1.8. These materials rank in the following order of damage resistance, with the first having the highest:

1. 2024-T3
2. 6Al-4V
3. 2024-T81
4. 7075-T6

Since damage tolerance is also dependent on material, material selection is a means of reducing structural degradation due to battle damage.

Effect of Applied Stress

If the stress level is sufficiently high to precipitate impact fracture, there will be an extension of damage beyond that obtained from lower stressed panels. Applied stress levels below this value may have a small influence on damage size and orientation; however, the extent of these effects has not yet been established.

III. 1.2 IMPACT DAMAGE IN FIBER COMPOSITES

There has been very little parametric impact-damage testing of fiber composites. Figure 15 shows typical projectile damage in a boron/epoxy sandwich panel. Some boron/epoxy test results are shown in

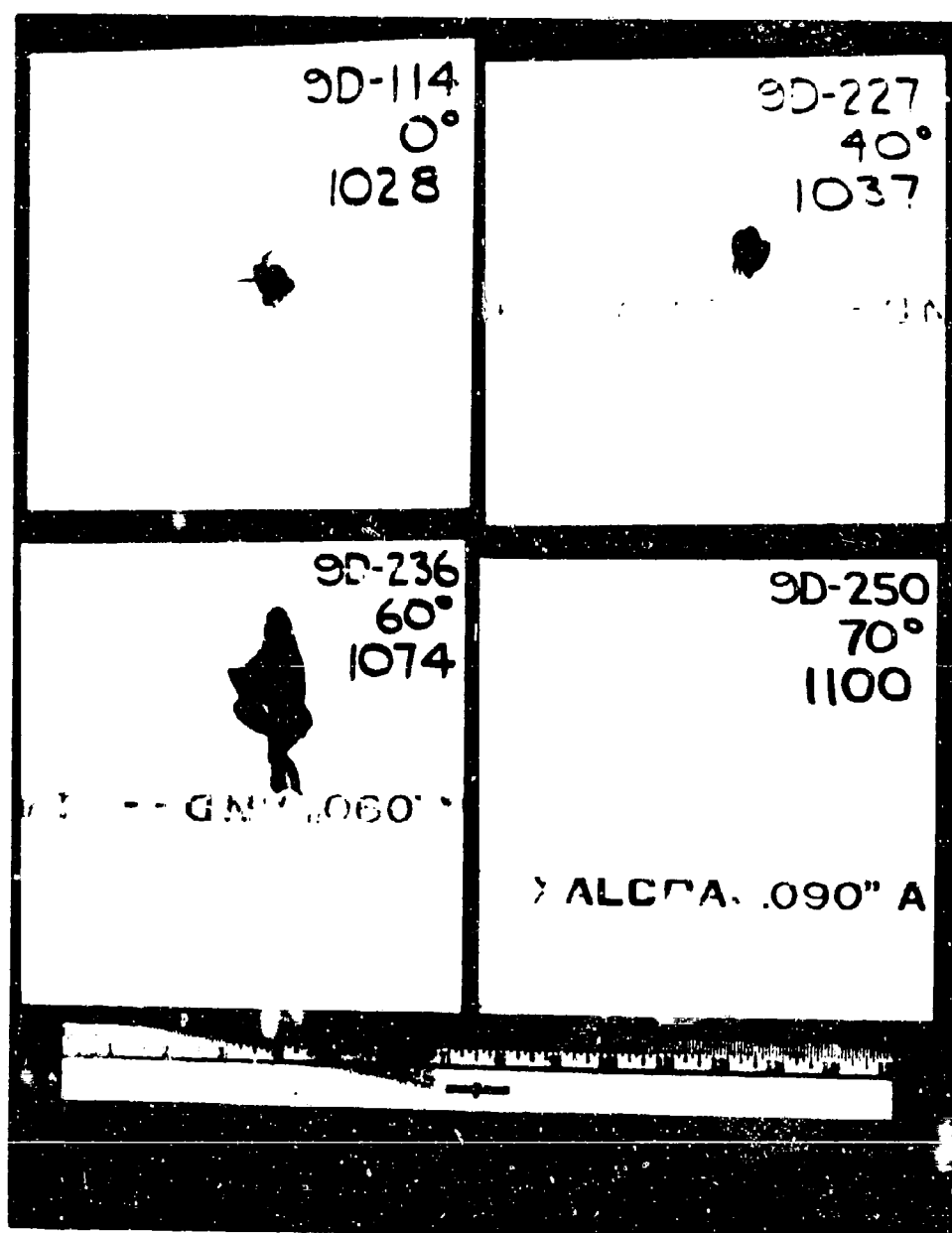


Figure 13. Effect of Impact Angle on Damage Size (0.050 7075-T6 Impacted by 0.30 Cal AP)

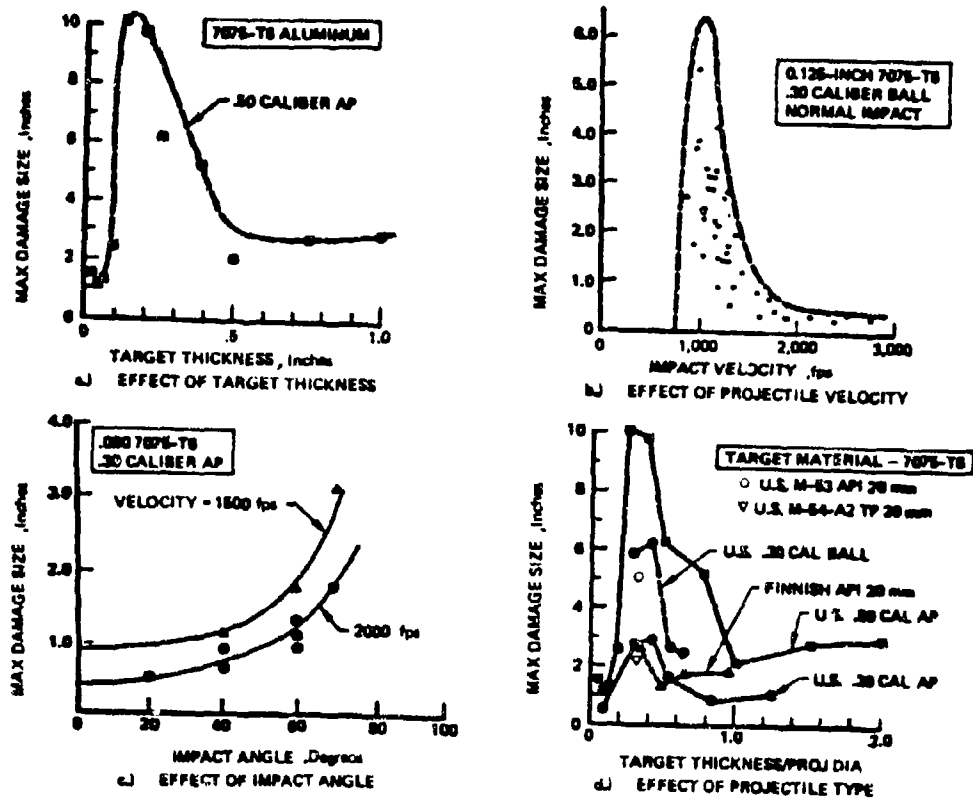


Figure 14. Effect of Several Parameters on Gunfire Damage of Metal Structure

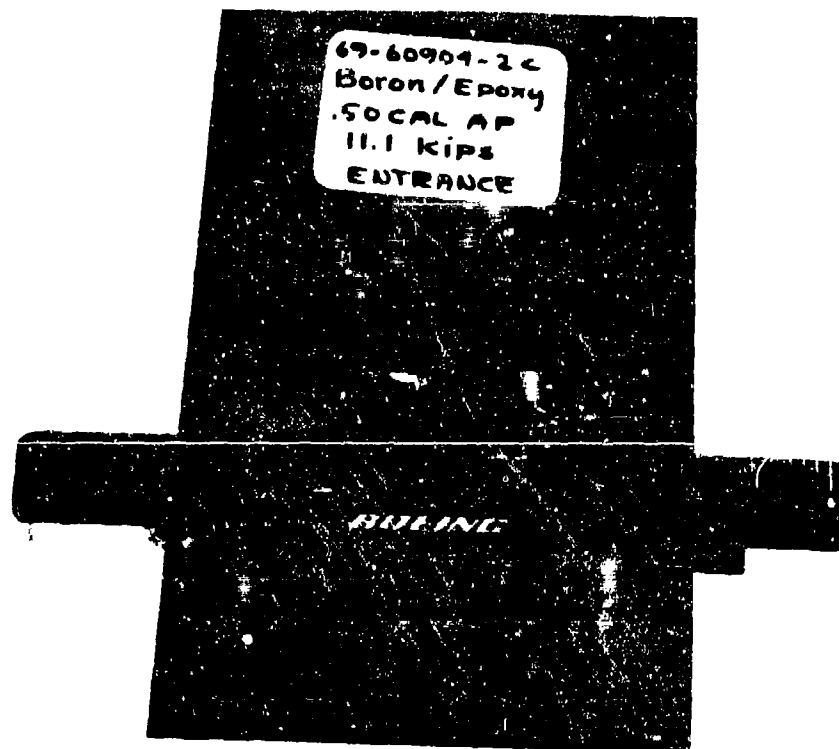


Figure 15. Typical Projectile Damage in Thin Fiber Composite Sheet

Figure 16 for comparison with the metal data (Figure 14). The dashed lines represent the size of the projectile projected onto the plane of the test panel. This is the minimum damage size corresponding to passage of the projectile through the panel. In contrast to the response of metals, there is a close correlation between the measured damage extent and the projected area of the projectile. The one exception is for the exit face of thicker laminates.

The available data indicate that extensive visible cracking extending from the impact point does not occur in thin panels of boron/epoxy and graphite/epoxy. These materials exhibit good damage resistance.

BORON/EPOXY STRUCTURAL PANELS

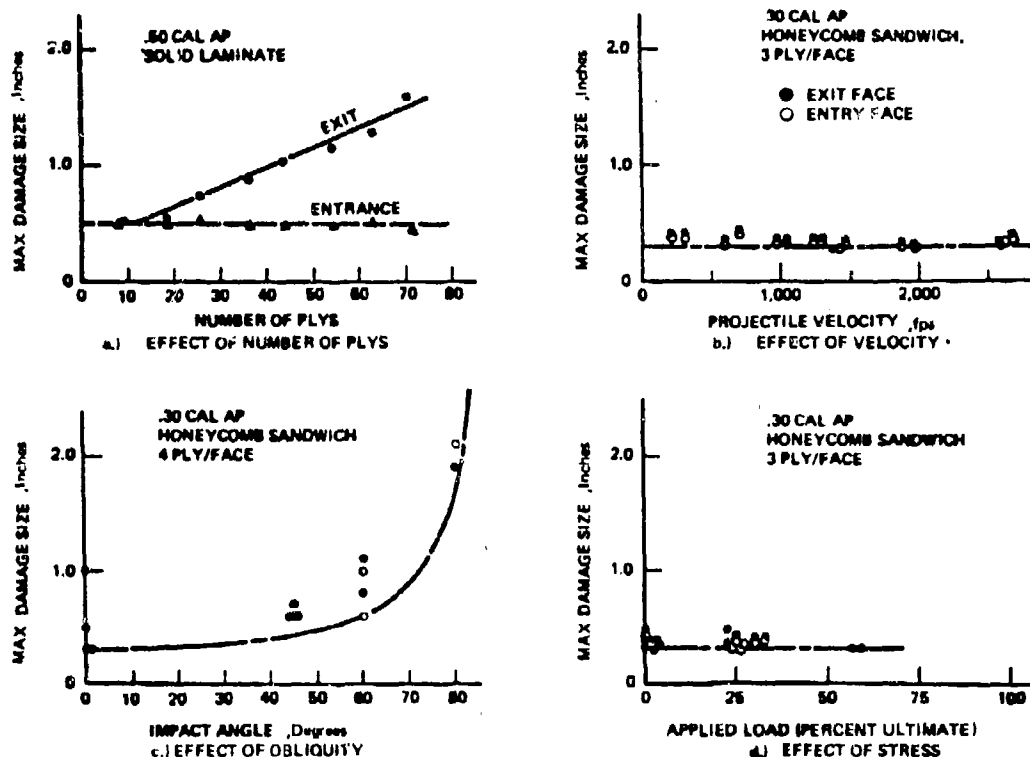


Figure 16. Typical Parametric Damage Data for Fiber Composites

III. 1.3 PROJECTILE IMPACT INTO FLUID FILLED CONTAINERS

In many aircraft applications, the structure serves the additional function of fuel containment, so that a penetrating projectile enters a fluid medium after passage through an adjacent element of structure. The term 'hydraulic ram' refers to the dynamic pressures generated within the fluid as a result of energy imparted by a penetrating projectile. These pressures are transmitted to the walls of the fuel tank, and they can cause severe structural damage to lightweight aircraft structure.

Hydraulic ram must be considered as a damage mechanism for any structural element that is wetted by fluid, or any element that is separated from fluid by a pressure transmitting component such as a flexible bladder. The structural damage caused by hydraulic ram consists of bulging and tearing, and fastener failure is common. Damage is especially severe at entrance and exit walls because the internal pressures extend the damage caused by penetration. Hydraulic-ram damage due to fragments and small-arms projectiles can be extensive and potentially catastrophic as suggested by Figure 17. Hydraulic-ram will be discussed more fully in a subsequent presentation.

III. 2 PREDICTION OF PROJECTILE IMPACT DAMAGE

The description and modeling of ballistic impact damage is a new and complex technology. The available prediction methods are primarily upper and lower limit techniques, and statistical reliability has not yet been adequately defined. These limitations in damage-prediction capability influence the reliability of structural vulnerability assessment and design.

The following paragraphs describe some techniques for predicting projectile impact damage size. The description is organized according to the type of projectile and the type of structural material, and includes:

1. Bullets impacting metal
2. Bullets or fragments impacting fiber composites
3. Fragments impacting metal
4. Impact damage from HE projectiles

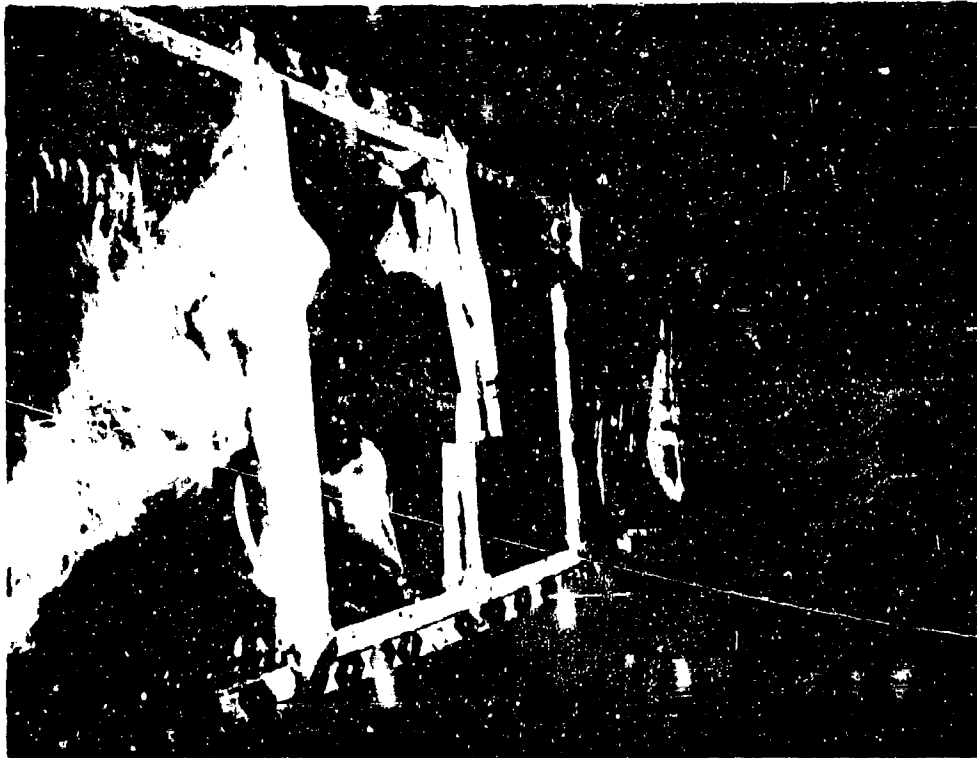


Figure 17. Hydraulic RAM Damage in Fuel Tank Caused by Small-Arms Projectile

BULLETS IMPACTING METAL

A damage-size model is described in Reference 4, and was incorporated into a design handbook in Reference 3. Because of the inherent scatter in damage size data, the model was designed to predict the upper and lower limits of damage size. The modeling is illustrated qualitatively in Figure 18, and a typical set of upper-limit damage-prediction curves is shown in Figure 19.

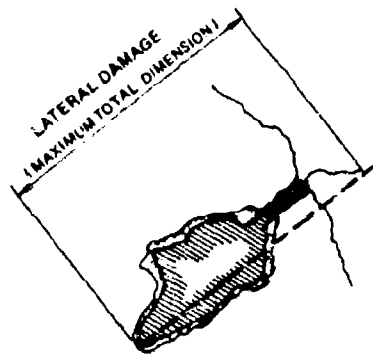
Upper and lower-limit prediction curves were plotted by computer for the following conditions:

- Projectiles: .30-caliber AP
.30 caliber ball
.50 caliber AP and ball
- Materials: 2024-T3 aluminum
2024-T81 aluminum
7075-T6 aluminum
6Al-4V titanium (except .30 caliber ball)
- Thicknesses: 0.032, 0.063, 0.090, 0.125, 0.160, 0.190, 0.250,
0.375, 0.500, 0.750, 1.000 inches
- Impact Angles: 0, 20, 40, 60, and 70 degrees

As a convenience, the upper-limit damage-size predictions have been reformulated in terms of maximum upper-limit damage for varying panel gages over a specified velocity range. Typical results are presented in Figure 20. These curves provide a condensation of the prediction curves shown in Figure 19. This is made possible by transforming the velocity variation into a velocity range (0 to 3200 fps).

BULLETS OR FRAGMENTS IMPACTING FIBER COMPOSITES

As discussed previously, there has been only limited parametric damage testing in composite materials. However, a tentative evaluation of the extent of damage in thin composite panels beyond the projected size of the projectile was made using available data. The results are reported in Reference 5. The average value found for all the data reported was about 0.2 inch, based on using linear elastic fracture mechanics for correlating residual tensile strength. From this result, an effective damage size was defined as shown in Figure 21. This provides a damage model for thin composite structure that relates projectile damage size to impact angle and projectile caliber. Figure 22 presents effective damage size results from this



a.) DAMAGE DEFINITION

DAMAGE SIZE MODEL

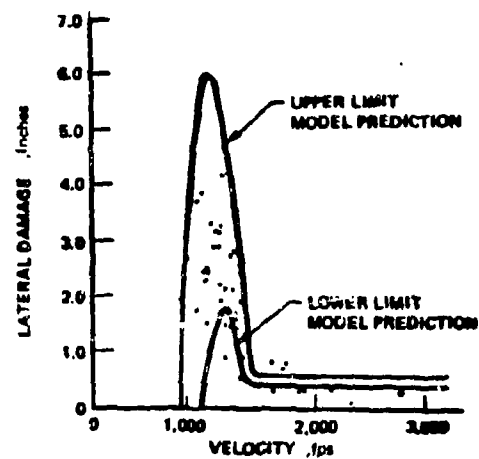
$$\text{LATERAL DAMAGE} = \begin{cases} 0 & \text{FOR } V^* < V_1 \\ K_D \text{ NIMLD} [a_4 V^4 + \beta_4 V^3 + \gamma_4 V^2 + \delta_4 V], & \text{FOR } V_1 < V^* < V_3 \\ \text{HVLD} & \text{FOR } V_3 < V^* \end{cases}$$

WHERE,

$$V^* = V (\cos \theta)^{0.7}$$

$$V = \frac{V^* - V_1}{V_3 - V_1}$$

$$\text{NIMLD} = C_1 D [\alpha_1 (V/D)^4 + \beta_1 (V/D)^3 + \gamma_1 (V/D)^2 + \delta_1 (V/D) + E_1]$$



b.) DAMAGE MODELING

Figure 18. Lateral Damage Size Prediction Model for Metallic Structure

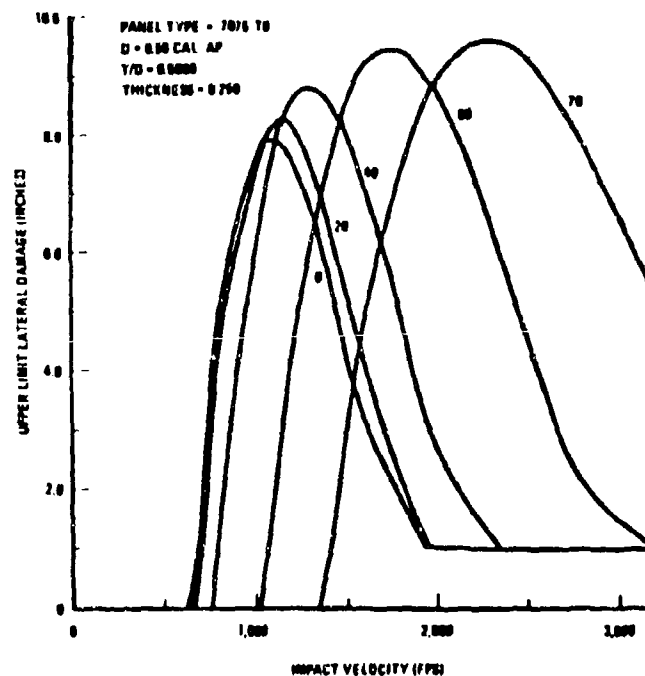


Figure 19. Lateral Damage Predictions From Analytical Model

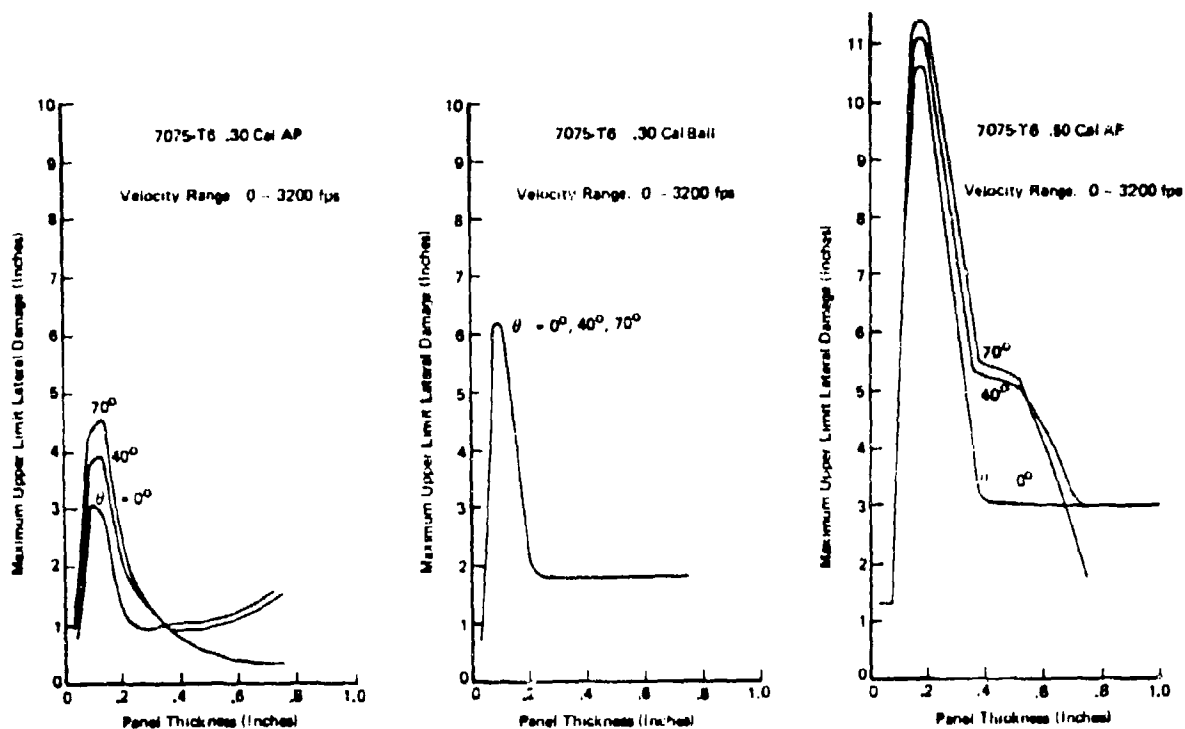


Figure 20 Maximum Upper Limit Lateral Damage for 7075-T6

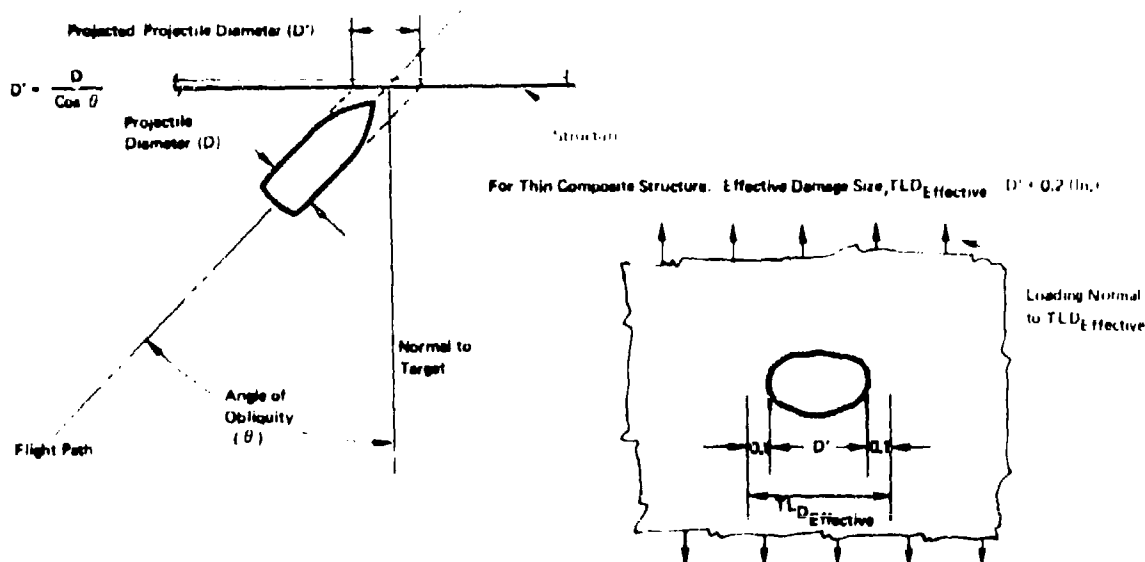


Figure 21 Boron Epoxy and Graphite Epoxy Effective Damage Size

model for 0.50 caliber non-piercing projectiles. Similar curves can be established for any projectile, including fragments.

FRAGMENTS IMPACTING METAL

Damage-prediction techniques for fragments impacting metal are not as well developed as the prediction techniques for bullets. This is partially due to the diversity in fragment sizes and shapes, ranging from cubes to continuous rods.

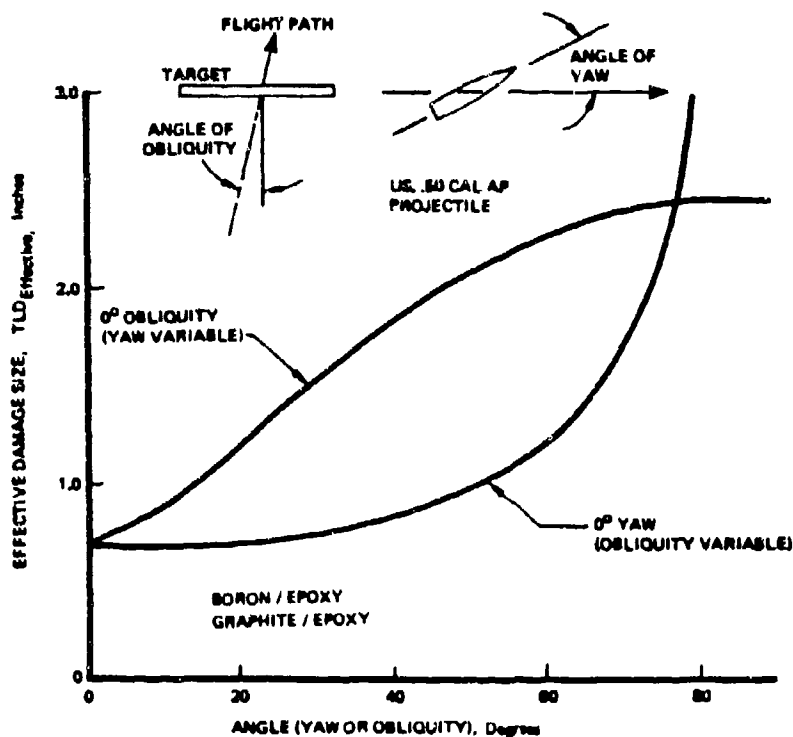


Figure 22. Variation of Effective Damage Size for .50 Caliber AP with Obliquity or Yaw Angle

A prediction model was developed in Reference 1 for damage size in aluminum due to singly impacting, high-velocity compact fragments. This model is described below, and should be applicable to low-density fragment impacts from SAMs or HE projectiles. High-density impacts involve the interactions between adjacent projectile damages, and there is currently no general method available for quantifying this type of damage.

Typical damage from high-velocity (greater than 2,000 fps) compact fragments is shown in Figure 23. Examination of compact-fragment data of this type indicated that the lateral damage is essentially independent of projectile velocity in the high-velocity range (2,000 to 6,000 fps). This behavior is similar to that established for bullets in Reference 3. The data also indicated that material effects were not pronounced in this range, as the damage sizes for 2024-T3 and 7075-T6 were very nearly the same.

These observations led to the development of a fragment damage model for aluminum alloys similar in form to the high-velocity damage model for bullets developed in Reference 3. The final expression is:

$$LD = \frac{b_e}{\cos^2 \theta} \left[1.16 + 0.6 \left(\frac{t}{D_e} \right)^2 \right]$$

where:

- LD = lateral damage size (inches)
- D_e = the maximum projected frontal dimension of the fragment (inches)
- θ = impact angle, measured between the flight path and a normal to the target surface
- t = target thickness (inches)

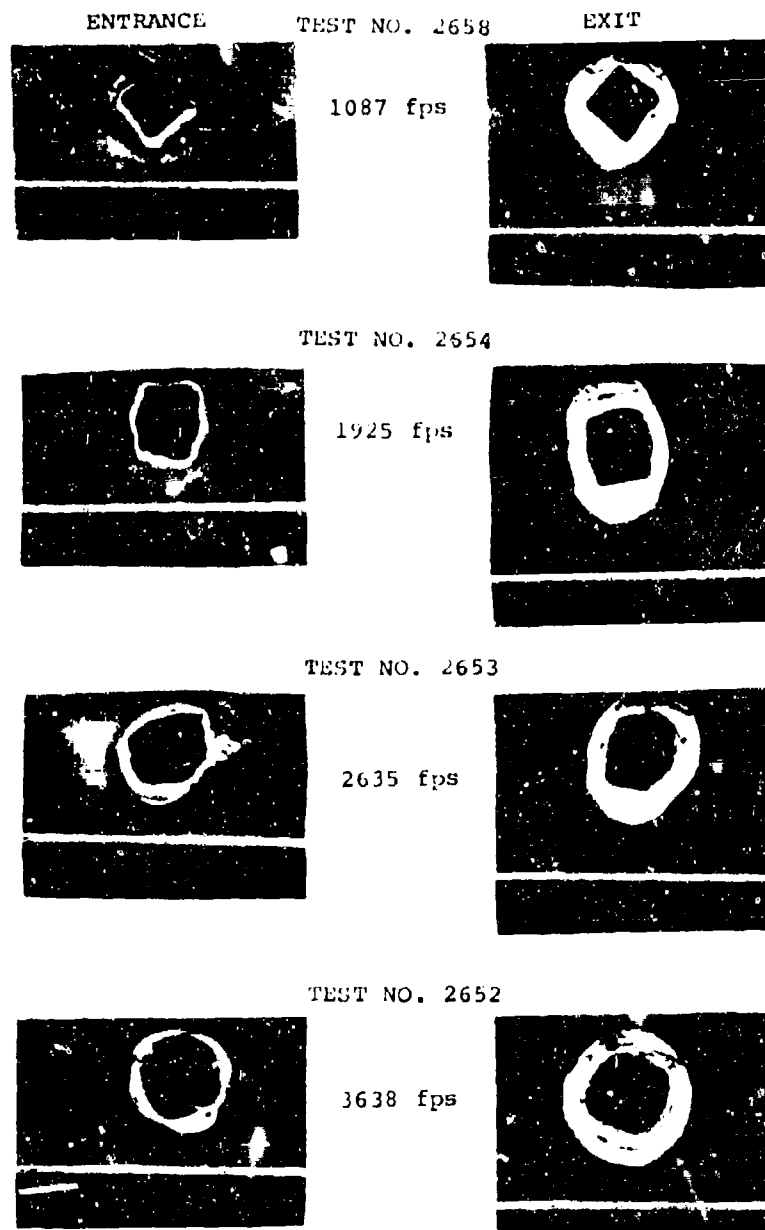


Figure 23. Damage Variation With Velocity for Compact Fragment Impacting 0.25 7075-T6 at Normal Obliquity.

IMPACT DAMAGE FROM HIGH EXPLOSIVE (HE) PROJECTILES

High-explosive projectiles of 20 to 37 mm caliber represent a probable threat for combat aircraft. Figure 24 shows several aspects of the terminal effects caused by HE projectiles. The resulting damage is due to the combined effects of fragments and blast (often internal).

The condition shown in the figure is for a projectile having an instantaneous fuze that detonates upon contact with the outer structure. Delay fuzes are also prevalent. In either case, a hole is punched in the outer skin, and a spray of fragments from the projectile casing emanates from the center of detonation. The spray forms a cone of fragments. The angle of divergence relative to the projectile flight path depends on projectile velocity and the fragment ejection velocity. This latter velocity is a characteristic of the projectile.

The development of methods for predicting damage due to HE projectiles has received recent attention, and certain of these methods will be described in subsequent presentations. The BR-1 computer code (Reference 6), for example, contains a fragmentation model for use in conjunction with the finite-element structural model developed for predicting the local damage and transient response of aircraft compartments subjected to the internal detonation of explosive projectiles.

The BR-1 code currently contains the characteristics of three HE rounds, including the static velocity, the mean static direction, the number of fragments and the mass distribution for the fuze, the fuze attachment, the side portion, and the base.

The velocity of the fragments is vectorially added in the BR-1 code to the velocity of the projectile relative to the target at the time of detonation to determine the relative velocity of the fragments to the target structure. For fragments emanating from the side of the projectile, the code automatically determines which finite elements in the structure are struck. For fragments emanating from the nose or base of the projectile, the user has to specify through the input data the elements struck. The BR-1 code determines what percentage of the fragments penetrate the structure, the impulse imparted to the finite elements because of the momentum change of the fragments as they encounter and/or penetrate the structure, and the loss in strain energy carrying capability and mass of the structure because of holes created by fragments that penetrate the structure.

III.3 INTERNAL LOAD REDISTRIBUTION

The infliction of damage in multiple load-path components causes a redistribution of internal loads among the elements. In addition, the availability of alternate load paths results in some level of residual strength capability in major structural components, even though element failures have occurred.

A powerful tool for determining load-redistribution in damaged structural components (a wing or wing segment, for example), is the finite-element structural analysis computer program. These programs are frequently used for design analysis, and their application to damaged or altered structure is a logical extension.

The operational theory of finite-element structural-analysis computer programs will not be discussed in detail here, as this theory is well known and well documented. The basic approach, however, is to develop a model or "structural idealization" of the component, using discrete structural elements such as plates, beams and rods having defined stiffness properties.

The utility of these techniques for structural vulnerability analysis lies in the fact that structural damage can be incorporated into the model by altering the stiffness properties of the damaged elements. This alteration must be made using damage models of the type discussed previously that relate damage size to threat, and that relate stiffness degradation to damage.

Using the altered element stiffness properties, the finite-element computer program can then reanalyze the structure and develop the redistribution of element stresses caused by the damage. The strength capability of the damaged structural component for any desired flight loading condition can then be determined by comparing the redistributed element stresses with structural failure criteria for damaged elements and crack-arresting structure.

Figures 25 to 28 show key aspects of the application of finite-element structural analysis to damaged structure. Figure 25 is the nodal diagram for a wing section under analysis. Considerable engineering judgment must be applied in preparing a nodal diagram that will ensure realistic results.

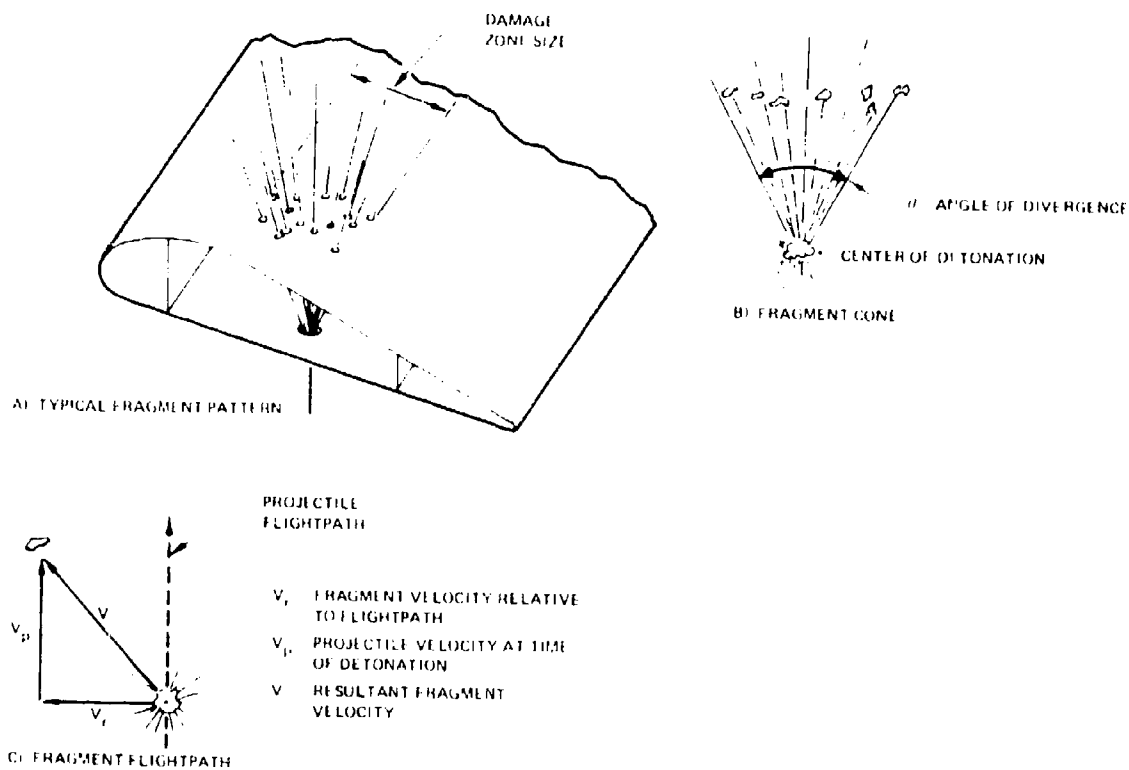


Figure 24 Fragment Phenomenology

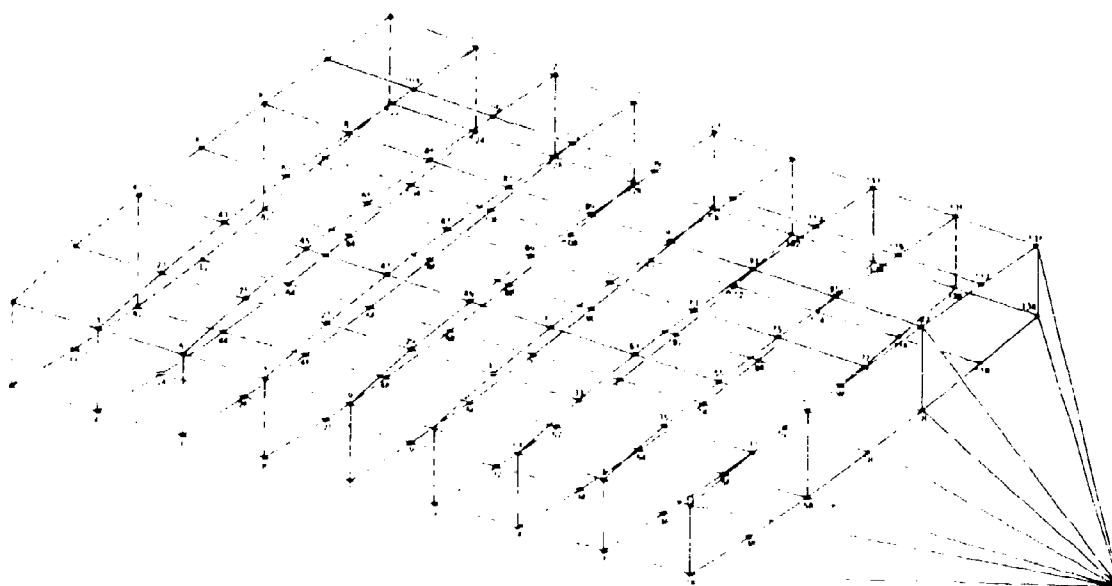


Figure 25 Wing Nodal Diagram

Figure 26 is the element diagram, indicating the various elements selected for the idealization. Typical element selection might include:

1. Upper and lower skin plates-- Stiffened plates carrying shear and axial load. Stiffeners were included as part of the plate properties.
2. Spar and rib web plates-- Spar webs were modeled as plates capable of carrying shear only.
3. Spar and rib stiffeners-- These elements were modeled as beams carrying axial load.
4. Spar chords-- All spar chords were modeled as beam elements carrying both axial and bending load.

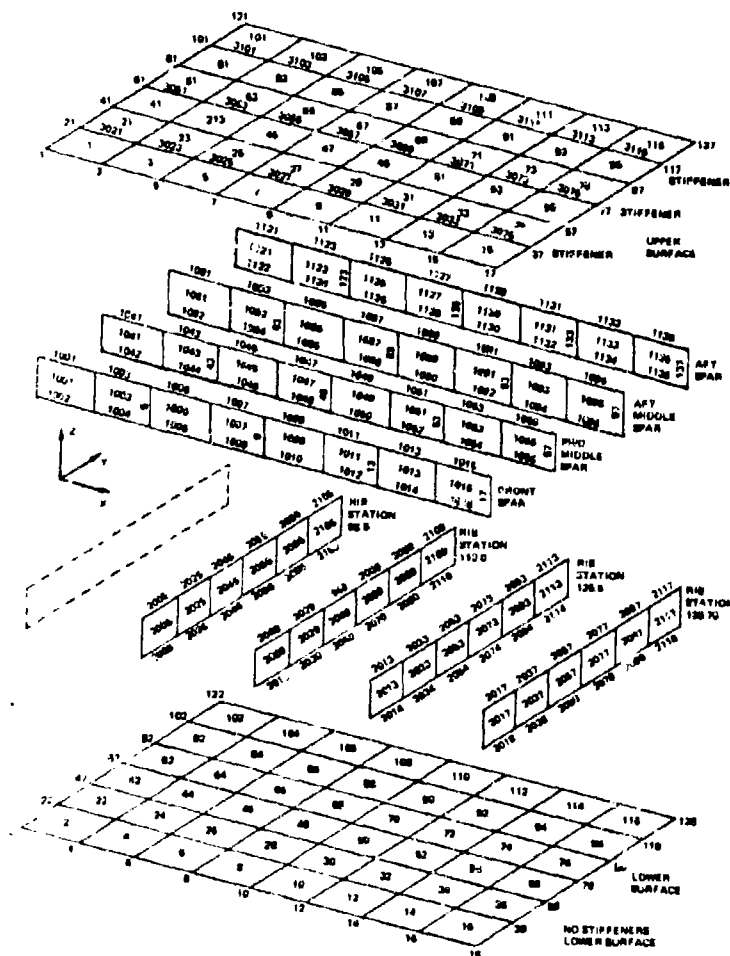


Figure 26. Wing Element Diagram

Figure 27 shows the loads applied at the nodes for a particular flight loading conditions. For example, these loads may be selected to represent flight conditions at limit load factor, or any load factor of interest.

The modeling developed at this point is that of the undamaged structure. The program should now be run so that element stresses and deflections for the undamaged case are available for comparison with the damaged cases. Following this, elements are altered as shown in Figure 28, in accordance with a damage model for the threat considered. The reanalysis is then completed to determine member stresses and deflections for the damaged component. These results must then be compared with failure criteria for both damaged and undamaged elements.

III.4 FAILURE CRITERIA FOR DAMAGED STRUCTURE

Having established the extent of damage, and the stress levels in members for a given external loading condition, residual structural performance can be estimated by comparing the stress levels in both damaged and undamaged elements with structural failure criteria. These failure criteria include net section strength, buckling, attachment failure, crippling, and fracture. Stiffness degradation may also lead to flutter-related failure modes.

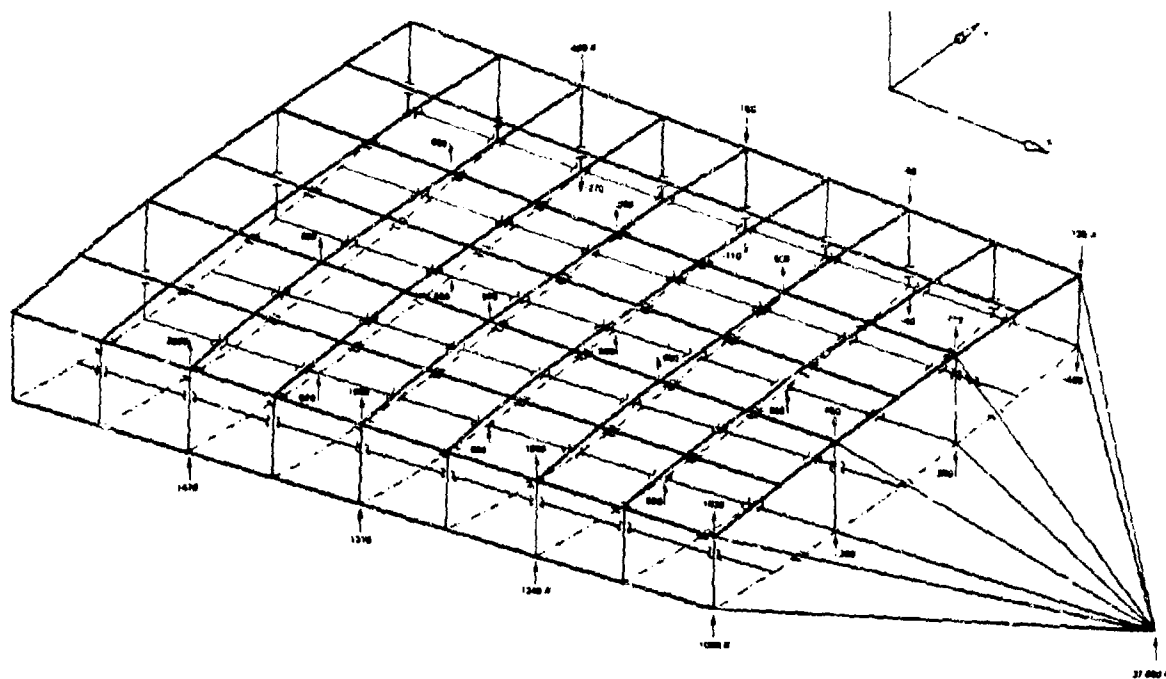


Figure 27. Wing Model Loads Diagram

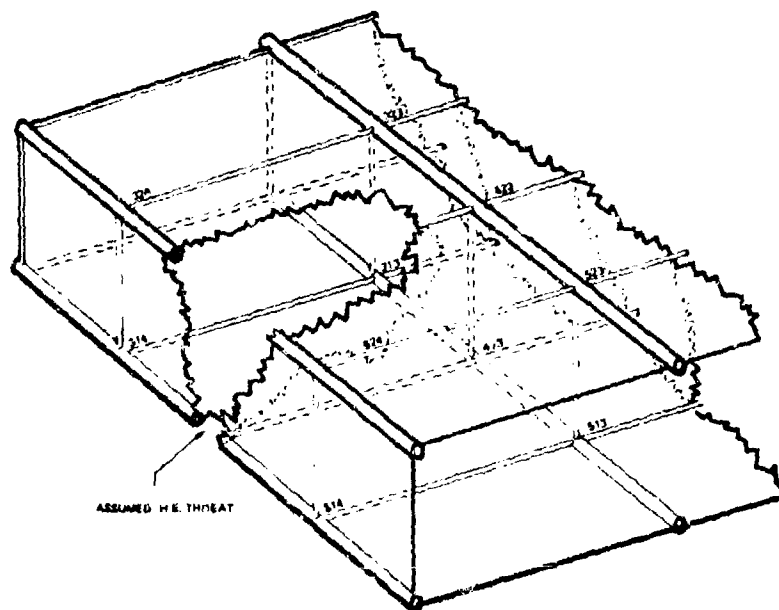


Figure 28. Schematic of Damaged Wing Model

Fracture of tension members is one of the most significant failure modes for projectile damaged structure, and considerable research has been done leading to the development of failure criteria. Some of this development is described in the following paragraphs, for both structural elements, and crack arresting structure.

III. 4.1 FRACTURE OF STRUCTURAL ELEMENTS

Typical element tensile strength behavior is shown schematically in Figure 29. In ductile materials, or when the type of damage results in low stress concentration, the residual strength behavior depends on the net area. This is defined as notch-insensitive fracture behavior. This behavior describes the least severe damage (greatest strength) for aircraft structure. The analysis of residual strength for this behavior is straightforward.

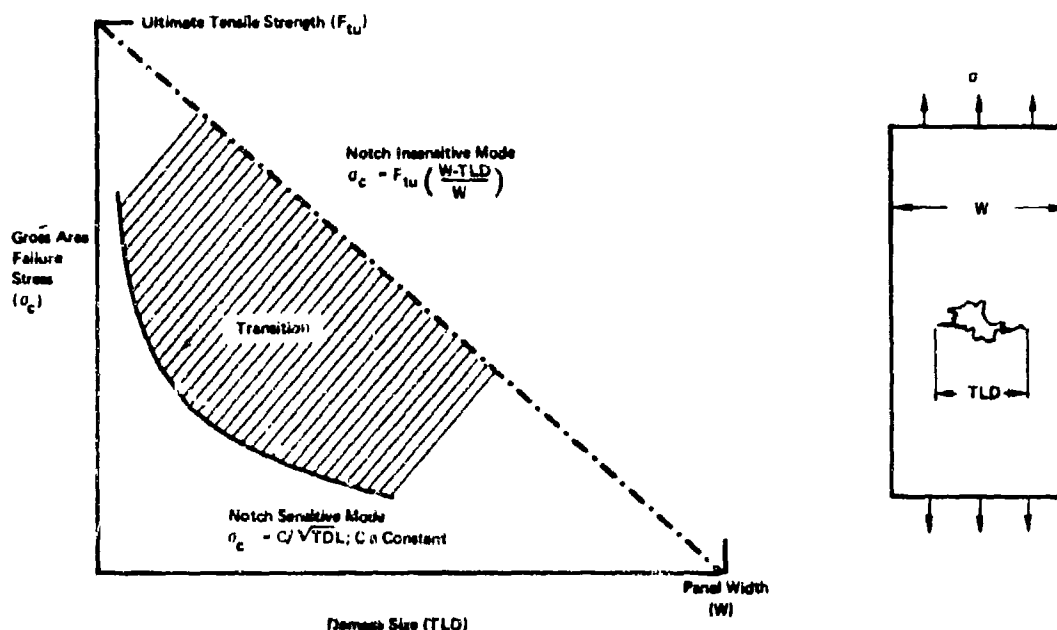


Figure 29. Variation in Fracture Response With Failure Mode

The most severe damage (lowest strength) consists of sharp cracks in brittle materials. This results in high stress concentrations with little ductility and a response characterized as notch-sensitive. This behavior is normally associated with fatigue-crack damage, and fracture mechanics (K_I) is used for the analysis.

The tensile strength of ballistic-damaged panels, based on transverse damage, often does not fit either of these categories, but is located in-between (referred to as transition behavior). The transition behavior for ballistic-damaged materials is due to the bluntness of the notch resulting from ballistic impact. A modification of the fracture mechanics technique has been developed from test data for predicting the residual strength of ballistic damaged structure (Λ_c).

An additional consideration is vital to structural vulnerability assessment: The strength of the structure is influenced by the loadings and effects induced by the impact. Because of this, structural elements may not be able to carry the same load during impact as immediately after impact.

Impact fracture is a term used to describe the fracture of a stressed tension panel immediately upon impact. This type of fracture occurs when local cracks, initiated by the impact, undergo rapid propagation through the structural member. Unless the crack propagation is arrested in some manner, the structural member will not survive the impact. This failure mechanism is distinct from the residual strength failure, in that residual strength failures occur when surviving (but damaged) panels are subjected to increased loadings until fracture occurs. Figure 30 depicts this distinction. From available data, a threshold level termed "impact fracture strength" can be defined, representing the onset of prestress influence. The analysis of impact fracture behavior follows a modification of the fracture mechanics technique using a parameter, Λ'_c , to define the threshold value for impact fracture (impact fracture toughness).

The remainder of this section describes analysis methods for predicting the tensile strength of damaged structural elements. As indicated in Figure 31, these methods are based on linear elastic fracture mechanics.

Λ_c - BALLISTIC DAMAGE RESIDUAL STRENGTH

A technique has been used for estimating the residual tensile strength of ballistic-damaged panels by defining a stress intensity factor for gunfire damage, Λ_c , by the relation:

$$\Lambda_c = \sigma_c \left(\frac{\pi}{2} \text{TLD} \right)^{1/2}, \quad \text{where}$$

$$\sigma_c = \text{gross stress at failure}$$

$$\text{TLD} = \text{maximum transverse lateral damage, as shown in figure.}$$

Figures 32, and 33 show a comparison of Λ_c values for 7075-T6 from Reference 3 compared with typical values of K_I .

It is believed that the trend shown in the figure is typical for metals and that the relative position of the ballistic damage fracture data depends primarily upon the extent of cracking inflicted by the impact. In general, the tendency to crack decreases as thickness increases beyond a t/D ratio of approx-

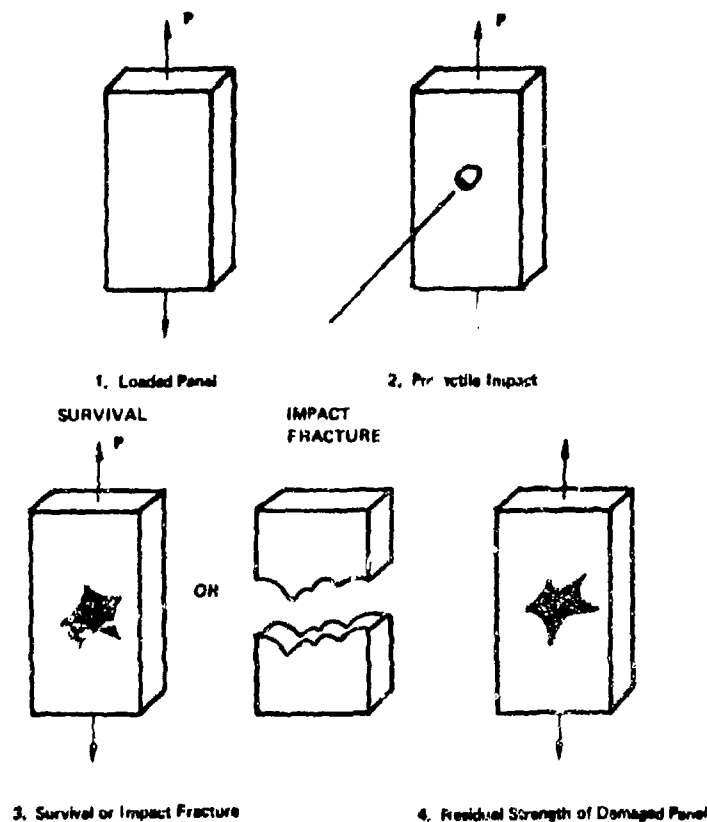


Figure 30. General Response of Loaded Panel Impacted by Projectile

RESIDUAL STRENGTH - FATIGUE DAMAGE

$$K_c = \sigma_c \left[\frac{\pi}{2} 2a \right]^{1/2}$$

σ_c - Gross Tensile Stress at Failure
 $2a$ - Total Crack Length

RESIDUAL STRENGTH - PROJECTILE DAMAGE

$$K_c = \sigma_c \left[\frac{\pi}{2} TLD \right]^{1/2}$$

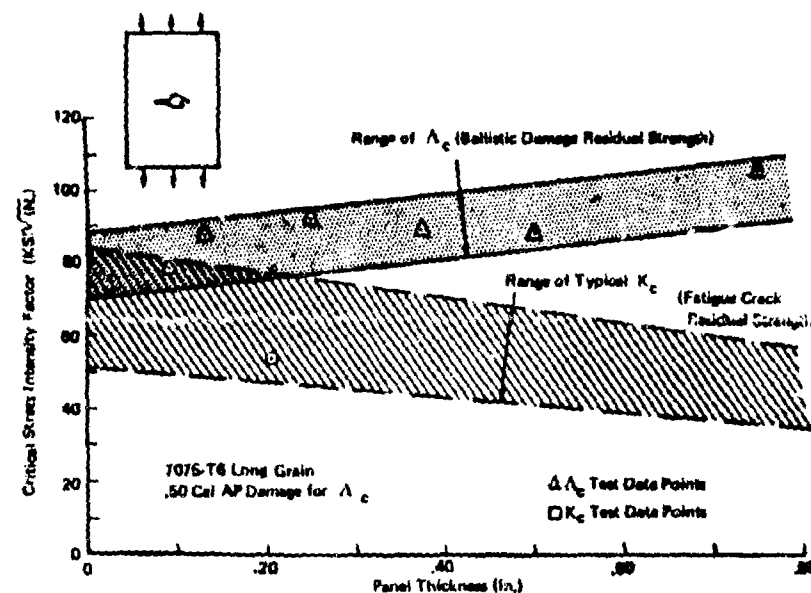
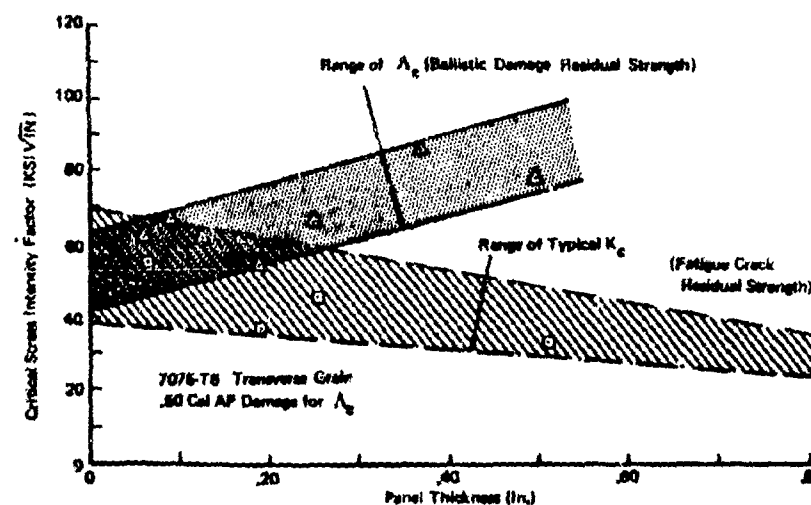
σ_c - Gross Tensile Stress at Failure
 TLD - Projectile Damage Normal to Gross Stress

STRENGTH AT IMPACT - PROJECTILE DAMAGE

$$K'_c = \sigma'_c \left[\frac{\pi}{2} TLD \right]^{1/2}$$

σ'_c - Gross Tensile Stress at the Onset of Impact Fracture
 TLD - Projectile Damage Normal to Gross Stress, based on Damage Response of Unloaded Panel

Figure 31. Summary of Fracture Mechanics Analysis of Damaged Structure

Figure 32. Comparison of A_c with K_c , Longitudinal Grain 7075-T6Figure 33. Comparison of A_c with K_c , Transverse Grain 7075-T6

imately 1:3. Consequently, it would be expected that the fracture response of impact-damaged sheets will become more notch-insensitive as thickness is increased.

A_c Values for Metals

Values of A_c are determined experimentally by pulling damaged panels until tensile failure occurs. Reference 3 presents a detailed analysis of A_c determinations for 2024-T81, 7075-T6 and 6Al-4V. The average values of A_c are summarized in Table I, along with the standard deviations and standard error of the mean.

It should be mentioned that cyclic loading after ballistic damage may increase the sharpness of the effective notch. This may occur quickly (with few cyclic load applications) in some applications, and a decision must be made whether to base strength predictions on A_c or K_c .

A_c Values for Fiber Composites

Analysis of available data (Reference 5) has indicated that the tensile strength of boron/epoxy and graphite/epoxy panels damaged by small caliber bullets can, in many cases, be predicted using a modification of the technique for metals. The modification consists of using an "effective" (transverse lateral) damage (LTD) as defined previously in Figure 21. This approach has also found application in fracture analysis of composites containing flaws other than ballistic damage.

TABLE I: Average Values of Λ_c

MATERIAL	Λ_c (ksi $\sqrt{\text{in}}$)	STANDARD DEVIATION (ksi $\sqrt{\text{in}}$)	STANDARD ERROR OF THE MEAN (ksi $\sqrt{\text{in}}$)	NUMBER OF TESTS n
2024-T81 (TRANSVERSE GRAIN)	53.5	8.3	4.2	4
7075-T6 (TRANSVERSE GRAIN)	65.6	12.6	2.8	20
7075-T6 (LONGITUDINAL GRAIN)	91.9	14.9	2.7	31
6A1-4V (TRANSVERSE GRAIN)	162.0	25.5	5.3	23

Available ballistic results for fiber composites layed-up in the 0, 45, 90 configuration family have been correlated effectively by the relation:

$$\frac{\Lambda_c}{F_{tu}} = \frac{\sigma_c}{F_{tu}} \sqrt{\frac{\pi TLD_{EFF}}{2}}$$

The data was presented as shown in Figures 34 and 35, and average values of Λ_c/F_{tu} were found for each material classification. In addition, statistical data was generated for each material to establish allowable values as presented in Table II.

TABLE II: Boron/Epoxy & Graphite/Epoxy Λ_c Data

MATERIAL	$\Lambda_c/F_{tu} \sqrt{\text{in}}$ AVERAGE	STANDARD DEVIATION	.95 CONF., .90 PROB.
Graphite/Epoxy	.574	.098	.393
Boron/Epoxy	.509	.059	.401

Graphite/epoxy on the average retained a greater percentage of its strength than boron/epoxy; but the variability was greater for the graphite/epoxy, resulting in nearly the same "B" allowable (.95 confidence, .90 probability) for the two materials.

Figures 36 and 37 define preliminary residual tensile strength allowable data for boron and graphite/epoxy panels of 0, 45, 90 lay-up, based on the test data available for consideration.

Impact Fracture Analysis

In Reference 3, the possibility of predicting impact fracture in a manner analogous to that used for residual static strength was examined. As described above, the static fracture behavior (residual strength) of impact-damaged panels has been characterized by Λ_c , the stress intensity factor for impact damage. A similar characterization for impact fracture is given by the formula:

$$\sigma'_c = \Lambda'_c \left(\frac{\pi}{2} TLD \right)^{-1/2} \quad \text{where}$$

σ'_c = threshold applied stress for impact fracture

Λ'_c = threshold stress intensity factor for impact fracture

TLD = transverse lateral damage, (the maximum component of damage transverse to the applied stress due to projectile impact).

There is very little data available, however, for pursuing this characterization, except for transverse grain 7075-T6 reported in Reference 3. Evaluations of Λ'_c for 7075-T6 are compared with a K_{IC} data envelope; in Figures 38 and 39. The Λ'_c estimates fall within the K_{IC} envelope; however, the Λ'_c data tends to fall in the lower region of the envelope. The range of Λ'_c for transverse-grain 7075-T6 is between 33 and 55 ksi $\sqrt{\text{in}}$. It should be noted that these values are substantially below the Λ_c values for this material, demonstrating that threshold levels for stressed panels are generally lower than the residual strength of similarly damaged panels.

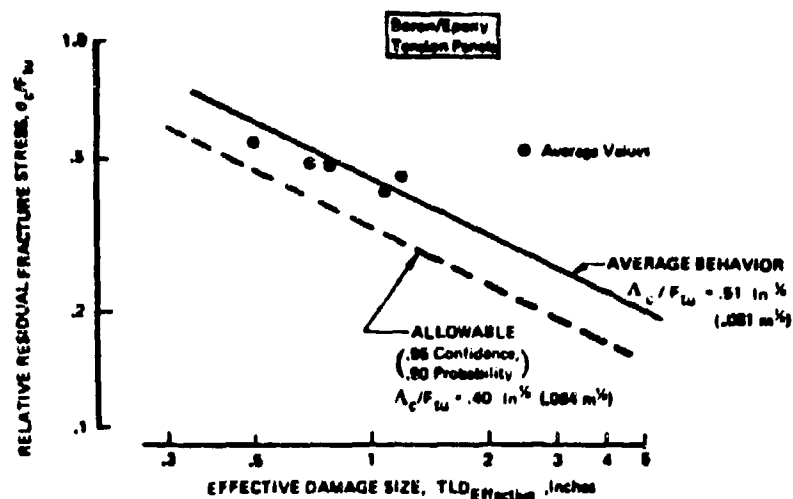


Figure 34. Residual Strength Data for Boron/Epoxy Panels Containing Projectile Damage

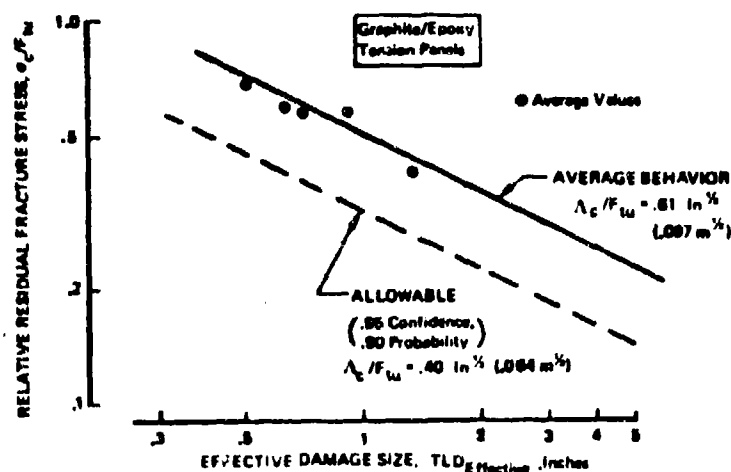


Figure 35. Residual Strength Data for Graphite/Epoxy Panels Containing Projectile Damage

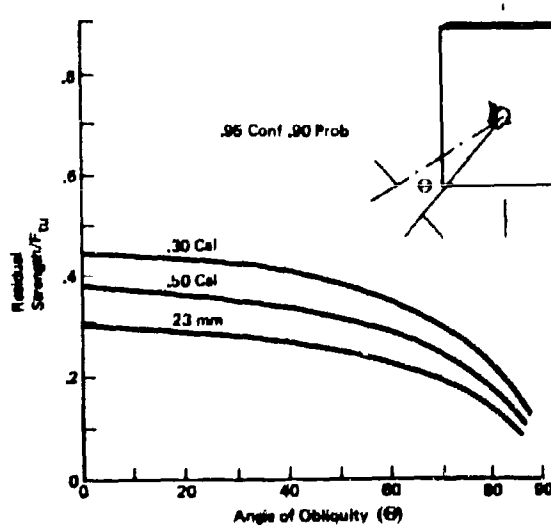


Figure 36. Residual Tension Strength Allowables for Boron/Epoxy

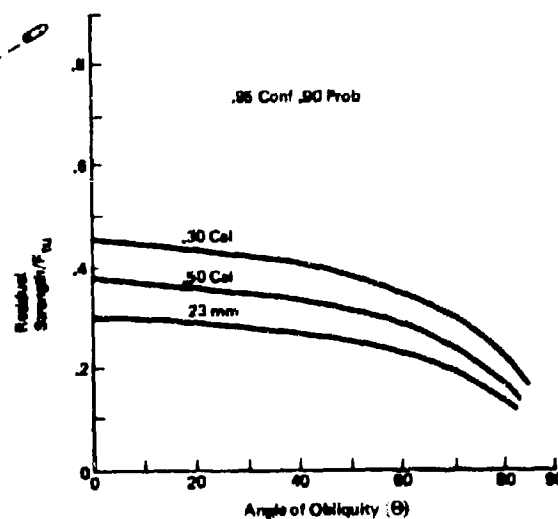


Figure 37. Residual Tension Strength Allowables for Graphite/Epoxy

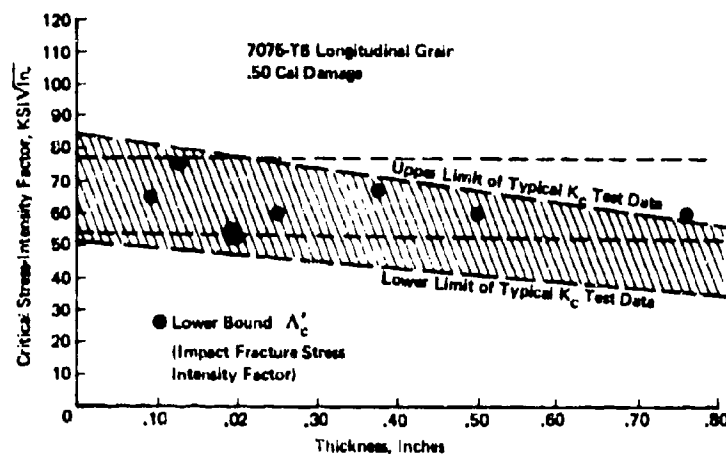


Figure 38. Impact Fracture Toughness Λ'_c and K_c of Longitudinal Grain 7075-T6

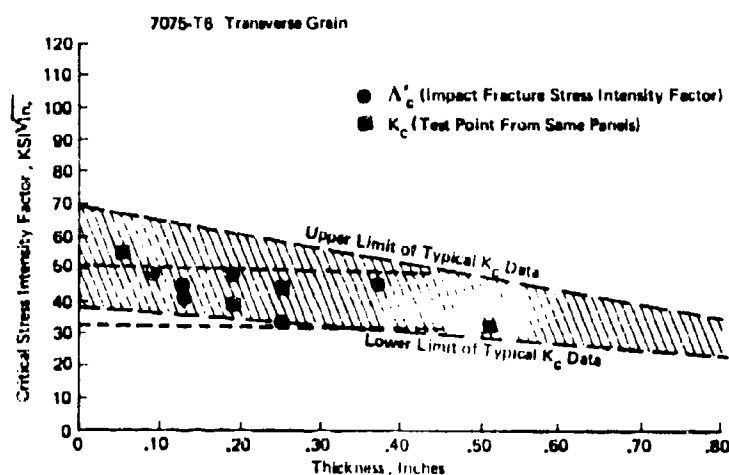


Figure 39. Impact Fracture Toughness Λ'_c and K_c of Transverse Grain 7075-T6

III. 4.2 FRACTURE OF CRACK ARRESTING STRUCTURE

Aircraft structure in most cases is not configured as a monolithic panel. For example, wing structure generally consists of skin with riveted stiffeners. The stiffeners can provide damage-containment or crack-arrestment capability that is not considered in the element residual strength analysis procedures described above. Since the crack-arrestment capability can significantly improve the residual strength of battle-damaged structure, the stiffening must be included in the analysis.

To determine the residual strength of stiffened structure damaged by weapon fire, the type of damage must first be established. Figure 40 presents several typical damage configurations. In Figure 40a the damage is confined to the skin area between the stiffening elements. This would be typical of a small-arms impact into the skin between stiffeners. In Figure 40b the damage is confined to the skin but reaches into the skin bays. This damage configuration, used in fatigue-damage analysis, is probably not typical for battle damage. When the skin damage extends into more than one bay, the intermediate stiffener normally will be damaged. This is illustrated in Figure 40c where both the skin and stiffener are damaged with the skin damage extending into two skin bays. Damage of this type generally would be considered the critical case for vulnerability analysis. Many impacts could damage several skin bays, and sever all the intermediate stiffening elements. For the particular case investigated, the threat and structural parameters such as stiffener spacing would be used in establishing the extent of damage.

The failure of a stiffened panel containing damage of the type illustrated in Figure 40c depends on the criticality of each panel component. Figure 41 illustrates schematically the critical components in the wing panels. As shown, the critical skin stress in an unstiffened panel follows the basic relationship for K_c . The critical skin stress is improved by the stiffeners when the crack tip is near the stiffeners ($1/D \approx 5$). As noted, however, the stiffener stress, because of the stress-concentration effect of the damage, can become critical for larger damage sizes. Also, the loading in the fastener attaching the stiffeners to the skin near the crack tip can approach a critical level resulting in an unzipping of the

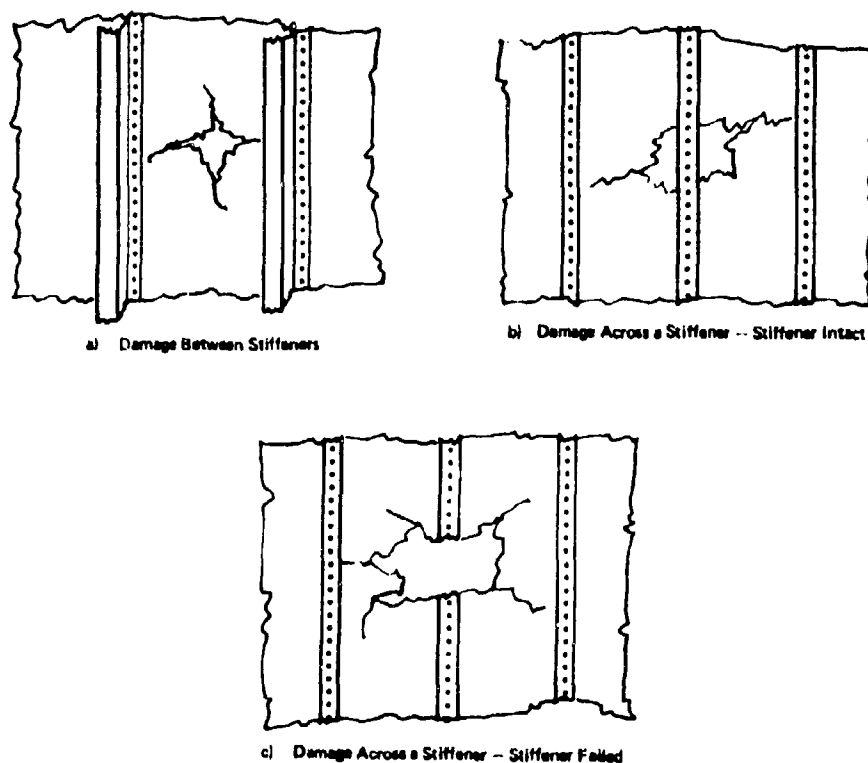


Figure 40. Typical Stiffener - Damage Configurations

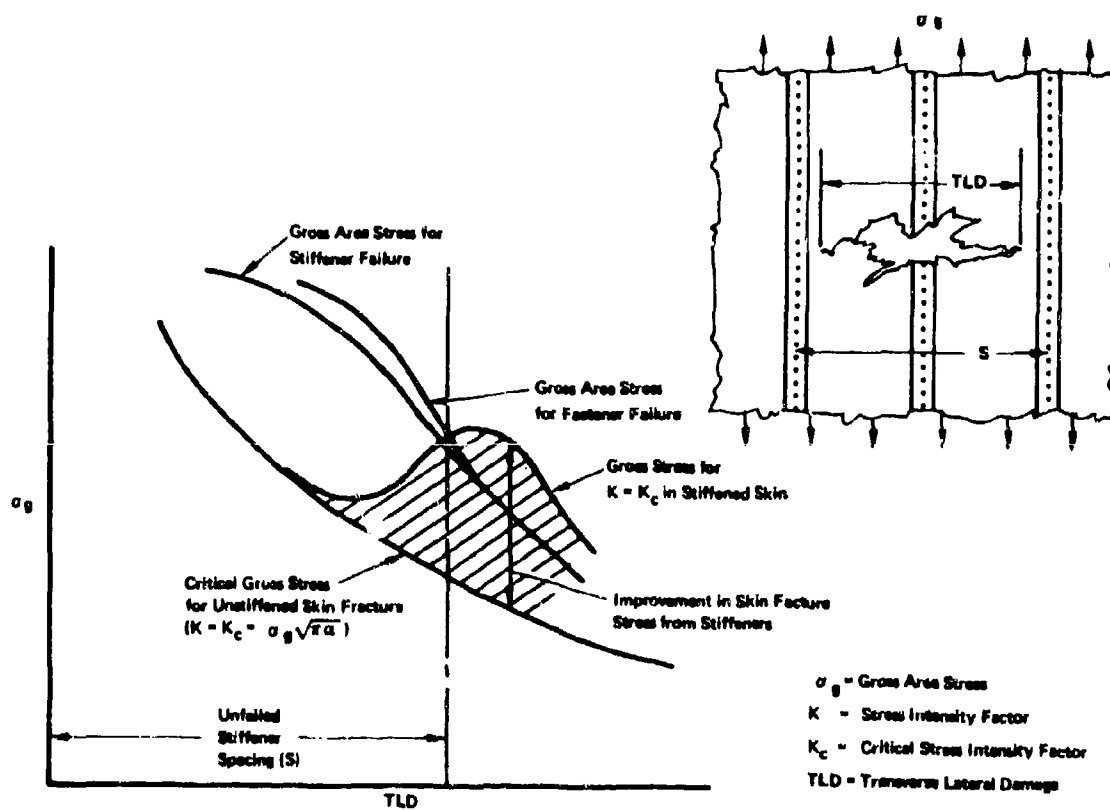


Figure 41. Schematic Description of Damaged Stiffened Panel Critical Components

attachment. For the total stiffened panel, the stress level for crack propagation corresponds to the critical skin stress ($K = K_c$ in the stiffened skin). As can be seen in the figure, for intermediate crack lengths (TLD less than S), the skin is more critical than for larger cracks (TLD \approx S). This results in cracks that run, but these may arrest at the stiffener.

Stress analysis must be performed in order to quantify the failure levels for specific built-up configurations. This analysis is identical to that performed for fail-safe requirements due to non-ballistic flaws, but must take into account the effective stress intensity factor for ballistic damage.

IV. CONCLUSIONS

This paper has described a methodology for integrating projectile damage tolerance considerations into the structural design process, along with related fatigue and fail-safe criteria. A key element for success in this task is the continued development of analytical methods that can establish criteria compliance in terms of design parameters.

V. REFERENCES

1. Avery, J. G., Porter, T. R., "Survivable Combat Aircraft Structures Design Guidelines and Criteria-Design Handbook," AFFDL-TR-74-50, April 1974.
2. Avery, J. G., Porter, T. R., "Designing Aircraft Structure for Resistance and Tolerance to Battle Damage," AIAA 4th Aircraft Design, Flight Test, and Operations Meeting, 1972.
3. Avery, J. G., Burch, G. T., "An Air Force Structural Combat Damage Model," AFFDL-TR-70-115, Nov. 1970.
4. Avery, J. G., Burch, G. T., Meiselman, J., "Techniques for Predicting the Structural Vulnerability of Aircraft to Ballistic Impact," AIAA 3rd Aircraft Design and Operations Meeting, 1971.
5. Avery, J. G., Porter, T. R., "Comparisons of the Battle Damage Response of Fiber Composites and Metals," ASTM STP 568, Foreign Object Impact Damage in Fiber Composites, 1974.
6. Jacobson, M., Yamane, J., and Brass, J., "Response of Aircraft Structural Compartments to Blast Pressures and Fragments from High Explosive Projectiles," AIAA/ASME/SAE 16th Structures, Structural Dynamics, and Materials Conference, 1975.

STRUCTURAL ANALYSIS OF IMPACT DAMAGE ON WINGS

by

Dipl.-Ing. Jürgen Massmann
Industrieanlagen-Betriebsgesellschaft mbH
8012 Ottobrunn, Einsteinstraße, Germany

SUMMARY

This paper gives a brief description of a recently-developed Structural Strength Model and examines in greater detail the functions and characteristics of a Damage Model. A discussion of a Shock Wave Model and how it analytically determines the dynamic response of a pressurized flat plate is also presented. Test and Finite Element results are compared with model-predicted results in order to determine model credibility. The pressures resulting from the detonation of ammunition are discussed and the contributions of each of the pressure components to the entire response are illustrated. Some advantages of an advanced Fragment Model are mentioned and the results from such a model are compared with appropriate test data. Lastly, the applications of the different Damage Submodels with respect to a honeycomb structure are shown.

1. INTRODUCTION

A relevant question for the design of a military aircraft is

how sensitive is the structure to impacts of different kinds of ammunition?

The investigation of this question results in the following statements: if the airplane has been hit

- the airplane is totally operational or
- only the mission can be finished or
- the mission ability is reduced or
- the airplane is no longer flyable.

Some tests have been performed to analyze the influence of

- different kinds of ammunition
- different airplane designs
- different locations of the hit points on the structure and so on.

As a result of these shooting tests and additional ultimate load tests, it has been determined that the most sensitive structural parts of an aircraft are the

- wings and the
- empennage.

The fuselage has also been partly destroyed. However, for most of this structural part the inside components are dominant.

This was the reason why damaged and undamaged wings and empennages have been investigated. These investigations have been done for

- given, specific wing and empennage designs and for
- different design principles.

(Fig. 1 shows some of the different investigated structural designs.)
For these analyses a computer model has been developed, a so-called

Structural Strength Model

2. STRUCTURAL STRENGTH MODEL

By using the Structural Strength Model it is expected that the reduced load carrying capacity of the damaged aircraft can be obtained. To acquire this information it is necessary to calculate the stress fields of a damaged aircraft structure loaded with the actual loads which are present during the mission. A very effective and powerful method to calculate the stress fields is the Finite Element Method. The most important advantage of this method is the flexibility in modelling structures. This becomes essential for structural changes which are caused by damage due to ammunition.

The damaged structural areas can be considered to be holes with cracks, removed panels, destroyed bars and so on. Apparently, there are different criteria which determine the reduction in load carrying capacity. Most of these criteria are

- fracture mechanic criteria
- ultimate strength or strain
- stiffness criteria
- stability criteria and so on.

(See Ref. 1 and 2)

The model used to predict the residual loads of damaged structures, taking into account the above criteria, is our so-called "Structural-Strength-Model" (see Fig. 2). Essential inputs for this model are

- data of the wing
- load distribution and the
- destroyed areas of the structure.

As a result of damaged structural areas the aerodynamic loads can also be changed. To take into consideration this additional effect, an Aerodynamic Model is available (see Fig. 2). This model is based on a Panel Method. However, the most important information is the description of the destroyed area of the structure. The prediction of these values has been accomplished by a Damage Model (see Fig. 2).

3. DAMAGE MODEL

The overall damage of a structure caused by projectile hits is based on different damage mechanisms. For high explosive ammunition these damage mechanisms are the

- penetration and perforation effect of the total ammunition (impact of the ammunition)
- shock wave effect caused by the detonation of the shell
- internal overpressure effect
- penetration and perforation effect of the fragments of the ammunition
- hydraulic ram effect and so on.

The flow chart of these models is shown in Fig. 3.

On the other hand, some results from real field tests with different types of wings and empennages are available. These test results are necessary to check and/or scale the model results and to obtain the degree of confidence in the model predictions. For the impact of the ammunition the destroyed areas can be described by a function in which the ignition delay, the material properties and the kinds of ammunition are included. The other effects are described by more complicated models.

3.1 Shock wave model

Fig. 4 shows the most critical areas for the influence of the internal overpressure and the shock wave of the ammunition as a result of different field tests with certain kinds of ammunition. This figure indicates that most of the sensitive areas can be described by time-dependent pressure-loaded thin flat plates.

A thin plate can be so highly loaded that the deflection is much larger than the thickness of the plate without failure. Therefore, a second effect, which can be described as a "cable-effect", occurs and leads to tension in the entire plate. In addition, it

must be taken into account that the material can be deformed into the elasto-plastic region. Hence, to describe the behavior of a loaded thin plate, the following physical effects have to be considered

- time dependent load function
- nonlinear stiffness of the structure
- nonlinear material behavior
- different failure modes.

Our investigation of this problem resulted in the decision to develop a model which is sensitive enough to take into consideration all of the above mentioned parameters. This model would be a one-dimensional, mass-spring system where the spring stiffness is a function of the deflection.

3.1.1 Static deflection behavior of a thin plate

The static deflection behavior of a thin plate has been described by a superposition of the bending mode and of the effect of extending the plate as a function of central deflection. The deflection as a function of loading has been considered for both

- elastic material behavior and
- perfectly plastic material behavior.

A more detailed description is shown in Tab. 1. It also shows the model used to describe the entire deflection behavior. The springs are nonlinear and the jump in the stiffness of the springs indicates the change of the material behavior.

To check the results of the described model, a Finite Element Program, which takes into consideration all of the mentioned nonlinear terms, was used. The applied program system was MARC. Figs. 5 and 6 show the comparison between the results of the Finite Element Program and the introduced theory for a clamped square plate which is statically loaded. Fig. 5 shows the central deflection as a function of the pressure for low pressures, and Fig. 6 shows the function up to very high pressures. The comparison shows that the theory used approaches the Finite Element results quite well for both material regions. Therefore this model is able to predict the central deflection of a pressure loaded thin plate.

3.1.2 Dynamic deflection behavior of a thin plate

The description of the dynamic deflection behavior of a thin plate has been performed by using the same mass-spring system with the developed nonlinear springs. A reduced value, which represents the effective mass has been used. With this modification this system gives nearly the exact first eigen frequency (see Ref. 3 and 4). The differential equation for this problem is nonlinear (see Tab. 2). The solution technique used is an integration of the piecewise linear differential equation with respect to the actual total plate stiffness. The different material behavior for loading and unloading has also been considered and the pressure has been described by a piecewise linear function of time (see Tab. 2).

A very important question was the precision of the prediction of the deflections and stresses with this model.

First, for test examples the dynamic behavior was calculated with both

- the model and with
- the Finite Element Method.

The Finite Element Program used was again MARC.

Fig. 7 shows the comparison of the results from both. The essential result is the maximum deflection, and these values differ by less than 3 %. Only the starting phase is different, but the maximum value is reached at nearly the same time.

Second, for some available test results from the U.S. (see Ref. 5), the deflection and failure modes were calculated. Fig. 8 shows the comparison of the calculated and measured results. For all of these examples the maximum deflection or failure modes are in good agreement (differences less than 10 %). Therefore, it is possible to predict the dynamic deflection behavior of thin plates with the described model and obviously with the Finite Element Method. However, for a large number of parametric investigations, the model is more economical.

3.1.3 Pressure as a function of time

The detonation of a high explosive ammunition inside a given volume results in an increase of pressure within the volume. There are two effects - the internal overpressure and the pressure from the shock wave.

Fig. 9 shows the overpressure from an ammunition as a function of time for two different venting areas. The overpressure is also a function of the size of the volume. However, the shock wave is governed by the distance from the detonation point to the investigated point. In Fig. 10 the reflected pressure as a function of time is shown for different radii. A result of this investigation is that the maximum pressure decreases and the action time increases with increased distance from the detonation point. The pressure values shown are obtained from a U.S. model which is available for these investigations (see Ref. 6). The internal overpressure charges the entire surface of the panels with the same magnitude of pressure. In the case of the shock wave the total load on the surface area must be determined by integrating over the entire panel surface. The pressure from the shock wave is constant on a circle of given radius (see Fig. 11). Fig. 12 shows the maximum shock wave pressure as a function of the radius r and the affecting pressure at a specified time after detonation. $R(t)$ represents the distance the shock wave has travelled as a function of time after detonation. A corresponding integration procedure is accomplished within the model.

3.1.4 Influence of internal overpressure and shock wave

In order to determine the correct response of a pressure-loaded panel it is necessary to consider the simultaneous influence of both

- internal overpressure and
- shock wave.

Fig. 13 graphically illustrates the interaction of the internal overpressure and the shock wave. In the example shown the deflection is greater than the allowable strain limit. The strain limit is not reached in the cases of the individual responses.

3.2 Hydraulic ram model

The Shock Wave Model is able to describe the deflection and also the stresses and strains in a dynamically loaded flat plate structure which is used for some tanks. However, when a hit occurs in the tank system a very complicated pressure-time-history has to be calculated. An additional problem is to find out the material properties as a function of strain rate for different types of e.g. rubber material. Hence, if this information is available, the Shock Wave Model can also be used to predict the hydraulic ram effect for the surrounding panels.

3.3 Fragment penetration model

Our first Fragment Penetration Model consisted of a box with all of the real cross sections of a portion of the wing. However, the format of this box was rigid (see Ref. 2). To improve the flexibility of this model, an advanced model has been developed. For the stress and strain calculation the Finite Element Method has been applied. Therefore, a definition of the structure with a similar description for both

- the Finite Element Method and
- the Fragment Penetration Model

has been found to be very useful. A further advantage is the applicability of this model to different kinds of structure. With this model it is possible to idealize structural parts in as much detail as necessary.

Fig. 14 shows an example of a portion of a modelled wing with honeycomb panels. The model predicts the fragment penetration points on the panels. In addition the model calculates the depth of fragment penetration, and this represents a distinct advantage of the new model. This analysis capability is essential in investigating relatively thick panels (for example, for the definition of three dimensional cracks in these thick panels).

In Fig. 15 a thick panel of a wing is shown. The letters indicate fragments which are not able to perforate the panel and the numbers indicate points where the panel is penetrated. (More than 60 % did not go through the panel.)

Figs. 16 - 19 demonstrate a comparison between model predicted results and field test data.

Fig. 16 shows the spars and ribs of the structure and Fig. 17 gives further information about the used honeycomb panels. The predicted results are shown in Fig. 18 and in Fig. 19 the real test result is illustrated. As a result of the comparison it can be seen that the model predictions are in good agreement with the test data.

4. HIT SENSITIVITY OF A HONEYCOMB STRUCTURE

For a military aircraft it is very important to choose a design which has a low structural response to impact damage. An analysis has been performed to investigate the behavior of a honeycomb structure which has incurred projectile hits. The honeycomb panels have a higher bending stiffness than that of a stiffened panel. In addition, the structure of the honeycomb panel consists of two plates and consequently different effects can be expected.

4.1 Pressure effect

Panel thickness is one of the essential values in determining the tension of a honeycomb structure and a stiffened panel.

To investigate the influence of different bending stiffnesses and equal entire thicknesses the Shock Wave Model has been applied. The results of this investigation are shown in Fig. 20.

This comparison shows that there is no significant difference between the designs. Hence, the increased stiffness does not give an advantage. (This result is in agreement with our shooting test data.)

4.2 Fragment effect

To determine fragment effect for the honeycomb structure and the stiffened panel designs the Fragment Penetrating Model has been applied. Fig. 21 shows a result for a stiffened panel design. A large region is destroyed by the fragments. In addition to that Fig. 22a shows the inside panel of a honeycomb structure. A comparison of Fig. 21 with Fig. 22a shows that the perforation of the panel for the inside honeycomb plate is slightly larger. However, the result for the outside plate is different. There are only a few fragments which have penetrated this plate. The prediction is, that the outside plate of the honeycomb structure is not destroyed by the fragments.

4.3 Combined effect

In the case of the example shown the pressure effect is dominant. Therefore, there is no significant difference between the honeycomb and the stiffened panel design if the number of ribs and spars and the thickness are the same. However, if the increased stiffness of the honeycomb panels used to reduce the thickness and/or the dimensions of the other structural parts an increased vulnerability would be expected. For a smaller ammunition or an ammunition with a smaller pressure effect, the honeycomb design provides some advantages.

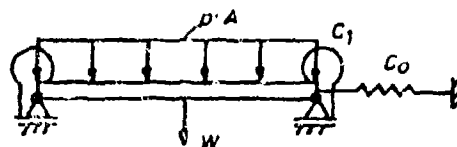
REFERENCES

1. Nassmann, J. (IABG): Investigation About Residual Strength of Damaged Structures. ICAF Conference 1973, LBF-Report S-108 ff.
2. Nassmann, J. (IABG): Structural Response to Impact Damage. AGARD-Report No. 633
3. Nassmann, J. (IABG): Schrittweise Entwicklung einer Berechnungs-, Prüf- und Konstruktionsvorschrift für luftstoßbelastete Schutzraumtore, dritter Schritt. IABG-Bericht Nr. B-TF-411, Ottobrunn - 30. 8. 73
4. Nassmann, J. (IABG): Gasschlagmodell zur Berechnung der Munitionswirkung in Flugzeughohlräumen. IABG-Bericht Nr. B-TF-484, Ottobrunn - 22. 12. 74
5. Proctor, J.F.: NOL-Internal Blast Damage Mechanism Computer Program. Naval Ordnance Laboratory, White Oak Silver Spring, Maryland, 31 August 1972

6. Ross, C.A. and W.S. Strickland: Response of Flat Plates to Fuel Air Explosive. Technical Briefings, Volume II, USA Ballistic Research Laboratories, Aberdeen Proving Ground, Maryland, 24 - 26 April 1974

TABLE 1

Static Deflection Behavior

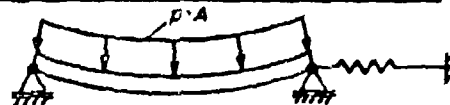
1. Plate

for elastic material behavior

$$p \cdot A \sim K_1 \cdot W$$

for perfectly plastic material behavior

$$p \cdot A = \text{const}$$

2. Thin plate with large deflection (without bending stiffness)

for elastic material behavior

$$p \cdot A \sim K_2 \cdot W^2 + K_3 \cdot W^3 + \dots$$

with

$$K_2 > K_3 \text{ also}$$

for perfectly plastic material behavior

$$p \cdot A = K \cdot W$$

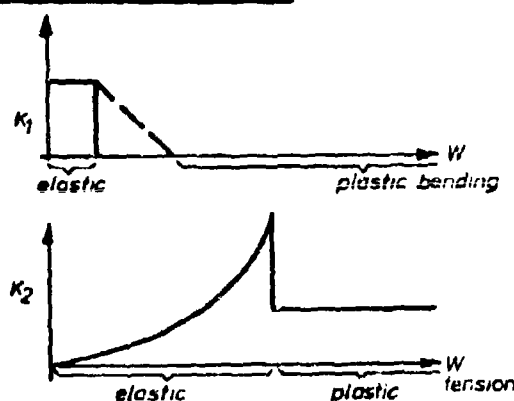
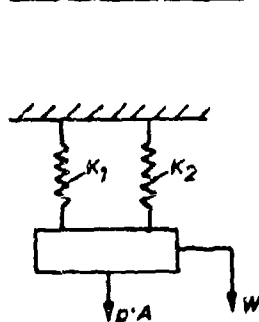
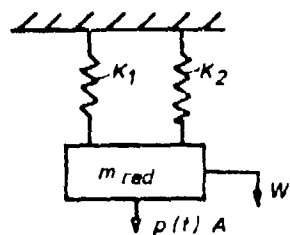
3. Model to describe the entire static deflection

TABLE 2
Dynamic Deflection Behavior

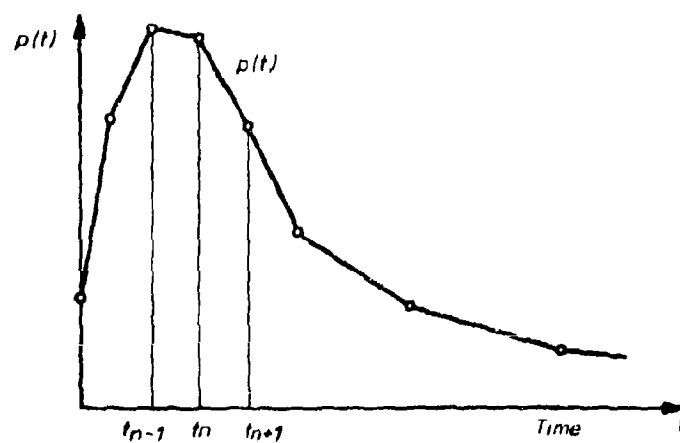
Model:



Differential equation:

$$m_{red} \cdot \ddot{W} + C(W) \cdot W = p(t) \cdot A$$

Pressure as a function of time:



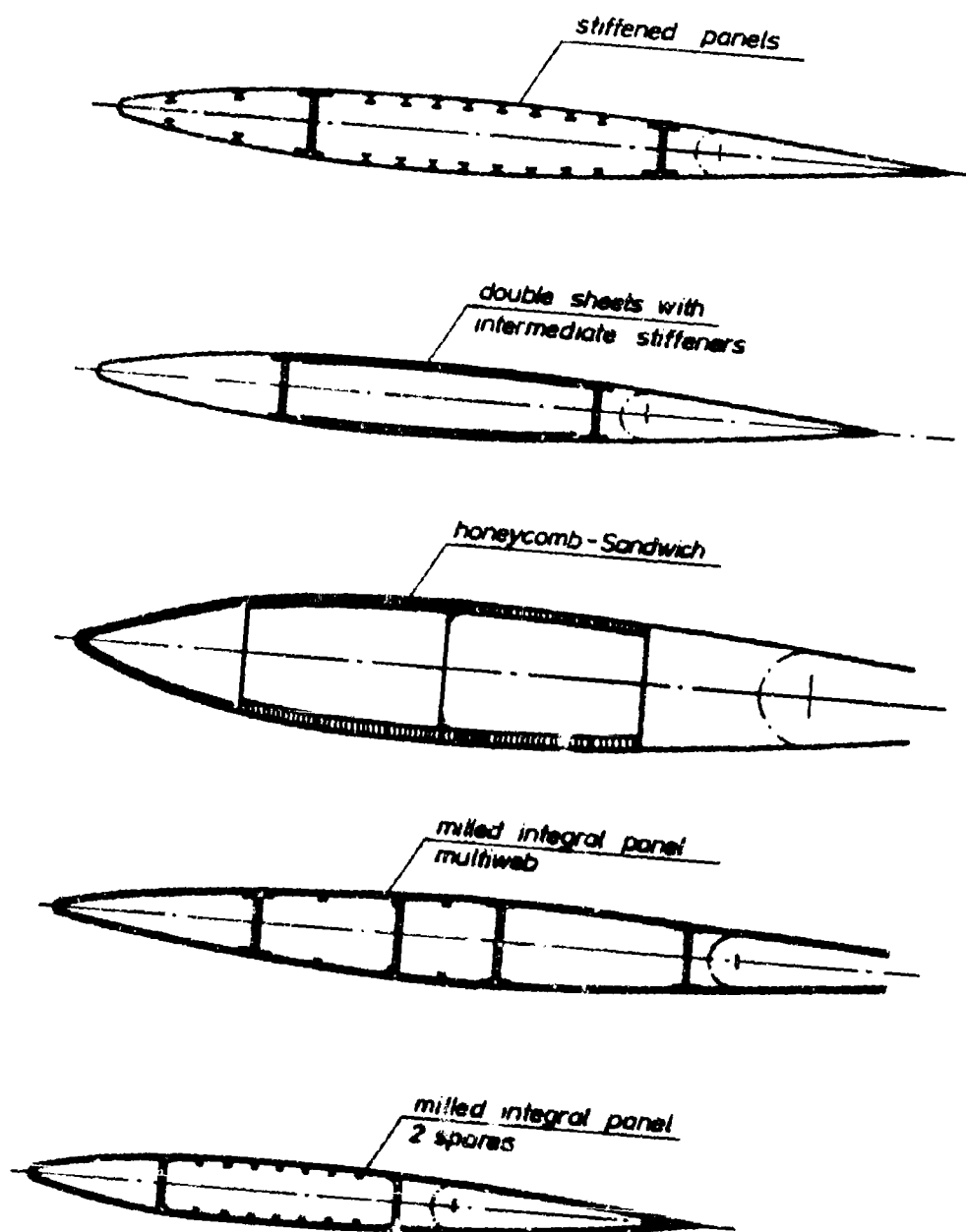


Fig.1 Comparison of various wing designs

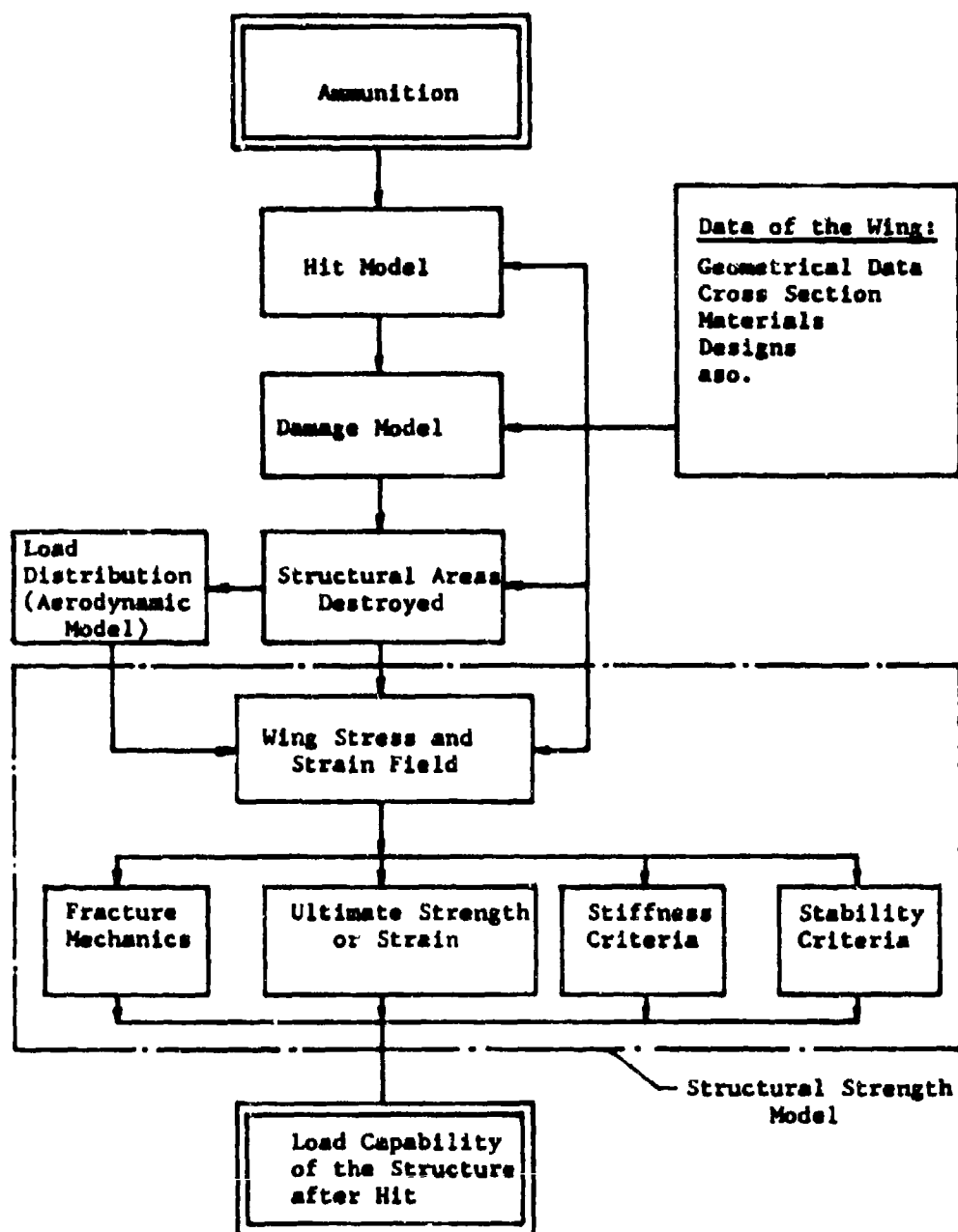


Fig.2 Structural strength model flow

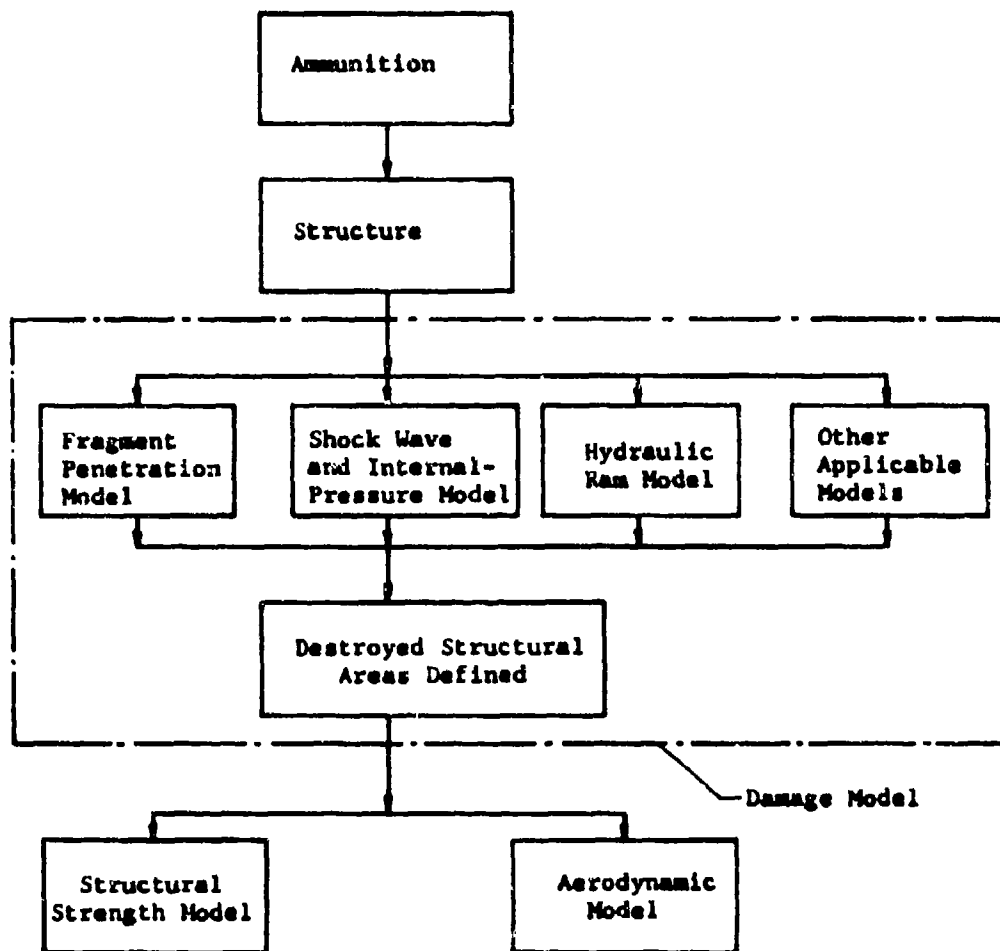


Fig.3 Damage model flow

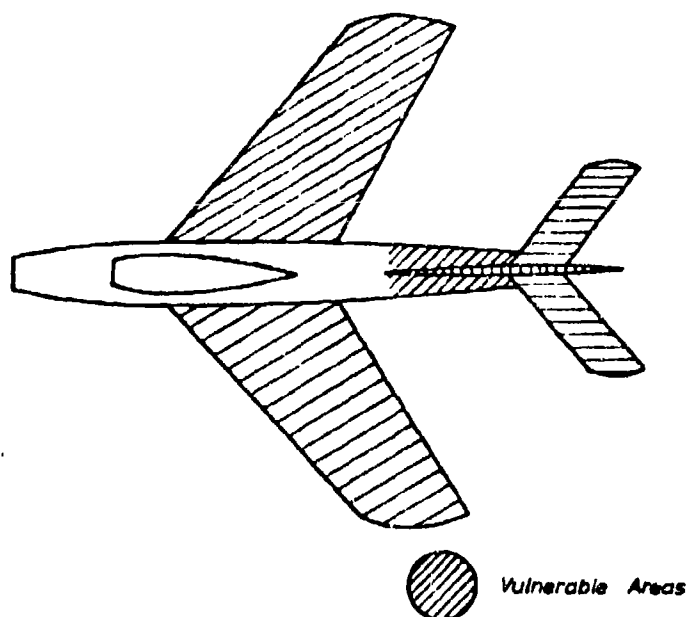


Fig.4 Structural areas vulnerable to shock wave

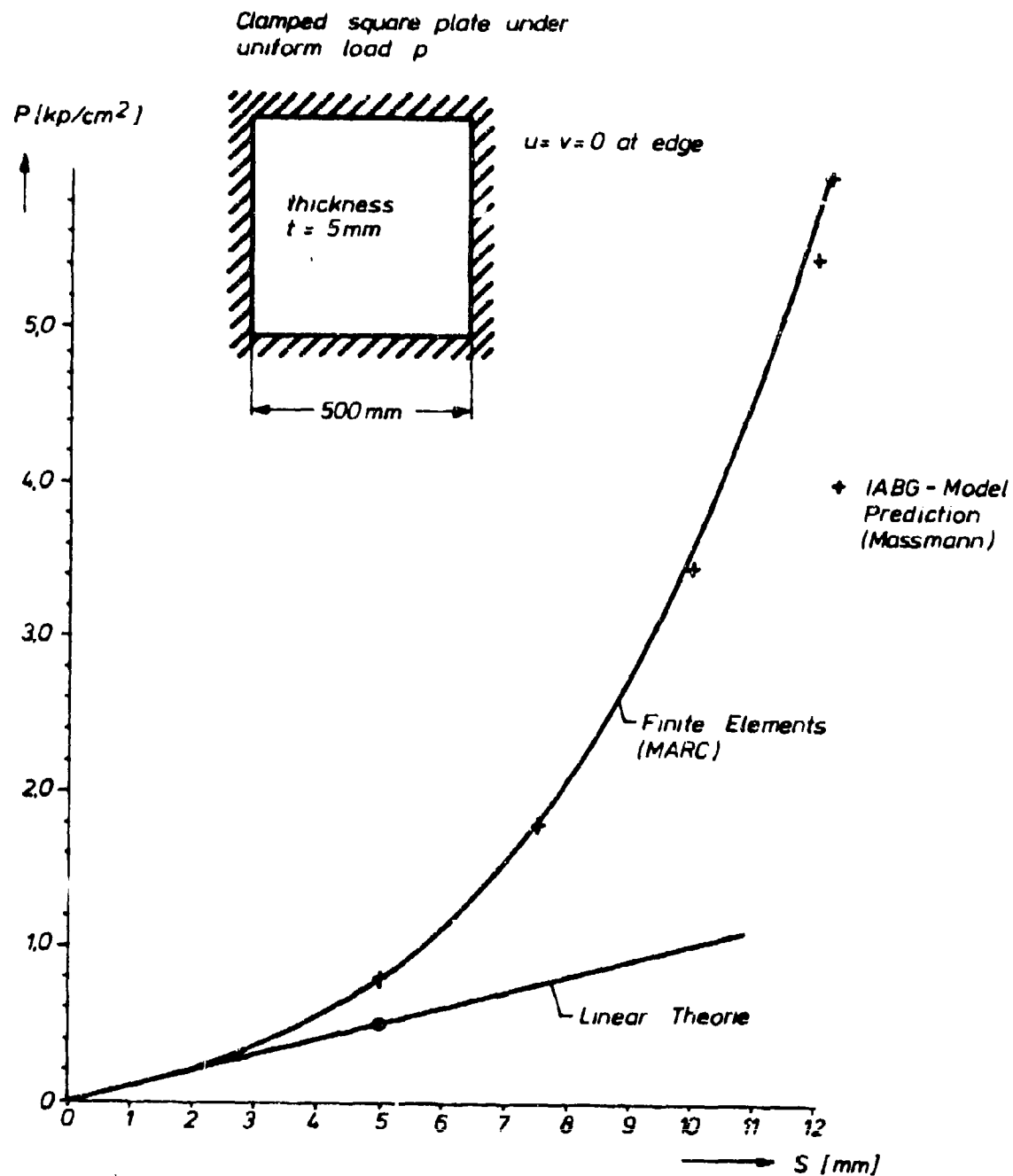


Fig.5 Comparison of finite element solution and model prediction for elastic deformation

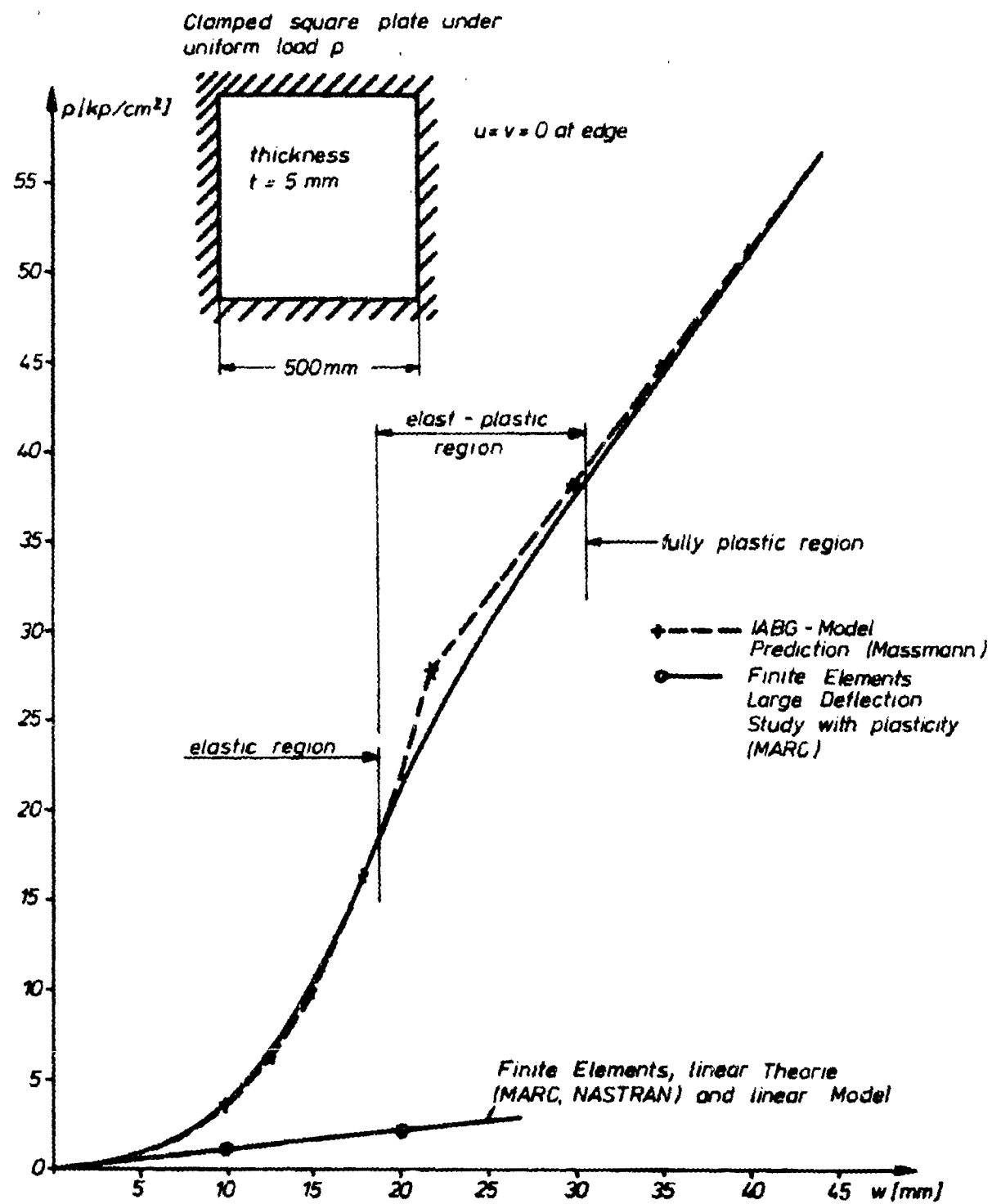


Fig.6 Comparison of finite element solution and model prediction for elastic and plastic deformation

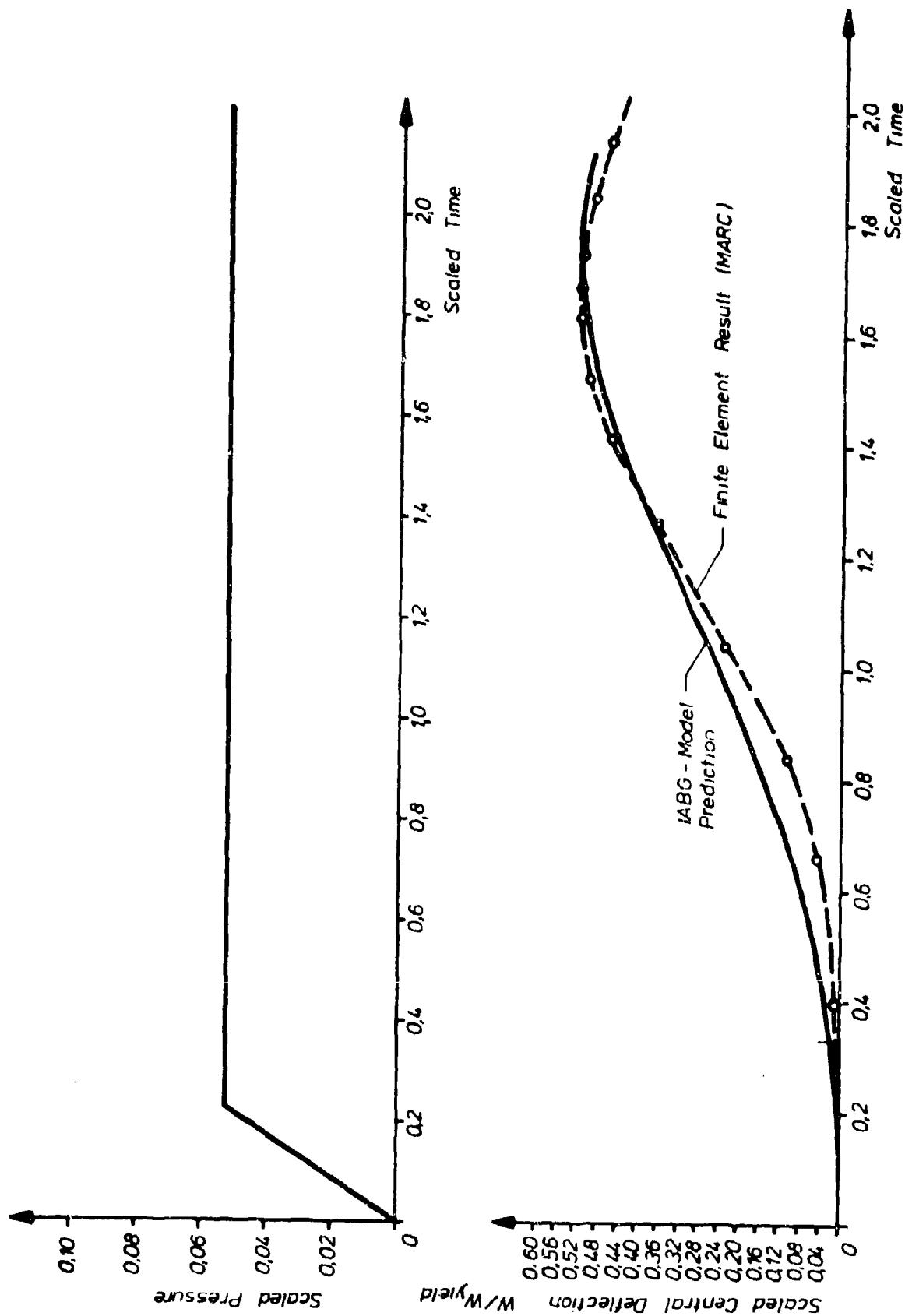


Fig.7 Comparison of results from model and finite elements

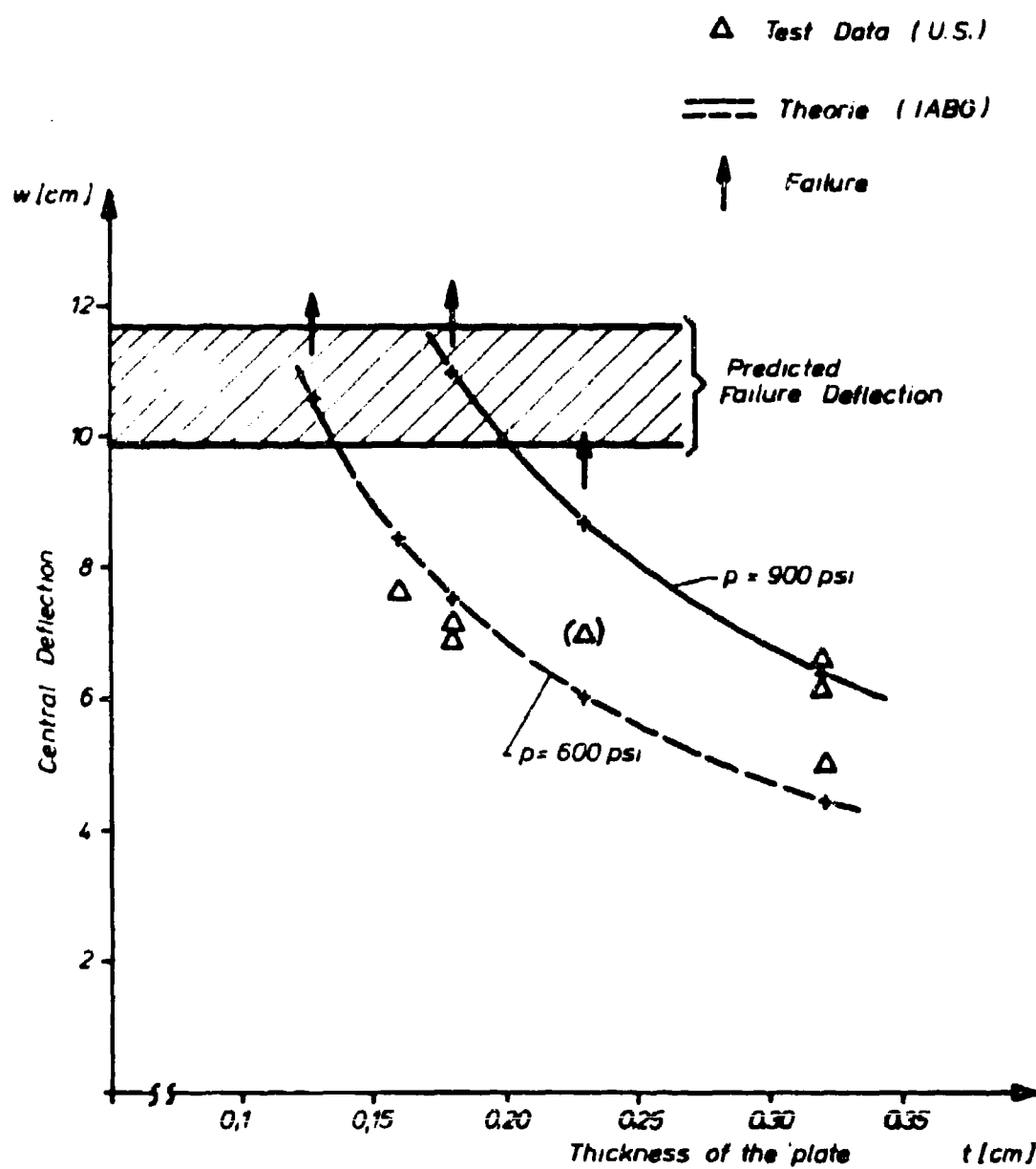


Fig.8 Comparison of the shock wave model results with US test data

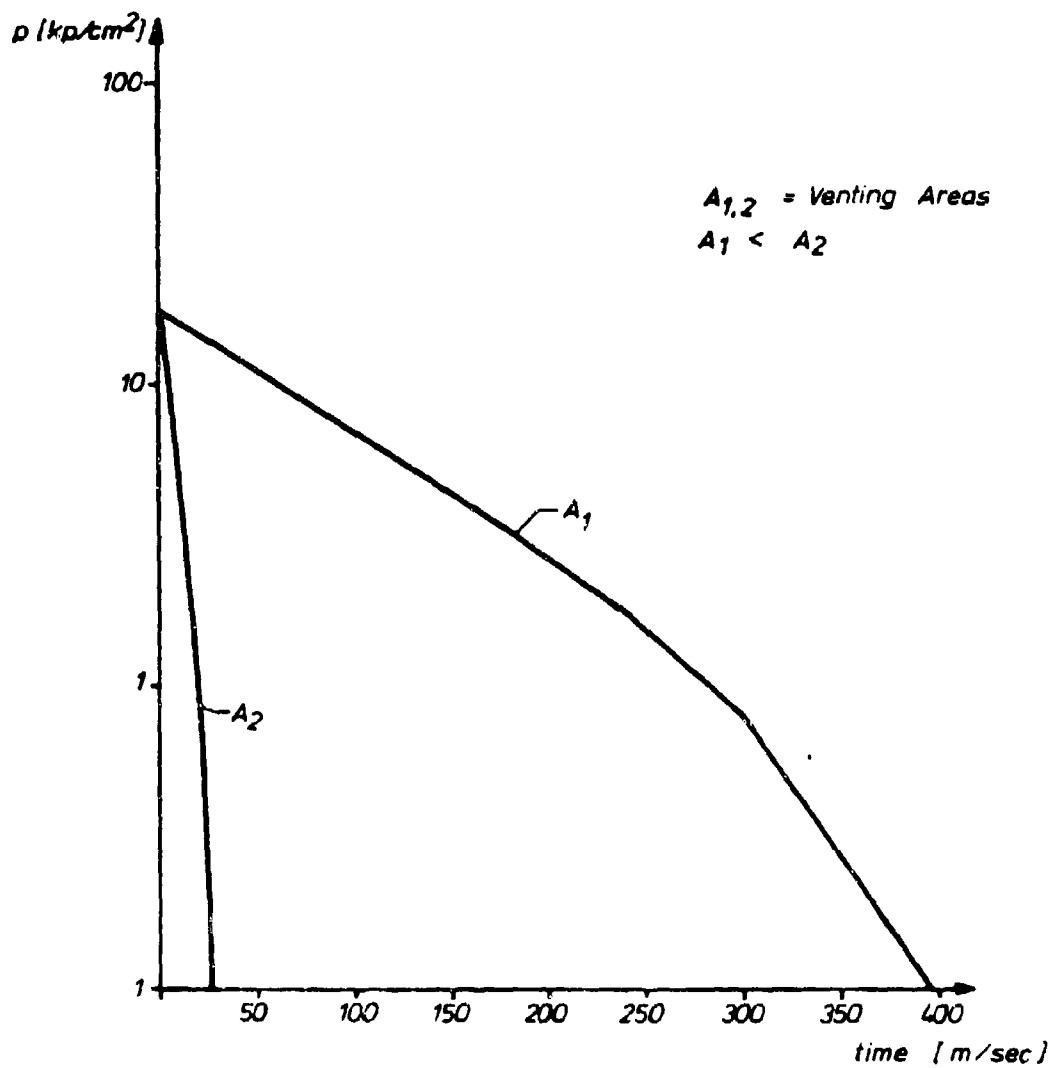


Fig.9 Internal overpressure for two different venting areas

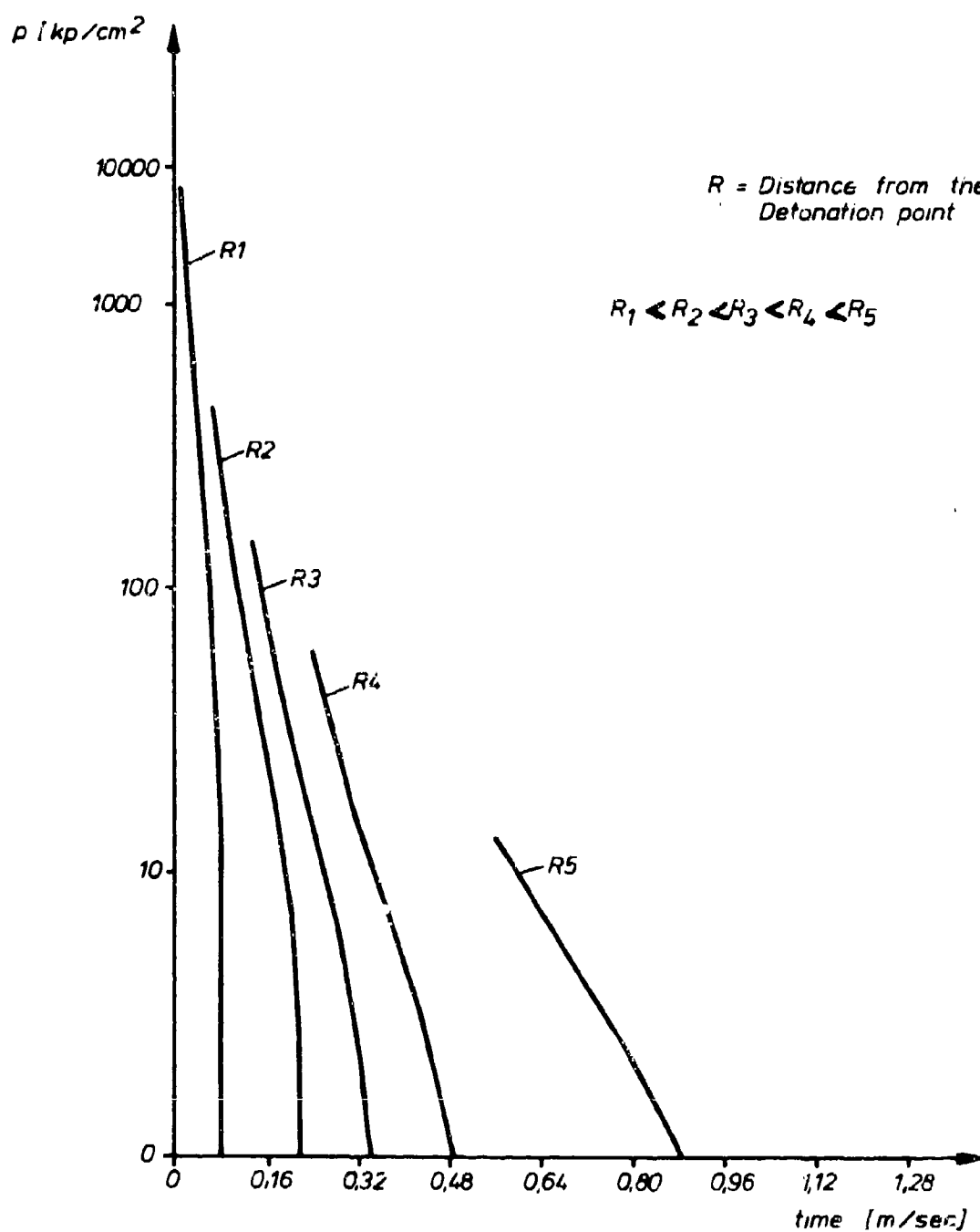


Fig.10 Shock wave pressure as a function of time at various distances from detonation point

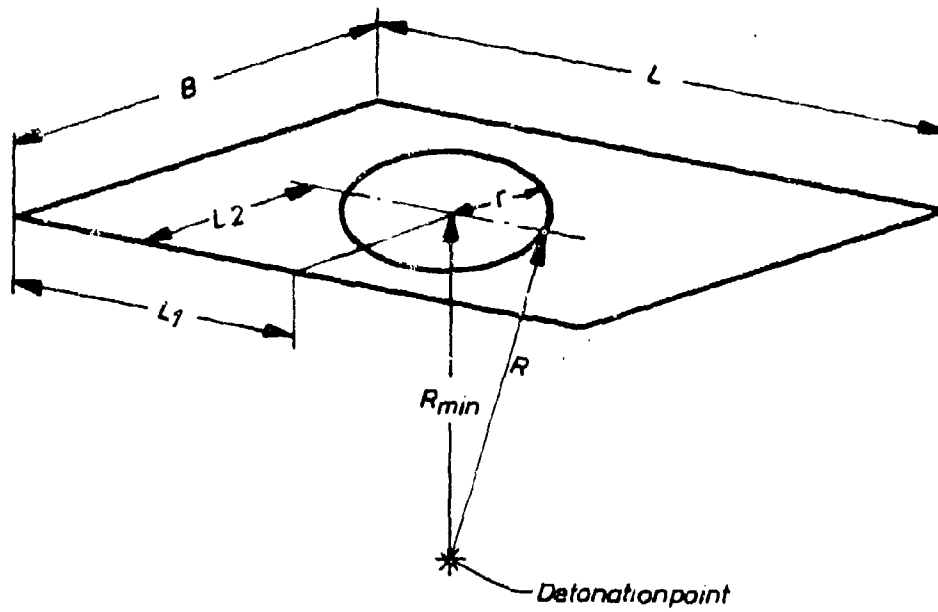


Fig.11 Location of the detonation point with respect to the affected panel

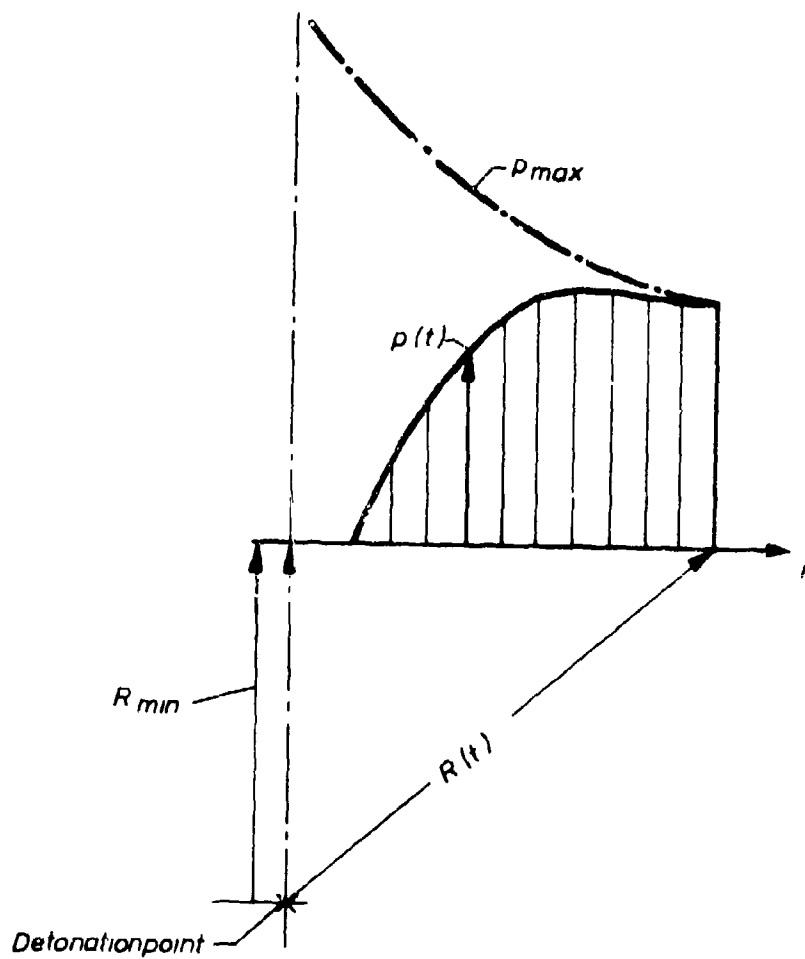


Fig.12 Maximum shock wave pressure and pressure/time distribution

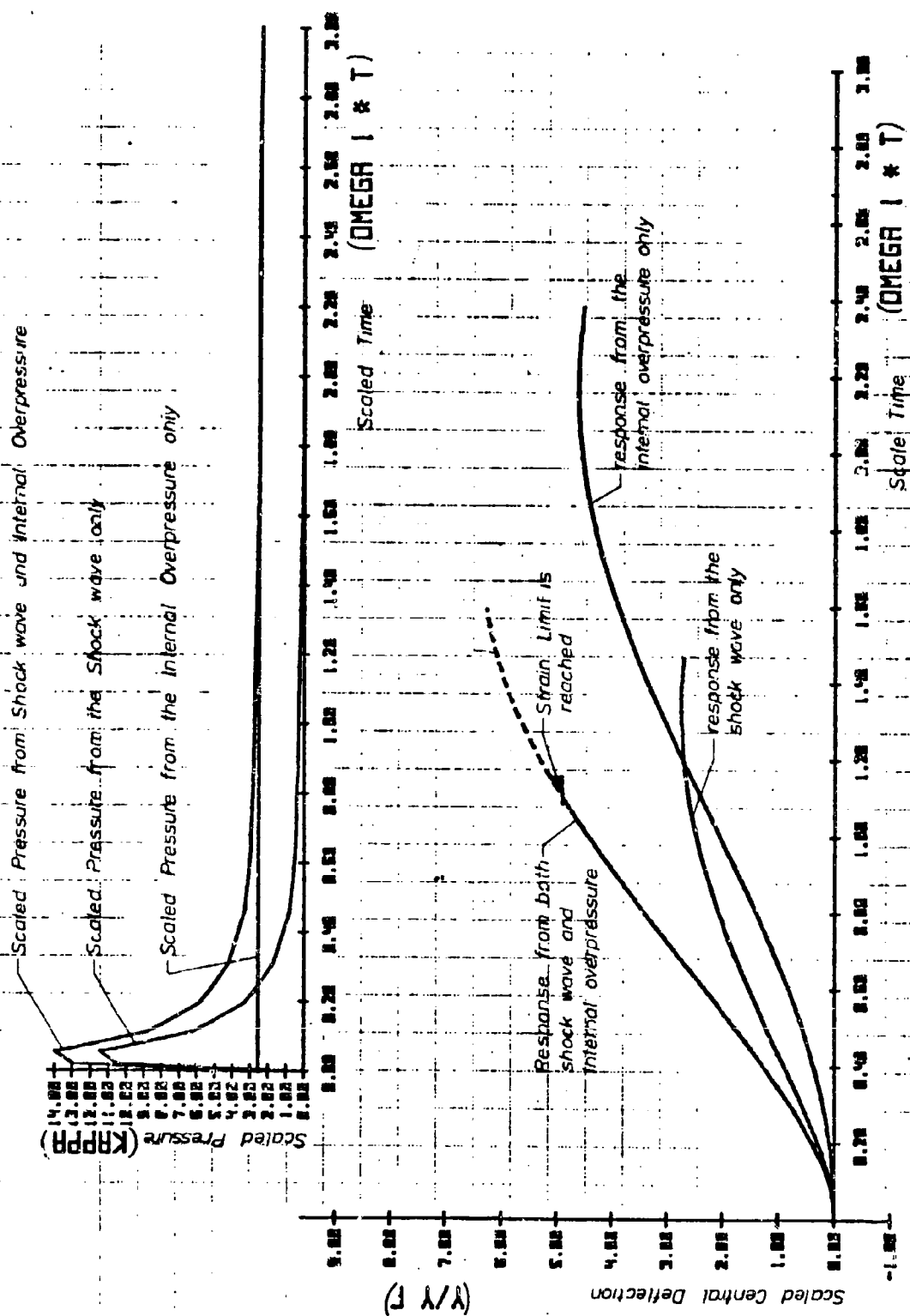


Fig.13 Influence of internal overpressure and shock wave

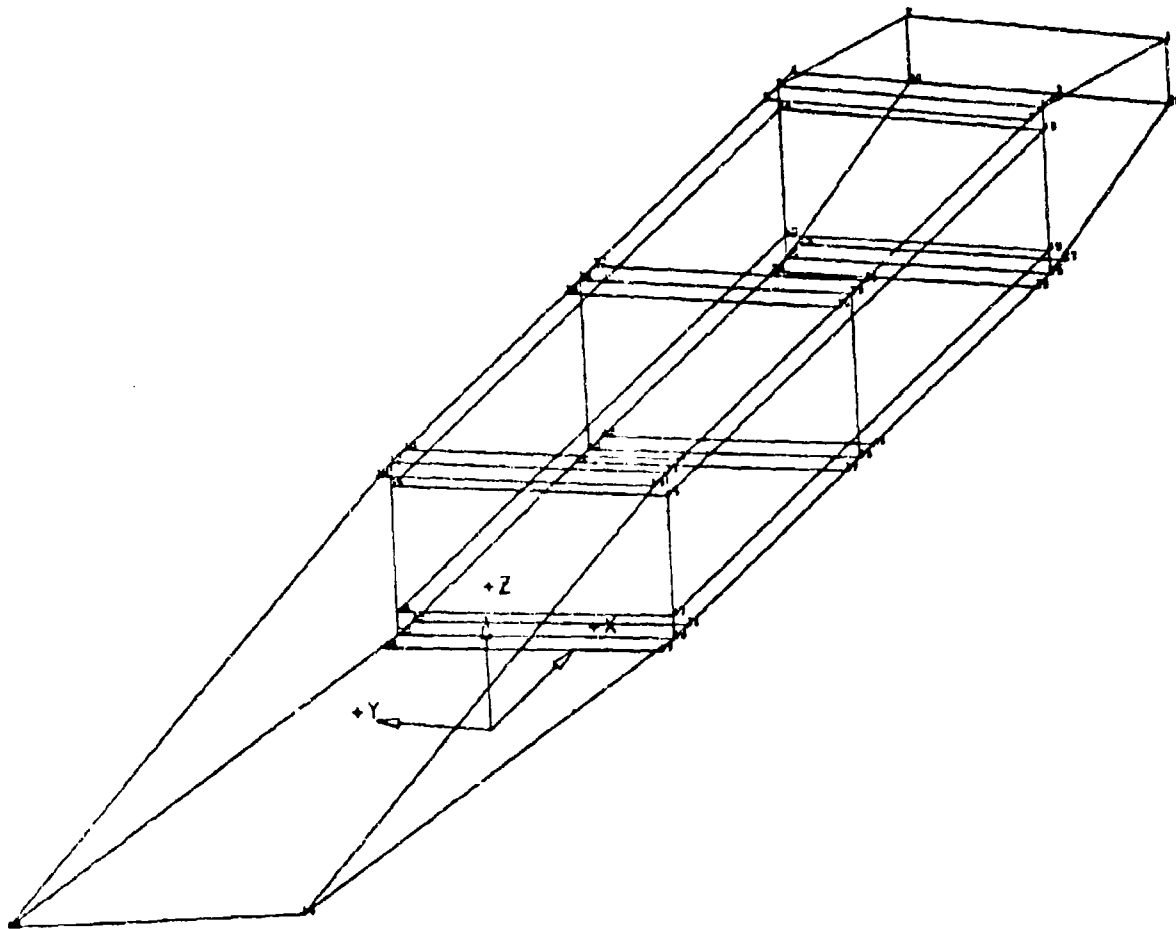


Fig.14 Modelled portion of wing with honeycomb panels

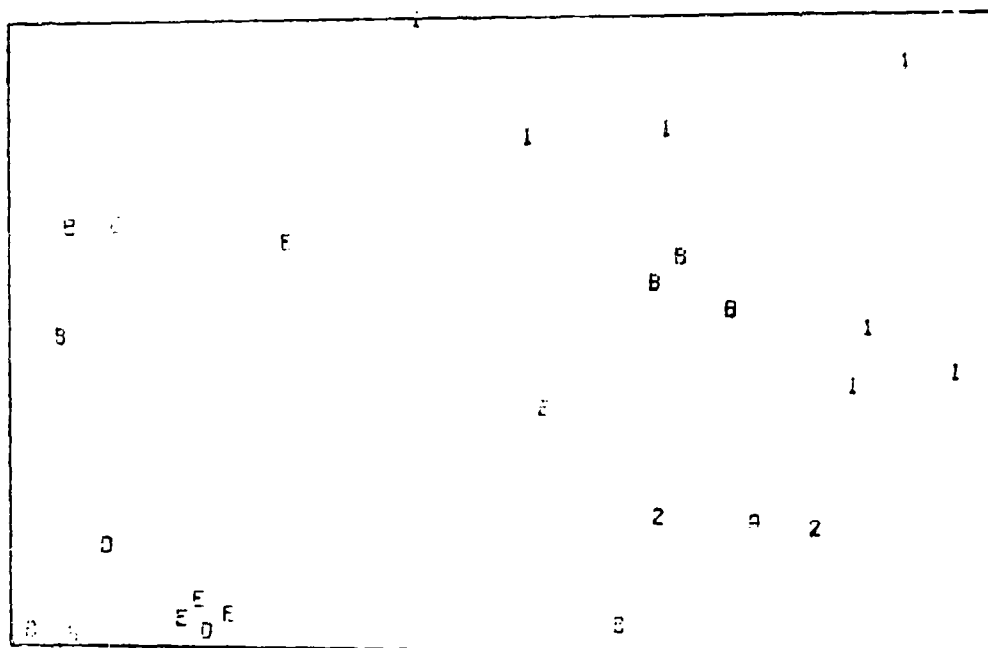


Fig.15 Predicted penetration of a thick panel

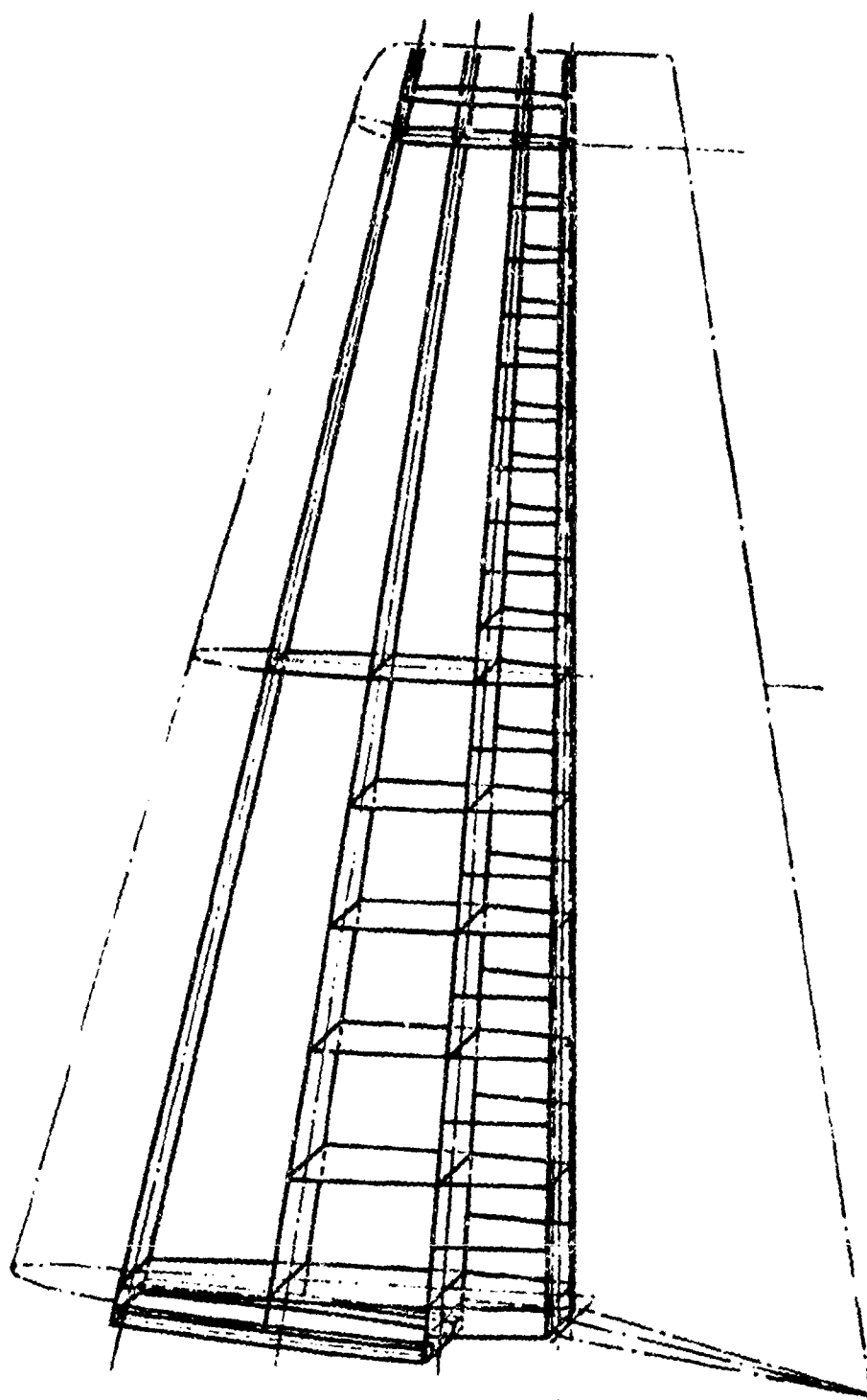


Fig.16 Inner structure

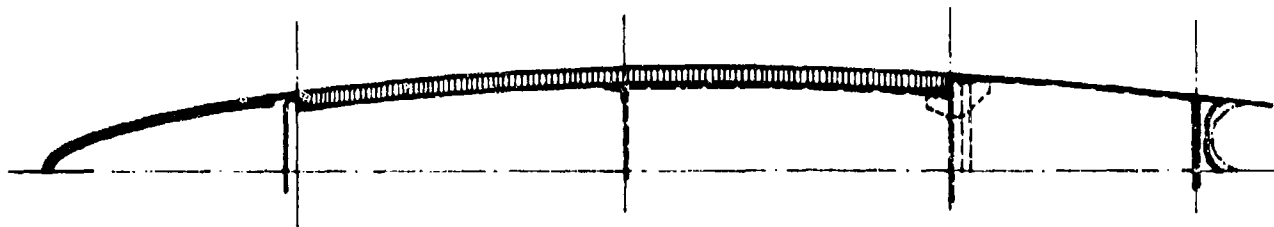


Fig. 17 Cross section of structure with honeycomb panels

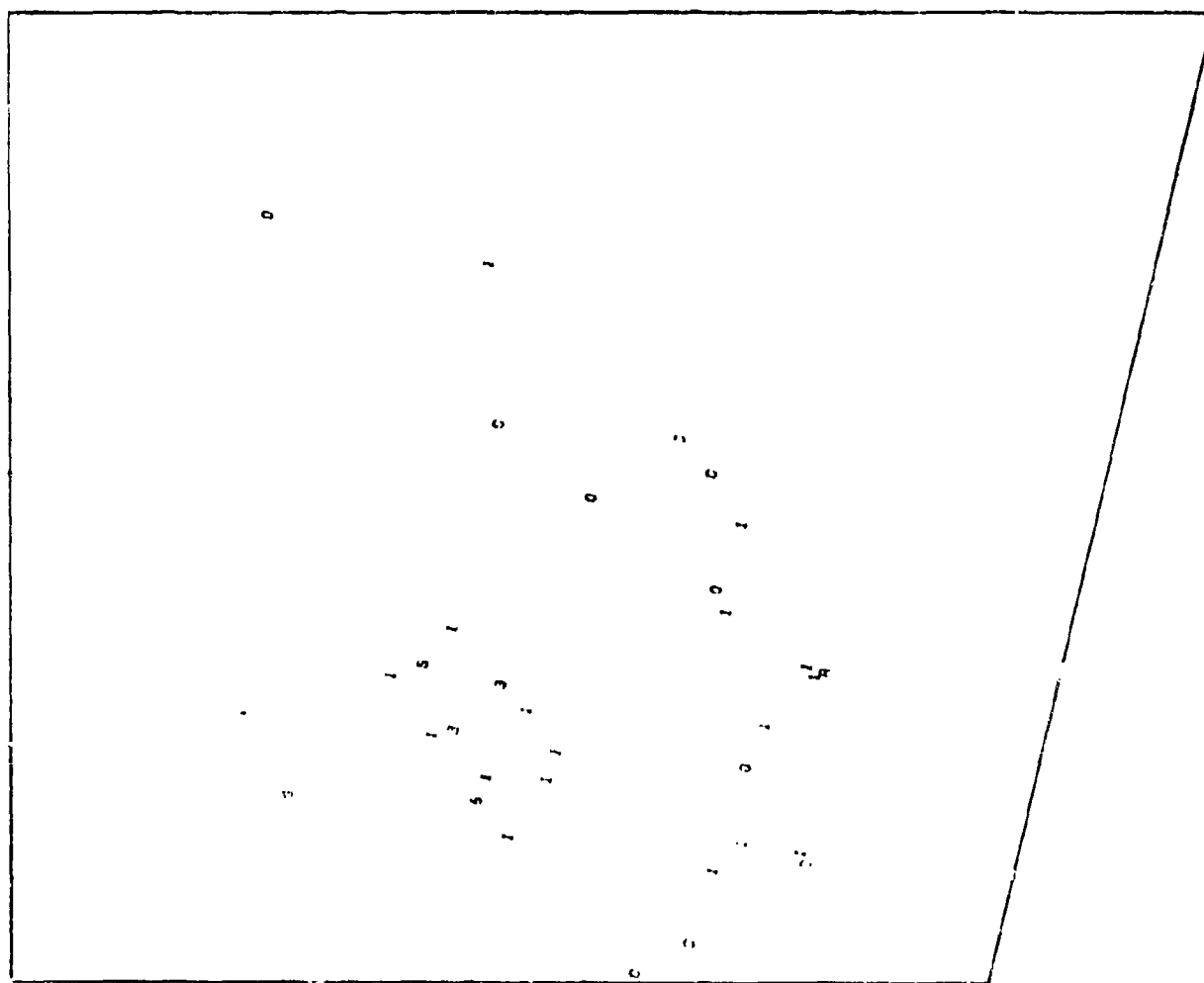


Fig. 18 Predicted penetration of a honeycomb plate for shooting test Nr. H1/4 (see Figure 19)



Fig.19 Shooting test results

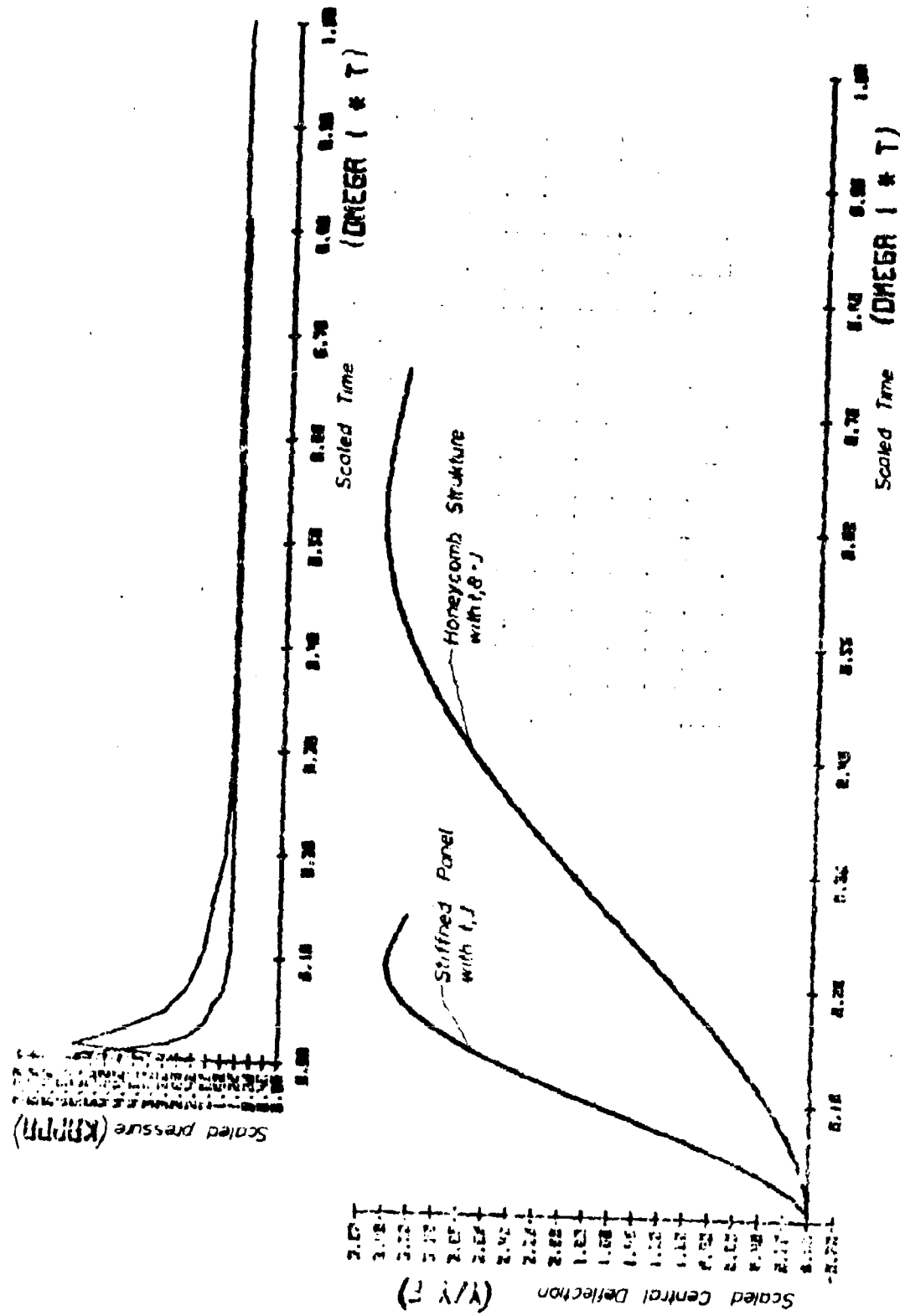


Fig. 20 Comparison of plates with different bending stiffnesses

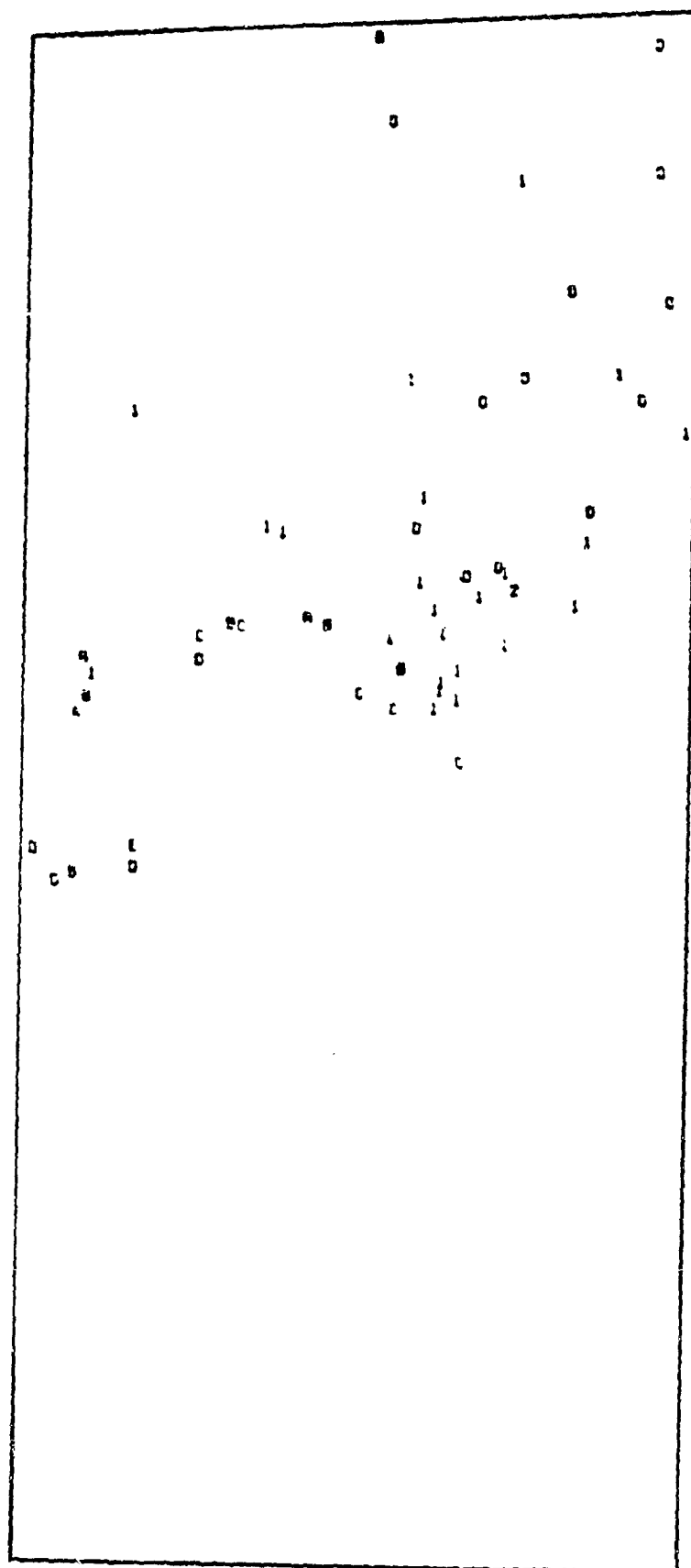


Fig.21 Predicted penetration of a stiffened panel

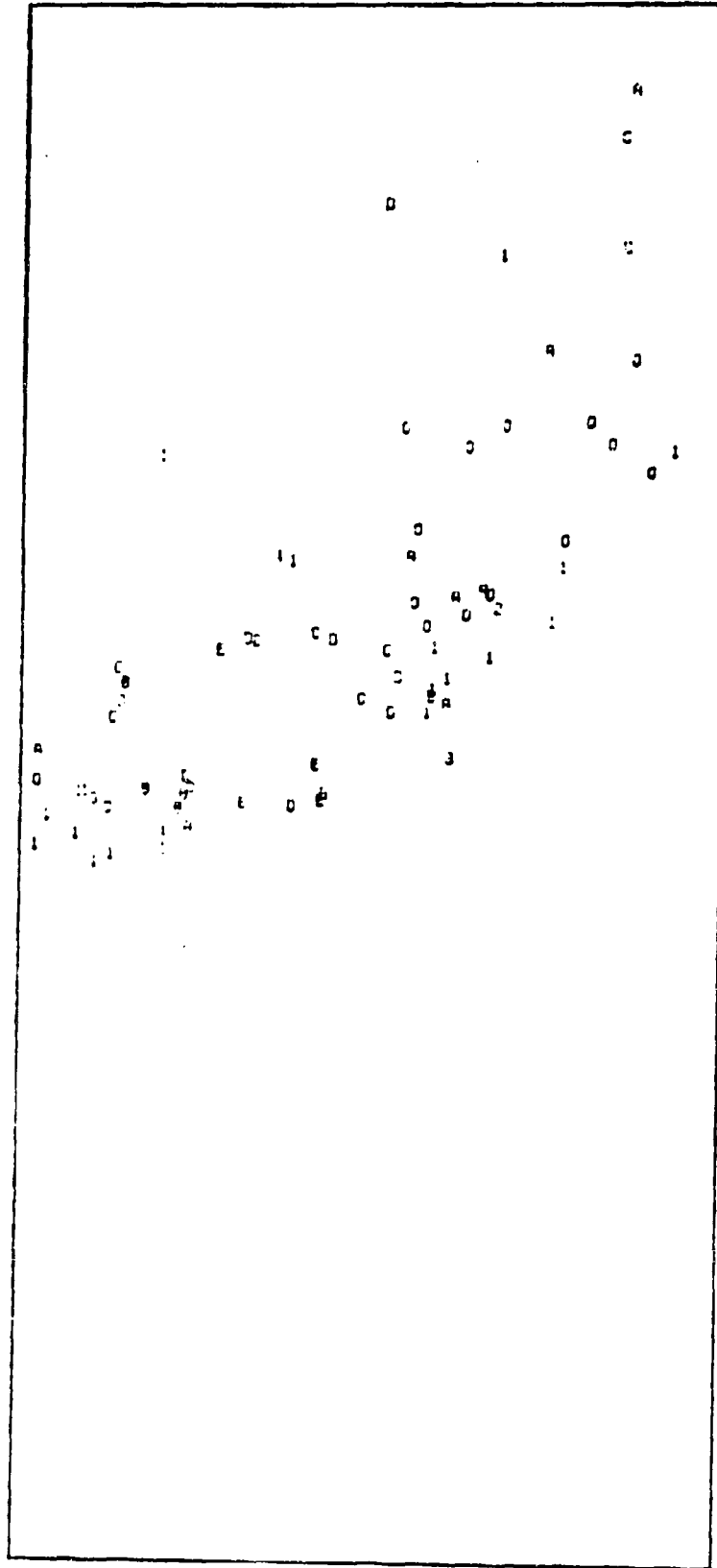


Fig.22(a) Predicted penetration of an inner honeycomb plate

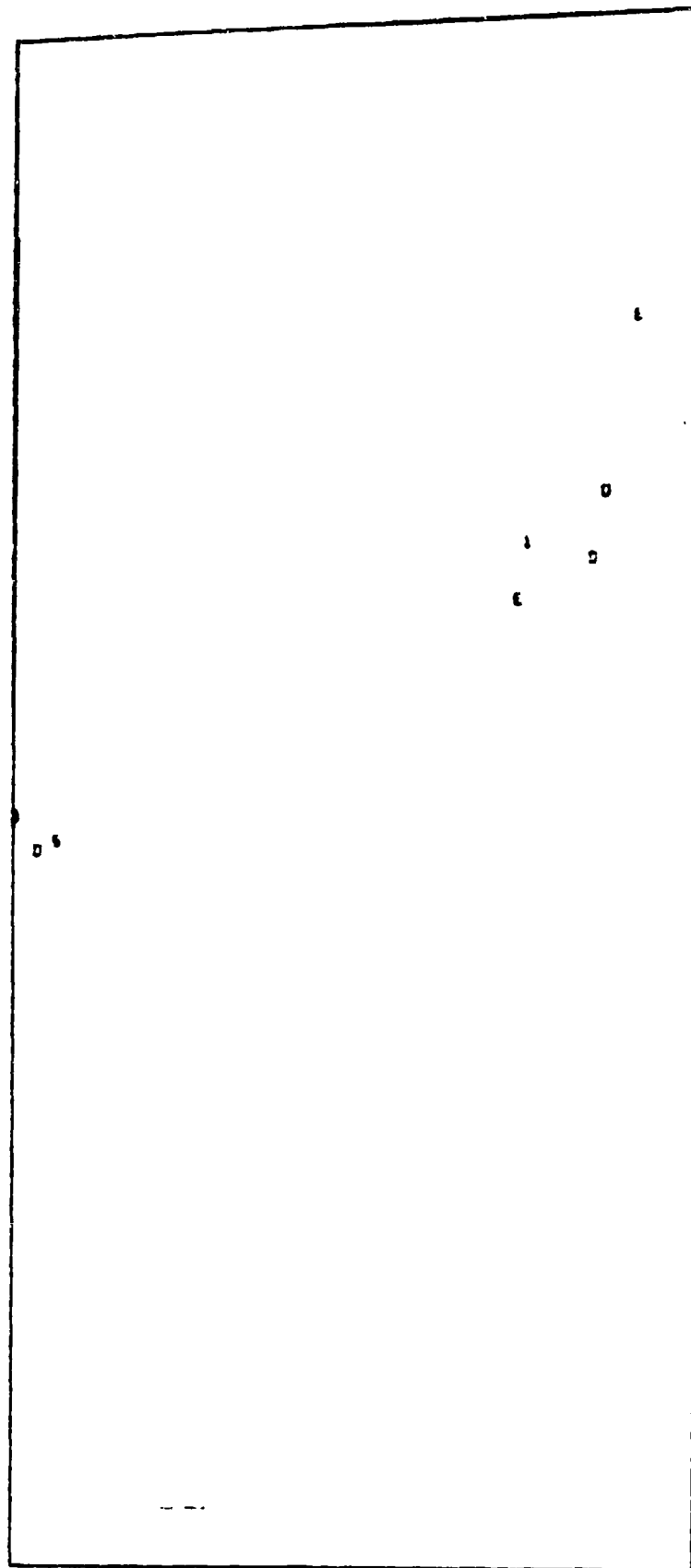


Fig.22(b) Predicted penetration of an outer honeycomb plate

FLUID DYNAMIC ANALYSIS OF HYDRAULIC RAM

by

Dr. Eric A. Lundstrom, Physicist
andWallace K. Fung, Aerospace Engineer
Naval Weapons Center
China Lake, CA 93555

SUMMARY

The hydraulic ram pressure loading associated with the ballistic impact of a projectile into an aircraft fuel cell can cause catastrophic failure of the cell and result in several modes of aircraft kill, such as fuel starvation, explosion, and fire. In addition, hydraulic ram pressure pulses in the fuel can damage critical components within the cell and components lying outside of and adjacent to the cell walls.

This paper summarizes ongoing work aimed at providing a theoretical basis for predicting hydraulic ram phenomena. A model has been developed for predicting fluid pressure fields generated by tumbling military ammunition. Derivation of the model is described, and comparison with experimental data is shown. Agreement of the model was quite good with shots fired into a test cell with 0-degree obliquity. Significant deviation of the model from experiment was obtained with 30- and 45-degree obliquity shots.

LIST OF SYMBOLS

- a = Cavity radius
- A = maximum cavity radius
- A_0 = value of A at point X_0 on the trajectory
- A_0 = projected frontal area of the bullet
- $B = \sqrt{p_0 - p_c} / \rho N$
- c = sound speed in the fluid
- C_D = drag coefficient
- E = projectile kinetic energy
- E_j = jacket kinetic energy at point X_j
- m = projectile mass
- N = $\ln W/A$
- p = fluid pressure
- p_c = gas pressure within the cavity
- p_0 = ambient pressure
- r = distance from point (x, y) to a point on the trajectory
- R_0 = distance from a point to the projectile
- R_0 = distance from a point to the projectile impact point
- t = time
- t_0 = time of projectile arrival at a distance X_0
- u = magnitude of the vector \vec{u}
- u = fluid velocity
- u_x = component of u in the x direction
- u_y = component of u in the y direction
- V = projectile velocity
- V_0 = initial projectile velocity
- x = position coordinate
- X_0 = distance along the bullet trajectory
- X_j = distance where jacket strips
- X_1, X_2, \dots = bullet tumbling distances
- α = parameter in Eq. (5)
- β = velocity decay coefficient
- B_1, B_2, B_3 = values of B for tumbling bullets
- B_j = value of B for bullet jacket
- Q = source strength
- ξ = dummy integration variable
- ρ = fluid density
- τ = retarded time given by $t - r/c$
- w = perpendicular distance from the bullet trajectory
- ω = integration limit on w

INTRODUCTION

Hydraulic ram is a phenomenon that may cause catastrophic failure of aircraft cells when they are subjected to ballistic impact. During impact and penetration of the fuel cell, intense pressure waves are generated by the projectile. The response of the fuel cell to this pressure loading varies according to its construction. For example, the walls of an integral fuel cell are formed by the aircraft skin, which is usually constructed of high-strength, often brittle metal designed to withstand normal flight loads. This type of structure can fail catastrophically in response to hydraulic ram pressure loading due to severe fracturing of entrance and exit walls of the cell. Self-sealing fuel cells can also be defeated due to hydraulic ram by gross tearing of the material or by misalignment of the wound edges, thereby defeating the self-sealing process. Both of these effects become increasingly severe as fuel cells become smaller and

projectile kinetic energies increases.

Fuel-cell failure can lead to numerous modes of aircraft kill. One particularly effective mode is fuel starvation resulting from a pump tank being hit or the failure of a cell which contains a large proportion of the total system's fuel. Other possible kill modes are explosion and fire, ignited by an incendiary projectile or by secondary ignition sources within the aircraft. In addition, the hydraulic ram pressure pulse can directly damage critical components, such as pumps and valves within the cell, or it can indirectly damage components that lie outside of and adjacent to the cell walls.

During penetration of the bulk of the fuel, a pressure field is generated that acts to displace the fluid from the projectile path. Applied to the projectile surface, these pressures form the source of the drag force that decelerates it. In this manner the projectile energy is gradually transformed into the kinetic energy of fluid motion.

One of the most striking phenomena associated with ballistic penetration of fluids is the formation of a large cavity behind the projectile. The cavity is filled with a liquid vapor evaporated from the cavity surface and air, which can enter the cavity through the entrance and exit wounds. The pressure of these gases is normally very low. The dynamic behavior of the cavity is loosely analogous to that of a cavity formed by an underwater explosion. The original outward motion of the fluid imposed by the passage of the projectile is opposed by the pressure difference between the ambient pressure of the fluid and the cavity pressure, together with the restraining effect of the fuel-cell walls. The cavity will thus expand to some maximum size, and then begin to contract until, eventually, it will close. For a constant velocity projectile, this process results in a cavity that is roughly ellipsoidal in shape. The maximum size of the cavity is indicative of the initial kinetic energy of the outward motion of the fluid and restraining forces.

In most laboratory experiments, bullets are fired into a fuel cell in a nonyawed attitude. Since a bullet is unstable in this attitude, it will tumble, usually within 1 foot of the impact point. In the tumbled configuration, the bullet loses more energy to the fluid by virtue of its hydrodynamic drag and, therefore, generates a much longer cavity. As the cavity begins to collapse, it usually relaxes into a spherical shape centered roughly at the point of bullet tumbling. The gas trapped will rebound. Thus, the cavity may oscillate through several such cycles until the energy of the fluid is dissipated. Each rebound of the cavity is accompanied by a pressure pulse. The peak pressure and pulse width depend on the total energy of the fluid, the amount of gas trapped in the cavity, and the extent of cavity shape deviation from spherical symmetry.

Bristow and Lundberg (References 1 and 2) as well as Yurkovich (Reference 3) have conducted extensive experimental and theoretical work on the fluid dynamics of hydraulic ram. The theory presented in this paper is a direct extension of the ideas reported in these three references.

BULLET DYNAMICS

Bullets are only marginally stable in their unyawed attitude. Asymmetric forces, acting on the bullet during impact into a fluid, often cause small perturbations in bullet attitude that are then magnified by the drag forces encountered. As a consequence, an experimentally fired bullet will tumble during fuel-cell penetration. While the bullet is tumbling, lift forces are generated perpendicular to the line of flight. Finally, the bullet is spinning very rapidly which, combined with the lift forces, produce a spiraling trajectory through the fluid.

For an aircraft in flight, an impacting bullet will either be tumbled at impact or it will start to tumble within inches of the point of entry. This is due to the relative motion of the aircraft, which gives the bullet a significant angular deviation from its unyawed attitude. The deviation will be magnified by the penetration of intervening aircraft structure so that, in the worst case, the bullet will be fully tumbled upon impact.

For calculating fluid pressures, it is necessary to know the velocity, the rate of kinetic energy loss, and the time of arrival of the projectile as functions of distance along the trajectory. To obtain estimates of these quantities, a simplified model of the complex bullet behavior is used.

The bullet is assumed to travel in a straight line. Along this line its velocity is given by

$$\frac{dV}{dx_b} = -\beta V \quad (1)$$

where V and x_b denote the bullet velocity and position, respectively. The velocity decay coefficient, β , is given by

$$\beta = \frac{1}{2m} \rho C_D A \quad (2)$$

where ρ is the fluid density, A is the projected frontal area of a bullet, m is the bullet mass, and C_D is a dimensionless drag coefficient, which, in general, depends on the velocity and yaw angle of the bullet.

The rate of kinetic energy loss, dE/dx_b , where $E = 1/2 mV^2$, is given by

$$\frac{dE}{dx_b} = m\beta V^2 \quad (3)$$

If β is a known function of x_b and V , Eq. (1) and (3) can be integrated to give the desired results.

Based on experimental observations, the variations of β with x_b for tumbling bullets is expected to be similar to that shown in Figure 1. The bullet enters the test cell with a 0-degree yaw with $\beta = \beta_1$, and

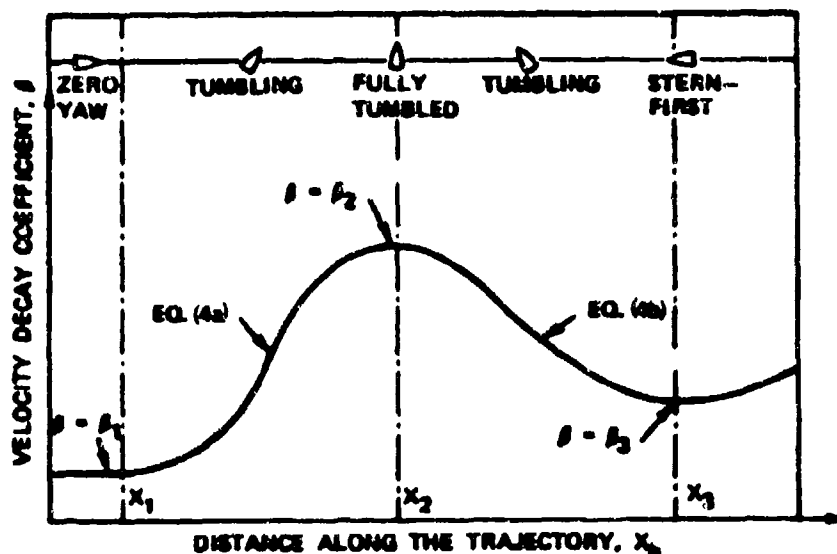


FIGURE 1. Variation of the Velocity Decay Coefficient.

continues until it reaches a point, X_1 , along its trajectory where it begins to tumble. At a further point, X_2 , the bullet is fully tumbled with $\beta = \beta_2$. As the bullet proceeds, it continues to tumble in a cyclic manner. An empirical function having these properties is

$$\beta(X_b) = \beta_1 + (\beta_2 - \beta_1) \left\{ \frac{1}{2} - \frac{1}{2} \cos \pi \left[\frac{X_b - X_1}{X_2 - X_1} \right] \right\}^n \quad (4a)$$

for $X_1 < X_b < X_2$,

$$\beta(X_b) = \beta_2 + (\beta_3 - \beta_2) \left\{ \frac{1}{2} - \frac{1}{2} \cos \pi \left[\frac{X_b - X_2}{X_3 - X_2} \right] \right\}^n \quad (4b)$$

for $X_2 < X_b < X_3$, and so on. The value, β_3 , corresponds to the bullet moving in a stern-first attitude. For simplicity in the following analysis it has been assumed that the tumbling proceeds at a constant rate, that is

$$X_2 - X_1 = X_3 - X_2 = X_4 - X_3 \dots$$

A value of the exponent $n = 3$ was found to be reasonable.

During many experiments it was noted that the jackets were stripped from the armor piercing core of the API (armor piercing incendiary) ammunition. The kinetic energy of the jacket and incendiary is approximately 40% of the total kinetic energy of the complete round. Deposition of this energy into the fluid is evidenced by a distinct pulse on the experimental pressure records.

A crude method for incorporating the jacket energy deposition into the hydraulic ram model is as follows. The projectile penetrates the fluid in a normal fashion for a distance X where the jacket strips. The kinetic energy of the jacket and incendiary material is calculated at this point. The energy deposition of the armor piercing core is then calculated in the normal manner except that values of β appropriate to the core must be used. The energy deposition of the jacket is assumed to be exponential, and is added to that of the core. The equation for the total energy deposition is then

$$\frac{dE}{dX_b} = -\frac{1}{2} \rho_c v^2 + \frac{\alpha E_j}{\beta_j} e^{-\beta_j (X_b - X_s)} \quad (5)$$

where the subscript c indicates properties of the core, and E_j is the kinetic energy of the jacket at X_s . The parameter, β_j , dictates the distance over which the jacket energy is deposited in the fluid. A reasonable value can be obtained from Eq. (2) using the jacket and incendiary mass, the area of the tumbled round, and a drag coefficient of 1.0. The factor, α , in Eq. (5) was included to allow adjustment of the pulse height to agree with the experiment. A constant value of $\alpha = 1/3$ was used throughout the analysis, and resulted in a reasonable description of the stripping pulse for most of the shots.

PRESSURE FIELD ANALYSIS

In the light of the previous work (References 1, 2, and 3), the problem of predicting the pressure field generated by a bullet in the drag phase will be reexamined. Because of the mathematical difficulties introduced by the wall boundary conditions, a simple model which neglects the wall effects will be considered here. A schematic of the model is shown in Figure 2. (The effect of the walls on the pressure field is discussed in the following section.)

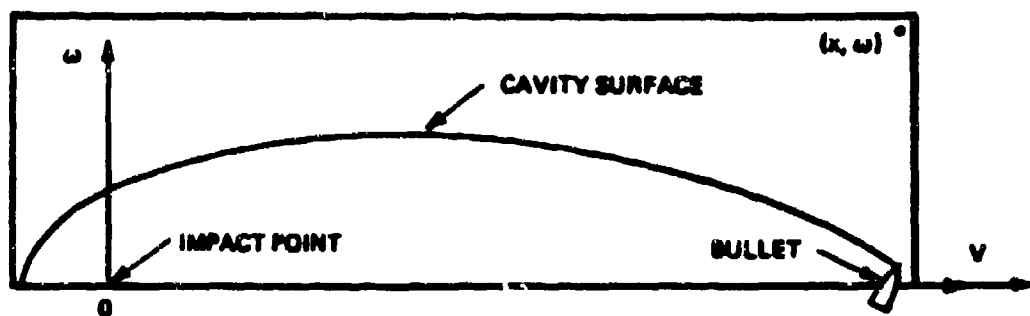


FIGURE 2. Model of Drag Phase of Hydraulic Ram.

In essence, the bullet shown in the Figure 2 model is initially stationary in an infinite body of fluid until $t = 0$. The bullet is then impulsively accelerated to an initial velocity, V_0 . At times $t > 0$, the bullet moves with a velocity, V , in a straight line along the axis in a prescribed manner as discussed previously.

It is assumed that the flow field can be described in terms of a potential function, ϕ , which satisfies the wave equation.

$$\nabla^2 \phi = \frac{1}{c^2} \frac{\partial^2 \phi}{\partial t^2} \quad (6)$$

where c is the speed of sound in the fluid. In terms of this potential the fluid velocity, \vec{u} , is expressed as

$$\vec{u} = \nabla \phi \quad (7)$$

and the fluid pressure, p , can be obtained from Bernoulli's Equation

$$p = p_0 - \frac{\rho}{2} \frac{\partial \phi}{\partial t} - \frac{1}{2} \rho u^2 \quad (8)$$

where ρ is the fluid density, p_0 is the ambient pressure, and u is defined as $|\vec{u}|$.

Since we have not yet included the effects of the walls, the proper boundary conditions for Eq. (6) are that the fluid velocity is tangential to the projectile surface and that $p = p_0$ on the cavity surface, where p_0 denotes the pressure in the cavity. It is assumed that p is constant throughout the cavity. Under these restrictions, the problem is to determine the pressure as a function of time at any arbitrary point (x, w) where, as shown in Figure 2, w is the perpendicular distance of this point from the x axis.

Even after these simplifications, the problem is enormously difficult to solve. Therefore, the approach taken here is to ignore the boundary conditions and then try to approximate the effect of the bullet and cavity on the fluid by the action of a line of sources distributed along the bullet path. Consequently, the resulting flow field is symmetric about the x axis. The potential due to these sources can be expressed as the integral

$$\phi(x, w, t) = - \int_0^{X_b(t)} \frac{\lambda(\xi, t - r/c)}{r} d\xi \quad (9)$$

where ξ is the distance along the trajectory, r is the distance from the point, ξ , to (x, w) and λ is the source strength at ξ . To account for the finite sound, the integral must be evaluated using the retarded time $\tau = t - r/c$. Methods were derived in the section on bullet dynamics to determine the bullet time of arrival, t_b , on the trajectory as a function of the bullet position, X_b . The results of the theory are not considered to be valid during the cavity collapse; therefore, the lower limit in this integral can be taken as zero. The upper limit, X_b , denotes the projectile position when $t = t_b$.

In order to determine the source strength, λ , an estimate is made by a method based on the conservation of energy. For this purpose assume that the flow is confined to a slice, dx , as shown in Figure 3, and that c approaches infinity. The fluid velocity in this slice is then

$$u = \lambda \frac{\partial \phi}{\partial t} \quad (10)$$

At the cavity radius, $w = a$ and $u = da/dt$ so that

$$\lambda = \frac{1}{2} \frac{da}{dt} \quad (11)$$

Following Birkhoff (Reference 4), the kinetic energy of the slice is added to the potential energy λ balanced against the energy deposited into the slice by the bullet. The result is a differential equation for the cavity radius, a , which, when integrated, can be used with Eq. (11) to give the source strength

$$\lambda = \frac{1}{2} \lambda A - \frac{1}{2} \lambda^2 (t - t_b) \quad (12)$$

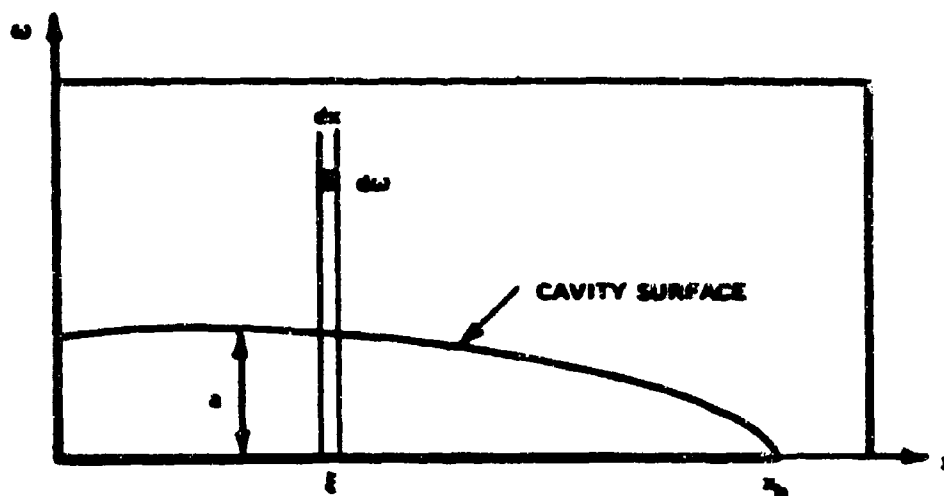


FIGURE 3. Flow Model for Estimating Cavity Growth and Source Strength Variation.

where the maximum cavity radius, A , is given by

$$A^2 = \frac{\left(\frac{dE}{dx_b} \right) \xi}{\pi(p_o - p_c)}$$

and

$$A^2 = \frac{p_o - p_c}{\rho N}$$

The parameter, $N = \ln \Omega/a$, comes from taking a finite limit, Ω , to the integral giving the kinetic energy of the slice. If the upper limit, Ω , were allowed to be infinite, the kinetic energy would become infinite, which is a physical impossibility. Hence, the limit, Ω , will be assumed to be finite. Since N is a slowly varying function of Ω , it will be treated as a constant. This is justified in that, for the special case in which a bullet is traveling with a constant velocity, the correct cavity shape is obtained for constant values of the quantity Ω/a in the 20-30 range (Reference 4). Physically, this step can be rationalized by considering the neglected influence of the noncylindrical divergence of the flow.

The pressure field resulting from this line of sources can now be calculated. Substituting Eq. (12) for the source strength in Eq. (9),

$$\phi(x, \omega, t) = -\frac{B}{2} \int_0^{x_b(\tau)} \frac{1}{r} \left\{ A(\xi) - B \left| t - \frac{x}{c} - t_b(\xi) \right| \right\} d\xi \quad (13)$$

Since ξ had to be expressed in terms of the retarded time τ , t in Eq. (12) was replaced by $t - r/c$.

The terms in Bernoulli's Equation for the pressure can be obtained by differentiating Eq. (13). For the time derivative one obtains

$$\frac{\partial \phi}{\partial t} = -\frac{BA_b}{2R_b} \frac{v}{1 - \frac{v}{c} \frac{x - x_b}{R_b}} + \frac{B^2}{2} \ln \left| \frac{x + R_o}{x - x_b + R_b} \right| \quad (14)$$

where R_o and R_b are distances from the point (x, ω) to the impact point and the bullet, and A_b denotes the value of A evaluated at x_b .

The fluid velocity component, u_x , is given by

$$u_x = \frac{\partial \phi}{\partial x} = +\frac{BA_b}{2R_b} \frac{\frac{v}{c} \frac{x - x_b}{R_b}}{1 - \frac{v}{c} \frac{x - x_b}{R_b}} + \frac{B}{2} \int_0^{x_b(\tau)} \left\{ A(\xi) - B \left| t - t_b(\xi) \right| \right\} \frac{x - \xi}{r^3} d\xi \quad (15)$$

Since the function $A(\xi)$ and $t_b(\xi)$ depend on the tumbling behavior of the bullet, the integral in Eq. (15) cannot be evaluated explicitly. The velocity component in the ω direction, u_ω , is given by

$$u_\omega = \frac{\partial \phi}{\partial \omega} = +\frac{BA_b}{2R_b} \frac{\frac{v}{c} \frac{\omega}{R_b}}{1 - \frac{v}{c} \frac{x - x_b}{R_b}} + \frac{B}{2} \int_0^{x_b(\tau)} \left\{ A(\xi) - B \left| t - t_b(\xi) \right| \right\} \frac{1}{r^3} d\xi \quad (16)$$

PRESSURE WAVE REFLECTIONS

Pressure wave reflected from the fuel-cell walls play an important, if not dominating, role in determining the total pressure field within the fluid and the pressure loading that acts on the walls.

To confirm theoretical predictions of the pressure field produced by the bullet and to visualize the hydrodynamic processes, a simple method of accounting for wave reflections can be used. This method is based on the solution of a problem given by Cole in his book on underwater explosions (Reference 5).

Consider the case of a plane, acoustic pressure wave that impinges normally upon an infinite, flat plate. Wave reflections within the plate are neglected so that the plate will react to the pressure loading as a rigid body with no internal stresses.

As representative of hydraulic ram in an aircraft fuel cell, consider the case of a 1-ms pressure pulse in JP-5 fuel incident on a 0.063-inch-thick aluminum panel. A common wall material used for windows in hydraulic ram experiments is 1-inch-thick plexiglass. Figure 4 illustrates the effect that walls constructed of these materials would have on records of the normalized total pressure taken at a distance of 5 inches from the wall.

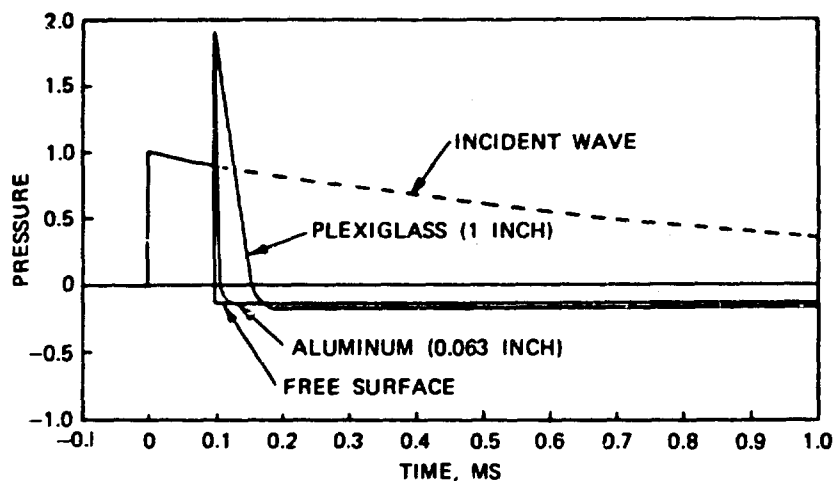


FIGURE 4. Total Pressure Versus Time of an Exponential Plane Wave Impinging Upon Plane Walls of Specific Construction.

It is obvious from this figure that the reflected pressure waves are extremely important in determining the measured pulse shape and impulse. For the rational correlation of any theory with experiment, the theory must include the wave reflection effects. The analysis also brings to attention the phenomenon of bulk cavitation in the fluid. As shown in Figure 4, the pressure becomes negative; that is, the fluid is in tension. When this occurs, cavitation in the form of a dispersion of small bubbles in the fluid is possible. After the inception of cavitation, the analysis is no longer valid.

A curve for the case of reflection from a free surface is also included in Figure 4. It is apparent that, for comparing experimental with analytical pressure measurements within the fluid, it is a good approximation to consider the walls as free surfaces. To a certain extent this is true even for heavily constructed walls such as thick plexiglass. If this approximation is made, then, for rectangular volumes, the method of images can be used to account for the pressure-wave reflections. The incident pressure due to bullet penetration has been approximated as arising from a line of sources. Reflections from a free surface near this line of sources (or sinks) can, therefore, be accounted for by adding the pressure due to a mirror image line of sinks (or sources).

BALLISTIC TESTING AND DATA REDUCTION

A total of 53 shots were fired at muzzle velocity into a water-filled test cell instrumented with five Kistler 601A pressure transducers. The rounds were .30 caliber AP, .50 caliber API, 12.7mm API, and 14.5mm API. The parameters that were varied were impact plate material and thicknesses, entrance angle obliquity, and bullet attitude on impact.

The test tank was a 5-foot cube. Entrance panels were 2 feet square, and two 1-inch-thick plexiglass windows were placed on opposite sides of the test tank for high speed photography. These provided a 30-inch-high and 36-inch-long field-of-view.

The five Kistler 601A pressure transducers were mounted at the end of 1/2-inch-diameter pipes extending beyond the open end of the tank. The pipes were, in turn, mounted to a separate frame isolated from shock and vibration in the test tank. The transducers were placed 6 inches above the expected trajectory of the 0-degree obliquity shots and spaced 6 inches apart.

The size of the test tank was sufficiently large so that pressure waves reflecting from the tank walls did not arrive at the transducer locations until approximately 1 ms after bullet impact. To avoid the complicating effects of the wall reflections, the analysis included only the 1-ms time interval. Wave reflections from the impact wall could not be ignored. Because of the lightweight construction of the entrance panel, it was assumed that the pressure waves reflected from it as if from a free surface. The reflected pressure wave could

then be calculated using the method of images.

Initial values of the drag coefficients for bullets in the 0-degree yaw attitude ($C_D = 0.05$) and in the tumbled attitude ($C_D = 0.30$) were obtained from Yurkovich (Reference 3). The drag coefficient used for the bullet traveling in a stern-first attitude was $C_D = 0.82$ corresponding to a circular disk. The trajectories were measured from high speed motion pictures of the shot. On the basis of this comparison, the drag coefficient of the .30 caliber AP round was doubled to $C_D = 0.60$ for the fully tumbled attitude. The accuracy of the experimental trajectory measurements was not sufficient to obtain direct verification of the drag coefficient for the 0-degree yaw attitude. Therefore, a comparison between theory and experiment was made of the initial part of the pressure pulse which was generated by the bullet in its 0-degree yaw attitude.

Much better agreement was obtained when the 0-degree yaw drag coefficients were doubled to $C_D = 0.10$ for the .30 caliber AP and the 14.5mm API rounds. However, the 0-degree yaw drag coefficients are particularly sensitive to the geometry of the bullet nose which can be considerably distorted during impact and penetration of the target panel. It is expected, therefore, that the 0-degree yaw drag coefficient will vary with impact obliquity and velocity as well as with target thickness and material. The drag coefficient for the armor piercing core were taken as identical as those of the complete round.

The tumbling distances, X_1 and X_2 , could not be accurately measured from the motion pictures. Therefore, a computer program was written which calculated those values of X_1 and X_2 that minimized the rms error between the experimental and theoretical pressure pulses.

COMPARISON WITH EXPERIMENT

The agreement of experiment with theory was, in general, quite good for all shots impacting at 0-degree obliquity into the test cell. The pressure pulse recorded at two of the transducers during one of the 12.7mm shots is shown in Figure 5 together with the theoretical curves. The origin of the time axis in these plots is arbitrary.

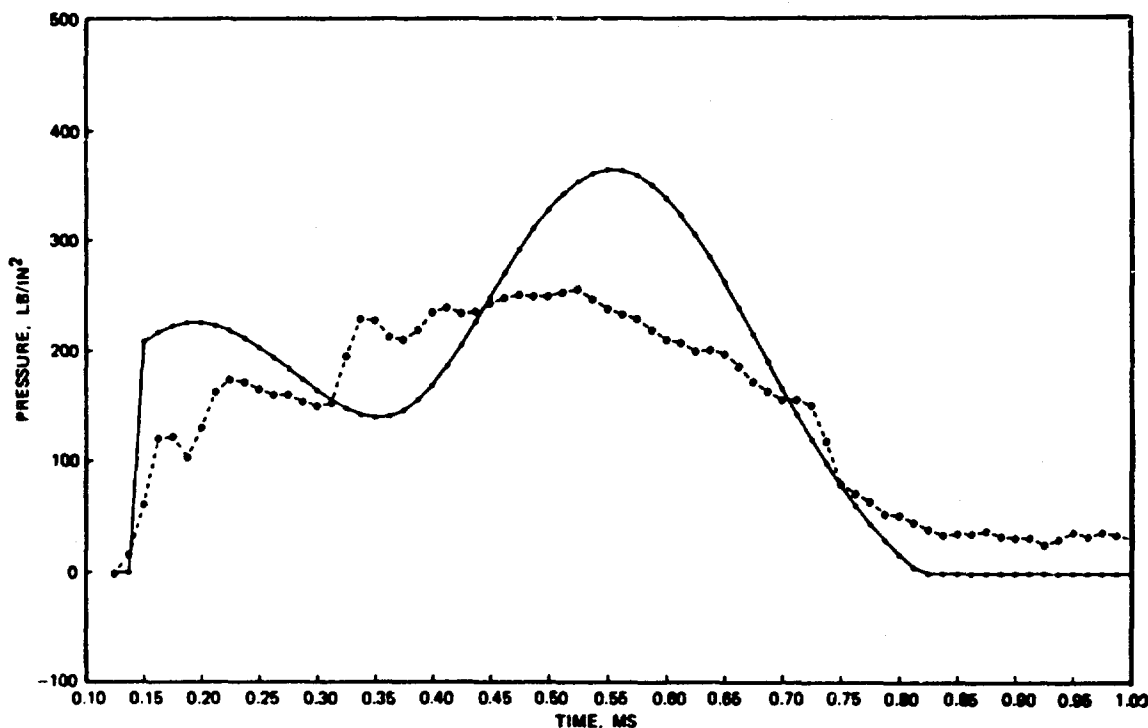


FIGURE 5a. Pressure Versus Time Plot; 12.7mm API; $x = 6$ in.; $\omega = 6$ in.

The overall accuracy of the theory can be assessed from Figure 6, where the experimental peak pressure is plotted against the corresponding theoretical values for 18 of the 12.7mm API shots. The theoretical values lie, in all cases, within a factor of 2 of the experimental values and are, in most cases, much better than that. Similar plots for the 14.7mm API, .30 caliber AP, and .50 caliber API show the same agreement.

Comparison of the theoretical bullet trajectories was made with experimental points taken from high speed motion pictures. Figure 7 shows the trajectory obtained for the same 12.7mm API shot whose pressure pulse was given in Figure 5. Similar plots were made for a number of other shots and showed somewhat worse agreement on the trajectory, but much better agreement of the tumbling distance, X_2 .

The tumbling distances varied quite widely from shot to shot. The actual distribution of theoretical values of X_1 and X_2 are shown in Figure 8 for the 12.7mm API shots.

The pressure pulse produced by the stripped-off jacket of the API rounds is of interest. A good example of this for a .50 caliber API shot is shown in Figure 9, where the pulse can be easily identified.

The agreement of experiment with theory was consistently bad for the 12 shots fired at 30 and 45 degrees obliquity. A plot of the experimental and theoretical peak pressures is shown in Figure 10 for the 12.7mm

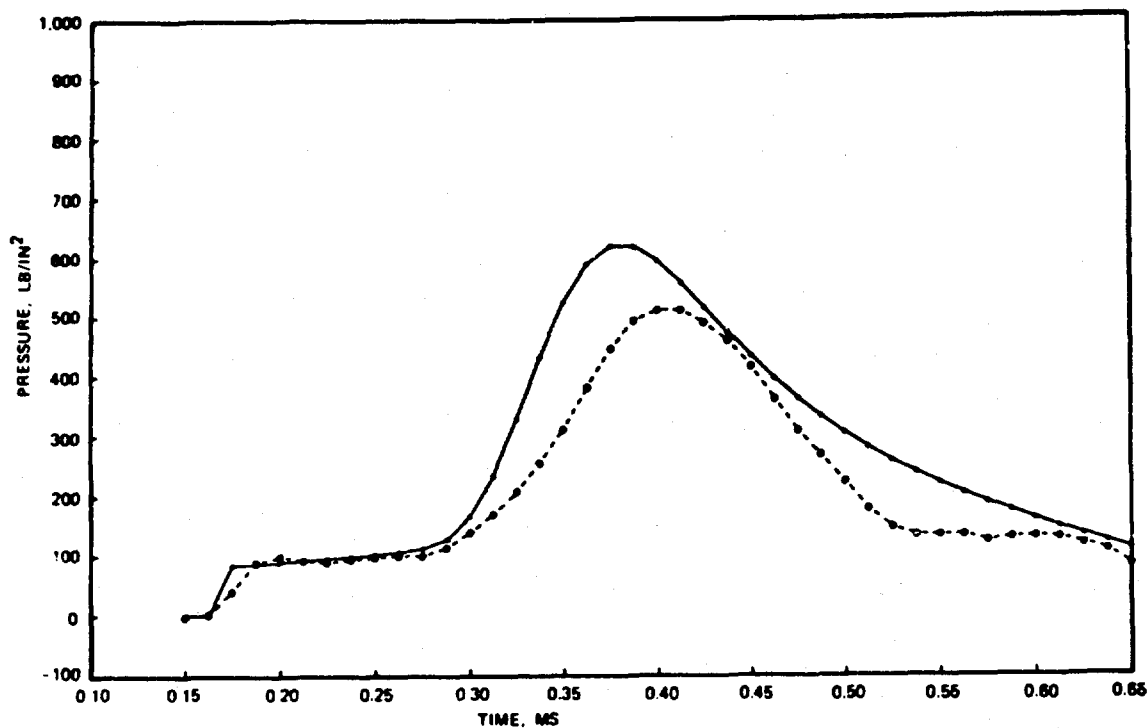


FIGURE 5b. Pressure Versus Time Plot; 12.7mm API; $x = 30$ in., $\omega = 6$ in.

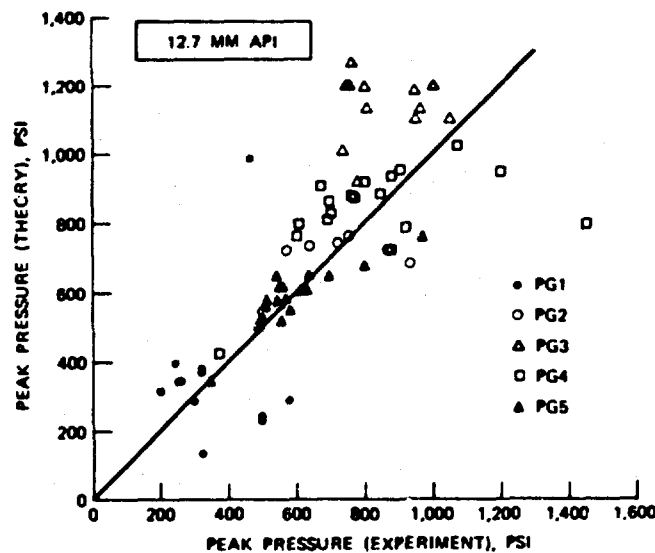


FIGURE 6. Peak Pressure; Theory Versus Experiment; 12.7mm API; 0-Degree Obliquity, 0-Degree Yaw.

API shots. The theoretical values are consistently too low. There are several possible sources for this disagreement. First, because of the nonzero impact obliquity, the path of the bullets could deviate considerably from a straight line. Second, the bullets could be deformed producing a different drag coefficient than in the 0-degree obliquity shots. In addition, the jackets could strip off in a manner different from the 0-degree obliquity shots. The actual source of the error could not be discerned from the pressure traces, and no motion pictures were taken of these shots. The possibility of faulty experimental technique exists. By comparison of Figures 9 and 10, the peak pressures measured for the oblique shots are much higher than those with 0-degree obliquity even though the latter shots passed much closer to the pressure transducers.

CONCLUSIONS

A theory has been derived for predicting the pressure field generated in a fluid during the penetration of tumbling, military ammunition. The theory was tested against pressure measurements taken during a large number of shots using a variety of ammunition. Agreement between the experiment and the theory was quite good for those shots impacting the test cell at 0-degree obliquity. Shots at 30 and 45 degrees obliquity

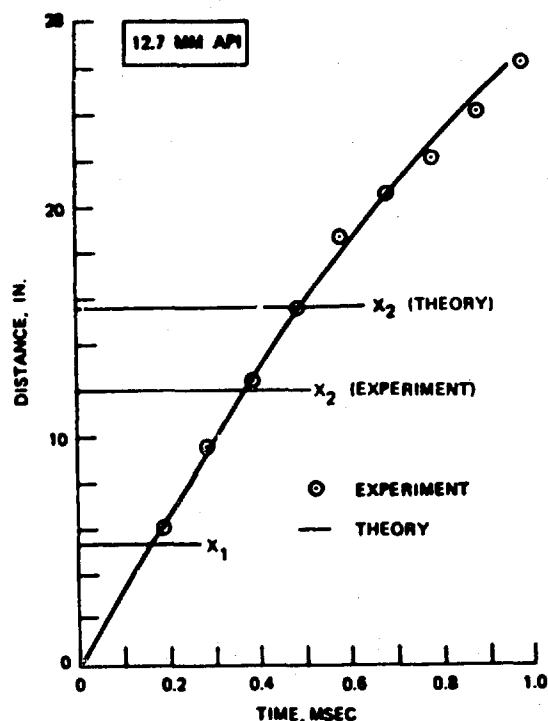


FIGURE 7. Trajectory; 12.7mm API.

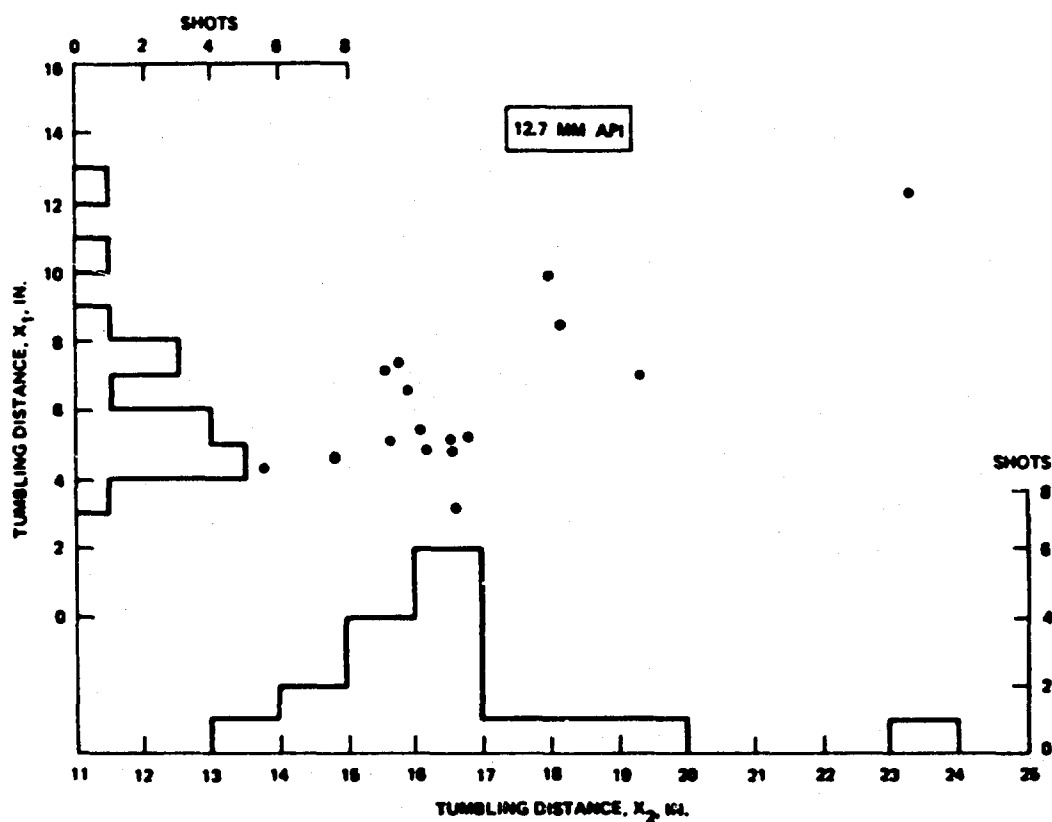


FIGURE 8. Tumbling Distance Distribution; 12.7mm API; 0-Degree Yaw, 0-Degree Obliquity.

were in serious disagreement; the predicted pressures being consistently too low. The reason for this disagreement could not be resolved.

Further ballistic testing is desirable, first to resolve the discrepancy with oblique impacts and, second, to test the theory at lower impact velocities.

Solutions of a simple problem illustrated the importance of wave reflections from the fuel cell walls on total pressure field. The problem of obtaining the total pressure loading on the walls will require

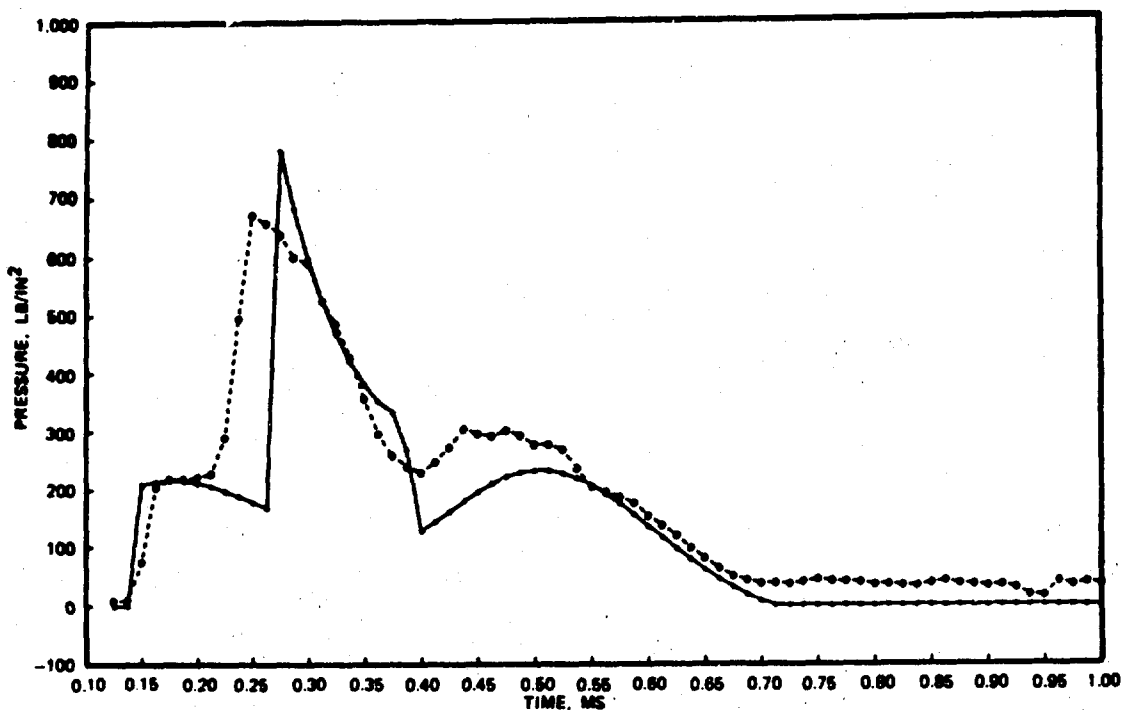


FIGURE 9. Pressure Versus Time Plot; .50 API; $x = 6$ in., $\omega = 6$ in.

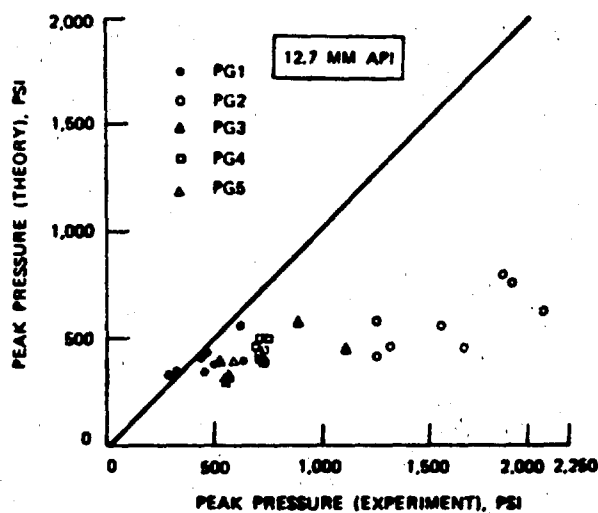


FIGURE 10. Peak Pressure Experiment Versus Theory; 30- to 45-degree Obliquity, 0-degree Yaw.

further theoretical advances.

REFERENCES

1. Bristow, R.J., and J.F. Lundeberg, Boeing Company. *Hydraulic Ram*. Seattle, WA., February 1969. (FAD S-66.)
2. Bristow, R.J., and J.F. Lundeberg, Boeing Company. *Projectile Penetration Through Rheopneumatic Fluids*. Seattle, WA., July 1968. (Report prepared under Contract No. F33615-68-C-1460 for USAF.)
3. Yurkovich, R., McDonnell Douglas Corp. *Hydraulic Ram: A Fuel Tank Vulnerability Study*. St. Louis, Mo., September 1969. (Report No. G964.)
4. Birkhoff, G., and E.H. Zarantonello. *Jets, Wakes, and Cavities*. New York, Academic Press, 1957.
5. Cole, R.H. *Underwater Explosions*. Princeton, NJ, Princeton University Press, 1948.

CALCUL DE QUELQUES PROBLEMES D'IMPACT SUR DES STRUCTURES AERONAUTIQUES

par

C. PETIAU

Avions Marcel Dassault - Bréguet Aviation
78 Quai Carnot
92214 SAINT-CLOUD
France

SOMMAIRE

Après le rappel de quelques méthodes, classiques et par éléments finis, utilisées aux AMD-BA pour le calcul des chocs, et des réponses transitoires, nous examinerons les possibilités d'application sur les problèmes suivants :

- Réponse de la structure après impact d'un projectile sur un blindage.
- Réponse des structures aux effets de souffle d'explosion.
- Calcul des atterrissages durs, catapultage et roulement.

On abordera le problème du calcul pratique de la tenue résiduelle des structures localement endommagées

SUMMARY

After reviewing some of the methods by finite elements, used at AMD-BA for calculating impacts and transitory responses, we shall examine the possibilities of application in the following cases :

- Response of structure upon impact of a projectile on an armor-plate.
- Response of structures to forces due to explosion blast.
- Calculation of hard landings, catapulting and taxiing.

Moreover practical calculation of the residual strength of locally damaged structures will be considered.

1 - INTRODUCTION

Les problèmes d'impact de projectiles sur les structures ne sont souvent traitables que par des méthodes semi-empiriques ; nous allons cerner certains des points où les techniques modernes de calcul, en particulier les méthodes d'éléments finis, peuvent apporter une aide :

- Réponse d'une structure après impact d'un projectile sur un blindage : la loi du choc sur le blindage étant supposée connue.
- Réponse des structures aux effets du souffle des explosions. On montrera que ce mode de destruction n'est pas déraisonnable pour les avions modernes. On évoquera le calcul de choc très bref sur des ogives cylindro-coniques.
- Réponse des avions lors des atterrissages durs, catapultage et roulement sur obstacle.

Ces types de problème étant tous traitables par une même modélisation numérique.

- Méthode des éléments finis pour la discrétisation dans l'espace.
- Méthode des différences finies implicites pour l'étude dans le temps.

On verra que ces modélisations conduisent malheureusement souvent à des calculs d'une telle complexité que leur utilisation systématique n'est pas actuellement industriellement rentable, tant du fait de la longueur des calculs que du nombre des données à rassembler pour décrire le phénomène.

L'autre point où les techniques de calcul par éléments finis sont évidemment fécondes est celui de la tenue résiduelle des structures après endommagement.

Ces calculs présentent deux aspects différents :

- Calcul de "fail safe"

Nous décrivons un procédé permettant d'effectuer très rapidement ce type de calcul sans avoir à effectuer une réanalyse complète de la structure.

- Calcul de propagation de fissure

Nous utilisons la méthode, maintenant "classique" dans les études de fatigue, de l'énergie de dislocation

2 - RAPPEL DES METHODES DU CALCUL DES REPONSES STRUCTURALES EN TRANSITOIRE

2.1 - Equation de la mécanique linéarisée

Soit X le vecteur représentant le déplacement des degrés de liberté de la structure ; en linéarisant les équations de la mécanique pour les petits mouvements, et en l'absence de frottement interne, il vient :

$$1 \quad [M] \ddot{X} + [K] \dot{X} = F(t)$$

Les matrices de masse et de rigidité $[M]$ et $[K]$ sont élaborées par la méthode des éléments finis, X représente alors les déplacements des noeuds du maillage, son rang est généralement de plusieurs milliers, voire dizaines de milliers.

Il est plus simple de ne pas tenir compte des frottements internes, car ceux-ci sont faibles et mal connus (de plus non linéaires), les négliger revient à être conservatif dans beaucoup de cas.

Nous pratiquons 3 types de façon d'intégrer dans le temps le système 1 :

- Intégration dans une base réduite de modes propres.
- Intégration sans réduction de base par méthode de différences finies implicites.

Remarque préliminaire importante

Toutes les méthodes que nous allons décrire résultent du fait que le plus gros des calculs sur ordinateur, est l'obtention de l'inverse de la matrice de rigidité $[K]$, ou celle d'une combinaison $[K] + \lambda[M]$.

Cette inverse est écrite sous une forme dite factorisée que nous calculons par la méthode de Gauss Frontale ; cette forme est relativement "creuse", cependant pour les problèmes dépassant quelques milliers de degrés de liberté, elle ne peut plus tenir dans la mémoire centrale des ordinateurs actuels.

Dans ce cas, il est préférable d'utiliser les méthodes de résolution à seconds membres simultanés plutôt que successifs pour minimiser les accès aux fichiers périphériques où se trouve la matrice factorisée.

Ce sont ces considérations tactiques qui ont inspiré le choix des méthodes que nous allons décrire.

2.2 - Intégration dans une base de modes propres

C'était jusqu'à ces dernières années la méthode la plus utilisée.

Son principe est le suivant :

- On calcule, ou on mesure, les modes propres de la structure, les vecteurs propres sont rangés en colonne dans une matrice $[B]$

On intègre dans une base réduite telle que $[X] = [B] z$

Le système 1 devient :

$$2 \quad [m] \ddot{z} + [k] \dot{z} = f(t)$$

avec

$$[m] = [B_t] [M] [B], \quad [k] = [B_t] [K] [B], \quad f_t = [B_t] F(t)$$

$[m]$ et $[k]$ sont alors des matrices diagonales et les équations du système 2 deviennent découplées (si elles ne sont pas couplées par $f(t)$).

L'intégration dans le temps ne pose alors plus de problèmes.

Nous effectuons le calcul des modes propres soit :

- par la méthode de Langzos-Brévan directe.
- par cette même méthode, mais utilisée sur une base réduite selon les principes du § 2.3.

Parmi les inconvénients de la méthode, on peut citer :

- de nécessiter le calcul des modes propres,
- ce calcul étant long, on est conduit à prendre une base trop restreinte,
- cette base trop restreinte empêche dans la pratique le calcul des efforts sur la structure à partir des déformations,
- elle est mauvaise quand les forces d'excitation sont concentrées,
- elle est exclusivement linéaire.

Son avantage est de pouvoir être pratiquée à partir des mesures des modes, et alors de conduire à des calculs extrêmement simples.

2.3 - Intégration sur une base réduite - base de chargement

La réduction de base est faite sur le même principe que celle du paragraphe précédent, mais la base réduite $[B]$ n'est plus une base de modes propres.

Dans la pratique cette réduction ne peut être arbitraire ; on a intérêt à ce que les déformées de base $[B]$ soient issues de chargement raisonnable $[P]$ (soit $[K][B] = [P]$), il est souhaitable que le second membre F_t puisse être exprimé totalement dans la base $[P]$ de façon à ce que cette réduction soit exacte en statique, on complète $[P]$ par des chargements d'inertie judicieusement intuités.

L'intégration dans la base réduite peut être conduite par les méthodes classiques.

Le coût de cette méthode est essentiellement celui des résolutions de système linéaire, avec seconds membres simultanés, qui sont peu onéreuses si on utilise la méthode de factorisation de Gauss Frontale.

Son avantage par rapport à la méthode modale est de pouvoir contraindre la structure dans une base comprenant au choix, des forces concentrées, forces de surfaces et forces d'inertie ; alors que la méthode modale contraint la structure par des seules forces d'inertie.

On remarque que la méthode classique de condensation de Guyan est équivalente à cette méthode si on prend pour $[P]$ des chargements concentrés sur certains noeuds.

Pour le calcul des modes propres du bas du spectre, nous avons constaté qu'en prenant des forces de volume pour $[P]$ le nombre de degrés de liberté à conserver semble pouvoir être divisé par 3 par rapport à la méthode de Guyan, ce phénomène s'accroît avec le raffinement des maillages d'éléments finis.

Cette méthode est bien adaptée aux problèmes à plusieurs dizaines de milliers de degrés de liberté, elle permet de récupérer pour les problèmes dynamiques les idéalizations du calcul statique (la matrice $[K]^{-1}$ est alors obtenue implicitement par la méthode des sous structures).

Cette méthode est exclusivement linéaire, cependant dans les problèmes de non linéarité locale, on peut coupler assez facilement les parties non linéaires par le second membre (voir § 2.52).

- Remarque sur la reconstitution des contraintes - Méthode déplacement, méthode forces

Dans les méthodes de réduction de base, le calcul des contraintes peut s'effectuer de 2 façons :

- Méthode déplacement

On reconstitue les contraintes à partir des déplacements calculés

$$\sigma = [L] X$$

L'opérateur linéaire $[L]$ exprimant le calcul des contraintes à partir de la loi de comportement et du calcul des déformations, à partir des déplacements X .

Pour simplifier les calculs, on transpose dans la base réduite, soit :

$$\sigma = [l] x \quad \text{avec} \quad [l] = [L][B]$$

L'opérateur $[l]$ est tabulé avant l'intégration pour les contraintes que l'on veut suivre dans le temps.

- Méthode forces

La réduction n'étant pas parfaite, les forces appliquées à la structure réellement, n'entraînent pas la relation

$$X = [K^{-1}] [F(t) - [M] \ddot{X}^a]$$

D'où l'idée de calculer les contraintes à partir de la déformation résultant des forces appliquées, soit :

$$\sigma = [L][K^{-1}] [F(t) - [M] \ddot{X}^a]$$

$$\sigma = [L][K^{-1}] [F_t - [M][B] \ddot{x}^a]$$

On tabule à l'avance les contraintes suivies, pour chaque composante de $F(t)$ et chaque accélération unitaire.

Cette deuxième méthode est généralement préférée surtout avec les réductions modales, car elle permet une compréhension, par le calculateur traditionnel, de "l'équilibre" et du "cheminement des efforts".

Notre opinion est que la réduction n'est correcte que si les 2 méthodes donnent sensiblement les mêmes résultats, au moins pour les efforts généraux.

2.4 - Intégration sans réduction de base

L'existence, dans un modèle d'éléments finis, de modes à fréquences très élevées, oblige à utiliser une méthode d'intégration dans le temps ne présentant pas de critère de stabilité.

Nous utilisons la méthode de Houbolt.

Dans cette méthode d'intégration pas à pas, on pose comme inconnue la position X_t à l'instant t , et on écrit l'équation 1 d'équilibre dynamique en calculant par extrapolation l'accélération à l'instant t .

Il vient :

$$X_t'' = \frac{1}{\Delta t^2} \left[2 X_t - 5 X_{t-\Delta t} + 4 X_{t-2\Delta t} - X_{t-3\Delta t} \right]$$

L'équation 1 devient :

$$\left[[K] + \frac{2}{\Delta t^2} [M] \right] X_t = F_t + \frac{1}{\Delta t^2} [M] \left[5 X_{t-\Delta t} - 4 X_{t-2\Delta t} + X_{t-3\Delta t} \right]$$

Dans les problèmes linéaires, cette méthode est relativement peu onéreuse car la matrice de rigidité dynamique

$$[K_D] = \left[[K] + \frac{2}{\Delta t^2} [M] \right]$$

est factorisée préalablement à l'intégration.

Dans la pratique, cette méthode n'est applicable que lorsque la matrice de rigidité dynamique factorisée tient en mémoire centrale ; ce qui nous limite à quelques milliers de degrés de liberté.

La méthode ne présente pas de critères de stabilité ; les modes élevés par rapport à Δt sont amortis par le calcul.

2.5 - Problème non linéaire

Dans les problèmes de choc, les effets non linéaires sont rarement négligeables, car ils apparaissent dans presque tous les processus d'absorption d'énergie, au point que c'est généralement plutôt le domaine linéaire qui est négligeable.

La plupart des types de non linéarité peuvent être représentés :

- changement de géométrie-grand déplacement
- travail des précontraintes
- plasticité
- viscosité d'amortisseur
- accélération de Coriolis

2.51 - Intégration directe

La méthode simple d'intégration directe est toujours théoriquement praticable en linéarisant au voisinage de chaque pas d'intégration.

Quand les non-linéarités ne sont pas prépondérantes, on peut rejeter dans les seconds membres les effets non linéaires, dans les autres cas on est amené à élaborer et factoriser la matrice de rigidité dynamique à chaque pas.

Dans les 2 cas, la méthode perd sa vertu qui est de ne pas avoir de critère de stabilité.

Elle n'est praticable que pour les problèmes à petit nombre de degrés de liberté ou dans les problèmes mono-dimensionnels (dans ce cas les matrices $[K]$ et $[M]$ sont tridiagonales) voir § 3.22

2.52 - Intégration directe avec confinement des non linéarités dans une sous-structure

Dans la plupart des problèmes de choc, la zone non linéaire est au voisinage du point d'impact dans la structure, ou dans des amortisseurs.

L'équilibre de la partie linéaire s'écrit par la méthode de Houbolt

$$1 \quad \left[K_l + 2 \frac{M}{\Delta t^2} \right] X_t = F_0 + F_{NL} + \frac{[M]}{\Delta t^2} \left[5 X_{t-\Delta t} - 4 X_{t-2\Delta t} + X_{t-3\Delta t} \right]$$

Le terme F_{NL} représente l'action des parties non linéaires sur la partie linéaire, elle n'a en général qu'un petit nombre de composantes non nul, qu'on rassemble dans un vecteur $\{f\}_{NL}$.

On pose

$$F_{NL} = [P] \{f\}_{NL} \quad 2$$

$$X_t = X_{0t} + [B] \{f\}_{NL} \quad 3$$

X_{0t} Solution de 1 pour $F_{NL} = 0$

avec

$$\left[K + \frac{2}{\Delta t^2} M \right] [B] = [P] \quad 4$$

Les degrés de liberté non linéaires de la frontière X_{NL} s'écrivent en fonction des $\{f\}_{NL}$

par $\{f\}_{NL} = [k_d] X_{NL} \quad 5$

avec

$$[k_d] = [B_t] [P]^{-1}$$

Cette matrice est appelée : matrice de rigidité dynamique des parties linéaires condensée à la frontière des parties linéaires.

L'équilibre dynamique des parties non linéaires^{*} au voisinage du pas $t - \Delta t$ s'écrit :

$$\left[[k_d] + [k_d M] \right] X_{NL} = \{f\}_0$$

$\{f\}_0$ comprenant des termes de précontraintes et d'inertie.

$[k_d M]$ étant la matrice de "rigidité dynamique" tangente des parties non linéaires.

L'algorithme d'intégration est résumé sur le tableau 1.

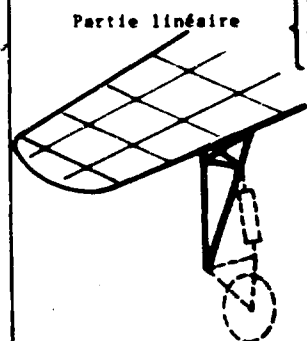
Cette méthode est très économique car en dehors des parties non linéaires les matrices sont constituées et inversées une seule fois préalablement à l'intégration.

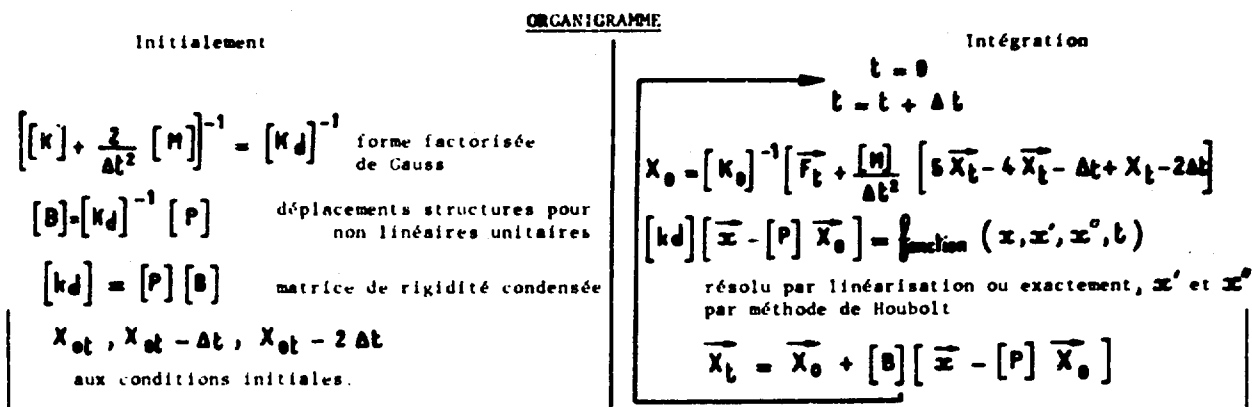
On notera que la base des parties linéaires peut avoir été réduite par la méthode des chargements, il est évidemment nécessaire que parmi les chargements de réduction figurent les $\{f\}_{NL}$.

* Il n'est pas toujours souhaitable de linéariser le comportement des parties non linéaires, dans la mesure où il peut être préférable de résoudre un petit système non linéaire à chaque pas plutôt que d'avoir un critère de stabilité (voir § 3.31).

Tableau 1

CALCUL DYNAMIQUE AVEC NON LINEARITES LOCALES	
Partie linéaire $\left\{ \begin{array}{l} \bar{X} \\ \bar{F} \end{array} \right.$ déplacement forces	Equations d'équilibre
	- Partie linéaire
	$[M] \ddot{\bar{X}} + [K] \bar{X} = \bar{F}(t) + [P] \{f\}$
	$[P]$: matrice rectangulaire de correspondance degrés non linéaires \rightarrow degrés linéaires
	- Partie non linéaire
	$\{f\}$ = fonction $(X, \dot{X}, \ddot{X}, t)$
Partie non linéaire $\left\{ \begin{array}{l} \bar{X} \\ \bar{F} \end{array} \right.$ déplacement forces	





2.53 - Flambage dynamique linéarisé élastique

C'est une méthode de l'analyse classique qui est plus simple que les méthodes précédentes pour le flambage, elle comporte cependant beaucoup d'hypothèses restrictives.

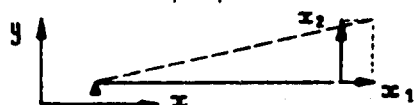
2.531 - Statique

Soit une structure soumise à un chargement restant proportionnel à lui-même λF_0 on peut poser quand $\lambda \rightarrow 0$

$$1 \quad \lambda F_0 = \left[[K] + \lambda [G] \right] X$$

La matrice $\lambda [G]$, rigidité géométrique, correspond au changement de direction des tensions internes, elle est fonction de F_0 .

- Exemple pour une barre de rigidité $ES/L = Rg$



rigidité géométrique perpendiculaire

selon y : $\frac{F}{L} = \epsilon Rg$

$$[K] + \lambda [G] = \begin{bmatrix} Rg & 0 \\ 0 & 0 \end{bmatrix} + \begin{bmatrix} 0 & 0 \\ 0 & \epsilon Rg \end{bmatrix}$$

On appelle charge critique la valeur de λ qui rend indéterminée l'équation 1.

λ critique est donc la plus faible valeur propre du système

$$[K] X + \lambda [G] X = 0$$

Qu'on calcule par la méthode de Lanczos-Brévan

L'équilibre avant charge critique se calcule classiquement dans la base des vecteurs propres $[B]$ du système 1.

Le système 1 s'y écrit :

$$\lambda \{ \}_0 = \left[[K'] + \lambda [G'] \right] x_{n2}$$

forme diagonale

$$\{ \}_0 = [B_t] F_0 [K'] = [B_t] [K] [B] [G'] = \lambda_{\text{critique}} [k]$$

d'où $x_{n2i} = \lambda \frac{f_{i0}}{k_i + \lambda g_i}$

avec $X = [B] x_{n2} + \lambda X_0$

2.532 - Extension à la dynamique

L'équation 1 s'écrit en dynamique :

$$[K_0 + K_g] X + [M] X'' = F_t \quad 3$$

On simplifie cette équation avec les 3 hypothèses suivantes :

- $F_t = \lambda_t F_0$ effort extérieur proportionnel à lui-même.
- les forces d'inertie $[M] X''$ sont négligeables dans l'effet linéaire (les déplacements de "compression" sont du second ordre par rapport aux "déversements latéraux", et il n'y a pas de grosse masse concentrée dont les forces d'inertie ne soient pas comprises dans $F(t)$).
- les contraintes provoquées par les forces d'inertie (supposées en flexion) ne provoquent pas de rigidité géométrique.

L'équation 1 peut alors s'écrire :

$$\lambda_t F_0 = K_0$$

Système qui réduit, donne en statique dans la base des formes de flambage

$$\lambda_t f_0 = [K_0] + \lambda_t [K_g] [x] + [m] x'' \quad 4$$

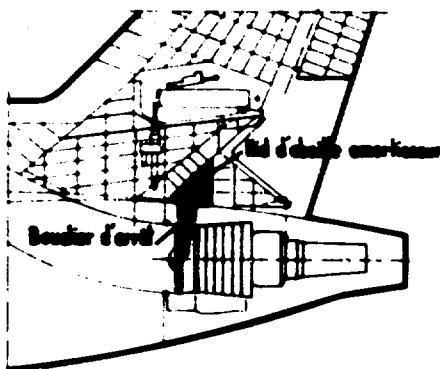
La matrice $[m]$ n'est en général pas diagonale.

L'équation 4 (type Mathieu-Hill) peut être intégrée classiquement (en diagonalisant arbitrairement $[m]$), ou pas à pas (en profitant du fait que $[K_0] + \lambda_t [K_g]$ est diagonale).

Cette méthode est certainement moins onéreuse que la méthode d'intégration directe mais ses hypothèses d'emploi rendent son application très spécifique à certains problèmes de coque avec matériaux fragiles et petites déformations.

3 - APPLICATION A QUELQUES PROBLEMES PARTICULIERS3.1 - Problème du choc sur un blindage avec amortisseur

C'est un problème que nous sommes en train de traiter actuellement pour le cas d'éclatement du réacteur arrière du FALCON 50.



Pour éviter un endommagement des parties sensibles de l'empennage, on a envisagé l'implantation de bouclier de protection selon le principe de la figure ci-contre.

Le bouclier est chargé d'arrêter ou de dévier le projectile, il est monté sur une plaque de nid d'abeille faisant office d'amortisseur.

Les premiers calculs sont faits classiquement en ne tenant pas compte de la souplesse du côté avion.

Dans le cas où le projectile est arrêté par le bouclier, par le théorème de la quantité de mouvement, on trouve en calculant l'énergie cinétique du bouclier et du projectile après le choc

$$\frac{W_{\text{bouclier}}}{W_{\text{projectile}}} = W_{\text{projectile}} \cdot \frac{M_{\text{projectile}}}{(M_{\text{projectile}} + M_{\text{bouclier}})}$$

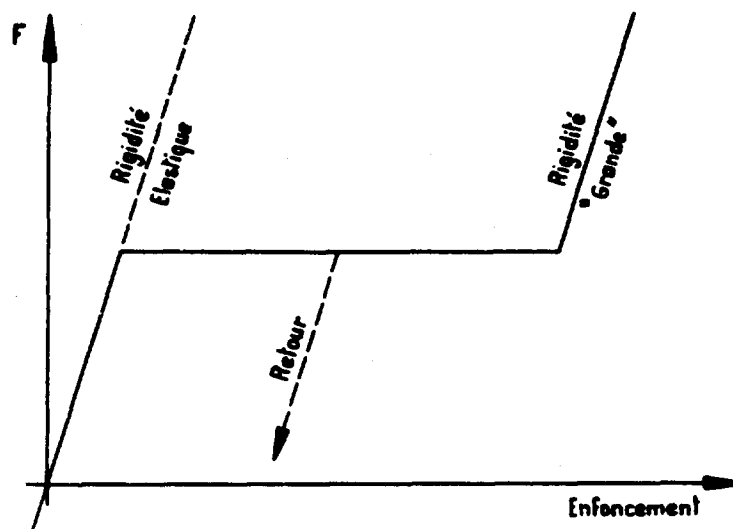
qu'on égale à l'énergie absorbable par le nid d'abeille en écrasement.

$$\frac{W_{\text{bouclier}}}{W_{\text{projectile}}} = H_{\text{Nida}} \times Q_{\text{critique Nida}} \times S_{\text{Nida}}$$

Le recours aux méthodes d'éléments finis dynamiques est nécessaire pour savoir comment s'équilibrent les forces appliquées par le nid d'abeille à la structure.

Nous sommes en train de tester l'utilisation de la méthode d'intégration directe du § 2.4 avec couplage non linéaire de l'amortisseur.

Le modèle de rigidité non linéaire pour les barres idéalise le nid d'abeille en compression est le suivant :



3.2 - Effet de souffle

Ce problème nous a été posé dans 2 cas de natures très distinctes :

3.21 - Effet de souffle sur un avion

Une étude classique rapide, résumée sur le tableau 2, permet de dégager rapidement les ordres de grandeur.

On modélise les surfaces portantes pour des systèmes à 1 degré de liberté (mode fondamental de flexion)

Il vient la relation :

$$\text{Pression statique équivalente} = 2 \times \pi \times f \times I$$

f = fréquence propre fondamentale

I = impulsion surfacique

Cette impulsion, soit se calcule par les méthodes de sphère de choc, soit est obtenue par essais.

Tableau 2

20 kg d'explosif à $z = 0$ km				
$d = 5$ m $I = 0,11$ T.s/m ²		$d = 10$ m $I = 0,025$ T.s/m ²		
	f	P. statique équivalente		Charges extrêmes
		$D = 5$ m	$D = 10$ m	
Voilure	9 Hz	6,2 T/m ²	1,4 T/m ²	4,1 T/m ²
Dérive	15 Hz	10,3 T/m ²	2,3 T/m ²	2,8 T/m ²

Ces valeurs sont à diviser sensiblement par 2 à $z = 10$ km

Les impulsions de la distance sont proportionnelles à la puissance 1/3 de la quantité d'explosif

Pour aller au-delà de ces ordres de grandeur, nous lançons une étude basée sur une réduction par base de chargement (§ 2.3).

Ces chargements de réduction sont de 2 natures :

- chargements de pression,
- chargement d'inertie correspondant à des champs d'accélération par zone.

3.22 - Onde de pression très brève sur des coques cylindro coniques

Ces études sont classiques sur certaines ogives : elles se caractérisent par le fait que la durée de la pression envisagée est nettement plus petite que le temps de parcours de l'onde de compression dans l'épaisseur de la coque, et que cette dernière est composée de plusieurs couches de matériaux différents et anisotropes.

Deux types de problèmes de choc sont posés, qui diffèrent par l'échelle des temps :

- transmission et réflexion d'onde de choc dans l'épaisseur de la coque,
- réponse générale en flexion de l'ensemble de la coque.

Nous avons traité le premier problème par la méthode de Houbolt avec un schéma d'éléments finis monodimensionnel qui a l'avantage de conduire à des matrices tridiagonales, donc un coût de calcul extrêmement faible même en introduisant une plasticité et une viscosité non linéaire.

Nous présentons sur la planche 1 quelques résultats de cette étude.

Le problème de réponse en flexion a été traité en linéaire par une méthode très voisine sur schémas d'éléments finis axisymétrique.

Pour le comportement en flambement, nous avons envisagé d'utiliser la méthode du flambement dynamique du § 2.53.

3.3 - Problème d'atterrissage, de catapultage et de roulement

Ce sont les problèmes où notre expérience est la plus grande et où nos méthodes de calcul ont été bien recoupées par l'expérience.

3.31 - Atterrissage dur

L'étude que nous présentons a été effectuée pour le Mercure.

La caractéristique du problème est de présenter des zones à très forte non linéarité (pneumatique et amortisseur, sonnette de train) mais sur un très faible nombre de degrés en liberté.

Nous avons utilisé la méthode d'intégration directe de Houbolt sur un modèle d'avion simplifié à 500 degrés de liberté (voir planche 2).

Les trains ont été couplés en tenant compte des non linéarités géométriques dues à la rotation de la sonnette, de la mise en rotation des roues, de l'aplatissement des pneumatiques, et des viscosités non linéaires des amortisseurs.

Tous ces effets non linéaires ont été linéarisés au voisinage de chaque pas d'intégration selon la méthode du § 2.52, à l'exception des termes de laminage et de frottement sec des amortisseurs qui n'ont pas été linéarisés.

On a été conduit après une sous structuration sur 2 niveaux, à résoudre à chaque pas un système non linéaire du type.

$$\text{signe de } \left(\frac{\partial \text{Enf}_i}{\partial t} \right) \left[\text{frottement} + C. \text{lamin.} \left(\frac{\partial \text{Enf}_i}{\partial t} \right)^2 - \frac{1}{2} - [k_t] \right] \text{enf}_i$$

avec

$$\frac{\partial \text{enf}_i}{\partial t} = \frac{1}{\Delta t} \left(\frac{3}{2} \text{Enf}_i - 2 \text{Enf}_{i-T-\Delta t} + \frac{1}{2} \text{Enf}_{i-T-2\Delta t} \right)$$

1 ≤ i ≤ Nombre d'amortisseurs

enf_i : enfoncement du ième amortisseur à l'instant T.

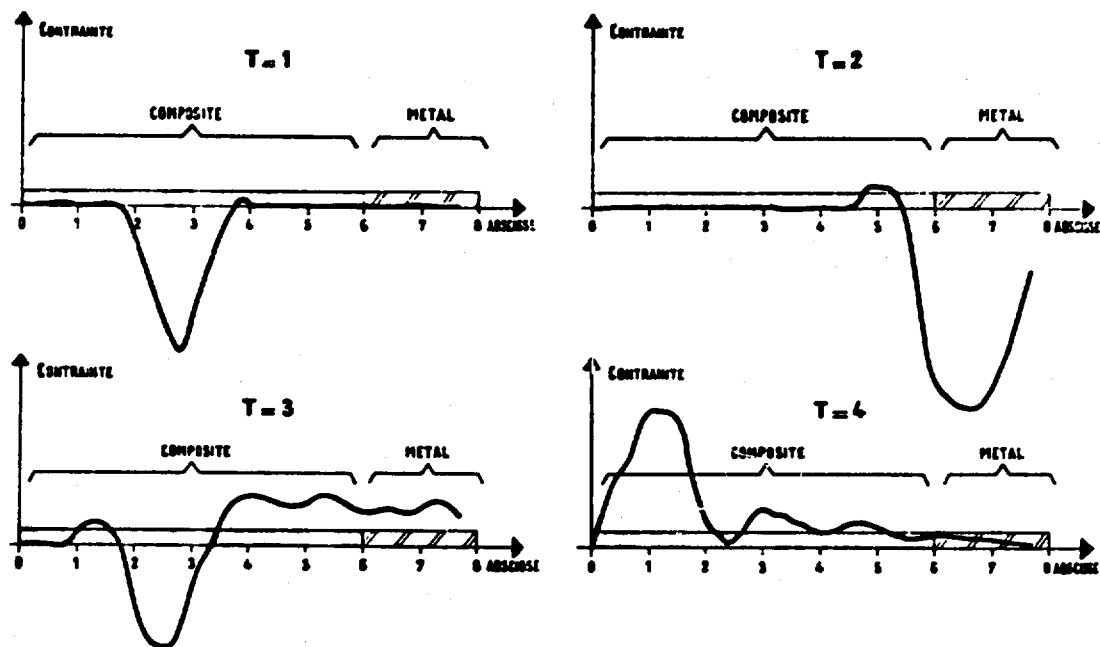
Ce système dont les inconnues sont nombre d'amortisseurs est résolu exactement par relaxation.

Nous présentons sur les planches 3 à 6 quelques-uns des résultats de cette étude comparés à des résultats d'essais en vol.

On remarquera que nous avons tenu compte de la souplesse du plancher et des passagers dont l'influence n'est pas négligeable.

CHOC SUR LES COQUES

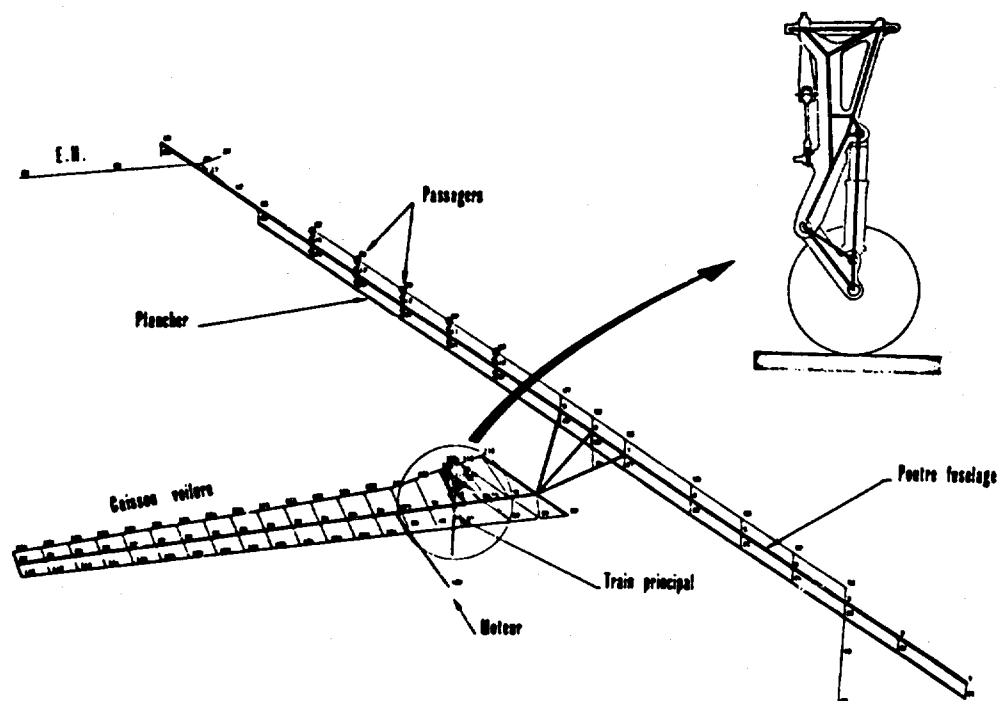
Propagation de l'onde de pression à travers l'épaisseur
Répartition des contraintes à différents instants



MERCURE

IDEALISATION POUR ATERRISSAGE DYNAMIQUE

PL 2



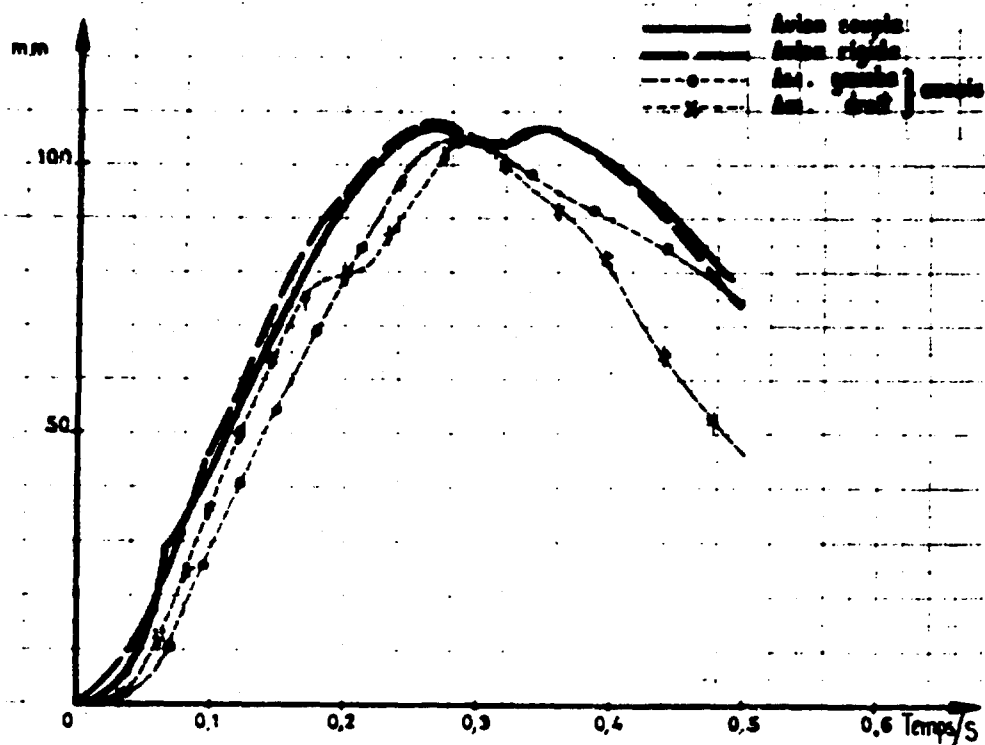
IDEALISATION MERCURE POUR ATERRISSAGE SOUPLE

Mercur
Atterrissage

COMPARAISON DU CALCUL AUX ESSAIS IN VOL 46

PL 3

ENFORCEMENT AMORTISSEUR

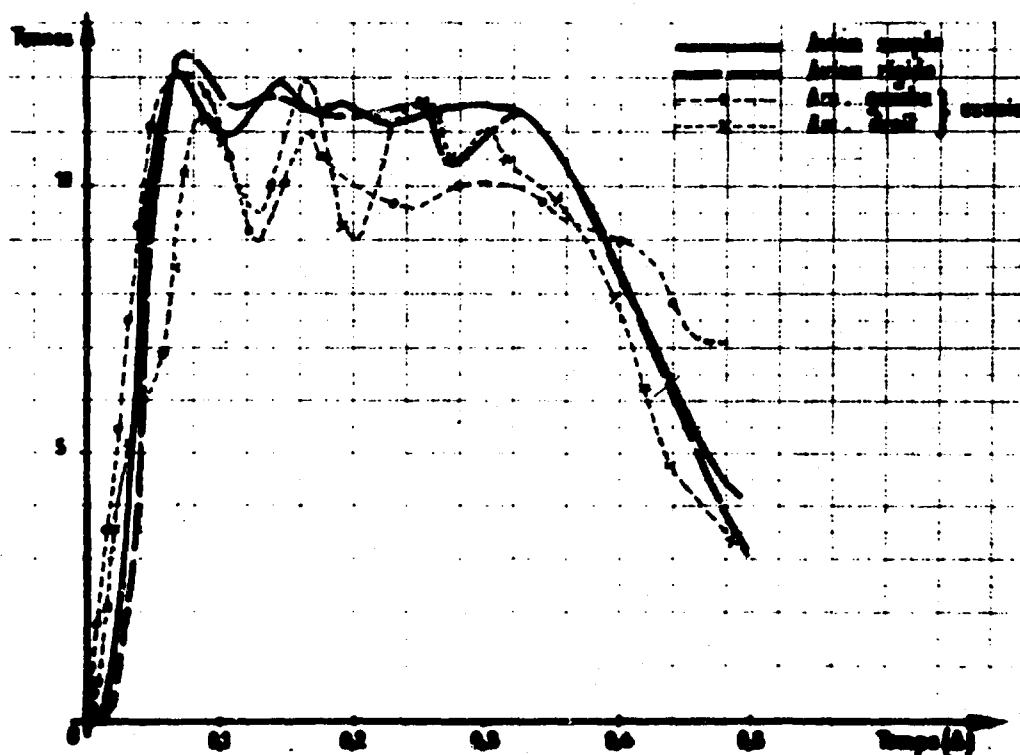


Mercur
Atterrissage

COMPARAISON DU CALCUL AUX ESSAIS DU VOL 46

PL 4

FORCE AMORTISSEUR

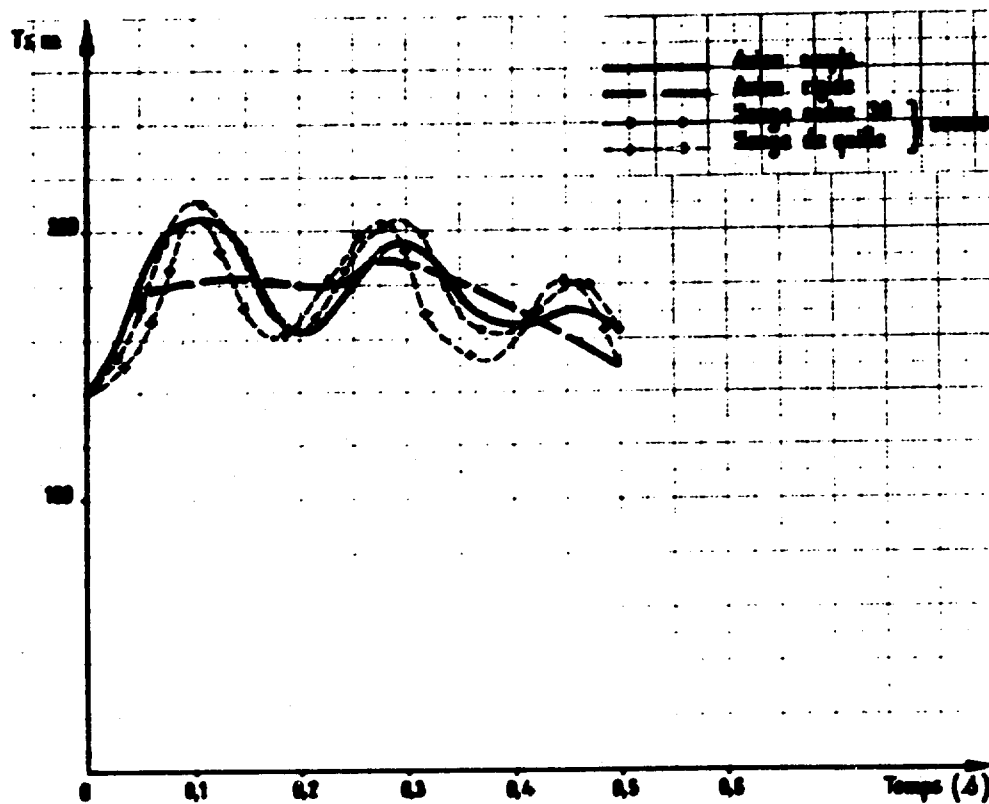


Mercur
Atterrissage

COMPARAISON DU CALCUL AUX ESSAIS DU VOL 46

PL 5

MOMENT DE FLEXION AU CADRE PRINCIPAL ARRIERE

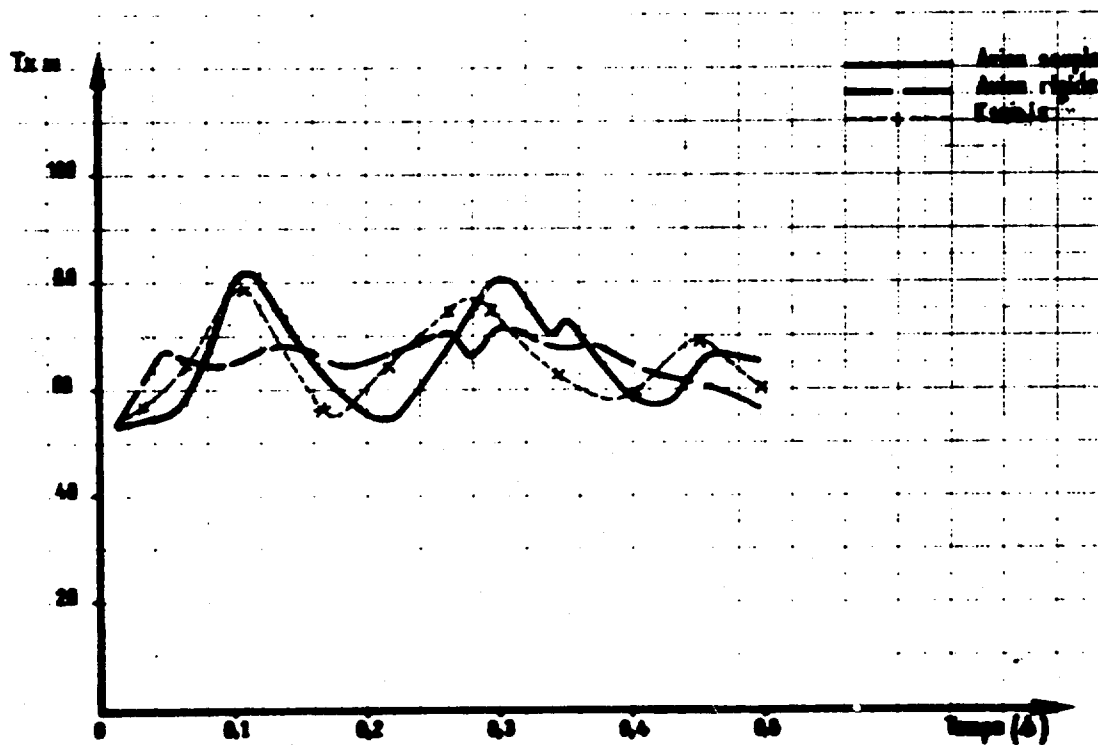


Mercur
Atterrissage

COMPARAISON DU CALCUL AUX ESSAIS DU VOL 46

PL 6

MOMENT DE FLEXION AU CADRE PRINCIPAL AVANT



Nous pensons qu'une réduction par base de chargement était aussi judicieuse que l'intégration directe sur ce problème, nous ne l'avons pas utilisée car l'avion n'était pas complètement idéalisé au moment de cette étude.

Une réduction modale essayée préalablement donnait des résultats très mauvais.

3.32 - Catapultage - roulement piste irrégulière

Nous avons utilisé un modèle très analogue pour la simulation du catapultage ; s'ajoute aux non linéarités du problème précédent, la simulation de la catapulte et de son élingue, ainsi que celle du Hold back et de sa rupture, voir planche 7.

Nous proposons d'étudier de façon analogue le roulement des avions sur piste irrégulière. Le modèle peut être linéarisé à l'exception du laminage et du frottement des amortisseurs ; en réduisant par base de chargement, le calcul par intégration directe doit être alors d'un coût extrêmement faible.

4 - PROBLEME DE TENUE RESIDUELLE

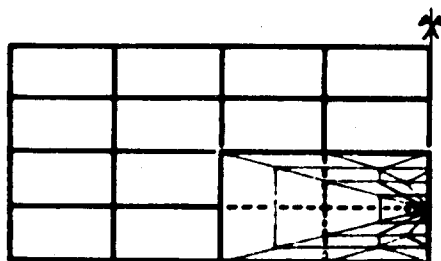
On peut artificiellement les décomposer en 2 familles.

4.1 - Calcul "fail safe"

C'est le calcul de la redistribution des contraintes après la destruction d'un élément structural.

Dans le domaine élastique ce type de calcul ne pose qu'un problème d'organisation et de prix de calcul, nous réduisons au mieux ces prix de calcul en utilisant une méthode de sous structuration "rigogne" (sous structure de sous structure) et du calcul de la matrice de flexibilité sur la frontière de la zone modifiée selon le principe suivant, l'équilibre de la partie modifiée s'écrit

$$[(K_0 - K_1) + K_2] X = F_0 - F_1 + F_2$$



K_0 = matrice de rigidité de la structure initiale condensée au niveau de la frontière avec la partie modifiée ; elle est obtenue par inversion de la matrice de flexibilité issue de chargement unitaire sur les points de la frontière.

K_1 = Matrice de rigidité initiale de la partie modifiée condensée à la frontière.

K_2 = Matrice de rigidité de la modification.

F_0, F_1, F_2 second membre réduit correspondant.

Par ce processus de calcul de la modification résulte uniquement de chargement supplémentaire sur le modèle initial et du maniement de matrices relativement petites.

On ne fournit, en donnée supplémentaire, que la modélisation de la modification.

Les résultats de ces calculs sont généralement analysés "classiquement", pour déterminer si la rupture va se propager.

Dans les cas où cette analyse n'est pas simple, on déduit de ces calculs les charges pour un essai partiel.

4.2 - Propagation de déchirure

Nous avons envisagé une approche du même type que celle utilisée en fatigue avec le coefficient concentration de contrainte.

Le coefficient :

$$K = \frac{1}{2e} \frac{\partial W}{\partial a} = \frac{1}{2e} X_t \left[\frac{\partial A}{\partial a} \right] X$$

W = énergie interne

a = longueur de déchirure

e = épaisseur

X = déplacement discrétisé en E.F

A = matrice de rigidité

K est considéré comme caractéristique de la propagation de la déchirure et permet la comparaison avec une éprouvette simple de même matériau.

Cette théorie, assez bien vérifiée en fatigue où la contrainte est en général perpendiculaire aux lèvres de la déchirure, demande encore à être développée et étayée par l'expérience, pour des charges quelconques, tel que l'on peut les trouver au bord des déchirures d'impact.

En outre, elle peut nécessiter des calculs non linéaires (cas de pression interne).

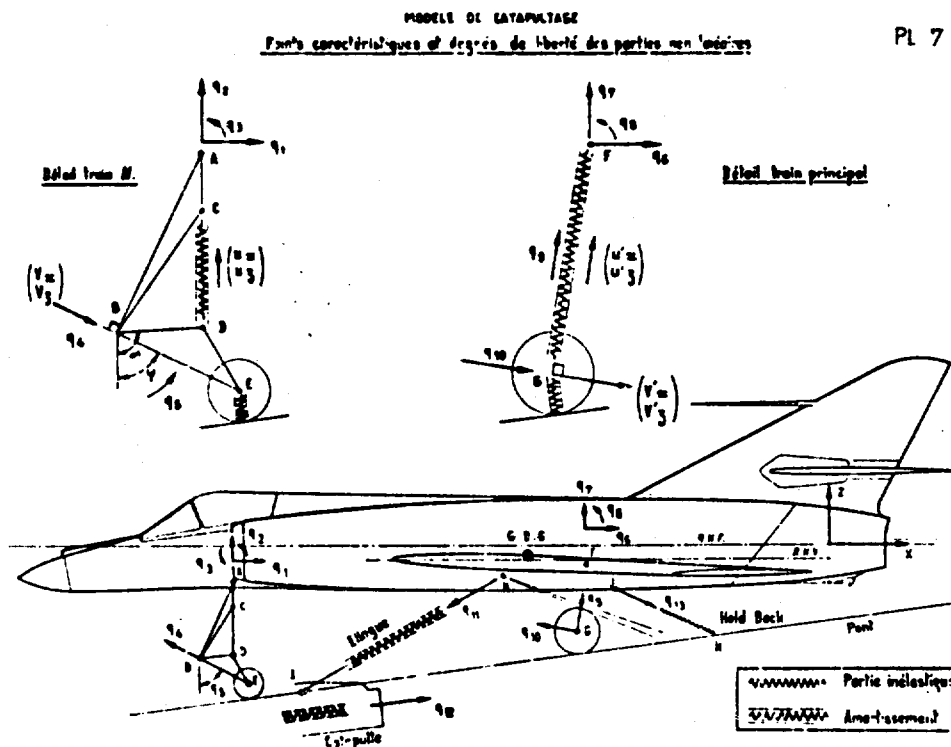
5 - CONCLUSION

Nous avons présenté une suite de méthodes de calcul que nous avons utilisé pour la plupart, notre sentiment est qu'en dehors des problèmes avec amortisseurs, elles ne permettent pas une confiance dans le calcul qui pourrait dispenser d'effectuer des essais.

La raison est qu'au voisinage de la rupture, l'énergie est absorbée par les mécanismes les plus complexes (plasticité, cisaillement ou arrachement de rivets, etc...) dont la représentation exacte est très complexe et souvent mal connue physiquement.

Il faut remarquer que dans les cas difficiles (choc d'oiseaux, et de projectiles sur structure courante), un calcul, non seulement peut apporter une aide à l'interprétation, mais permet de vérifier les conditions aux limites des éprouvettes d'essais et de réduire la taille et le coût de ces derniers.

Nous pensons bien mieux dominer les problèmes de choc sur amortisseur comme l'a montré le problème de l'atterrissage : c'est heureux car les charges induites dans ce cas sont dimensionnantes pour les fuselages d'avion civil.



COMPUTER METHOD FOR AIRCRAFT VULNERABILITY
ANALYSIS AND THE INFLUENCE OF STRUCTURAL
DAMAGE ON TOTAL VULNERABILITY

by

Dieter K a r d e l s

INDUSTRIEANLAGEN-BETRIEBSGESELLSCHAFT MBH
8012 O t t o b r u n n , Einsteinstrasse
W e s t - G e r m a n y

S U M M A R Y

This paper presents an overview of the methodology developed by the Industrieanlagen-Betriebsgesellschaft (IABG), Ottobrunn, West Germany, for the analysis of aircraft vulnerability. This methodology consists of two basic computer models, the so-called ammunition and target models. These models are so constructed that the evaluation of ammunition types such as AP, API, HEI with both impact and proximity fuzes, and fragmenting warheads is possible, as is a detailed vulnerability assessment of a particular aircraft. The approach taken in this paper is the interaction of various submodels in order to show the different types of possible outputs. A special emphasis is given to the influence of structural damage and aerodynamic capabilities on total aircraft vulnerability. Some test data and model prediction results are also graphically presented.

With regard to the objective of this meeting to discuss available methodology and test results related to the assessment of in-flight damage tolerance as a part of the structural design process, the purpose of this briefing is to present a methodology developed by the IABC for an overall Aircraft Vulnerability Assessment.

The analysis and evaluation of a complex process such as in-flight damage inflicted by military weapons is, in general, possible only if a sufficiently sophisticated abstraction of this process can be materialized in a model. Hereby, the quality and confidence of the output data is directly dependent upon the quality of the weapon and target input data as well as the resources available for experimental investigations.

Due to the design complexity of high performance aircraft and their representation as relatively soft targets it is advisable to describe the aircraft as real and as detailed as possible. With regard to the operational capabilities of the aircraft, the description must be so managed, that the influence of damage to components of the major-subsystems, the structure or the engine can be evaluated with the desired accuracy.

The objective of the study is to establish an adequate data base for systems analysis and operational research studies relating to

- o Air Defense Weapon Systems Effectiveness
- o Aircraft Vulnerability
- o Military Requirements and System Specifications
- o Operational Procedures and Tactics for AAA-, SAM- and Aircraft Weapon Systems.

The output of the below-mentioned submodel data analysis will be

- o the effective vulnerability analysis for a special aircraft type when considering different ammunition and warhead configurations
- o the determination of design weakpoints
- o the criteria for use in design, development and evaluation relating to
 - allocation and efficiency of armor
 - change from component location
- o assessment of critical components within a failure mode and effects analysis
- o development of kill categories for classification of the effects of damage on the operational capabilities of the aircraft
 - effect of subsystem arrangements and assembly upon A/C vulnerability.

A necessary prerequisite to assessing the effects of specified damages involves developing classification of those damages. These classifications, called kill or damage categories, are defined as those damages which result in a particular class of effects on the operational capability of the aircraft. For use in this study a set of four categories were developed. On the basis of a failure mode and effects analysis a list of critical components was categorized.

Some examples for these categories:

- o Catastrophic aircraft loss ($t = 15$ sec.):
such a condition will usually arise when one or more of the following conditions apply:
 - Loss of pitch control
 - Loss of control in at least two axes
 - Injury of single pilot (assuming that, for a two seat version, the navigator is not able to control the aircraft)
 - Total loss of engine power
 - Residual load factor less than 2 g
- o Aircraft attrition ($t = 5$ min)
 - Loss of all flight control power
 - Loss of aileron and stabilator power
 - Bleed air duct rupture in close proximity to fire vulnerable components
 - Uncontrolled fuel leakage
 - Uncontrolled fuel and oil fire
 - Loss of minimum engine power requirement
 - Flight load due to structural damage e.g. of less than 3.8 g (depending on the flight profile)
 - Evaluation of the flight qualities on the basis of Mil-F-8785 F Category 1, 2 and 3:
 - Cat. 1 - Flight capability during the entire mission phase
 - Cat. 2 - Flight capability remains, but higher g's on the pilot and/or a certain decrease in the mission capability
 - Cat. 3 - Aircraft still controllable, but increasing high g's on the pilot or the mission can no longer be accomplished, or both
- o Mission inability
 - Loss of engine power
 - Degradation of aircraft control
 - Performance limits
 - Flight load factor for damaged structures less than the value is needed for the mission
- o Unable to land normally
 - Landing gear failure
 - Brake failure.

Fig. 1 shows the basic model concept of the study. The overall vulnerability model is divided into two large models, the ammunition model and the target model. A brief description of these models is published in the AGARD ADVISORY Report No. 47 Volume 3 on Aircraft Vulnerability Analysis. The nature of the methodology generated for the ammunition and target model is so generalized, that an evaluation of various ammunition types such as AP, API, HEI with impact

and proximity fuzes and fragmenting warheads is possible.

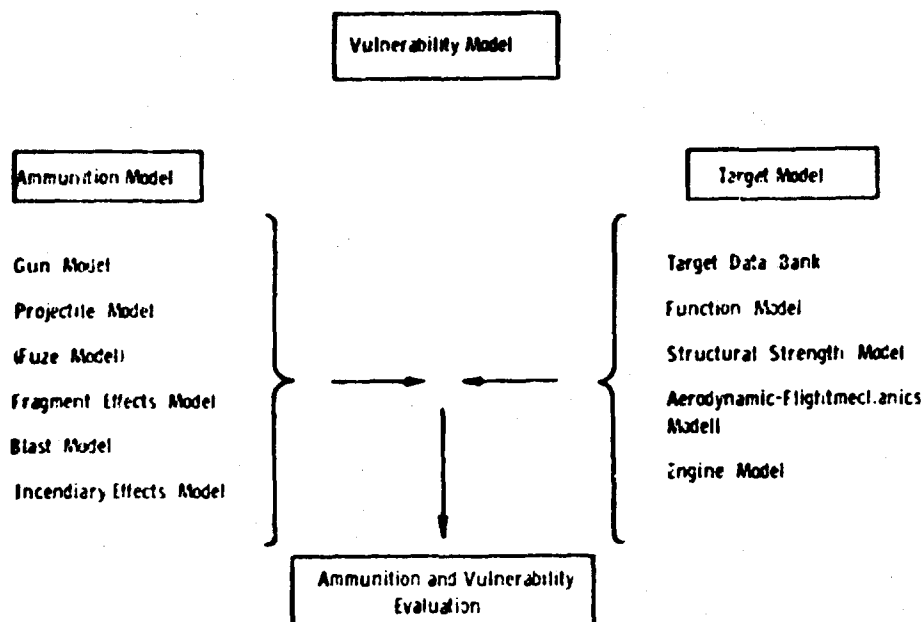


Fig. 1: The basic model concept of the study

The threat situation is defined in terms of the basic damage mechanism. Each of the mechanisms is represented by a mathematical submodel which calculates the damage, depending on the type of weapon and the encounter situation.

The ammunition model incorporates five major submodels, namely the

- Gun Model
- Projectile Model with Fuze Model
- Fragment Effects Model
- Blast Model
- Incendiary Effects Model.

While the ammunition model simulates the physical process taking place from the moment when projectiles arrive in the target area, the target model provides information as to the operational effects of ammunition damage on particular aircraft in a dynamic manner.

To this end, the target model consists of a detailed target data bank and four major submodels relating to

- Interrelation of Aircraft System Function:
- Structural Strength Determination
- Aerodynamic and Flightmechanic Estimations and
- Engine Power Determination.

Fig. 2 shows the outer surface of the aircraft, which is approximated by relatively simple mathematical functions for example, ellipsoids, cones and elliptic truncated cones.

Nearly 5000 components of the equipment systems such as the fuel system, pneumatics, control, electrical, engine and also structure, are incorporated into the mathematical descriptions of the fuselage, wings and the empennage. The shapes of these components are idealized by geometrical bodies.

The function model represents the functional interconnection of the aircraft's components in order to determine the results of causalities and failures among the elements of a system. All systems have been analysed with respect to their functional process. By means of circuit algebra all the components of a system have been connected and described in a logical circuit diagram.

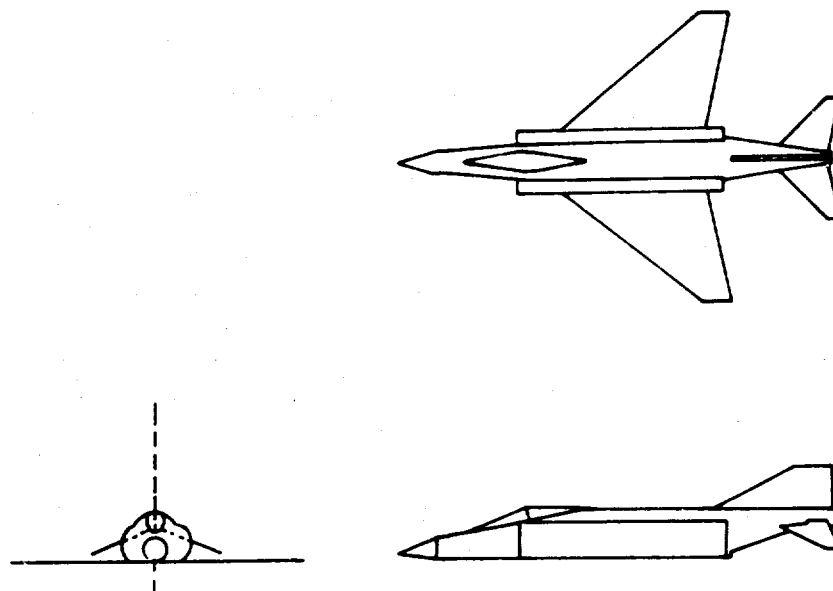


Fig. 2: Geometrical description of an aircraft as used in the computer program

Fig. 3 shows for example the network of a typical hydraulic system. The interrelation of the logical networks of all the subsystems (fuel, electrical, control, etc.) describes the integrated functional process of the aircraft.

In case of a hit, failing parts can be identified as belonging to a system or a subsystem. The resulting information as to the state of one system may be an initial value for the determination of the state of another one. Fig. 4 and 5 illustrate a typical model output.

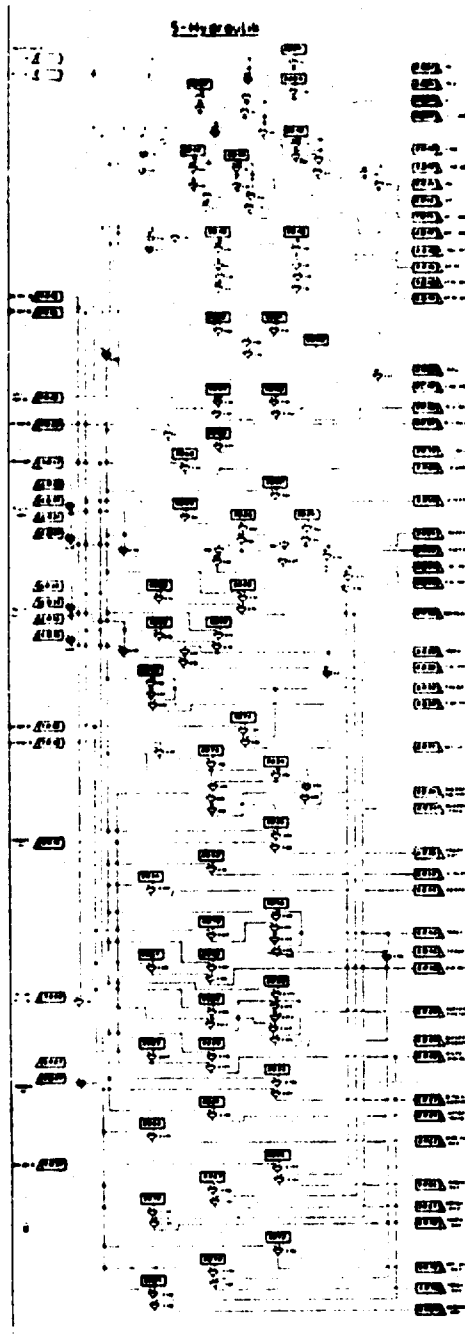


Fig. 3: Network of a typical hydraulic system

EFFECTS OF 1. HIT ON A/C STATUS

EFFECTS OF 1. HIT ON ENGINE

STARTER WITHOUT FUEL SUPPLY
 PRIMER DUCT WITHOUT FUEL SUPPLY
 HYDR. PUMP 1 FAILURE AFTER 10 MIN. AT THE LATEST
 HYDR. PUMP 2 FAILURE AFTER 10 MIN. AT THE LATEST
 GENERATOR 1 FAILURE AFTER 10 MIN. AT THE LATEST
 GENERATOR 2 FAILURE AFTER 10 MIN. AT THE LATEST
 TACHOGENERATOR FAILURE AFTER 10 MIN. AT THE LATEST
 RESTARTING IMPOSSIBLE AFTER 10 MIN. AT THE LATEST

EFFECTS OF 1. HIT ON CONTROL SYSTEM

LEFT AILERON OPERABLE RETARDATION POSSIBLE
 RIGHT AILERON OPERABLE RETARDATION POSSIBLE
 STABILATOR IS OPERABLE RETARDATION POSSIBLE
 RUDDER HYDRAULICALLY OPERABLE FOR 2-4 TIMES
 LEFT SPOILER FAILURE
 RIGHT SPOILER FAILURE
 FLAPS FAILURE
 LEFT AIRBREAK FAILURE
 RIGHT AIRBREAK FAILURE

EFFECTS OF 1. HIT ON FUEL SYSTEM

BOOSTERTANK SYSTEM FAILURE
 MAINTANK FAILURE. SELECTING VALVE FOR WING TANK OPERABLE
 FUEL SYSTEM FAILURE, EMERGENCY LANDING IN GLIDE
 TOTAL BREAKDOWN OF FUEL SYSTEM

EFFECTS OF 1. HIT ON HYDRAULICS

POWERSYST. EMERGENCY SUPPLY, GEN.PUMP INDICATOR 1500 PSI
 UTILITYSYST.FAILURE, LANDING GEAR BY EMERGENCY PUMP OPERABLE
 ELEVATOR EMERGENCY OPERATING
 RUDDER CAN BE OPERATED 2-4 TIMES BY HYDRO RESERVOIR
 AILERON ACTUATOR EMERGENCY OPERATING
 SPOILER ACTUATOR FAILURE.
 AIR BREAKS NOT OPERABLE
 FLAPS NOT OPERABLE
 LANDING GEAR EMERGENCY OPERATING
 BREAKS EMERGENCY OPERABLE
 COMPRESSOR FAILURE
 AERIAL REFUELING SYSTEM NOT OPERABLE
 BOOSTER RELEASE MECHANISM NOT OPERABLE
 UTILITY SYSTEM PRESSURE INDICATOR FAILURE

Fig. 4: Output of the functional model

Fig. 5

HIT-CODE	TR 1 1 1
DISTANCES FROM AAA	HX = 1405 M HY = 400 M HZ = 374 h
SLANT-RANGE	1508 M
IMPACT-VELOCITY	721 M/S
IMPACT-ANGLE	37 deg.
IMPACT-LOCATION	FUSELAGE
IMPACT-COORDINATES	X = 640 CM Y = -0 CM Z = 12 CM
SIZE OF HOLE	115 QCM

APPLICATION OF DAMAGE CRITERIA ON THE AIRPLANE AFTER THE 1.HIT

THE AIRPLANE IS NOT ABLE TO FULFILL THE MISSION

CAUSED BY FOLLOWING EFFECTS:

BREAK DOWN OF CABIN AIRCONDITION

EQUIPMENT-COOLING LIMITED BY AIRSPEED AND DYNAMIC
PRESSURE

Within the Aircraft Vulnerability Analysis the influence of impact damage on aircraft wing and empennage structures has been of special interest in relation to the operational capability of the aircraft.

The methodology and applicable computerized techniques, which together can be used to predict the reduced load carrying capacity of inflight damaged structure in relation to several types of threat and aircraft design, is discussed in detail in Mr. J. Massmann's paper "Structural Analysis of Impact Damage on Wings" (Ref.4). This paper gives a brief description of a recently-developed Structural Strength Model and examines in greater detail the functions and characteristics of a Damage Model. A discussion of a Shock Wave Model and how it analytically determines the dynamic response of a pressurized flat plate is also presented. Test and Finite Element results are compared with model-predicted results in order to determine model credibility. The pressures resulting from the detonation of ammunition are discussed and the contributions of each of the pressure components to the entire response are illustrated. Some advantages of a new Fragment Model are mentioned and the results from such a model are compared with appropriate test data.

With regard to the necessary core storage and computer time for a special structural analysis of impact damage on wings, a simplification of the Structural Model was performed.

In accordance with the experimental and model data, the wing was subdivided into areas of similar vulnerability. On the basis of these calculations, we made the assumption that every point within the area has the same reduced maximum load factor after a hit has occurred.

Fig. 6 shows, depending on the location of the impact and the type of high explosive ammunition, the calculated residual load factors for a typical wing configuration. Within the computer model these residual load factors are stored in a special matrix for calculation of the residual strength after a hit.

Within the scope of the simulation model, the following Figures depict the results of 71 single wing hits. For the sample calculation, the effects of a special ammunition caliber on a two spar cantilever wing of the RF-84 have been investigated.

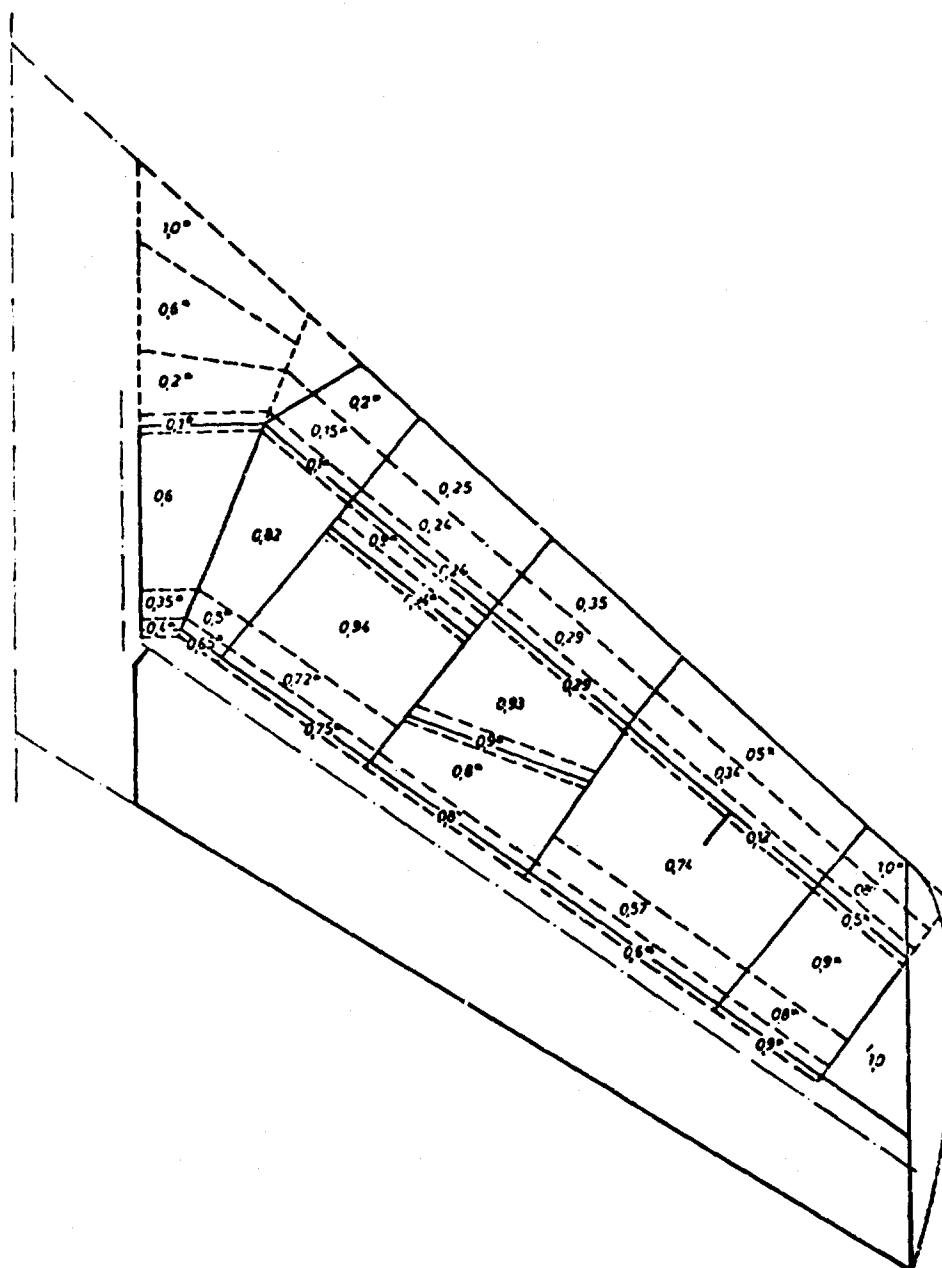


Fig. 6: The calculated residual load factors for a typical wing type

Fig. 7 gives, for example, a survey of the hit distribution on the target. The data analysis enables one to make precise statements about the status of the aircraft according to the damage categories. The information on hits causing attrition by system or structural failure is demonstrated by different symbols on the Figures.

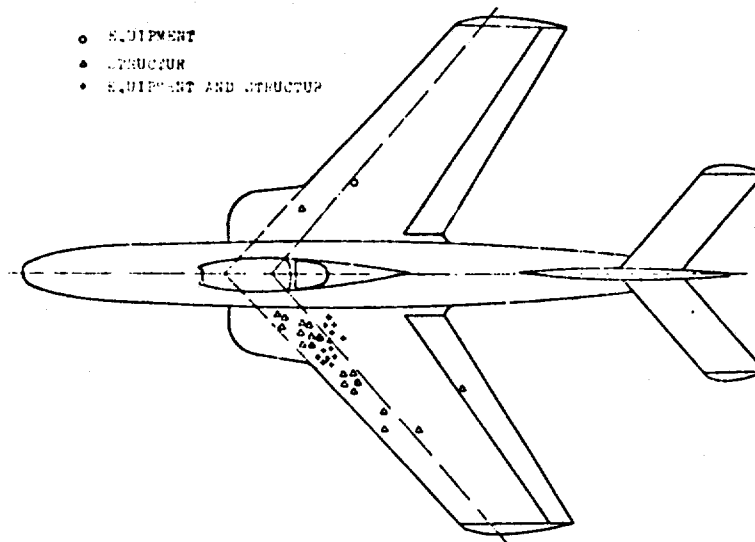


Fig. 7: Hit distribution on the target

Fig. 8 shows the detailed damage analysis subdivided into damage relating to mission inability and attrition. For each category the portion of damage is cataloged in relation to system failure, structure failure and both system and structure failure. The results of this calculation, the effect of ammunition at the target, as well as the resulting consequences for the target, cannot be transferred in general to other aircraft types.

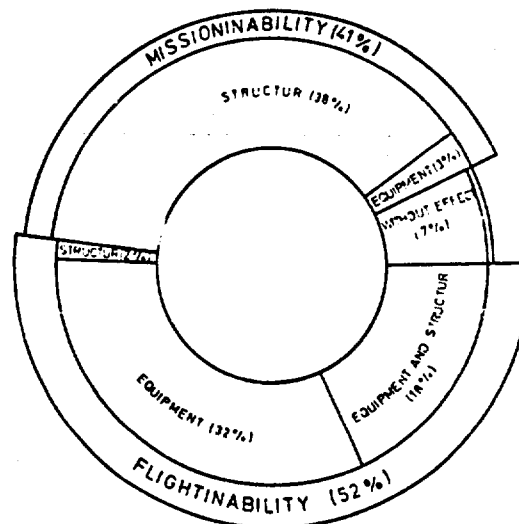


Fig. 8: Percentage of A/C wing failures due to equipment and structural damage

With the forementioned submodels, aircraft damage was analyzed only from the viewpoint of equipment and structure with a rough correction for the influence of aerodynamics. With a special submodel developed by MBB in Hamburg the analysis of stability, maneuverability and performance capability for a damaged aircraft can be made (Ref. 5).

Fig. 9 shows the block diagram of the aerodynamic-flightmechanics model. As input for the two main blocks, a number of input data must be specified.

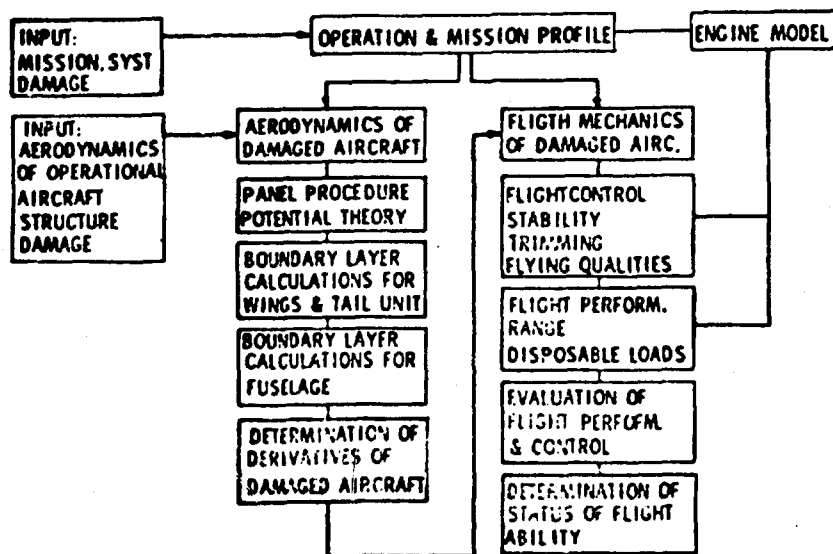


Fig. 9: Block diagram of the aerodynamic-flightmechanics model

This data includes the full airframe geometry and the complete aerodynamic characteristic of the undamaged aircraft as well as the range of flight conditions of the mission, the damage geometry (position and size of damage) and type of system damage (damage of engines, automatic control systems or actuators).

When we started the work on the aerodynamic portion of the program, there were no methods known to us for calculating the aerodynamic data of, for example, a wing with a hole. However, some wind tunnel test results on additional drag of open bomb bays and some results of wind tunnel tests on a damaged vertical tail were available. Two ways of solving the problem were considered:

- A number of windtunnel tests involving the changing of parameters over a wide range of wing and damage geometry
- A theoretical method to calculate influence of damage on the aerodynamics of wing and compare the results with wind tunnel test data.

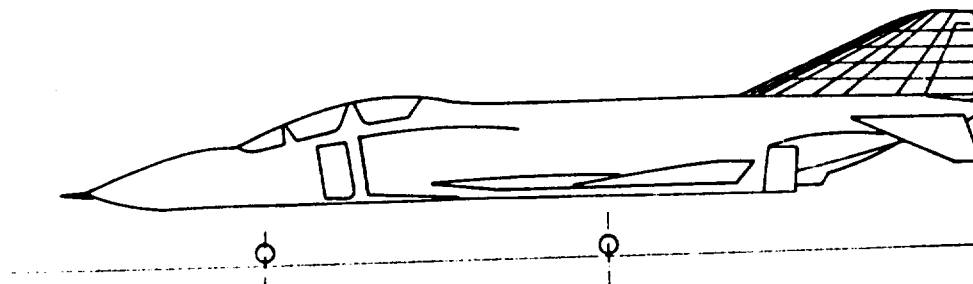
The available and successful methods for calculating the aerodynamics of undamaged wings such as lifting line theory or lifting surface theory are unsuitable for calculating wing damage. So only the panel method was useful for our purpose of investigating the effects of local disturbances on the wing surface.

The panel method (a singularity method) calculates the potential flow around the body under consideration. This means that no friction or boundary layer separation and compressibility effects are taken into account. This must be done by special corrections from DAS, JACØB and JUNGCLAUS in the procedure. Using the panel method,

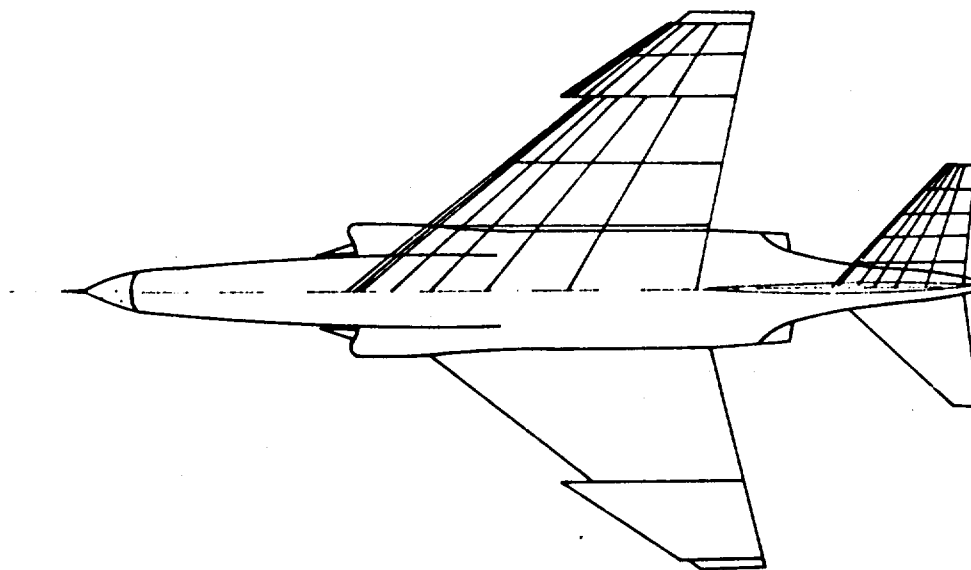
the surface of the airframe is covered with panels, each fitted with a source-sinkpoint and a pivot point. On wing and tail surfaces, series of horse shoe vortices are also provided.

To save computation time the aerodynamic data for wing, fuselage and tail surfaces were calculated separately.

The distribution of panels was performed in the following way: Wing or horizontal tail was covered with 140 panels (10 strips for 14 panels) and fitted with corresponding horse shoe vortices. This is the minimum number to obtain accurate results and the maximum number to obtain short computation times or low costs (see Fig.10).



Panelling of vertical tail surface



Panelling of wing and horizontal tail surface

Fig. 10: Panelling of wing and tail surfaces for calculations with the aerodynamic model

Now, how can damage or a hole in a wing be simulated?

Damage to the wing by ammunition can be of many forms and there is no chance of realizing all these forms in the simulation. Wind tunnel test results showed that the main influence is exercised by the hole position and hole size and that there is only a small effect of the hole form. So the parameter "hole form" will be neglected.

To obtain a good simulation many different ways of panel distribution around the hole were tried. But the simplest form of simulation produced the best results. To describe a hole by the panel method, we only have to omit the panels which correspond to the hole, which is assumed to be circular. Different positions or areas of the real hole or damage and the substituted panel hole are corrected by special factors. In the case of damage to the wing leading edge - and only in that case - the pannelled airfoil must be closed in the front part by additional panels.

Past experience has shown that correct absolute values of aerodynamic data cannot be expected from singularity methods for damaged or for undamaged aircraft. So a trick was used to get usable aerodynamic data for the damaged aircraft: By the aid of the panel method we calculated the data for the undamaged aircraft as well as for the damaged aircraft. The difference between these values - that is the influence of the damage - is added to the known data for the undamaged aircraft from flight or wind tunnel tests.

As well as these calculations, a series of wind tunnel tests was performed on a semispan-rectangular wing model with holes to check the calculation results.

Test results and calculation results are compared in the diagrams 11 - 15 (the shadowed area on the wing sketch shows the damaged area).

In the mathematical model the aerodynamic data are converted into derivatives which are used in the flight mechanics model part. Now, with this data, the flight characteristics will be calculated in the flight mechanics block for aircraft with or without automatic control systems. For this purpose, methods are chosen which are frequently used during the development of an aircraft.

For example, the dynamic longitudinal and lateral stability are determined from so called eigenvalues, special forms of the damping and frequency of the uncontrolled aircraft motion. This form of result is favorable for the assessment of the aircraft since the requirements for flight characteristics (for example, in the MIL SPEC 8785 B) are represented by limitations in damping and frequency for all modes of aircraft motion. Later in the program the ability of the aircraft to be trimmed is checked. Rudder, elevator and aileron deflection available after trim are the basic data for the determination of the maneuverability.

In the flight performance program block the loss of range due to additional drag and the ability for curved flights are checked.

The results of the flight mechanics program blocks for the damaged aircraft in the operation points will be compared within the program with minima and maxima of the allowable range for these values. Most of these requirements are taken from MIL SPEC 8785 B, i.e., the minima and maxima for stability of aircraft motion. Some nominal values must be fed into the program by the user/operator (for example, operational range and information about curved flight).

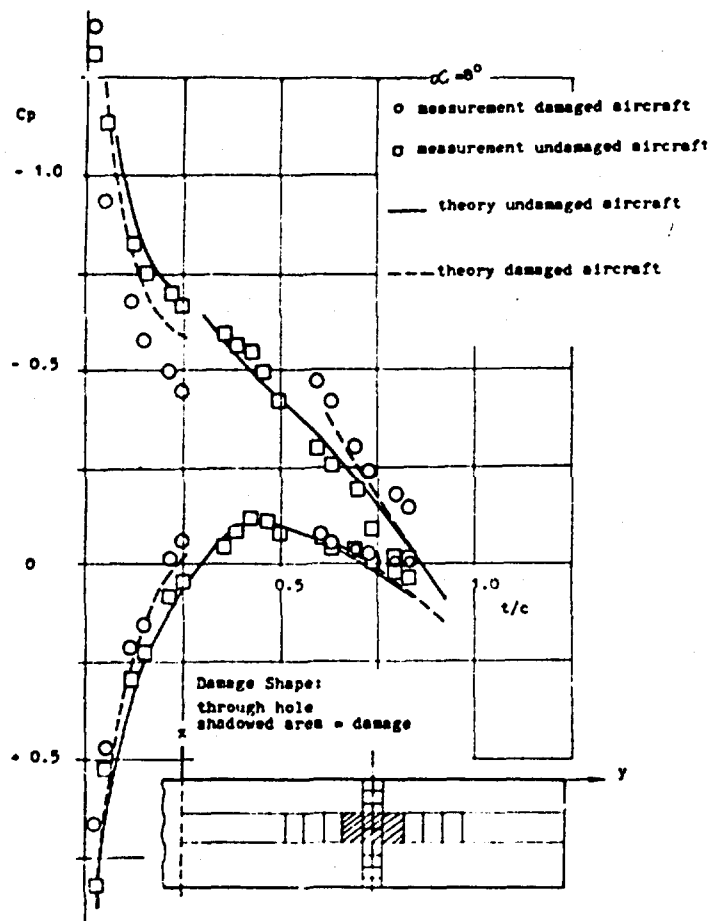


Fig. 11: Comparison of measured and calculated chordwise pressure distributions of damaged and undamaged rectangular wing

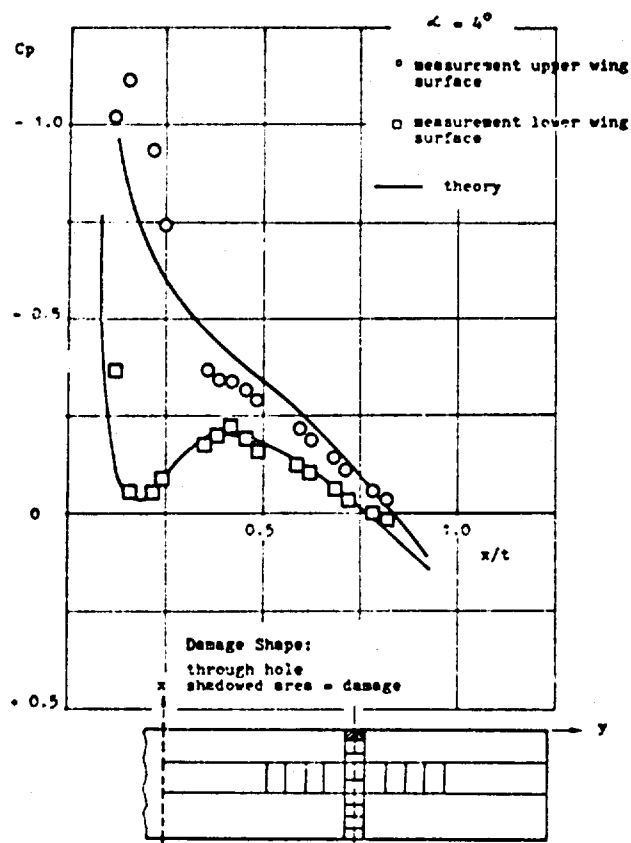


Fig. 12: Comparison of measured and calculated chordwise pressure distribution on a damaged rectangular wing (nose damaged)

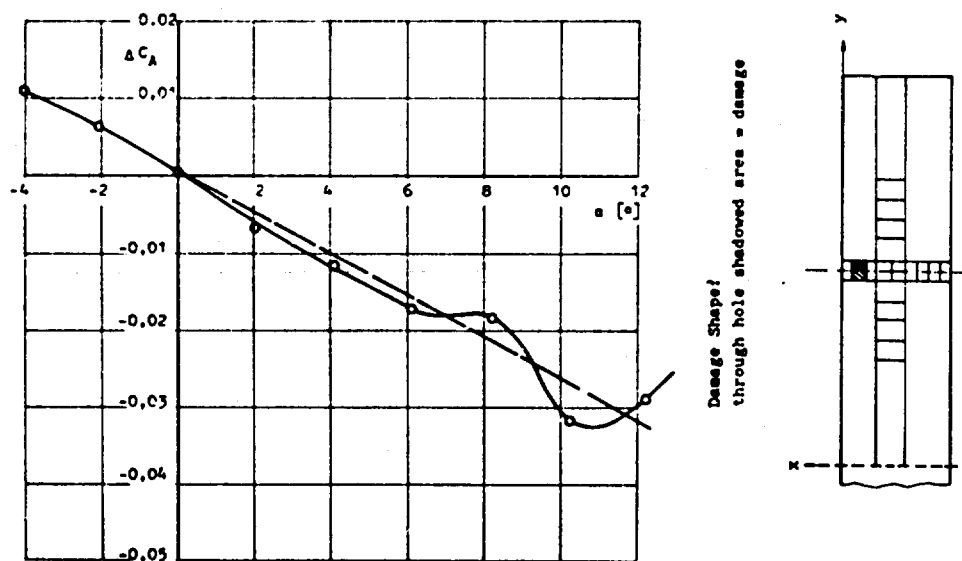


Fig. 13: Change of lift coefficient due to damage on a rectangular wing

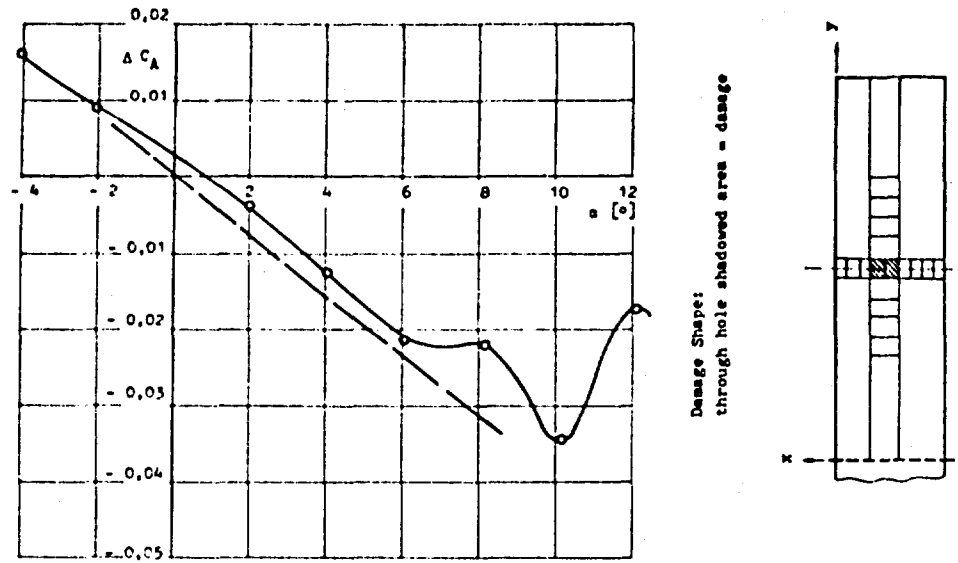


Fig. 14: Change of lift coefficient due to damage on a rectangular wing

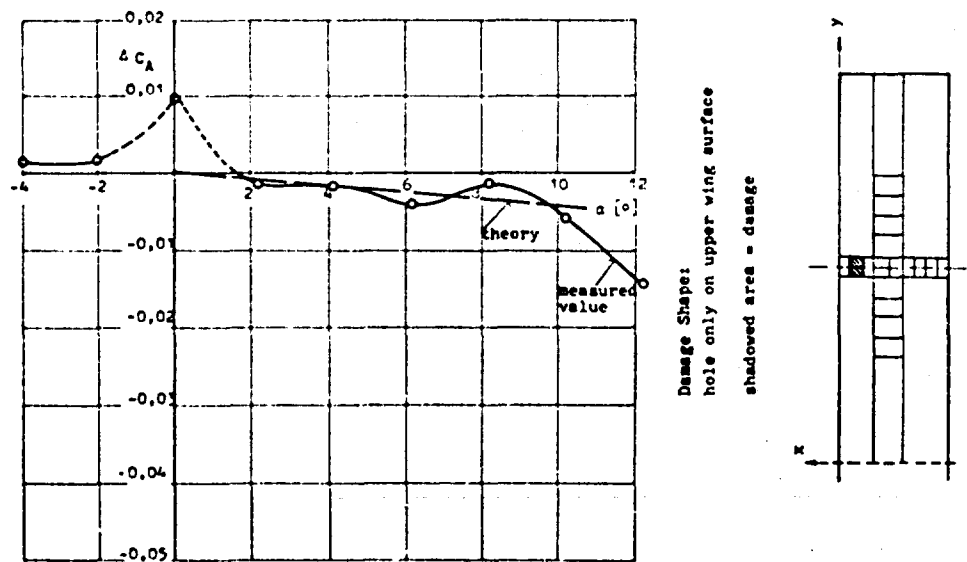


Fig. 15: Change of lift coefficient due to damage on a rectangular wing

After the assessment of the characteristics and performance, the results are stored on computer tapes and are printed out on line printer.

The next Figure shows some results from calculations:

Fig. 16 shows the roll moment coefficient due to wing assymetry for different wing damages of an RF-4. The hole is, as in the following diagrams, a hole through the entire wing (i.e., a through hole) with equal damage area on upper and lower wing surface. (Specified hole areas are those of only one hole, for example, that of the upper wing surface). The aircraft can, independent of attack, produce a roll moment coefficient by aileron deflection of maximum $C_l = 0,020$. The roll moment due to damage is linear and dependent on the angle of attack and, in the landing phase, is about three times the value shown in the graph. So it is clear that, at low speeds, a special A/C with a damage of more than 3 ft^2 in the leading edge area of the outer wing cannot be trimmed by aileron and it will be lost.

Fig. 17 shows the value $\Delta(\omega_o^2/n_d)$, a measure of dynamic longitudinal stability. Good flyable fighter-aircraft need a $\Delta(\omega_o^2/n_d) = 0,28$ or more. At less than $\Delta(\omega_o^2/n_d) = 0,16$ the aircraft can no longer be flown safely. This means that by a change of $\Delta(\omega_o^2/n_d) = -0,12$ the aircraft can become unflyable. This value can be reached by leading edge damage (through hole) of about 5 ft^2 as shown in the diagram.

The usage of this program is limited in certain respects. Such limitations are caused by the mathematical methods which are used or by the scheme of the program. It can only be used to analyze subsonic flight ($Ma = 0.9$). Because of the linearity of the panel method the aspect ratio of the wing must not be too low ($A \geq 1.8$). The speed must be ($V \geq 1.2 V_S$). The program is so formed that the aircraft must be a monoplane (no biplane!), one horizontal tail and one vertical fin. Wings or tail surfaces may have only one inconstancy of contour on each side and the contour must be unchanged during one computer run. These limitations can be removed by moderate changes in the program.

The engine model, developed by the DFVLR in Braunschweig, consists of three sub-models which describe mathematically

- the position, shape and material of the components of the engine and its subsystems. (Fig. 18 illustrates, for example, the geometrical description of the compressor section)
- the capability of the engine-subsystems when components of these systems are damaged
- the performance of the engine, when the actual gaspath-components are damaged

in order to

- determine the point of impact and the damaged components and
- to obtain on the basis of a failure mode analysis information about the disturbed function of the
 - o fuel system
 - o lubrication system
 - o hydraulic system
- calculate the performance data of the undamaged and damaged engine for any chosen flight altitude and Mach number and the demanded thrust.

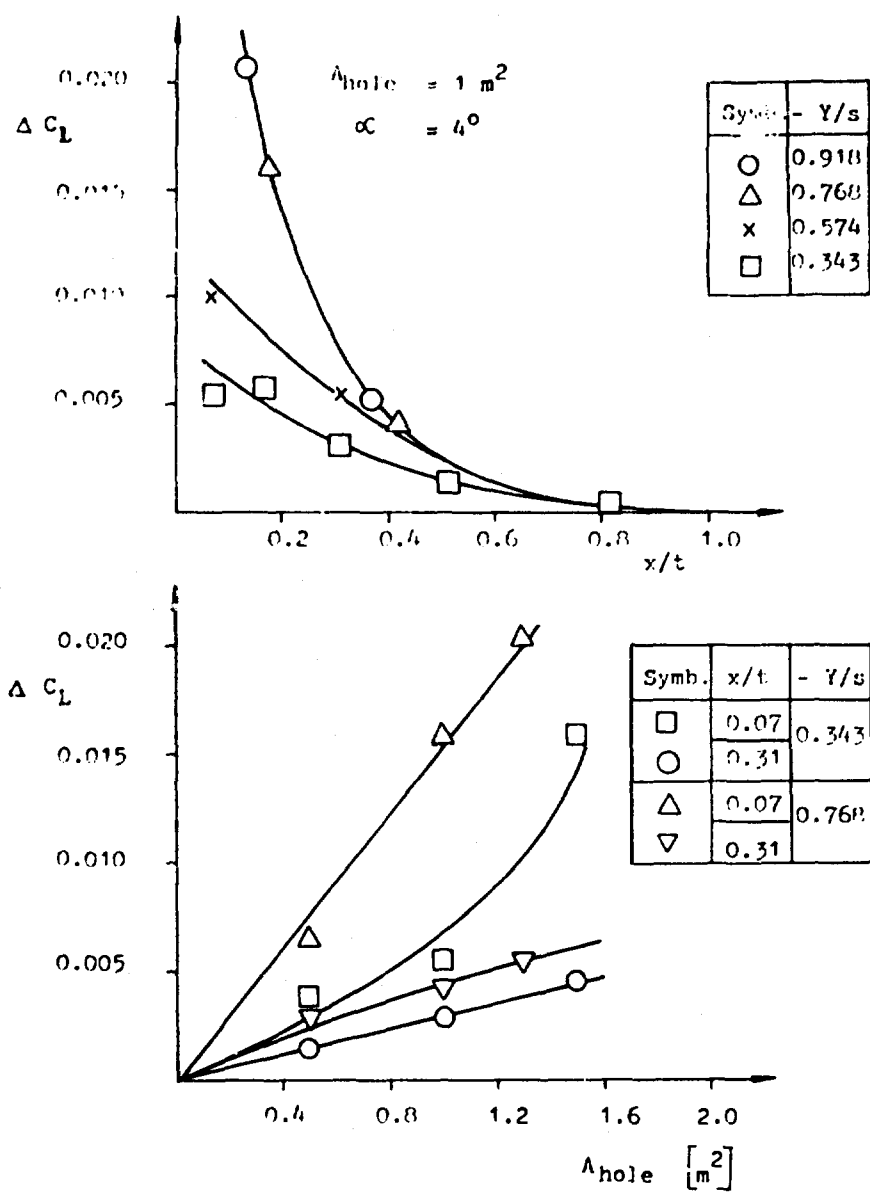


Fig. 16: Rollmoment due to wing asymmetry by wing damage

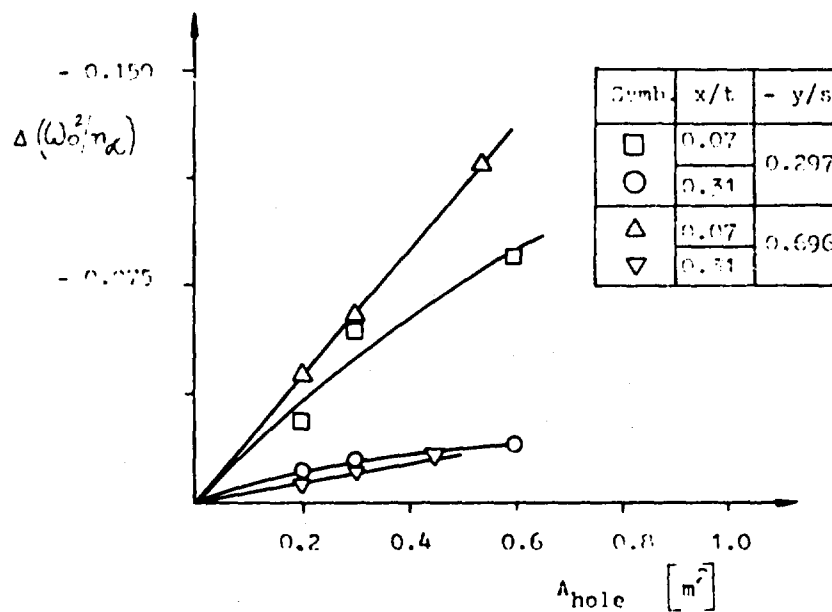
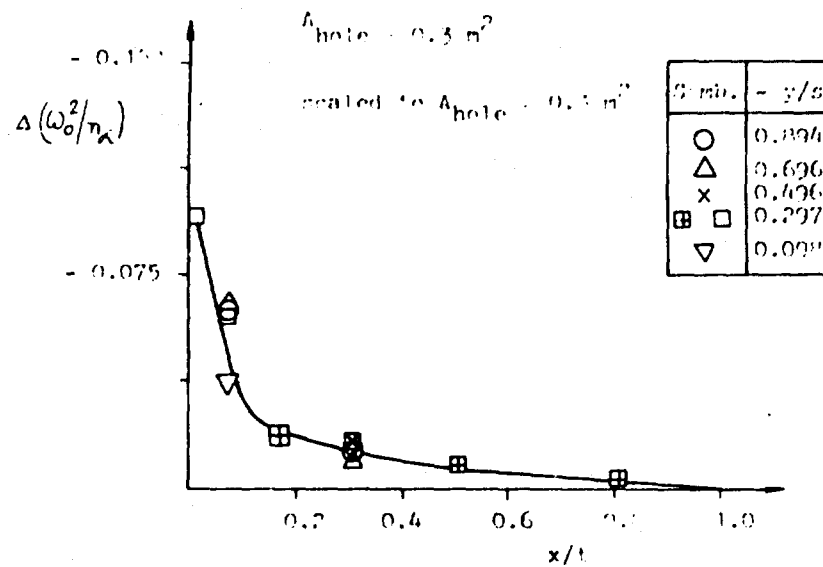


Fig. 17: Change in $\Delta(\omega_o^2/\eta_\lambda)$ of the longitudinal short period oscillation of the A/C due to horizontal tail surface damage

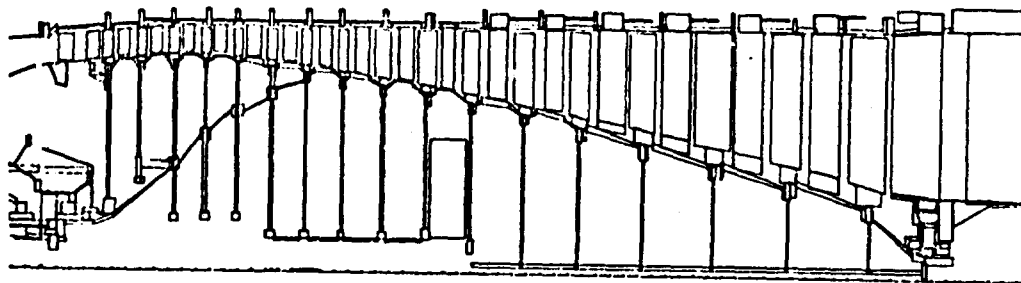


Fig. 18: Geometrical description of the compressor section

The computation of the influence of damage on the engine systems takes into consideration the

- o variable guidevan-system
- o variable nozzle-system
- o fuel control
- o lubrication system
- computing the influence of damaged gas-path-components for, e.g.,
 - o air inlet ramps
 - o compressor
 - o combustion chamber
 - o turbine
 - o after burner
 - o exhaust nozzle.

Fig. 19 gives a survey of the relationship between the different submodels for a vulnerability assessment.

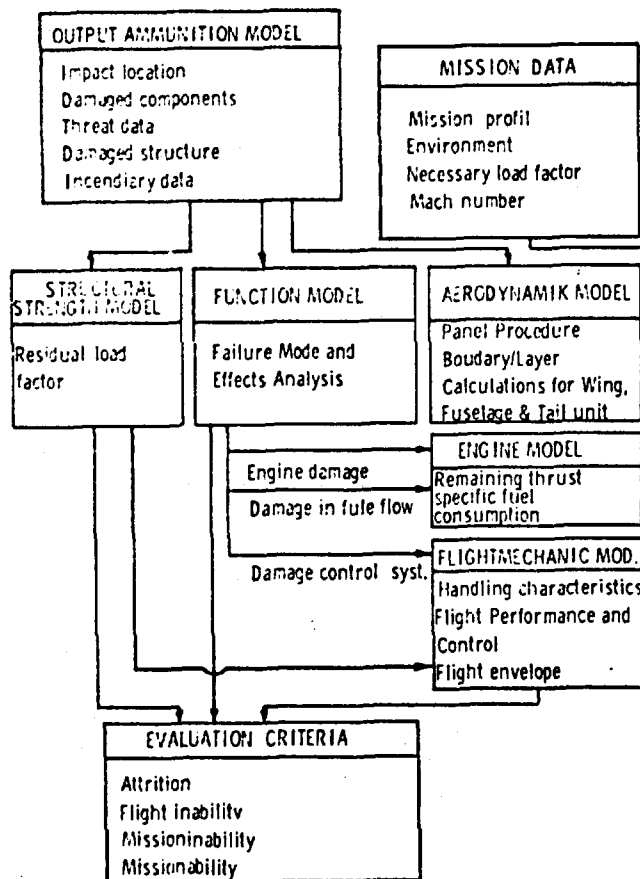


Fig. 19: Relationship between the different submodels of the study

The output of the ammunition model provides input data for the

- structural strength
- the function and
- the aerodynamics analysis.

With regard to the computer time the analysis will be done in three steps taking into consideration the specific damage criteria. If the conditions are satisfied, the computer run stops automatically.

This, in general, is a brief overview of the total structure of the IABG model which is currently operational on our CDC computer system. It can be said in conclusion that this model is serving our purposes well and is providing an accurate means of evaluating the effects of damage on the operational capability of aircraft.

REFERENCES

1. AGARD ADVISORY REPORT No. 47
Volume 2 on The Physical Vulnerability of Aircraft
2. AGARD ADVISORY REPORT No. 47
Volume 3 on The Physical Vulnerability of Aircraft
3. Program Description of the IABG
F-4-Vulnerability Model
B-SO-2007/02
4. Structural Analysis of Impact Damage on Wings
by J.Massmann, IABG/TFS
5. Aerodynamic-Flightmechanics Model
Dr.Weise, Messerschmitt-Bölkow-Blohm GmbH

DAMAGE TOLERANCE OF SEMIMONOCOQUE AIRCRAFT

Donald F. Haskell, Ph.D.
 Mechanical Engineer
 U.S. Army Ballistic Research Laboratories
 Aberdeen Proving Ground, Maryland 21005
 United States of America

SUMMARY

A combination of simple theory and test has been used to investigate the damage tolerance of semi-monocoque aircraft structure. The simple theoretical method which has been developed may be used to predict deformation, strain, and fracture of aircraft skin subjected to blast attack. Test results and predictions of the theory compare favorably. The method is used to analytically delineate the factors that significantly affect skin damage tolerance. For the conditions studied these factors, in decreasing order of influence, are: standoff distance, panel width, skin thickness, aspect ratio, skin ultimate strength, rivet spacing, and rivet hole diameter to skin thickness ratio.

In addition, test results of two types of semimonocoque helicopter tail booms damaged by bare explosive charges and small-caliber, high-explosive projectiles while under simulated maximum flight load show that both skin and the skin stiffening system are important in the damage tolerance of these structures. Damage tolerance of these structures is proportional to the section modulus of the undamaged section and inversely proportional to the amount of skin removed from the structure by the damaging agent. Furthermore, it is also demonstrated that large increases in damage tolerance can be achieved by increasing longitudinal stiffness.

INTRODUCTION

The genesis of this study lies in the need for a method for determining the tolerance of aircraft structure to the damaging effects of high explosive munitions. This need encompasses the requirements that the method be reasonably accurate and account for all the pertinent factors that influence aircraft damage tolerance. In addition, the method should be simple in form and execution so that practical answers can be easily obtained with minimum time and effort. These requirements represent a somewhat formidable task for a structural system, the aircraft, which depends in large measure for its successful operation upon the fine details of its design.

The present study addresses the subject: damage tolerance of semimonocoque aircraft to skin loss from blast attack. The object of the study is to develop an analytical base that can be used to delineate those factors that affect skin blast damage, their relative influence on skin damage tolerance, and the effects of skin damage in turn on the structural damage tolerance of the overall aircraft. Such knowledge of damage tolerance may then be employed in the design process, both in the design of damage-tolerant aircraft as well as in the design of antiaircraft munitions. It can also be used to assess the vulnerability of existing or proposed aircraft as well as in the vulnerability reduction of existing aircraft.

The report describes those factors that affect the blast damage tolerance of semimonocoque aircraft skin, discusses the relative sensitivity of skin blast damage tolerance to these factors, and relates these factors to the overall blast damage tolerance of helicopter tail booms and aircraft structure in general. The method that was developed and employed to analyze aircraft skin panels for blast damage and delineate the role of the various factors that influence skin blast damage tolerance is described and comparison between predictions of the method and skin panel blast test results is discussed. In addition, the test results of two types of helicopter tail booms damaged while under simulated flight load by bare explosive and/or small caliber, high-explosive projectile fire are discussed in terms of the tolerance of these structures to the incurred damage.

SKIN DAMAGE THEORY AND TEST

A combination of simple theory and test is used to investigate and evaluate the terminal effects of high-explosive antiaircraft munitions fuzed to detonate inside helicopter tail booms and aircraft fuselage structure. The analytical formulation treats the structure between frames as panels supported by frames and longerons. To account for inherent variations in fuze delay and projectile aimpoint, the model is capable of treating detonation at any point within the structure. The damage caused by detonation at such a spatially variable point is treated by an assumed first mode deformation pattern. The blast-deformation damage process is characterized by the law of conservation of energy and tail boom/aircraft fuselage fracture criterion. Expressions for the work done on the structure by the blast and structure strain energy are derived. The work done on the panel by the blast is found by considering the energy fluence of the blast wave incident upon the panel. Because of the gross deformation incurred by blast, the panel is assumed to behave as a rigid-linear strain hardening material. This allows the strain energy to be reduced to a simple expression which, when combined with the energy from the blast in the conservation of energy relation, yields explicit equations for deformation, strain, and stress. This inplane stress is combined with the average transverse shear stress at the panel edge to obtain the principal stress. Fracture is characterized by the maximum normal stress criterion. In this manner, all the pertinent material, geometrical, and explosive factors that characterize skin fracture from blast are accounted for.

The law of conservation of energy states that the work E done by the external forces in altering the configuration of the natural (or unstrained) state to the state at time t is equal to the sum of the kinetic energy K and the strain energy U . The strain energy U may be conceived as the energy stored in

the body when it is brought from the configuration of the natural state to the state at the time t . This law may be expressed by the equation

$$E = K + U. \quad (1)$$

The body system here is taken as an individual skin panel in the aircraft. The functions E , K , and U are defined as follows:

$$E = \iint [u\bar{X} + v\bar{Y} + w\bar{Z}] \cdot dA \quad (2)$$

$$K = \frac{1}{2} m (v_f^2 - v_i^2) \quad (3)$$

$$U = \int_V \bar{U} \cdot dV \quad (4)$$

where u, v, w = panel displacement in the short panel dimension direction, long panel dimension direction, and transverse directions, respectively;

$\bar{X}, \bar{Y}, \bar{Z}$ = external stresses in the u , v , and w directions, respectively;

A = surface area of the body over which the external forces are applied;

m = mass of the body;

v_f, v_i = final and initial velocities of the body;

\bar{U} = strain energy volume density;

U = strain energy; and

V = volume of the body.

The time interval over which this relation is applied is from an instant immediately preceding arrival of the blast wave to the time when the panel has come to rest. Since the initial and final relative velocities of the panel are zero, $K = 0$ whereby the conservation of energy law reduces to

$$E = U. \quad (5)$$

For convenience it is assumed that $\bar{X} = \bar{Y} = 0$. Further, if the external work is measured in terms of blast energy fluence, or rate of energy flow through a surface of unit area E_F , external work on the panel may be expressed as

$$E = \iint E_F \cdot dA \quad (6)$$

where the integration is taken over the panel surface and energy fluence is defined as

$$E_F = \int_0^{\Delta t} p u dt, \quad (7)$$

where E_F = blast energy fluence,

p = incident overpressure,

u = particle velocity, and

t = time from occurrence of the peak overpressure.

The typical blast wave pressure-time history may be expressed by the empirical equation

$$p = P \left(1 - \frac{t}{\Delta t}\right)^3 e^{-\frac{t}{\Delta t}} \quad (8)$$

where P = peak overpressure,

e = base of the natural system of logarithms, and

Δt = time duration of the positive overpressure phase.

Substitution of the pressure-time relation, Eq. (8), into the energy fluence definition, Eq. (7), and subsequent integration over the time duration of the overpressure Δt results in the relation

$$E_F = 0.1137 P u \Delta t. \quad (9)$$

Values of P , u , and Δt for a given explosive charge weight and standoff distance to the structure for 50/50 Pentolite may be obtained from Reference 1. Performing the integration of E_F given by Eq. (9) over the surface of a rectangular panel as indicated by Eq. (6) yields the following expression for the work done by the blast wave on the panel if it is assumed that the loading is uniform over the panel surface,

$$E = 0.1137 P u \Delta t a b, \quad (10)$$

where a is the short edge and b is the long edge of the panel. The term in the conservation of energy statement that remains to be evaluated is the panel strain energy U .

To develop an expression for the panel strain energy, the skin may be treated as a uniformly loaded, thin rectangular plate that undergoes large transverse deflection of the form

$$w = C \left[.8 \cos \frac{\pi x}{a} \cos \frac{\pi y}{b} + .2 \cos \frac{3\pi x}{a} \cos \frac{3\pi y}{b} - .6 \cos^2 \frac{\pi x}{a} \cos^2 \frac{\pi y}{b} \right], \quad (11)$$

where C is deformation amplitude. This deformation pattern corresponds to a rectangular plate with combined simply supported and clamped edges. The plate is assumed to deform in this manner with increasing amplitude until the principal stress becomes equal to the ultimate tensile strength of the material. At this point the plate is assumed to fracture, or tear.

A general expression for the strain energy of deformation of a flat plate U is

$$U = \iiint (\sigma_x e_x + \sigma_y e_y + \sigma_{xy} e_{xy}) \, dx \, dy \, dz, \quad (12)$$

where $\sigma_x, \sigma_y, \sigma_{xy}$ are the normal and shear stresses in the x and y plane of the plate and e_x, e_y, e_{xy} are the strains in the plane of the plate with $dx \, dy \, dz$ an incremental volume in the plate. Since the blast attack produces gross deformation throughout the plate and the material is assumed to be rigid-linear strain hardening, the stress components are

$$\begin{aligned} \sigma_x &= F_y + E_p e_x \\ \sigma_y &= F_y + E_p e_y \\ \sigma_{xy} &= S_y + G_p e_{xy} \end{aligned} \quad (13)$$

where F_y = tensile yield strength,

S_y = shear yield strength,

E_p, G_p = normal and shear moduli in the plastic region, respectively,

and the strain energy equation, Eq. (12), becomes

$$U = \iiint (F_y e_x + F_y e_y + S_y e_{xy}) \, dx \, dy \, dz. \quad (14)$$

Expressions for the strains accompanying finite deformations are

$$\begin{aligned} e_x &= \frac{1}{2} \left(\frac{\partial w}{\partial x} \right)^2 - z \frac{\partial^2 w}{\partial x^2} \\ e_y &= \frac{1}{2} \left(\frac{\partial w}{\partial y} \right)^2 - z \frac{\partial^2 w}{\partial y^2} \\ e_{xy} &= \frac{\partial w}{\partial x} \frac{\partial w}{\partial y} - 2z \frac{\partial^2 w}{\partial x \partial y} \end{aligned} \quad (15)$$

where z is the distance from the midsurface of the plate.

Substitution of the deflected shape and its derivatives into Eqs. (15), substitution of the resultant expressions into the strain energy, Eq. (14), and subsequent integration yields the following expression for membrane (U_m) and bending (U_b) strain energies, with the plastic moduli taken to be zero for simplicity:

$$\begin{aligned} U_m &= 5.1888 F_y h \left(B + \frac{1}{B} \right) C^2 \\ U_b &= 3.9669 F_y h^2 \left(B + \frac{1}{B} \right) C \end{aligned} \quad (16)$$

in which S_y has been taken equal to $F_y/\sqrt{3}$, h is the skin thickness, and $B = h/a =$ aspect ratio. Now, by equating the sum of these strain energies to the external work expression, Eq. (10), and solving for deformation amplitude, we have

$$C = \frac{1}{2} \left[- .7645 h + \sqrt{.5845 h^2 + .08765 \frac{P_u \Delta t a b}{F_y h (B + 1/B)}} \right] \quad (17)$$

The highest inplane strain occurs at the midpoint of the long panel edge (i.e., length a) and is given by

$$e_{xm} = \left(\frac{\pi}{a} \right)^2 (.02C^2 + .6hC). \quad (18)$$

With the strain known, the inplane stresses can be obtained from the stress-strain relation, Eq. (13).

The transverse shear stress is obtained by considering the average normally reflected pressure from the blast wave that acts on the skin panel. For the form of the wave given by Eq. (8), the average normally reflected pressure is equal to $0.2073 P_n$ where P_n is the peak normally reflected pressure.

As before, the blast wave is assumed to be uniform over the panel, so the transverse load becomes $0.2073 P_n ab$. The net cross sectional area of the skin along the rivet line is equal to

$2h(a + b)(1 - kh/D)$ where k is the rivet hole diameter to skin thickness ratio and D is the center-to-center spacing of the rivets. Therefore the transverse shear stress at the edge of the skin panel, given by the transverse load divided by the net cross sectional area of the skin at its edges, becomes

$$\tau = \frac{0.1037 P_n ab}{h(a + b)(1 - kh/D)} \quad (19)$$

With both the inplane normal stress and transverse shear stress known, the principal stress, σ_1 , may be obtained and compared to the ultimate tensile strength of the skin, F_{TU} , which is used here to characterize fracture. So, when the ratio of ultimate strength to principal stress defined here as the safety factor,

$$SF = \frac{F_{TU}}{\sigma_1}, \quad (20)$$

becomes equal to or less than one, the skin is assumed to fail.

Equations 17 through 20 are used here to demonstrate the effects of the various independent parameters on safety factor. The information generated by use of these relations is listed in Table I and is shown in Figures 1 through 7. Since the safety factor indicates the level of maximum stress in the skin and is also a measure of structural integrity, it represents structural tolerance to damage. Consequently, it is selected here as one of the indicators of damage tolerance.

A total of 25 bare explosive charge test firings were performed against individual panels of two different types of helicopter tail booms to substantiate the theory just presented. These tests comprised two different skin sheet materials, one a magnesium alloy and the other an aluminum alloy. The panels tested varied in width from 3.5 inches (8.89 cm) to 6.6 inches (16.764 cm), in length from 13 inches (33.02 cm) to 21 inches (53.34 cm), and in thickness from 0.021 inch (0.5334 mm) to 0.040 inch (1.016 mm). Aspect ratio varied over the range from 2.9 to 5.3. The explosive used in the tests was bare, spherical 50/50 Pentolite. Charge size ranged from 0.00375 pound (1.7 grams) to 0.0703 pound (31.9 grams). Standoff distance measured along the normal to the panel skin from the midpoint of the panel to the center of the explosive charge ranged from 4 inches (10.16 cm) to 15 inches (38.1 cm). This combination of charge sizes and standoff distances used in the tests provided a range in peak incident overpressure, time duration, and particle velocity from 39.2 psi (0.27 MPa) to 792 psi (5.46 MPa), 28 to 259 microseconds, and 14,685 inches/second (373 meters/second) to 85,085 inches/second (2,161 meters/second), respectively. These ranges mean that peak incident overpressure, time duration, and particle velocity were varied in the tests by a factor of 20, 9 and 6, respectively.

In these tests strain gage measurements were made at the midpoint of the panels and at the midpoint of the long edges. Unfortunately, some of the desired data was lost because of technical difficulties of one kind or another. For example, in some cases leads were broken during test; in others, gages partially or totally debonded. However, nineteen successful panel midpoint strain records were obtained

along with twelve successful records at the long edge midpoint location. Correlation between predicted strains and these test results was found to be favorable. The theoretical strain predictions and test results compared within an average error of 6 percent at the panel midpoint and within an average error of 11 percent at the midpoint of the long edge. Correlation between the fracture predictions and test results was also found to be favorable. According to the theory, three skin panels were predicted to fracture. These three did fracture along with two additional panels. The maximum deviation between the predicted and test safety factor was 13 percent for those two panels that were not predicted to fail but did.

TAIL BOOM DAMAGE TOLERANCE TESTS

Two different types of semimonocoque helicopter tail booms were tested. Both were roughly the same size. One, labeled type A for the purposes of this report, consisted of eight bays along its length plus its empennage. This tail boom was essentially an all-aluminum alloy boom. The other tail boom, labeled type B, consisted of ten bays plus empennage, with an aluminum alloy stiffening system. Its top and bottom skins were of aluminum alloy with a magnesium alloy for its side skins.

For some of the tests these tail booms were modified with additional longerons and stringers to determine their influence on damage tolerance. These longerons and stringers were obtained from other, untested type B tail booms. Identical longerons and stringers were used in the modifications of both tail boom types. One type A tail boom was modified. Two longerons and two stringers were added to the predominately tension side of the boom. Two of the type B tail booms were modified. In this case two longerons and two stringers each were added to both sides of the type B tail booms. In all, a total of seven booms were tested: three unmodified and one modified type A booms, and one unmodified and two modified type B booms. (See Table II.)

In order to test these tail booms while loaded, they were bolted at their manufacturing joint to a rigid fixture and deadweight-loaded at their elevator and tail rotor attachment points. The boom axis in this arrangement was horizontal. In all tests but one, the tail booms were loaded to simulate their maximum flight load conditions. These conditions were different for the two types of tail booms. In one test the type B tail boom was loaded to only 63 percent of its maximum flight load.

Two types of damaging agents were employed, a 0.0395-pound (18-gram) bare spherical 50/50 Pentolite explosive charge and a small-caliber, high-explosive projectile. The bare charges were statically detonated at various standoff distances from the helicopter structure to achieve the desired levels of damage. These charges were all detonated within the tail boom interior at points located midway between adjacent frames of the bays tested. The projectile was fired so as to strike the boom normal to its longitudinal axis at the longitudinal midpoint of the selected target bay. The striking speeds were approximately equal to 60, 67, and 100 percent of the projectile muzzle velocity. All projectiles detonated within the interior of the tail booms. The aimpoints were varied from test to test.

Measurements of overall tail boom deflection and skin loss were made. Two surveyor's transits located roughly along the tail boom longitudinal axis and about 40 feet (12.2 meters) behind the tail boom were used to measure deflection at the tail end of the booms. These measurements were made both after the load was applied to the boom and then after the boom was damaged by the explosive or projectile. In this manner, the increase in deflection caused by the damage was obtained. Gross skin loss was also measured. Included in this measurement was the total area of the skin that was blown away or otherwise removed from the structure by the damaging agent. The area removed by fragments that perforated the skin was not included in the skin loss measurements.

The test results are given in Table II. In this table the test number, modification (yes or no), applied load, bays damaged, skin loss to total skin affected ratio, and scaled deflection increment are listed. The test number indicates the type of boom (A or B), the number of the boom tested (given by the first digit after the letters A or B), and the number of the test performed on the boom. For example, A1-2 refers to type A tail boom, the number 1 tail boom, and the second test firing into boom number A1. A total of five test firings were performed on boom number A1. Four of these were in bay 4-5 (tests A1-1 through A1-4), and one test firing was made in bay 7-8 (test A1-5). Bare explosive charges were used in these tests. The high-explosive projectile was used as the damaging agent in all the other tests listed in Table II. In this table the applied load is listed as maximum flight load for all the tests except test B1. The applied load employed in test B1 was 63 percent of the maximum flight load. The extent of skin damage to the structures is listed in Table II as the ratio of skin that was lost because of the damaging agent to the total skin area in all bays affected by the damaging agent. Damage to the skin in terms of skin actually removed from the structure generally occurred over more than the target bay. The two adjacent bays generally suffered some skin loss as well as the target bay. Consequently, the total skin area affected was either the skin area in one, two, or three bays, depending upon whether skin loss was confined to only one bay or extended to a second or third bay, respectively.

The measures of damage tolerance used in these tests are: (1) whether the tail boom failed or sustained the applied load under fire, and (2) scaled deflection increment. Scaled deflection increment is defined here as the ratio of deflection caused by the incurred damage to the overall length of the tail boom. As described previously, this additional deflection is obtained by measuring the deflection after a test and subtracting from it the deflection of the tail boom under the applied load measured before the firing test. Scaled deflection increment is proportional to the maximum strain in the structure and as such is considered in this study a good measure of damage tolerance. The lower the scaled deflection increment for a given amount of skin loss, the higher is the damage tolerance of the structure.

The data listed in Table II is discussed in the next section. The deflection data for the type A tail booms is shown in Figures 8 and 9.

DISCUSSION

In this discussion, damage tolerance is characterized either by safety factor or by scaled deflection increment. Safety factor is employed in the discussion concerning skin panel damage. Scaled deflection increment is used to gauge the tolerance of the complete helicopter or aircraft fuselage to structural damage.

Skin Damage Tolerance

Of the seven independent variables studied in the skin panel analysis, as they increase in value, four serve to increase damage tolerance and three tend to decrease it. As to be expected and as shown by Figure 1, safety factor increases with standoff distance from the explosive detonation point. Standoff is varied here over the range from 2 inches (0.0508 m) to 40 inches (1.016 m). This corresponds to a range in scaled distance in charge radii from 4 to 81.1. Over this range the safety factor increases from 0.2 to 7.2, a 36-fold increase. The figure also shows that, for the conditions studied, the skin will fracture if the explosive detonation point is within 9 inches (0.2286 m) of the skin. Blast damage tolerance of skin then can be increased by keeping structure as far away as possible from possible points of detonation. This, of course, suggests that structures should be as large as possible to maximize blast damage tolerance.

Figure 2 shows the effect of panel width on safety factor. The panel area is kept constant at 180 square inches (0.116 m²) as the panel width is varied from about 2 inches (0.0508 m) to 14 inches (0.3556 m). Over this range the aspect ratio varies from 45 to a little over one. As shown, safety factor, or blast damage tolerance, decreases as panel width increases. Blast damage tolerance is highest for long, narrow skin panels and least for square ones. Figure 2 demonstrates the trend of safety factor with variation in panel width and aspect ratio for a constant area panel. However, for the particular conditions studied it also shows that the skin is only expected to be blast tolerant in widths less than 4 inches (0.1016 m), or with an aspect ratio greater than 11.25. Such a situation is generally not practical nor feasible in aircraft or helicopter fuselage construction. Aspect ratios typically range from one to around six or so. Therefore, some other combination of the independent variables would have to be found to provide damage tolerance. In any case, the curve of Figure 2 serves to illustrate the role of panel width and aspect ratio in blast damage tolerance: blast damage tolerance increases with an increase in aspect ratio, or a decrease in panel width, if panel area remains constant.

As to be expected, Figure 3 shows safety factor to increase with skin thickness. It also shows that the rate of this increase declines with thickness increase. An increase in thickness from 0.02 inch (0.508 mm) to 0.04 inch (1.016 mm) yields about a 58 percent increase in safety factor, whereas a change in thickness from 0.04 inch (1.016 mm) to 0.08 inch (2.032 mm) yields only a 38 percent safety factor increase. These large increases in damage tolerance certainly show that skin thickness is a significant factor in damage tolerance. However, it should be noted that even though damage tolerance can be increased by increasing skin thickness, a region of diminishing returns is reached where the benefit to be gained diminishes in the thicker skin region.

Figure 4 illustrates the effect of aspect ratio on safety factor if the panel width is kept constant over the aspect ratio range from one to twelve. As shown in this case, safety factor decreases with increasing aspect ratio. This occurs because, with constant width, panel area grows as the aspect ratio is increased and this causes the total load on the panel to increase, which more than offsets the otherwise beneficial increase in aspect ratio. (The benefit to be gained by employing aspect ratios greater than one were demonstrated in Figure 2 for the constant area case and were described in the discussion of the figure.) The largest decrease in safety factor occurs over the range in aspect ratio from one to about five or six for constant panel width. Beyond this range the safety factor becomes relatively constant.

Figure 5 shows safety factor variation with skin ultimate strength. This curve was constructed from data points corresponding to the properties of AZ31B magnesium alloy, 2024-T3 aluminum alloy, and 7075-T6 aluminum alloy sheet. As illustrated and as expected, safety factor increases with ultimate strength. However, this increase levels off in the high range over strengths from 60,000 psi (414 MPa) to 70,000 psi (482 MPa). For example, a strength increase from 40,000 psi (276 MPa) to 50,000 psi (345 MPa) yields a 27 percent increase in safety factor while a strength increase from 55,000 psi (379 MPa) to 70,000 psi (483 MPa) corresponds to only a 4 percent safety factor increase.

The influence of rivet spacing on safety factor for the conditions studied is illustrated by Figure 6. Rivet spacing from 0.5 inch (12.7 mm) to 2 inches (50.8 mm) is covered by this figure. As shown, the distance between rivets has much less influence on safety factor than the variables discussed previously. Doubling the rivet spacing from 0.5 inch (12.7 mm) to 1 inch (25.4 mm) results in only an 8 percent increase in safety factor. Furthermore, over the range of rivet spacing considered the rise in safety factor is rather shallow.

The influence of rivet hole diameter to skin thickness ratio on safety factor as shown by Figure 7 is also small. In this case safety factor is decreased by an increase in the size of the rivet hole relative to skin thickness. Safety factor decreases about one percent as the rivet hole diameter to skin thickness ratio is doubled from one to two.

The sensitivity of the safety factor (or damage tolerance) to the various independent variables discussed can be judged by comparing the slopes of the curves over the various ranges of interest of the independent variables. Actually, a somewhat more objective measure of sensitivity is given by variation in safety factor with respect to the ratio of independent variable to the range in the independent variable. This measure is evaluated at a certain value of the independent variable. These sensitivities are listed in Table I. The independent variable, its range, the specific value at which sensitivity is evaluated, and the various safety factor sensitivities are listed in the table. The independent variables are listed in order according to their relative influence on safety factor. As

shown, standoff distance from the skin to the explosive detonation point has the highest influence on safety factor. At 5.70 the safety factor sensitivity to standoff is 81 times higher than its sensitivity to rivet hole diameter to skin thickness ratio, which at -0.07 is the least influential variable studied. Also listed in Table I are the safety factor sensitivities relative to standoff as well as sensitivities relative to panel width at constant panel area (which has the second highest influence on safety factor). Panel width at constant panel area and skin thickness exert roughly the same influence on safety factor although in opposite directions. Safety factor decreases by 0.80 with an increase in panel width at constant panel area, while an equal percentage increase in skin thickness raises the safety factor by 0.71. Besides standoff, these two variables, panel width at constant panel area and skin thickness, exert the next highest influence on damage tolerance. As shown, aspect ratio at constant panel width and ultimate strength have about one-quarter and one-sixth, respectively, the effect on damage tolerance as panel width at constant panel width and skin thickness. At one-tenth of both the sensitivity of panel width at constant panel area and skin thickness, rivet spacing and rivet hole diameter to skin thickness ratio have the least effect on damage tolerance. As stated previously, the values listed in Table I correspond to the calculated sensitivities for the conditions studied, evaluated over the listed range of values of the independent variables. For other conditions and values of the independent variables outside the stated ranges, sensitivity of the safety factor to the various variables can and probably will differ from those values listed in Table I.

The table clearly shows those parameters that have the highest impact on damage tolerance. In those cases in which it is possible to provide large standoff between point of explosive detonation and the aircraft structure, the structure will be inherently damage tolerant. This, of course, is true with-in reason at least for projectiles with explosive charge weights up to certain maximum values that depend upon the combination of the other pertinent parameters discussed herein. For those regions in the aircraft which must be small for other reasons, damage tolerance can be obtained by utilizing thick skins. This, along with use of a large structure to obtain damage tolerance, of course incurs a weight penalty. However, to keep increases at a minimum for a given sized structure with lightweight skin, a judicious selection of panel width and aspect ratio can be used to increase damage tolerance. To do this, panel width must be minimized and the aspect ratio should be maximized. As discussed previously, aspect ratios around five to six provide a good compromise. Since decreasing panel width is achieved by increasing the number of longerons or stringers, this means an added benefit is obtained -- the load per longitudinal member is decreased with a consequent decrease in the probability of loss in bending capability if a certain number of longitudinals are lost from blast damage or fragment perforation.

As indicated in Table I, skin ultimate strength plays a relatively small role in damage tolerance. This is partly because of the level and range of strengths studied: from 39,000 psi (269 MPa) to 70,000 psi (483 MPa). These strengths are already high since they are inherently necessary to sustain flight loads. Higher strength materials are, of course, available although they were not considered for a variety of reasons, some of which are: (1) some are not as lightweight as aluminum and magnesium alloys, and (2) the use of some is not economically feasible at this time. If the skin strength range were extended to include strengths from say 20,000 psi (138 MPa) to 60,000 psi (414 MPa), the sensitivity value would change from the present 0.124 to around 0.7. This would make the skin strength influence comparable to skin thickness. However, this is unrealistic since typical skin materials used in aircraft construction have strengths much higher than 20,000 psi (138 MPa).

Even though the effect of skin ultimate strength on damage tolerance is quite small compared to the effect of standoff, it still can be used to increase damage tolerance, particularly if a specific region in the aircraft is marginal. As shown in Table I, ultimate strength has 15 percent the effect of panel width at constant panel area. So at least some benefit can be gained by changing a skin that may be marginal to a new skin material with higher ultimate strength. In this modification fracture strain must not be overlooked. The fracture strain of the higher strength material should be about the same as or higher than (if possible) that of the skin material that is to be replaced. If the fracture strain of the new higher strength material is lower than that of the replaced skin material, the potential benefit of the higher ultimate strength may not be realized.

As in the case of skin ultimate strength just discussed, the potential benefit to damage tolerance obtained from variation in rivet spacing or rivet hole diameter to skin thickness ratio is not very promising at about 10 percent of the effect of panel width at a constant panel area. However, with skin ultimate strength, a change in rivet spacing or rivet hole diameter to skin thickness ratio, or preferably a change in both, could be employed to correct a marginal skin situation. As indicated in Table I, to increase damage tolerance, rivet spacing should be increased and the rivet hole diameter to skin thickness ratio should be decreased.

Tail Boom Damage Tolerance

The test data listed in Table II for two separate bays of the type A tail booms are shown plotted in Figures 8 and 9. The abscissa in these figures is skin loss from blast divided by the total area of skin in all bays damaged by the explosion. The ordinate in these figures represents the added deflection at the endpoint of the tail boom caused by the blast-induced skin loss. As described previously, the tail booms were damaged by either a statically detonated bare charge explosive or a small-caliber, high-explosive projectile fired into the tail boom while the boom was statically loaded to simulate the maximum flight load condition. Figure 8 concerns damage inflicted on bays 4 and 5 located near the middle of the tail boom. Figure 9 concerns damage inflicted on bays 7 and 8. These bays are located near the tail end of the boom. If the tail boom is treated as having a circular cross section, the ratio of moments of inertia about a diameter for bays 4-5 and 7-8 is about 1.8.

As described previously, each tail boom was loaded by the simulated flight load. Under this load the boom deflected a certain amount. Then the boom was damaged by either the high-explosive projectile or a bare charge. Because of the damage incurred, which consisted of blown-away skin, cut longitudinals, bent frames, etc., the tail boom suffered additional deflection. This additional deflection divided by the overall boom length is defined here as "scaled deflection increment" and is the ordinate in Figures 8 and 9. Boom strain is directly proportional to this scaled deflection increment.

Both Figures 8 and 9 show that damage-induced deflection increases with an increase in skin loss and that for the conditions investigated, deflection caused by skin damage is approximately linearly related to the amount of skin lost. The intent here of presenting the data shown in these figures is purely to indicate trends and is not meant to be definitive. The vertical line labeled "failure" in both figures corresponds to the relative amount of skin removed by the bare charge or projectile in those tests in which the boom failed under the applied flight load. The skin loss associated with these failures does not necessarily represent the minimum amount of skin that has to be removed to cause the boom to fail. This value should be fairly well represented by the failure line of Figure 8 since the nearest data point, at skin loss/total skin area equal to about 0.3, is fairly close to the failure line where skin loss/total skin area equals 0.35. However, the modified structure failure line of Figure 9 at skin loss/total skin area = 0.34 is far removed from the next nearest data point at skin loss/total skin area equal to about 0.1.

The slope of the data line in Figure 8 corresponding to damage in bays 4 and 5 is 0.022 while the slope of the modified boom data line in Figure 9 corresponding to damage in bays 7 and 8 is 0.032, indicating that the damaged structure of bays 4 and 5 is 1.45 times stiffer than that of bays 7 and 8. This is understandable, particularly since the moment of inertia in the undamaged state of bays 4 and 5 is approximately 1.8 times the moment of inertia of bays 7 and 8 in their undamaged condition; that is, the bulk of the structure in bays 4 and 5 is located farther from the boom cross section neutral axis than that of bays 7 and 8. This basic foundation of beam theory, that structural stiffness increases as section size increases, parallels the previously discussed obvious relationship between standoff and damage tolerance that damage tolerance increases as the distance between detonation point of the explosive and the skin of the aircraft increases. This fact that damage tolerance increases with an increase in section size and structural stiffness was predictable before testing.

Figure 9 illustrates the result of longitudinally stiffening the tail boom. In this case two longerons and two lightweight stiffeners were added to the predominately tension side of the tail boom. These longerons and stiffeners were identical to those used in the original, unmodified tail boom. The resultant slope of the modified structure deflection - skin loss line is 0.018. This represents a 44 percent increase in stiffness over the original, unmodified tail boom structure. Also, as indicated on the figure, at a skin loss to total skin area ratio equal to 0.34, the unmodified tail boom failed. (This value may actually be high since tests were not performed at skin loss/total skin area values between about 0.1 and this 0.34 figure.) However, the modified tail boom was able to carry the maximum flight load while sustaining skin loss/total skin area equal to 0.35 -- essentially the same value at which the unmodified tail boom failed. So, the additionally stiffened tail boom, with 35 percent of the skin in two adjacent bays lost due to blast damage, was able to sustain its load while an unmodified tail boom with the same damage failed. Furthermore, the stiffeners added 44 percent to the rigidity of the tail boom.

As described in the test description section, the effect of added stiffening on damage tolerance was also evaluated on the type B tail booms. Longerons and stringers identical to those used to modify the type A tail booms were employed on the type B booms. Two longerons and two stringers each were added to both sides of the type B booms whereas they were added to only one side of the type A booms. Three of the type B tail booms were tested. One was used as a control and was tested in its original unmodified condition. The other two booms were tested as modified. As indicated by Table II, a single shot into the unmodified tail boom caused it to fail, and this occurred with only 63 percent of maximum flight load applied to the tail boom. However, the modified tail booms, hit at the same point by the same type of projectile under the same firing conditions, were able to sustain the full, maximum flight load. Furthermore, as shown in Table II, a total of three projectiles each were fired into both of the modified tail booms -- both of which sustained the full, maximum flight load. Therefore, it may be seen that the added stiffening allowed the type B tail booms to carry their maximum flight load while sustaining multiple hits in adjacent bays, whereas the unmodified tail boom failed at only 63 percent of its maximum flight load from the action of a single projectile.

CONCLUSIONS

Both the skin and the skin stiffening system of a semimonocoque aircraft are important in the damage tolerance of the structure. For a given size structure, a judicious selection of skin panel width and aspect ratio can be used to increase damage tolerance. To do this, panel width must be minimized and aspect ratio should be maximized. For the conditions studied, aspect ratios around five or six provide a good compromise. Damage tolerance of the helicopter tail booms investigated in this study have been found to be proportional to the section modulus of the undamaged section and inversely proportional to the amount of skin removed from the structure by the damaging agent.

For the conditions studied, damage tolerance of the aircraft skin is influenced by the following parameters which are listed in decreasing order of their effect on damage tolerance. The relative values of the skin damage tolerance sensitivity to these parameters are also listed:

• Standoff distance	1.00
• Panel width at constant area	-0.140
• Skin thickness	0.125
• Aspect ratio at constant panel width	-0.035
• Skin ultimate strength	0.021
• Rivet spacing	0.014
• Rivet hole diameter/skin thickness	-0.012

It has also been found that an increase in longitudinal stiffening, achieved in this particular study by addition of longerons and stringers, can provide an increase in structural damage tolerance of at least 44 percent. Furthermore, it has been demonstrated that the simple addition of a few lightweight longitudinal stiffening members can mean the difference between catastrophic failure of an aircraft from the damage caused by a single high-explosive projectile and an aircraft that can continue to carry its maximum flight load with multiple hits in the same critical area by the same projectile.

REFERENCE

¹ Goodman, H. J., US Army Ballistic Research Laboratories, "Compiled Free-Air Blast Data on Bare Spherical Pentolite," February 1960, BRL Report No. 1092.

TABLE I. SKIN PANEL DAMAGE TOLERANCE SENSITIVITY

FACTOR	RANGE	SENSITIVITY EVALUATED AT POINT	SENSITIVITY	SENSITIVITY RELATIVE TO STANDOFF	SENSITIVITY RELATIVE TO PANEL WIDTH
S STANDOFF	2-40 in. (0.051-1.02 m)	S = 5 in. (0.127 m)	5.70	1.000	-7.125
a PANEL WIDTH AT CONSTANT AREA	2-12 in. (5.08-30.5 cm)	a = 6 in. (15.24 cm)	-0.80	-0.140	1.000
h SKIN THICKNESS	0.02-0.08 in. (0.508-2.032 mm)	h = 0.04 in. (1.016 mm)	0.71	0.125	-0.888
B ASPECT RATIO AT CONSTANT PANEL WIDTH	2-12	B = 5	-0.20	-0.035	0.250
F _U SKIN ULTIMATE STRENGTH	39,000-70,000 psi (269-483 MPa)	F _U = 59,000 psi (407 MPa)	0.12	0.021	-0.150
D RIVET SPACING	0.5-2 in. (12.7-50.8 mm)	D = 1 in. (25.4 mm)	0.08	0.014	-0.100
k RIVET HOLE DIA. SKIN THICKNESS	1.4-4.8	k = 1.8	-0.07	-0.012	0.088

TABLE II. TAIL BOOM TEST DATA

TEST NO.	MODIFICATION	BAYS DAMAGED	APPLIED LOAD	SKIN LOSS TOTAL SKIN AREA	SCALED DEFLECTION INCREMENT, 10 ⁻³
A1-1	NO	4-5	MAXIMUM	0.093	2.2
A1-2	NO	"	"	0.193	4.2
A1-3	NO	"	"	0.305	6.3
A1-4	NO	"	"	0.351	FAILED
A4	NO	7-8	MAXIMUM	0.05	1.8
A1-5	NO	"	"	0.11	3.2
A2	NO	"	"	0.34	FAILED
A3	YES	"	"	0.35	6.5
B1	NO	3-4	.63 MAX.	*	FAILED
B2-1	YES	2-3	MAXIMUM	*	SUSTAINED LOAD
B3-1	YES	"	"	*	"
B2-2	YES	3-4	MAXIMUM	*	SUSTAINED LOAD
B3-2	YES	"	"	*	"
B3-3	YES	4-5	MAXIMUM	*	SUSTAINED LOAD

* NOT MEASURED

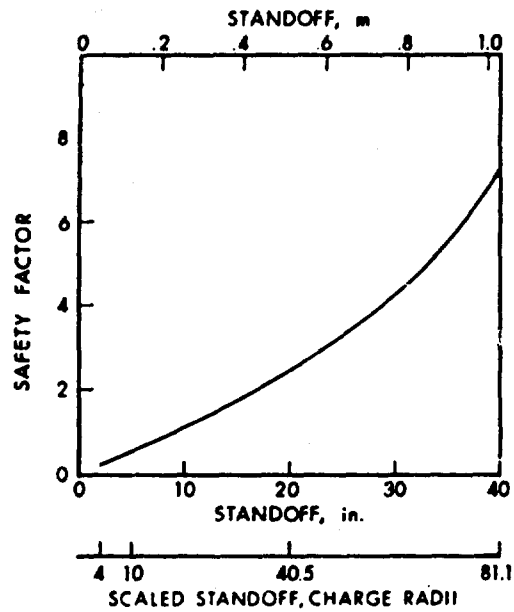


Figure 1. Effect of Standoff on Safety Factor.

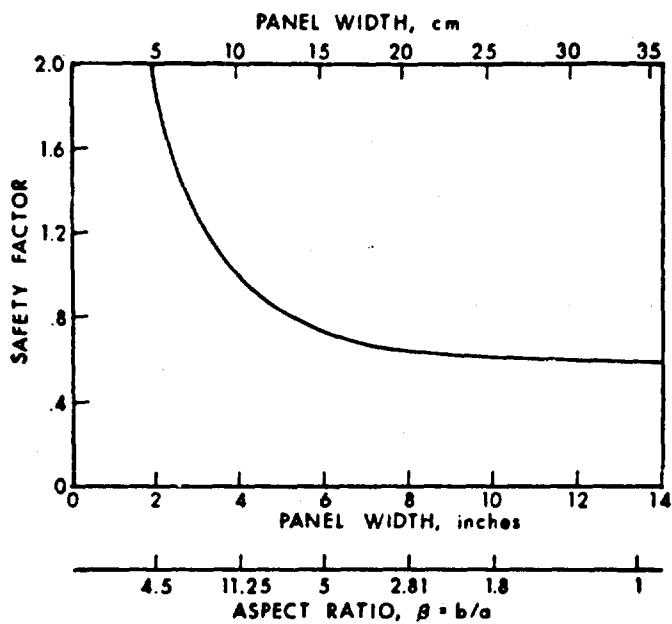


Figure 2. Effect of Panel Width on Safety Factor for Constant Area Panel = 180 in.² (0.116 m²).

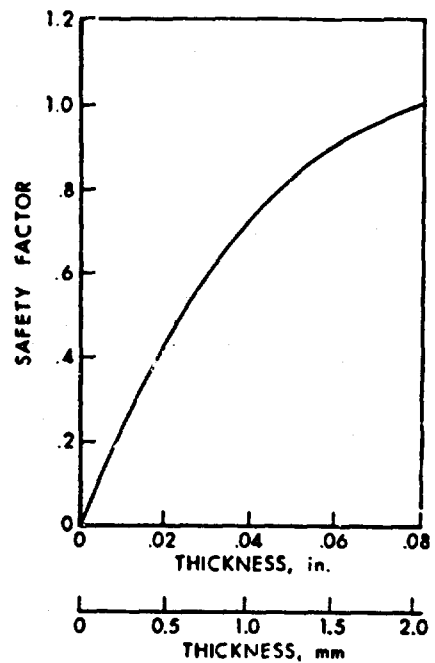


Figure 3. Safety Factor Variation With Skin Thickness.

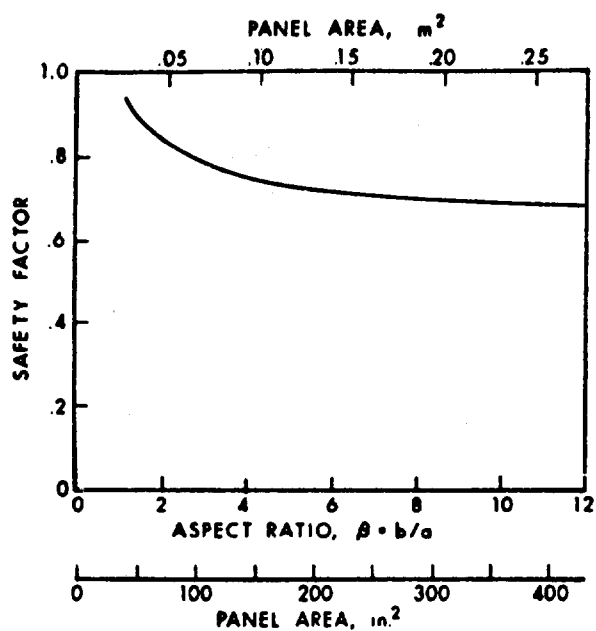


Figure 4. Effect of Aspect Ratio on Safety Factor.

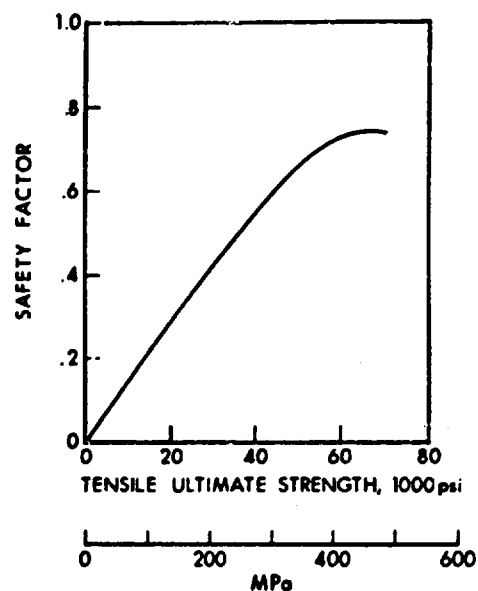


Figure 5. Safety Factor Variation With Ultimate Strength of Skin.

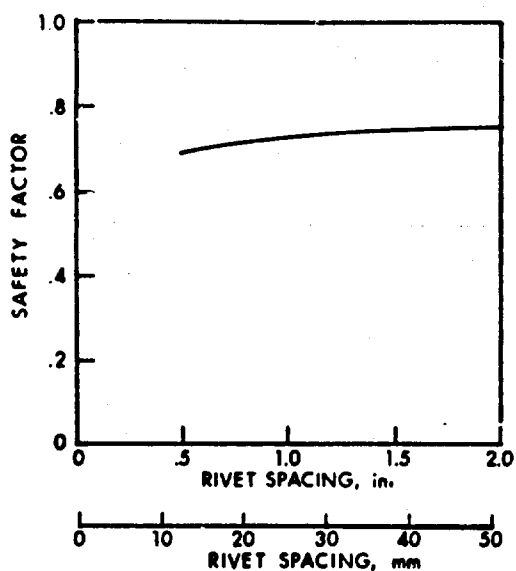


Figure 6. Effect of Rivet Spacing on Safety Factor.

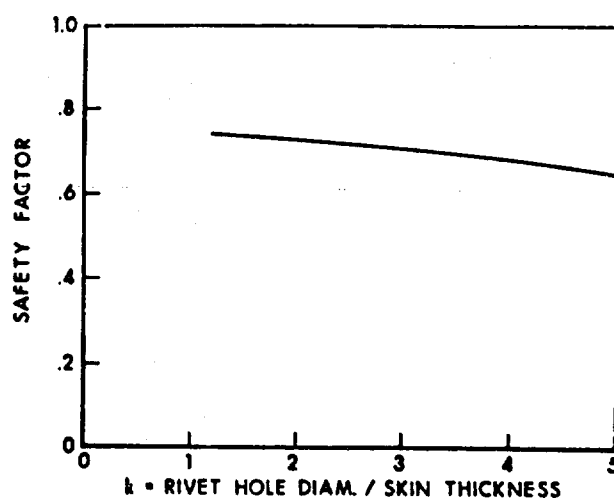


Figure 7. Safety Factor Variation With Rivet Hole Diameter to Skin Thickness Ratio.

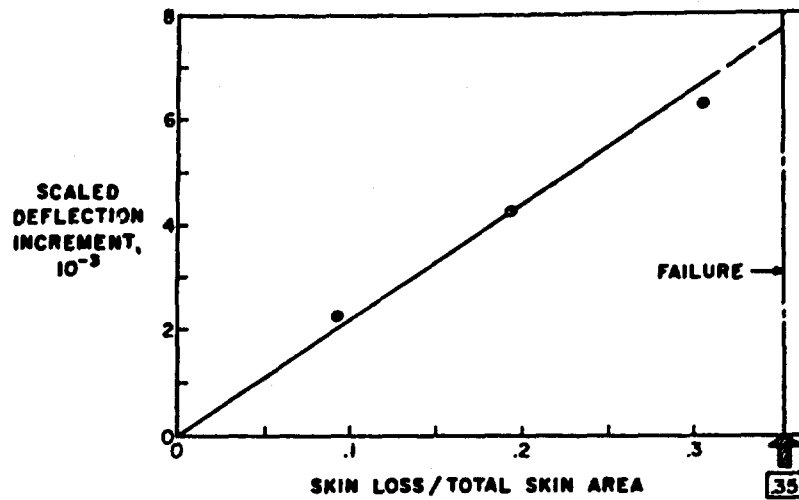


FIGURE 8. DEFLECTION INCURRED BY SKIN LOSS IN BAYS 4-5.

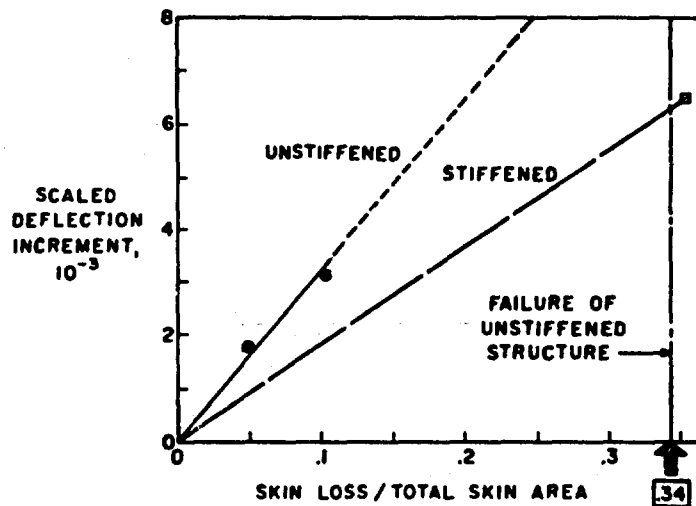


FIGURE 9. DEFLECTION INCURRED BY SKIN LOSS IN BAYS 7-8. FOR UNMODIFIED AND MODIFIED TAIL BOOMS.

DEFINITION OF ENGINE DEBRIS AND SOME PROPOSALS FOR REDUCING POTENTIAL DAMAGE TO AIRCRAFT STRUCTURE

by

D. McCarthy
Chief Engineer - Staff Engineering
Rolls-Royce (1971) Limited
Derby Engine Division
Moor Lane
P.O. Box 31
Derby DE2 8BJ
U.K.

SUMMARY

For the aircraft designer to be able to take proper precautions against the potentially damaging effects of non-contained engine failures, he needs to know the likely size, weight, energy and direction of attack of debris that might be released by the engines. From an analysis of a large sample of past non-contained engine failures in commercial service the above parameters have been established for any given engine.

Protection of sensitive parts of an aircraft beyond that implicit in the aircraft/engine layout could be provided by recently developed deflector systems capable of deflecting high energy fragments in a harmless direction.

Continuing work on the basic causes of non-contained engine failure has led to changes in engine design to make these failures less likely. Beyond this, improved containment characteristics of casings are under development, notably in the control of the way in which debris is released.

INTRODUCTION

The purpose of this paper is to provide a basis for minimising the hazard of non-contained engine failure. The objectives are:-

1. To define the debris that might be released by a given engine in the event of non-contained failure, in terms of the weight, direction of release, energy and size of fragments.
2. To examine ways of reducing the potential effect of such debris upon the aircraft.
3. To explore the practicability of making non-contained engine failure less likely.

Non-contained engine failures do not occur very often, the average rate in commercial service has been less than one per million engine hours world-wide in recent years. Further, the probability of this once-per-million-hour event causing an aircraft accident, defined as penetration of fuselage or damage to wings or vital services, has proved to be about 1 chance in 8.5. In other words, aircraft accidents due to non-contained engine failure have occurred, on average, less than once per 8.5 million engine hours. The statistics shown in Fig.1 put it another way and show that 97.2% of all aircraft accidents and 99.9% of all fatalities have been the result of events other than non-contained engine failure.

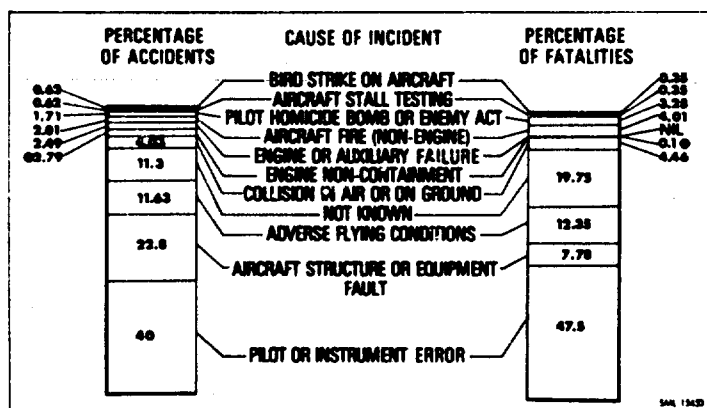


Fig.1. Analysis of Aircraft Accidents & Fatalities - 1954 to 1974

Nevertheless, to reduce the accident rate we must work to eliminate all known causes of accidents, and non-containment is one of them. Recent research work has indicated some possible ways of improving the situation without the need for large increases in weight and ultimately a balance must be struck between weight increase and the effect upon an already low probability of hazard.

To provide a definition of the kind of debris likely to be generated by non-contained failure in a given engine, we have examined the results of non-containment in our commercial engines over the years and recorded the weights of fragments, their direction of release, their energy and their size, wherever the information is known. The statistics cover a wide range of engine sizes and types, including prop-jet, pure-jet, by-pass and fan engines, in single-shaft, two-shaft and three-shaft configurations. The experience covers over 124 million hours of engine operation in service.

WEIGHT OF FRAGMENT

Fig.2 shows the weight of the largest fragment released in each incident as a percentage of the bladed disc weight. The fragments vary from part of a blade to a complete disc. The incidents categorised as aircraft accidents are indicated, showing that complete discs are less likely to cause a problem than disc fragments, but fragments of any size are capable of causing unacceptable damage if they hit certain parts of the aircraft. Compressor and turbine non-containment are indicated on the plot and it shows that only turbine discs have been released complete, probably because a turbine disc has easier access to freedom than a compressor disc.

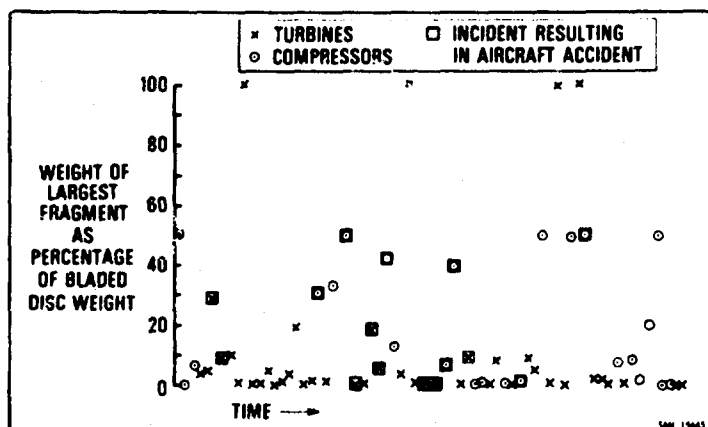


Fig.2. Non-Contained Failures 1954 To 1974 Inclusive

Fig.3 gives the percentage of incidents in which the weight of the largest fragment released was a given percentage of the bladed disc weight or less. It is a way of showing the reduction in the number of non-contained failures that would be achieved by providing an ability to contain an increasing weight of fragment. For example, the ability to contain a fragment weighing 5% of the bladed disc weight would have prevented 56% of all non-containments. If the former figure were 10% we would have prevented 72% of the non-containments. Thereafter the gains are less spectacular.

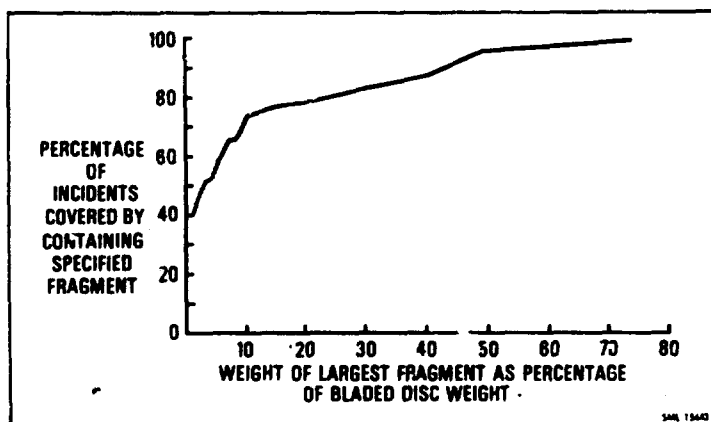


Fig.3. Number of Incidents V Fragment Weight

When a fragment strikes the inside of an engine casing and it is not contained, it is sometimes deflected on its way through the casing. Fig.4 illustrates the effect of such deflection upon the subsequent path of a fragment. Since the point of penetration of the casing is at a random circumferential position, the probability of an aircraft item in line with a disc being struck by a fragment is unaffected by deflection of the fragment by the casing. But the axial deflection of the fragment is important in that it affects the axial length of the possible impact area on the aircraft.

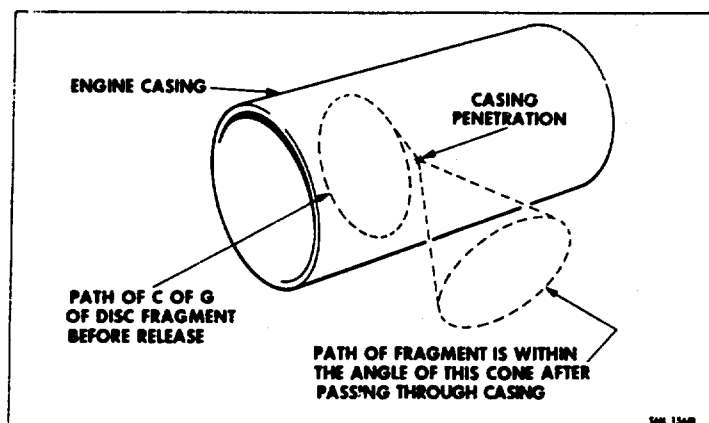


Fig.4. Debris Spread

A study of the axial deflection of debris in actual incidents produced the result shown in Fig.5 where axial deflection is plotted against weight of fragment. It shows that only the lighter fragments were appreciably deflected, the maximum deflection being $\pm 33^\circ$ whereas the heavy fragments were not deflected more than $\pm 5^\circ$. Thus, the situation may be as shown on Fig.6 where a pack of discs creates over-lapping fields of possible debris distribution so that any protection or special measures taken by the aircraft designer will require sensibly uniform application over a length slightly greater than the length of the rotor pack, tailing off to zero beyond each end of the rotor as shown in the Figure.

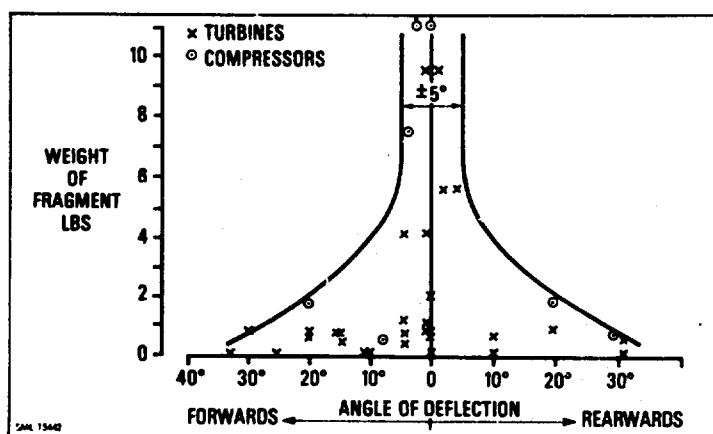


Fig.5. Debris Spread V Weight of Fragment

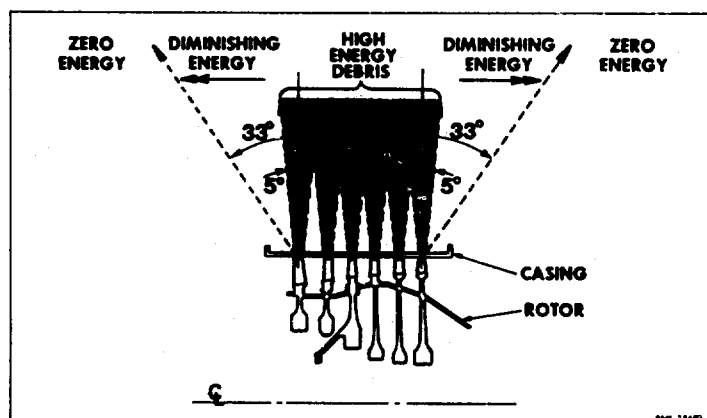


Fig.6. Direction & Energy of Emerging Debris

ENERGY OF FRAGMENT

A fragment has two kinds of energy when it leaves an engine, see Fig.7. It has kinetic energy along its flight path which is tangential to the radius described by its c of g when it was part of the disc, and it has rotational energy about its own c of g. Experience shows that for practical purposes it is the former, i.e. its translational energy, that causes the real damage on impact and this is because the translational energy is in the direction of the impact and, for realistic fragments, it is invariably much greater than the rotational energy.

Fig.7 also shows a plot of disc sector size against its translational energy. The fragment with maximum translational energy is a disc segment subtending an angle of 133.6° . An unbroken disc has no translational energy unless it picks some up as a result of friction developed in rubbing against static parts which may throw it sideways out of an engine with a relatively low velocity.

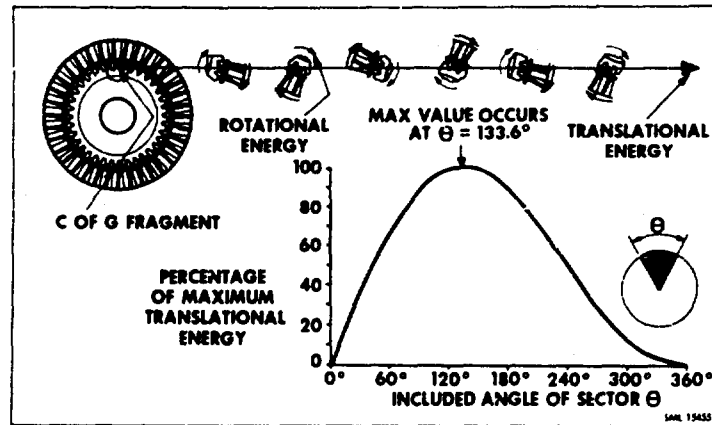


Fig.7. Definition of Fragment with Maximum Energy

The energy with which a fragment leaves an engine is less than its initial energy because it expends some energy in penetrating the engine casing. In calculating the energy of an emerging fragment a proportion of the amount of energy the engine casing is capable of containing should be subtracted from the initial energy of the fragment.

To determine the blade containment ability of a casing we plot blade energy against a function of blade dimensions and casing properties for all known cases of blade release including experimental tests and service experience. The result is shown in Fig.8 where contained and non-contained failures are identified.

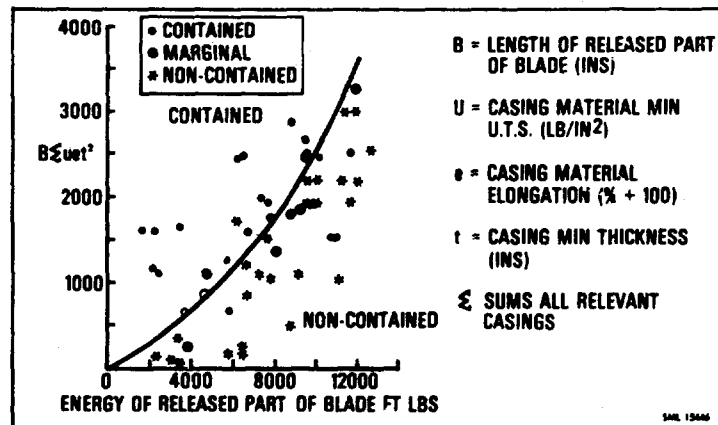


Fig.8. Blade Containment Criterion

The dividing line between containment and non-containment becomes apparent and although, in the nature of things, there are occasional results out of line with the overall trend, the method provides a guide to the thickness of casing, in a given material, required to contain a blade of given energy. It also provides a measure of the energy a given casing is capable of destroying in the blade release case.

Unfortunately the behaviour of a casing is not quite as straightforward as to destroy an equal amount of energy regardless of the initial energy of the fragment. In containment tests a fragment with an energy level just beyond the containment capabilities of a casing lost 90% of its energy in passing through the casing. But when a portion of a rotor, comprising four blades and a piece of disc, was released from a rotor rotating inside a casing designed to contain a single released blade, the fragment passed through the casing with a near-zero loss of energy. That some energy was lost was shown by damage and distortion to

the casing and to the blades in the fragment but the loss was too small to be measured in terms of fragment velocity before and after penetration. Evidently, the casing did not develop its full containment potential when subjected to loadings far beyond its capabilities.

Further containment tests are in progress to build up more data on this problem and to establish a formula for the amount of energy destroyed in a range of fragments when they pass through a casing of known blade containment ability. Meanwhile, until we have more data it seems reasonable to assume that the loss of energy varies from 100% for a single blade, to zero for the 4-blade fragment tested, or any larger fragment. The 4-blade fragment weighed 6.5% of the weight of the bladed disc.

There is an additional loss of energy in fragments that are deflected on passing through the casing. The amount of this loss depends upon the degree of deflection, and from theoretical considerations and practical observations the relationship between deflection and residual energy is as shown in Fig.9.

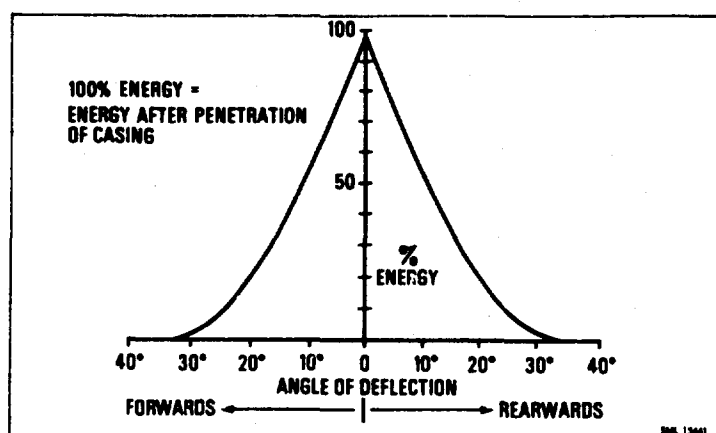


Fig.9. Energy after Deflection v Angle of Deflection

This relationship can be used in calculating the possible energy of deflected fragments in the forward and rearward fields covered by the possible axial spread of debris.

SIZE OF FRAGMENT

The maximum dimensions of a fragment thrown by an engine is important in terms of the probability of striking a given vulnerable item of the aircraft. Fig.10 shows that for a given aircraft layout the larger the fragment the more likely it is to strike a given object. The chances of the small fragment striking the object are θ_1 in 360° , but for the large fragment they are θ_2 in 360° and clearly the larger the fragment the greater the probability of a strike.

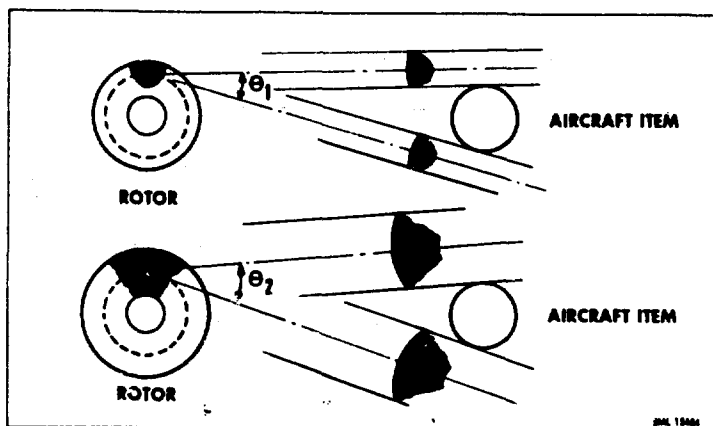


Fig.10. Fragment Size Effect Upon Probability of Strike

Fig.11 shows actual non-contained failures in terms of the arc of disc released against percentage of incidents. These results can be used for calculating the probability of impact of fragments of various sizes upon aircraft vulnerable items for various aircraft/engine arrangements. The results for turbines and compressors are shown separately to illustrate that compressors have tended to release larger arcs of disc rim than turbines. This is due to factors such as disc proportions.

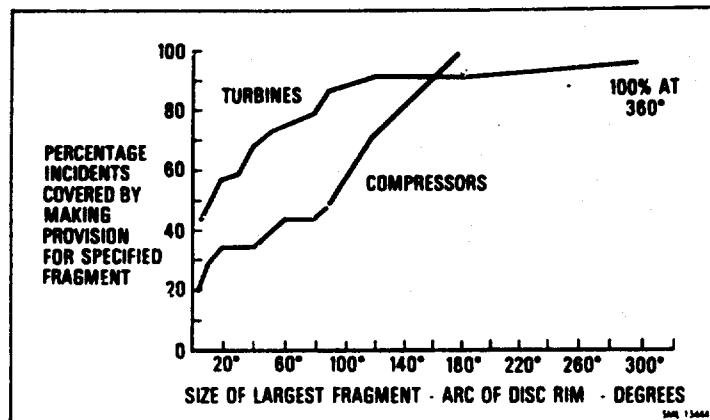


Fig.11. Size of Fragment

AIRCRAFT TREATMENT

Having defined the possible debris from engine failure the problem of dealing with it falls to the designers of aircraft and engines. The aircraft designers can minimise its probable effects by careful planning of engine rotor positions relative to vulnerable aircraft items. He can make use of duplicated and triplicated runs of vital aircraft services to reduce the probability of a hazard to the aircraft in the event of damage in any particular region. He can avoid, for example, siting the distribution unit of a multiple system in line with an engine rotor. Where there is no other possible course he can rely upon the statistical improbability of the coincidence of adverse events. The safety record of existing aircraft, designed long before the information now available to us had been generated, provides a high level of confidence in the safety of new aircraft designed with this wider knowledge of the hazards to be avoided. Finally, it is possible to provide protection for vital regions of an aircraft if the pressures of meeting other essential requirements of an aircraft design do not permit the required safety standards to be achieved by manipulating the aircraft/engine layout.

Tests have been carried out in the U.K. both on armour plating and upon devices capable of protecting vital regions by deflecting approaching debris in a harmless direction. Lightweight angled deflector plates mounted on collapsible mountings have been shown to be capable of deflecting fragments of any given energy in a consistent manner without subjecting the mounting structure to the intolerable shock loads associated with the devices capable of absorbing the whole energy of high energy fragment.

Fig.12 shows the concept of the deflector system.

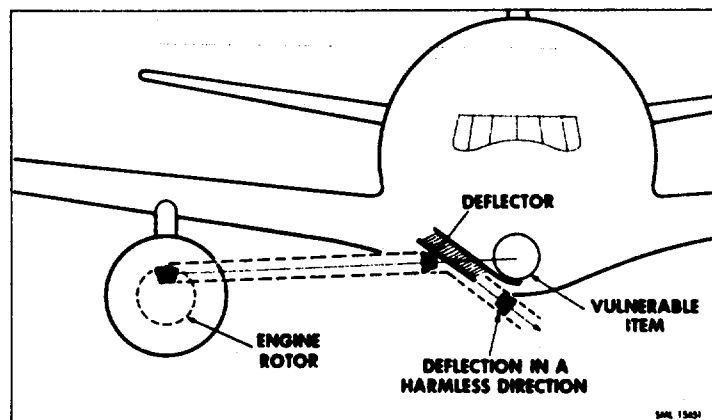


Fig.12. Debris Deflector

ENGINE TREATMENT

It has been suggested from time to time that the hazard of non-containment could be completely eliminated if the engine could be designed to contain all rotor failures including segmental disc failure through the bore. Studies of this solution, based upon limited rig test results, indicate that in the case of a large transport engine, the weight increase for complete containment would be of the order of 50% of the Basic Engine Weight. Further, if the most effective use were to be made of the extra weight, the casings would have to be a single thickness and the thermal lag of casings of such thickness would impose severe restrictions on engine handling (throttle movement) and we would have an engine of weight and handability suitable for a power station but not for an aircraft.

Instead the approach has been to examine the reasons for all past non-contained failures on development and in service and to work towards eliminating the causes by careful design and development. The causes can be put into the following categories -

1. Disc failure due to primary or secondary fatigue i.e. due to fatigue imposed by normal engine operation or due to fatigue under abnormal conditions arising from engine malfunction.
2. Disc failure due to overheating as a secondary effect of a malfunction such as loss of cooling air or an internal engine fire.
3. Disc failure as a result of loss of relative axial location between rotating and adjacent static parts leading to a rub on a sensitive part of a disc.
4. A failure precipitating the shelling-out of a complete row of blades from the disc.
5. Shaft failure leading to turbine overspeed to burst or blade release.
6. Multiple blade failure due to ingestion of exceptionally large bird or other foreign object.
7. Detachment of complete disc.
8. Disc failure due to material defects.

We do not propose to deal with all these items in detail in this paper but the general approach to each item can be stated.

Primary fatigue failure from the bore of a disc has been avoided in the past by establishing safe low cycle fatigue (LCF) lives on the basis of extensive cyclic rig testing of engine discs, including sample discs taken from service engines after given exposure to service operation, cycled on to failure. A typical result is shown in Fig.13 where the disc failed from an origin in the hub. This form of failure is avoided in service by limiting the number of stress cycles accumulated by any disc in service to substantially less than the number established by the rig tests to be within the capabilities of the disc under service conditions. These measures have rendered LCF failure a very rare occurrence but discs have found other ways of failing in fatigue.

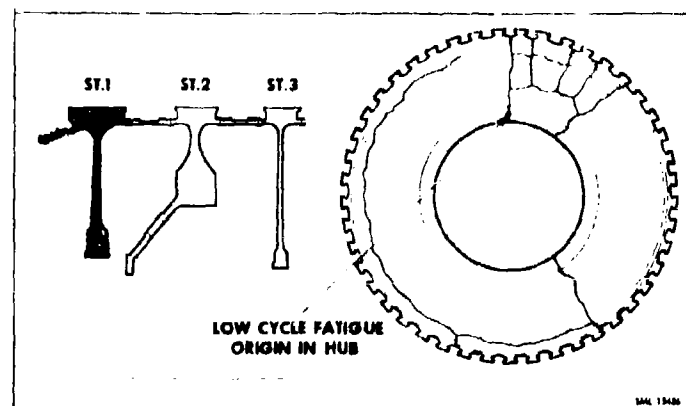


Fig.13. Cyclic Spinning Fatigue Test to Failure

Examples of disc fatigue failure in service are shown in Fig.14. Item 1 shows a rare case of failure through the bore from a crack in the rim of a turbine disc. Item 2 shows a turbine disc rim crack initiated by blade excited high cycle fatigue (HCF) and progressing in a circumferential direction to release a piece of disc. Items 3 and 4 similarly show compressor disc failures which have released pieces of disc rim where the crack has not run into the bore of the disc. The important point about these failures is that in some designs of disc, a crack propagating from the rim follows a line that releases only a small piece of disc rim whereas in other designs the crack will take a different course and release a large fragment. Clearly, by studying the mode of failure and relating it to the direction of crack propagation in the disc we can establish the features of design and environment that determine the size of fragment released and we can move towards designing discs disposed to release small rather than large fragments.

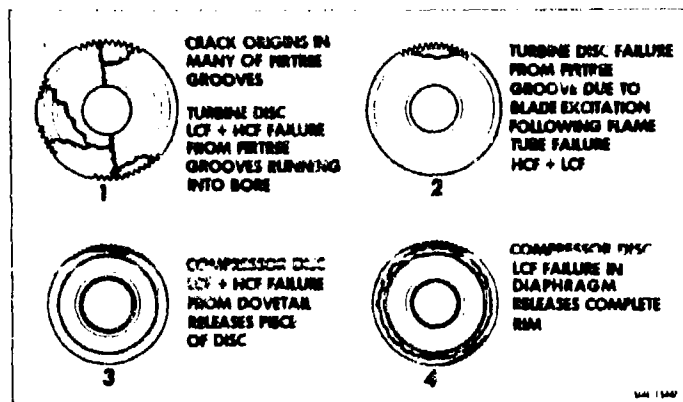


Fig.14. Typical Service Disc Failures

Disc failures due to overheating through lack of cooling air have been due to straightforward mechanical failures of air ducts or air seals and experience has shown how such failures can be avoided or the effect of their failure can be reduced. Oil fires have caused disc failures too, but we have learned how to inhibit the engine against internal fire by avoiding the possibility of conditions in the engine that will permit the ignition or continued burning of oil vapour.

In the case of disc overheating due to rubs, if the loss of axial location of a rotating assembly, due to bearing or shaft failure, permits rubs to occur between rotating and static members, the rub can be arranged to occur in a relatively harmless position on the disc. It is known that a rub on a sensitive part like the disc diaphragm can cause overheating leading to disc failure due to loss of creep properties. See Fig.15.

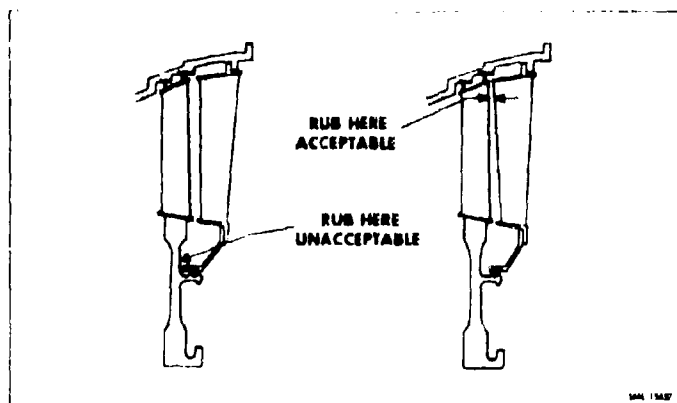


Fig.15. Control of Rubs

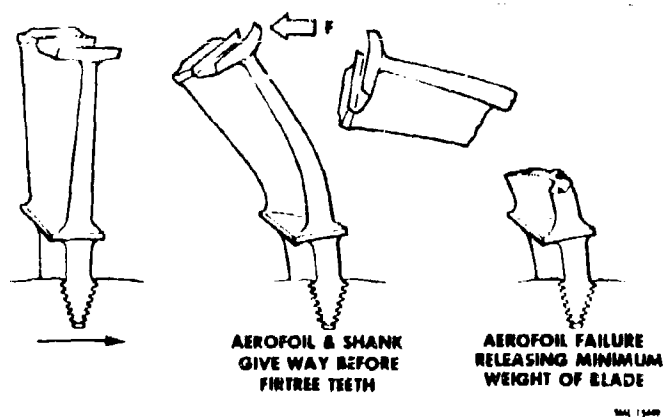


Fig.16. Prevention of Shelling-Out of Blades

It has been known for complete rows of blades to shell out of a disc, complete with roots, to precipitate a non-contained failure. To avoid this, blades and their fixings can be designed to allow the blade to break off in the aerofoil or in the shank without failing the fixing itself, see Fig.16. With such a design, fouling of the blades which might otherwise cause wrenching of the blades out of the disc, will instead either bend the blades over or break them in the aerofoil, releasing fragments more likely to be contained by the casings.

In the case of shaft failure a study of all causes of failure carried out some years ago identified a variety of different failure mechanisms. The causes were largely eliminated in later engines but the assumption should be made that despite all precautions, rare cases of shaft failure may conceivably occur, components are continually finding new ways of failing, and appropriate precautions should be taken, such as providing sufficient braking in the inevitable rubs between rotating and static components to prevent unacceptable overspeeding of the turbine in the event of a shaft failure with loss of turbine axial location.

With regard to the problem of bird or other ingestion, an engine would have to be impossibly rugged to tolerate every possible bird strike. Engines are designed to ensure that failure from this cause is acceptably rare. The ability of engines to ingest birds without serious effect has been greatly improved over the years by the more extensive use of stronger blade materials, stronger shafts and shaft joints, by increases in clearances between rotor and stator blades to avoid fouling, and by the introduction of stronger stator fixings. But there are bound to be occasions when exceptionally heavy ingestion will cause multiple blade failure and possible non-containment.

Disc detachment has been overcome principally by the steps taken to eliminate shaft failure. But in a case of a disc breaking up it may cause sufficient damage to the shaft and surrounding structure to lead to the release of an adjacent disc and here we must rely upon reducing the likelihood of failure of the first disc. Some discs on early engines were lost due to failure of their retaining bolts or flanges and these incidents are included in the non-containment statistics but more stringent criteria on bolt and flange design have been applied for a number of years with satisfactory results.

Our safeguard against disc failure due to defects in the material is a high standard of quality control of manufacturing and inspection. Having established manufacturing procedures giving reliable and consistent material properties throughout the disc, and having established the cyclic life of the disc by rig and engine cyclic spinning tests at extreme conditions, no change in manufacturing procedure should be permitted without a repeat of a comprehensive test programme. Further, techniques for the external and internal inspection of discs for material flaws must always be the best available and we are continually endeavouring to improve the inspection standard.

IMPROVED CONTAINMENT

Having taken all reasonable steps to prevent disc failure and having designed the discs so that in the event of failure the size of fragment likely to be released is as small as possible the question arises as to how much farther the engine man should go. He could improve on the containment capability of engine casings by making them heavier but this would require an international ruling because no engine manufacturer is going to put himself in an uncompetitive position on weight relative to other engine manufacturers.

At first sight any improvement in containment capability would require a general thickening of the casing in the plane of the disc and any worthwhile improvement would involve a considerable weight penalty. But the layout of many aircraft is such that the escape of a high energy fragment from the engine could only affect the aircraft if it emerged from a particular small arc of engine casing, see Fig.17. Thus, an improvement in the containment ability of this arc of casing alone would provide the same benefit to the aircraft as improving to the same degree the containment over the complete circumference of the casing.

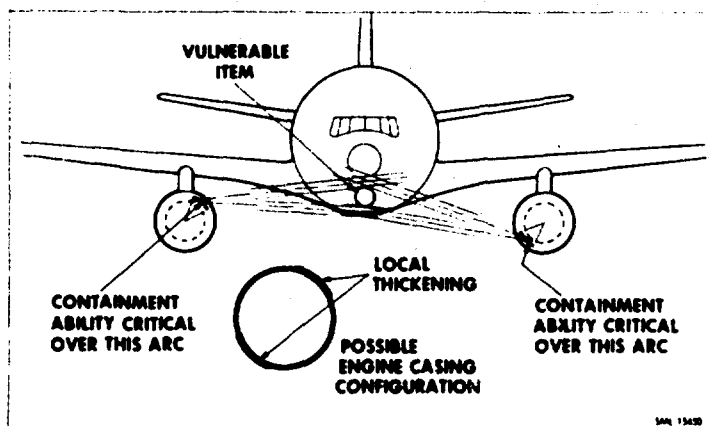


Fig.17. Control of Direction of Release

Containment rig tests have been carried out on locally thickened casings and it has been shown that because only a local region of a casing takes part in destroying the energy of a fragment by stretching and distorting, a local thick area of casing behaves as though it were part of a complete ring of the same thickness. By applying this principle, a given standard of protection could be provided for a given aircraft for a minimum engine weight penalty.

FUTURE

Research work is required in the subjects listed below and to some degree, it is in progress.

- (a) Control of direction of fatigue crack propagation in discs.
- (b) Loss of energy of a fragment due to passing through a casing.
- (c) Effect of blade/disc configuration upon loss of energy in passing through a casing.
- (d) Containment criteria for a group of blades and a piece of disc, as opposed to a single blade.
- (e) Containment ability of casings of various materials and configurations.
- (f) Directional release of debris.

ACKNOWLEDGEMENT

The research work referred to in this paper was carried out with the support of the Procurement Executive, Ministry of Defence.

PROBABILITE DE PERFORATION D'UNE STRUCTURE D'AVION PAR DES DEBRIS DE MOTEURS

Michel HURET
AEROSPATIALE - DIRECTION DES ETUDES AVIONS
B.P. 5155
51055 - TROUILLOUSE

Les besoins de l'analyse de sécurité imposée par l'éjection de débris de moteurs conduisent à l'élaboration de schémas de perforation des structures d'avion. Pour être pratiquement utilisables dans ce but ces schémas doivent être simples tout en restant réalistes. Pour ce faire, il apparaît préférable d'utiliser différents schémas adaptés à chaque situation suivant la nature des obstacles et des projectiles en présence. Un ensemble d'essais relativement simples permet en particulier de justifier et d'adapter à la situation étudiée un tel schéma pour la perforation des structures et des blindages métalliques. Ce schéma peut alors être utilisé à la détermination de la probabilité de perforation des structures par des débris définis par un modèle d'éjection élaboré par le motoriste. Le développement de cette méthode fournit des bases rationnelles à un jugement objectif de la situation. Il permet de dégager de nouvelles perspectives pour la recherche et l'analyse de solutions plus performantes.

1. POSITION DU PROBLEME

1.1 L'objectif sécurité

La sécurité du transport aérien reste un objectif fondamental des constructeurs, avionneurs et motoristes, et des exploitants sous la conduite des Autorités Officielles. Les efforts inlassables déployés par tous en ce domaine ne sont pas vains si on en juge par l'amélioration constante du niveau global de sécurité. A l'heure actuelle le transport aérien tient une place honorable dans ce domaine, intermédiaire entre l'automobile et le train. Ce résultat, pour encourageant qu'il soit, ne conduit cependant pas à relâcher les efforts en ce domaine. L'expérience acquise permet à chaque nouvelle génération d'avions de transport d'améliorer cette situation. C'est ainsi qu'en dépit de sa percée dans le domaine du transport supersonique, vous pouvez être assuré que tout a été mis en œuvre pour que CONCORDE ne faillisse pas à cette règle. Nous allons vous présenter un aperçu des développements effectués dans un domaine très particulier de ce vaste problème. Ce faisant, il convient de ne pas perdre de vue deux des aspects qui nous paraissent essentiels en ce domaine : je me permets de le rappeler ici car plongés dans une analyse parcellaire nous risquons de perdre de vue ces éléments fondamentaux.

a) La sécurité n'est pas un problème déterministe.

Un problème de sécurité ne peut se poser de par sa nature même qu'en termes de probabilité. Il est clair que si les choses étaient parfaitement déterminées il y a bien longtemps qu'il n'existerait plus de catastrophe. Mais notre ignorance ou l'imprévisibilité de certains phénomènes nous posent ce problème. En matière de sécurité, la certitude absolue n'existe pas. On ne peut parler de risque nul ni à fortiori l'exiger même pour le transport aérien. Cependant nous nous permettons par abus de langage de dire qu'un risque est nul ou plutôt négligeable en nous référant au moins implicitement à un niveau général de plusieurs ordres de grandeur supérieur.

b) La sécurité ne se partage pas.

L'impact psycho-sociologique considérable de la catastrophe aérienne est lié nous semble-t-il à l'importance du nombre des victimes et à l'absence quasi générale de rencap. Les raisons de la catastrophe lorsqu'on peut les déterminer n'intéressent que peu le public. C'est seulement affaire de spécialiste. Il est tout à fait vain de chercher à réduire un risque particulier à néant si simultanément un effort homogène n'est pas effectué sur l'ensemble des autres risques. Ceci n'aura pas modifié la situation du passager et ne peut servir qu'à donner l'illusion d'une bonne conscience à certains spécialistes.

Il convient tout particulièrement de ne pas perdre de vue ces considérations générales puisque nous n'allons plus nous intéresser qu'à un aspect très particulier de la sécurité, celui des conséquences d'éjection de débris de moteurs. C'est pourquoi ceci nous conduit forcément à aborder ce problème du point de vue des probabilités et non d'un point de vue purement déterministe et à nous intéresser essentiellement à l'ordre de grandeur relatif de ces probabilités.

1.2 L'écèlement des disques

Il arrive malheureusement que pour diverses raisons les rotors des réacteurs éclatent en projetant dans l'espace environnant des débris variés.

En raison des conséquences catastrophiques pouvant en résulter pour l'avion il est maintenant généralement admis par les motoristes d'assurer la rétention de ces débris dans le carter du moteur en cas de rupture d'aubes. Mais il peut se produire des incidents plus graves : des ruptures de disques.

Dans ce cas les motoristes ne s'engagent pas à l'heure actuelle à assurer la rétention de ces débris. Il appartient alors aux avionneurs d'apprécier le risque en résultant et de rechercher les moyens adéquats pour minimiser à un niveau convenable la probabilité de conséquences catastrophiques pouvant en découler. Naturellement les motoristes font tout leur possible pour chercher à réduire le nombre d'incidents de cette sorte. Ces efforts ne sont pas vains d'ailleurs, si on en juge d'après la décroissance lente mais régulière depuis une dizaine d'années de la fréquence de ce phénomène.

C'est en se basant sur cette vaste expérience et compte tenu des précautions adoptées lors du développement de ce nouveau moteur que ROLLS ROYCE a avancé la valeur de 0,55 incidents de ce type par million d'heures de vol avion. Cette valeur s'entend pour le quadri-réacteur CONCORDE effectuant une étape type d'une durée moyenne de trois heures.

Cependant ce risque est encore suffisamment grand pour avoir fait l'objet d'une étude particulièrement importante de la part des avionneurs. Pour s'en convaincre il suffit de comparer cette valeur à celle

du risque global, Fig. 1. Il convient donc de justifier pour cette seule cause un risque de conséquence catastrophique notablement inférieur.

Naturellement pour en juger l'avionneur doit disposer d'informations sur les caractéristiques des éjections :

- trajectoire des débris,
- nature des débris,
- énergie des débris.

Ces informations associées à des répartitions de probabilité constituent le modèle d'éclatement.

1.3 Le modèle d'éclatement

L'analyse minutieuse de tous les incidents de ce type survenus à ce jour alliée à une connaissance approfondie du moteur ne nous semble pas encore suffisante aujourd'hui pour élaborer sur des bases strictement rationnelles un modèle complet d'éclatement. Il convient de ne pas perdre de vue ce caractère hautement hypothétique du modèle. En particulier, on ne peut en déduire plus que des ordres de grandeurs de certains risques et on ne peut espérer atteindre aucune conclusion certaine. Ceci est cependant suffisant compte tenu des remarques générales précédentes si on se place naturellement en dehors de tous cadres déterministes.

A titre d'exemple, dans le modèle utilisé la définition des trajectoires est du même type pour tous les débris. Elle est basée sur une trajectoire de base constituée par la tangente dans le plan de rotation du disque au cercle décrit par le centre de gravité du débris avant rupture. La probabilité d'éjection est la même dans toutes ces directions. Cette trajectoire de base peut être déviée à la traversée du carter moteur d'un certain angle θ par rapport au plan de rotation du disque. La valeur maximale de cette déviation est fonction de la nature des débris. Elle est de $\pm 30^\circ$ pour les débris mineurs, de $\pm 5^\circ$ pour les débris majeurs et de $\pm 3^\circ$ pour les tiers de disques de turbine. A cette déviation est associée une répartition de densité de probabilité triangulaire symétrique sur l'intervalle des déviations maximales considérées. Cette distribution est représentée sur la Fig. 2 pour les débris mineurs.

Par nature les débris inclus dans ce modèle sont de trois types :

- aube
- fragment de disque
- tiers de disque de turbine

Il convient de préciser ici pourquoi dans ce modèle on trouve des débris du type aube bien qu'il s'agisse d'un modèle d'éclatement de disque et que les ruptures d'aubes sont supposées contenues par ailleurs. A la suite de l'éclatement d'un disque les débris primaires ne sont pas contenus et perforent le carter. Par l'orifice ainsi créé peuvent alors d'échapper des aubes qui peuvent se détacher de la partie intacte du disque. Il s'agit donc en fait de projectiles secondaires.

La forme de chacun de ces débris est définie par ailleurs.

La combinaison de ces différents débris permet de définir huit cas d'éclatement. Ces huit cas sont répertoriés dans le tableau ci-dessous avec leurs fréquences relatives.

	Cas	Fréquences	Nombre de débris et nature
Turbine 75 %	1 Tiers de disque	5 %	2 tiers de disque - énergie maximale
	2 Fragment de disque	20 %	1 fragment de disque - énergie maximale
	3 Aubes haute énergie	8 %	1 aube - énergie répartie entre 55 et 100 % 1 aube - énergie répartie entre 0 et 55 %
	4 Aube basse énergie	40 %	1 aube - énergie à 55 %
	5 Débris multiples	2 %	Equiprobable entre N/3 et N/12 aubes* toutes à 100 % d'énergie.
Compresseur 25 %	6 Fragment de disque	5 %	1 fragment de disque - énergie maximale 1 aube - énergie répartie de 55 à 100 % 2 aubes - énergie répartie de 0 à 55 %
	7 Aubes haute énergie	5 %	1 aube - énergie répartie de 55 à 100 % 1 aube - énergie répartie de 0 à 55 %
	8 Aube basse énergie	15 %	1 aube - énergie à 55 %

* N : nombre d'aubes de l'étage considéré.

Les risques associés sont supposés être équi-répartis respectivement entre les deux étages de turbine et les 14 étages de compresseur.

Les niveaux d'énergie maximale ou à 100 % des divers types de débris sont définis par ailleurs avec ce schéma pour tous les étages du compresseur et de la turbine.

Pour les débris du type tiers de disque de turbine ou fragment de disque cette énergie ne dépend pas de l'angle de déflexion. Par contre, pour les débris du type aube cette énergie est fonction de l'angle de déflexion suivant la loi indiquée sur la Fig. 3.

Lorsque le niveau d'énergie est indiqué comme réparti entre deux limites il est considéré que tous les niveaux d'énergie entre ces limites sont équiprobables.

Ceci étant, on ne peut s'empêcher de remarquer la complexité de ce schéma. Naturellement, il est unanimement reconnu que les débris susceptibles d'être éjectés sont très variés. D'où une certaine tendance naturelle pour augmenter le réalisme à multiplier les types de débris. En fait on est certainement encore très loin du compte car il n'y a probablement pas deux éjections comportant les mêmes débris. Cependant, il faut bien noter que chaque type de débris pris en considération doit être accompagné d'un ensemble d'hypothèses définissant : trajectoires, déflexion, énergie, probabilité d'occurrence associées à ces caractéristiques.

A l'heure actuelle la valeur de la quasi totalité de ces hypothèses repose essentiellement sur un jugement. Il est clair dans ces conditions que l'amoncellement d'hypothèses de cette sorte risque d'éloigner rapidement le modèle proposé du réalisme souhaité. Autrement dit il conviendrait dès l'élaboration du modèle proposé aux avionneurs de ne pas perdre de vue le caractère hautement aléatoire de l'ensemble des phénomènes considérés.

1.4 L'analyse de sécurité

Face à cette situation et à l'aide de ce modèle d'éclatement, l'avionneur va rechercher tous les moyens à sa disposition pour essayer de réduire à un minimum acceptable les risques de conséquences catastrophiques pouvant résulter de ce phénomène. Il est commode de distinguer parmi ces moyens les moyens actifs et les moyens passifs.

La définition des trajectoires fournie par le modèle d'éclatement permet de déterminer un volume entourant les réacteurs qui risque d'être balayé par des débris. L'intersection de ce volume et de l'avion définit alors un volume critique à l'intérieur de l'appareil, Fig. 4.

Naturellement le premier soin à prendre est d'éliminer de ce volume tous les éléments dont la destruction par les débris risquerait d'avoir des conséquences catastrophiques. Malheureusement cette solution simple ne peut être appliquée à tous les cas. En effet le volume critique coupe l'appareil en deux. L'intercommunication vitale entre ces deux parties nécessite donc de faire traverser le volume critique par un certain nombre de circuits.

Pour réduire le risque en résultant on applique alors le principe de la duplication des circuits vitaux. Sur CONCORDE tous ces circuits sont triplés. Il y a lieu de noter que cette duplication résulte également d'autres considérations. Il convient néanmoins d'attribuer à ce phénomène pour la part qui lui revient les pénalités associées à la réalisation de ce principe.

La duplication a pour corrolaire obligatoire la ségrégation de façon à éviter la rupture des divers circuits par un seul projectile. Chaque circuit constitue un objectif d'une taille relativement faible. Du seul point de vue géométrique la probabilité d'atteindre un tel objectif est faible, généralement largement inférieure à 10^{-2} pour fixer les idées. La probabilité d'atteindre deux ou trois circuits séparés par des projectiles indépendants est donc encore plus largement inférieure à 10^{-4} ou 10^{-6} . Ceci est tout à fait négligeable devant les risques associés aux catastrophes naturelles que constitue par exemple l'éjection de deux tiers de disque de turbine avec l'énergie maximale.

Sous réserve de contrôler simplement l'application des principes de duplication et de ségrégation des circuits il apparaît qu'il pourrait être fait l'économie dans le modèle proposé de tous les cas d'éjections multiples. Il nous semble que ceci serait de nature à clarifier notablement la situation au bénéfice certainement d'une meilleure compréhension des points fondamentaux de l'analyse de sécurité.

Enfin il reste à déterminer le choix des cheminement les plus appropriés compte tenu en particulier des possibilités de protection contre les débris offerts par les structures naturelles de l'avion.

Cette possibilité est illustrée par un incident survenu à une CARAVELLE de la Compagnie A.U.A. peu après un décollage de BUCAREST. Un débris éjecté du moteur a traversé la paroi de nacelle et a perforé la paroi de fuselage. L'énergie absorbée par ces perforations a été suffisante pour protéger la nappe hydraulique située sous la peau du fuselage et l'appareil a pu se reposer en évitant une catastrophe.

Il est certain donc que le choix des cheminement est particulièrement important pour minimiser les risques. Pour motiver ce choix sur une base rationnelle il convient de disposer d'une méthode d'évaluation de la probabilité de perforation des structures de l'appareil par ces débris.

Enfin si l'analyse de sécurité ne conduit pas dans ces conditions à un niveau de risque jugé acceptable, l'avionneur peut avoir recours à des moyens actifs constitués par des blindages supplémentaires destinés à arrêter plus ou moins partiellement ou à dévier les projectiles se dirigeant vers des points sensibles. La méthode d'évaluation de ces blindages ne sera pas essentiellement différente de la méthode précédente et de toute façon il y aura lieu de tirer partie de la protection naturelle des structures. En effet ce type de solution est dans l'état actuel de la technologie extrêmement pénalisant en particulier sur le plan des masses.

Ces quelques considérations préliminaires permettent de se convaincre de la nécessité du développement d'un tel moyen d'évaluation pour aborder aussi raisonnablement que possible ce type de problème.

2. SCHEMATISATION THEORIQUE

2.1 Objectif du schéma

Il convient de noter tout particulièrement et de ne pas perdre de vue que la schématisation théorique recherchée n'a pas besoin d'être très précise pour les trois raisons fondamentales suivantes :

a) L'application dans le cadre de l'analyse de sécurité ci-dessus évoquée de ce schéma ne demande que l'évaluation de l'ordre de grandeur du niveau d'un certain nombre de risques. Il est bien certain que tous les risques doivent être relativement bien évalués. Compte tenu de la multiplicité des débris inclus dans le modèle, 56 débris différents rien que pour le compresseur, aubes et fragments de disque de chacun des 14 étages avec différentes énergies, de la multiplicité des cibles critiques à envisager, de la multiplicité des obstacles, paroi de nacelle, intrados de voilure, nervures, extrados de voilure, paroi de fuselage etc ..., il convient naturellement de sacrifier quelque peu la précision du schéma à sa simplicité de mise en oeuvre pour pouvoir aboutir raisonnablement à une évaluation exhaustive.

b) Les caractéristiques des débris fournies par le modèle ne peuvent être considérées comme absolument certaines. Il est donc tout à fait inutile que le schéma ait une précision supérieure à celle qui peut être accordée aux données du modèle et qui, dans l'état actuel de nos connaissances, reste extrêmement modeste.

c) Enfin par nature les phénomènes de perforation sont extrêmement complexes. Il nous paraît tout à fait vain sur le plan technique de chercher à analyser en détail tous ces phénomènes dans toutes leurs généralités. Par exemple on sait que les phénomènes diffèrent suivant la nature des corps en présence : projectiles et structures ou blindage. Nous préférons donc développer plusieurs schémas simples adaptés à chacune de ces situations plutôt que de rechercher un schéma plus complexe pouvant les englober toutes.

Par contre, les schémas retenus devront prendre en compte les caractéristiques essentielles qui proviennent du problème posé par l'éclatement non contenu des moteurs. Deux de ces caractéristiques nous paraissent particulièrement importantes.

La première est l'incidence des trajectoires (par rapport aux structures ou au blindage). En effet les structures de l'appareil sont souvent constituées d'éléments successifs orthogonaux. Un cas type est le suivant : paroi de nacelle verticale, intrados de voilure horizontal, nervure verticale, extrados de voilure horizontal, paroi de fuselage verticale. Par suite de l'obliquité et de la diversité des trajectoires on est amené à considérer pratiquement toute la gamme des incidences possibles de zéro à 90°.

La seconde est la présentation de ce projectile à l'impact sur sa trajectoire. Il est indéniable que le pouvoir perforant d'un projectile comme une aube de réacteur n'est pas le même suivant que ce débris se présente à plat ou la pointe en avant. De ce fait le problème est essentiellement différent de celui posé aux armuriers par les artilleurs qui s'appliquent à expédier des projectiles pointus axés et stabilisés sur leurs trajectoires. Il est implicitement admis dans le modèle, que chaque débris peut se présenter sur sa trajectoire de toutes les façons possibles avec la même probabilité. Il est donc essentiel du point de vue des probabilités de tenir compte de cette situation.

2.2 Schéma pour un blindage plastique

2.2.1 Considération énergétique globale

Les deux corps en présence, c'est-à-dire :

- le projectile constitué ici par une aube ou un fragment de disque
- le blindage constitué ici par une plaque avec éventuellement son support,

peuvent être caractérisés par leurs énergies cinétiques E^c et leurs énergies internes E^i . Globalement le principe de la conservation de l'énergie permet d'écrire la relation suivante entre les variations de ces grandeurs entre deux instants successifs et plus particulièrement entre le début et la fin du choc :

$$\Delta E_B^i + \Delta E_B^c + \Delta E_A^i + \Delta E_A^c = 0$$

avec l'indice B pour les caractéristiques du blindage et A pour celles de l'aube.

Globalement il y aura naturellement transfert de l'énergie cinétique de l'aube incidente E_A^c vers les autres formes d'énergie. Cette relation est naturellement trop générale pour être d'une grande utilité, mais il semble possible dans le cas présent de l'explicitier un peu plus tout en la simplifiant. Compte tenu de la nature des matériaux en présence, il est raisonnable d'admettre que le projectile se comporte comme un corps rigide indéformable.

La relation précédente se réduit alors à : $\Delta E_B^i + \Delta E_B^c + \Delta E_A^c = 0$

En ce qui concerne le blindage on peut chercher à éliminer le terme énergie cinétique. L'analyse ultérieure permettra de préciser ce point de vue.

2.2.2 Considération énergétique partielle

Même simplifiée dans le cadre du présent problème, la relation énergétique globale précédente est trop générale pour être utilisable. Pour progresser dans notre analyse, il est nécessaire de préciser les actions de contact entre le projectile et le blindage au cours du choc.

La première hypothèse est de considérer le blindage comme homogène bien qu'il soit constitué d'une matrice de résine renforcée par des nappes de fils synthétiques. Pour ce faire il sera vérifié que la plus grande des distances caractéristiques entre les fils est bien inférieure à la plus petite des dimensions caractéristiques de l'aube d'une part et que d'autre part la structure du réseau de ces fils est isotrope à cette échelle. Dans ces conditions l'aube pour pénétrer dans le blindage doit rompre ces fils et on peut admettre que l'énergie nécessaire δE est, du fait de la densité du réseau des fils proportionnelle au volume du cratère ainsi constitué δV . Soit : $\delta E = p \delta V$ en négligeant par ailleurs l'effort de pénétration dans la matrice de résine.

En désignant par \vec{n} le vecteur unitaire normal à la surface de contact S entre l'aube et le blindage, par \vec{V}_{AB} la vitesse de la paroi de l'aube par rapport à celle du blindage, le volume constitué pendant l'intervalle de temps Δt est égale à :

$$\delta V = \int_S \vec{n} \cdot \vec{V}_{AB} dS \Delta t$$

d'où

$$\delta E = p \int_S \vec{n} \cdot \vec{V}_{AB} dS \Delta t$$

Si f est la force de contact, son travail est aussi égal à :

$$\delta E = \int_S \vec{f} \cdot \vec{V}_{AB} dS \Delta t$$

Il en résulte que : $\vec{f} = p \vec{n}$

Autrement dit, l'effort de contact est assimilé à une pression constante s'exerçant sur la surface de contact et caractéristique de l'énergie volumique de décohésion du blindage. Les auteurs du document AD 601-200 ("Study of mechanisms of armor penetration resistance" du Ballistic Research Laboratory d'Aberdeen - "Mathematical model for energy loss mechanisms in composite media" des Drs S. TSAI et D. ADAMS) arrivent à la même conclusion après un examen visuel de la surface des cratères créés dans des blindages de ce type. Il y a lieu de noter que ces phénomènes sont bien différents en statique ou à vitesse lente. La pression caractéristique p est la contrainte de rupture dynamique différente de la contrainte de rupture statique σ en traction des fils par flexion de la plaque.

Suivant la nature des constituants du blindage, le rapport p/σ évolue entre 1 et 2 d'après les essais rapportés dans ce document.

En admettant cette conception, la variation de l'énergie interne de décohésion du blindage prend donc la forme :

$$\Delta E_B^i (\text{décohésion}) = p \int_S \vec{n} \cdot \vec{V}_{AB} dS \Delta t$$

D'autre part, la variation de l'énergie interne de déformation du blindage et de son énergie cinétique est égale au travail des forces extérieures $p \vec{n}$ sur la surface de contact S du blindage avec l'aube qui se déplace à la vitesse \vec{V}_B

$$\Delta E_B^i (\text{déformation}) + \Delta E_B^c = p \int_S \vec{n} \cdot \vec{V}_B dS \Delta t$$

D'où en sommant

$$\Delta E_B^i + \Delta E_B^e \text{ (décohésion)} + \Delta E_B^i \text{ (déformation)}$$

$$\Delta E_B^i + \Delta E_B^e = p \int_S (\bar{V}_{AB} + \bar{V}_B) dS \Delta t$$

Or, la vitesse de l'aube est égale à :

$$\bar{V}_A = \bar{V}_{AB} + \bar{V}_B$$

d'où

$$\Delta E_B^i + \Delta E_B^e = p \int_S \bar{V}_A dS \Delta t$$

D'autre part pour l'aube, on a de la même façon : $\Delta E_A^e = -p \int_S \bar{V}_A dS \Delta t$

Par élimination de p, ces deux relations conduisent à la relation énergétique globale du § 2.2.1. Cependant, cette analyse a permis de préciser la structure des échanges énergétiques entre l'aube et le blindage.

2.2.3 Schématisation des caractéristiques dynamiques du blindage

Afin de poursuivre cette analyse il nous faut maintenant exprimer de façon plus précise les caractéristiques dynamiques du blindage qui permettent de déterminer les expressions de son énergie cinétique et de son énergie de déformation.

Nous supposons que le blindage est constitué par une plaque carrée de cotés a simplement appuyée sur son contour sur un cadre infiniment rigide. Nous supposons de plus, pour ne pas multiplier les calculs, que l'aube vient percuter le blindage en son centre.

Nous allons chercher à représenter le blindage par une masse ponctuelle équivalente appelée élastiquement et placée au point d'impact. En ne considérant que la première forme propre de cette plaque, la masse équivalente est égale à :

$$\mu = \frac{4}{\pi^2} M$$

en désignant par M la masse totale du blindage.

De la même façon le coefficient de rappel élastique peut être évalué à : $f = \frac{E h^3}{\alpha a^2}$

E désignant le module d'Young et h l'épaisseur de la plaque; α est une constante numérique ($\alpha = 0,13$).

Ces relations pour calculer μ et f ne sont données qu'à titre indicatif pour déterminer ci-après quelques ordres de grandeur. Il serait intéressant de les déterminer expérimentalement compte tenu des conditions d'appuis réels de la plaque, des caractéristiques plastiques du matériau et éventuellement en fonction des caractéristiques de l'entaille provoquée par le projectile.

2.2.4 Formulation simplifiée pour un projectile cylindrique

Considérons un projectile cylindrique attaquant normalement le blindage. Soit A la section de contact qui est constante dans ce cas. L'ensemble des hypothèses faites précédemment permet de décrire le mouvement de pénétration par les deux équations suivantes :

$$\begin{aligned} \text{- mouvement de l'aube : } m \ddot{z} &= -pA \\ \text{- mouvement du blindage : } \mu \ddot{\xi} + f \xi &= pA \end{aligned}$$

en désignant par z le déplacement de l'aube de masse m et par ξ celui du blindage.

Soit h leur déplacement relatif, c'est-à-dire la profondeur du cratère créé par l'aube dans le blindage : $h = z - \xi$

on a :

$$h \frac{dh}{dt} = -pA \left(\frac{1}{m} + \frac{1}{\mu} \right) + \frac{f}{\mu} \xi$$

A l'instant initial $h = 0$ et $h' = V$ vitesse de l'aube. L'aube cesse de s'enfoncer dans le blindage lorsque $h = 0$. On a donc :

$$\frac{1}{2} m V^2 = pA \left(1 + \frac{m}{\mu} \right) h + \int_0^h \frac{m f \xi}{\mu} dh$$

Si on néglige l'énergie de déformation élastique du blindage représentée par le terme intégral on obtient la relation approchée :

$$h = \frac{\frac{1}{2} m V^2}{pA \left(1 + \frac{m}{\mu} \right)}$$

Avant de généraliser cette formule pour les applications en vue, nous allons la comparer avec la formule de TSAI et ADAMS dans laquelle K est un coefficient de forme qui vaut d'ailleurs 1 dans le cas d'un projectile cylindrique à fond plat : $h = \frac{m}{K p A} \cdot \log \left(1 + \frac{K p V^2}{2 p} \right)$

Les conceptions avancées sont très voisines des nôtres sauf en ce qui concerne le calcul de l'énergie cinétique prise par le blindage. En effet, ces auteurs écrivent que le travail de la force de contact est égal à l'énergie cinétique prise par l'élément de volume du blindage surmontant l'aire d'impact. En fait nous pensons que ceci est incorrect pour les raisons suivantes :

- le travail de la force est égal à la variation d'énergie cinétique et non à l'énergie cinétique.
- la vitesse de blindage n'est pas celle de l'aube sinon il n'y aurait pas pénétration.
- l'élément de masse intéressé n'est pas uniquement l'élément au-dessus, mais tout le blindage est entraîné plus ou moins.

Il est alors clair qu'en approximant le terme $\log(1+x)$ par x, ce qui revient à négliger l'énergie cinétique du blindage on retrouve identiquement la même formule.

L'évaluation numérique de quelques ordres de grandeur permet d'ailleurs de justifier cette hypothèse pour les applications envisagées.

2.2.5 Extension de la méthode

Dans le cas d'une aube d'une géométrie en définitive fort tourmentée, on peut établir un critère tout aussi simple. En effet en revenant à l'équation de base on peut également intégrer lorsque l'aire de contact A est variable avec h.

On a alors :

$$\int_0^h A dh = \frac{1}{2} m v^2 - \frac{m \int_0^h \frac{dh}{p(1+\frac{h}{p})}}{p(1+\frac{h}{p})}$$

et le premier membre n'est autre que le volume du cratère créé par l'aube si bien qu'en négligeant éventuellement l'énergie de déformation élastique du blindage on obtient le critère : $\gamma = \frac{1/2 m v^2}{p(1+\frac{h}{p})}$ qui nous semble généraliser d'une façon convenable la formule précédente.

Ceci permettrait en particulier de traiter également le cas d'une trajectoire à incidence non normale.

Enfin dans le cas d'une aube, il est clair que les forces de contact vont créer également un couple qui va engendrer une énergie cinétique de rotation de l'aube. Ceci va avoir pour effet :

- d'améliorer l'efficacité du blindage car cette énergie cinétique de rotation ne peut provenir que de l'énergie cinétique initiale de l'aube ce qui réduit d'autant ce que le blindage doit absorber en énergie de décohéation, de déformation ou cinétique.
- d'augmenter le volume du cratère pour une même épaisseur traversée car la rotation induite va avoir pour effet de coucher l'aube sur le blindage, ce qui va augmenter l'aire de contact A.

Le traitement complet du problème vu sous cet angle nous semble sortir complètement du cadre limité que nous nous sommes fixé. Néanmoins, je pense qu'il était bon de préciser les limitations de certaines approximations.

2.3 Schéma pour un blindage métallique ou une structure

2.3.1 Considération générale

Dans le cas d'un blindage ou d'une structure métallique, le mécanisme des phénomènes de perforation est apparemment tout à fait différent de celui avancé ci-dessus pour la perforation d'un blindage plastique.

Naturellement les considérations énergétiques globales restent les mêmes. Nous admettrons également que le projectile se comporte comme un corps rigide indéformable bien que ceci soit certainement beaucoup moins vraisemblable que précédemment. Par contre l'expérience montre que dans les cas étudiés, les déformations du blindage sont relativement faibles, ce qui permet de négliger plus facilement les termes d'énergie de déformation élastique et d'énergie cinétique de ce type de blindage.

2.3.2 Considération énergétique partielle

Il est maintenant nécessaire de revoir les actions de contact entre le projectile et le blindage au cours du choc. Un examen visuel rapide d'un certain nombre de résultats d'essais effectués dans ces conditions nous a conduit à admettre que le mécanisme fondamental de perforation est une rupture par cisaillement dynamique. Ce mécanisme est naturellement tout à fait différent de celui examiné précédemment pour la perforation d'un blindage plastique. Comme il a été souligné ab initio ceci provient de la nature différente des corps en présence.

Suivant ce point de vue l'effort de pénétration est proportionnel à l'aire cisailée. Dans le cas d'une plaque, cette aire est proportionnelle au produit du périmètre L de la projection suivant la vitesse V du projectile en admettant que ce dernier ne tourne pas durant l'impact, par l'épaisseur cisailée $\frac{L}{\cos i}$, e étant l'épaisseur de la plaque et i l'incidence de la vitesse du projectile, angle de cette vitesse avec la normale à la paroi.

Il convient de bien noter pour éviter toute confusion, que ceci ne veut pas dire que la déchirure de la plaque s'effectue strictement suivant le périmètre. L n'est en fait qu'un paramètre d'échelle. Ceci veut dire en fait que l'énergie de perforation sera finalement proportionnelle à la taille du projectile et que nous avons trouvé commode pour caractériser la taille de nos débris de prendre ce paramètre.

Il en résulte que la variation d'énergie cinétique de l'aube doit pouvoir se mettre sous la forme : $\Delta E_A = - \frac{E_L \cos^2 i}{\cos^2 i}$

ce qui définit un coefficient de proportionnalité γ . Ce coefficient a les dimensions d'une contrainte. Nous l'appellerons la contrainte apparente de rupture en cisaillement dynamique de la plaque. Elle n'est naturellement pas directement liée aux caractéristiques habituelles du matériau et doit être déterminée dans chaque cas par des essais aussi représentatifs que possible de l'ensemble du phénomène.

Ce schéma nous semble bien répondre aux objectifs généraux exposés ci-avant. En particulier il prend bien en compte l'effet de taille du projectile et l'effet d'incidence. Il y a lieu de noter que pour un projectile sphérique, le périmètre projeté L est inversement proportionnel à $\cos i$, ce qui n'est pas vrai ici pour une aube de forme complexe, le contour apparent se modifiant suivant la direction de \vec{V} dans l'aube. On retrouve alors dans ce cas l'effet d'incidence en cosinus cube de la loi de Smith, ce qui nous paraît être un recoupement intéressant pour justifier cet aspect de la formulation présentée.

2.3.3 Extension aux structures

Les structures avion sont constituées bien souvent de plaques munies de raidisseurs, soit obtenues par un usinage dans la masse, soit rapportées comme des cornières. L'énergie de perforation de ces éléments ne peut être négligée devant celle de la paroi proprement dite au moins pour les plus importants d'entre eux.

Pour ces éléments l'effet de taille n'est manifestement plus relié directement à la taille des projectiles si ce n'est par le nombre d'entre eux qui doivent alors laisser le passage aux projectiles.

Nous sommes donc amenés à relier cet effet de taille à celle du raidisseur. Nous admettrons que la rupture se fait suivant la section la plus faible, c'est-à-dire la section droite S_j du raidisseur. Nous conserverons néanmoins l'effet d'incidence en prenant pour section cisailée $\bar{S}_j = \frac{S_j}{\cos i}$ dans le cas où le tir est dans la direction du raidisseur.

De la même façon le déplacement de l'effort de perforation est ramené à la hauteur cisailée h_j.

Dans le cas d'un raidisseur de section rectangulaire, la dimension caractéristique est choisie en fonction de celle du tir, on a alors : $\bar{h}_j = \frac{h_j}{\cos i}$ ou $\frac{h_j}{\sin i}$ suivant l'orientation.

Ces considérations nous conduisent à généraliser notre formulation sous la forme suivante:

$$\Delta E_A^c = -G \left[1 - \frac{v^2}{c^2} \right] - \sum_j \bar{G}_j \bar{h}_j$$

en étendant la sommation j à tous les éléments de renfort de cette nature interposées sur la trajectoire du projectile.

Pour un même matériau le coefficient \bar{G}_j n'est pas forcément égal à G car il inclut une schématisation des phénomènes de rupture qui ne peuvent être identiques. Il serait cependant extrêmement difficile de pouvoir déterminer ces valeurs expérimentalement et nous admettrons de prendre en première approximation une valeur unique. Nous obtenons alors la formulation définitive suivante :

$$\Delta E_A^c = -G \left[1 - \frac{v^2}{c^2} + \sum_j \bar{G}_j \bar{h}_j \right]$$

Il y a lieu de noter que cette conception de décomposition et de sommation des éléments n'est certainement pas très justifiable a priori, le mécanisme de rupture d'un ensemble d'éléments pouvant être fort éloigné de la superposition de ceux des différents composants. C'est ainsi que pour un raidisseur intégré nous avons admis qu'il y avait deux sections j cisailées alors que pour un élément disjoint nous n'en considérons qu'une. En effet dans ce cas nous estimons que le travail de déformation de cet élément pour livrer passage au projectile après rupture suivant une section n'est pas très important vis à vis de l'énergie de rupture d'une seconde section.

3. AJUSTEMENT EXPERIMENTAL DU SCHEMA

3.1 Objectifs

L'analyse des considérations théoriques ne peut que nous convaincre de la nécessité d'une justification expérimentale de ces schémas. En outre, chacun de ces schémas comporte une caractéristique dont la détermination expérimentale est nécessaire. Tout ceci doit naturellement être réalisé dans les conditions les plus réalistes possibles car la simplicité voulue de ces schémas interdit naturellement toute transposition.

C'est ainsi que ces essais ont été réalisés avec des tirs d'aubes de réacteur. Il a été possible d'explorer entièrement la plage des énergies couvertes par les débris du modèle à la seule exception des tiers de disque de turbine qui se trouvent avoir un niveau d'énergie de deux ordres de grandeur supérieur.

Les tirs ont été effectués sur :

- des plaques de matériaux divers pour la recherche des blindages,
- un caisson de voilure de CONCORDE très représentatif des structures avion considérées,
- un élément de blindage monté sur ce caisson pour l'étude des problèmes de fixation.

Les essais sur des plaques de blindage en matériau plastique nous ont rapidement conduit à abandonner cette solution compte tenu :

- des performances de ce type de matériaux dans ces conditions,
- des problèmes de fixation de ce type de blindage sur la structure avion,
- des contraintes d'encombrement.

C'est pourquoi nous allons maintenant nous limiter uniquement à la considération de blindage et de structures métalliques. Naturellement ces conclusions sur le mérite des blindages plastiques sont toutes relatives et provisoires et nous souhaiterions bien sûr que le développement de matériaux nouveaux nous permettent d'améliorer la présente situation.

3.2 Moyens d'essais

Ces essais ont été réalisés par le Centre d'Essai Aéronautique de TOULOUSE. Le moyen de propulsion est un canon à air comprimé comprenant un réservoir de $1m^3$, une vanne à ouverture rapide, une culasse et un tube de 12m de long et 150mm de diamètre. Pour le tir les aubes sont enrobées sur une partie de leur longueur dans un cylindre de polystyrène expansé de ce diamètre. A la sortie du canon des couteaux sont chargés de déchiqueter cet emballage.

Avant le tir chaque aube est pesée et son positionnement repéré. Le diamètre du canon ne permet que les tirs axiaux pour les plus grandes aubes. C'est pourquoi la quasi totalité des essais a été réalisée dans cette configuration - la plus défavorable - Cependant pour les plus petites il a été possible de réaliser des tirs sur le tranchant ou à plat.

La vitesse du projectile à la sortie du canon est mesurée par un système classique. En outre, il a été installé une caméra FASTAX à grande vitesse de prise de vue (8 000 images/seconde) pour pouvoir observer l'impact du projectile, sa pénétration et éventuellement sa sortie. Une base de temps s'inscrivant sur le film permet également de déterminer la vitesse du projectile à l'entrée et à la sortie. Le fonctionnement de cette caméra est synchronisé par la séquence de tir. Malheureusement, les conditions d'essais n'ont que rarement permis de tirer partie de cette instrumentation dont la mise en oeuvre s'est révélée plus délicate que prévue.

Par contre, la mise en oeuvre du canon s'est révélée excellente, les vitesses désirées ayant toujours été obtenues. La cible est placée verticalement devant le canon. Son orientation permet d'obtenir tous les angles d'incidences. Enfin une enceinte de protection permet d'éviter l'endommagement des installations environnantes et de récupérer les débris après chaque tir.

3.3 Analyse des résultats

Nous avons analysé globalement l'ensemble des résultats d'essais obtenus pour des tirs sur des plaques en AU20NT6 et sur le caisson de voilure. Pour ce faire nous avons reporté dans un diagramme le résultat observé de la perforation en fonction de l'énergie cinétique initiale du projectile et des paramètres de similitude. Le diagramme ainsi obtenu est représenté sur la figure 5.

On peut distinguer très nettement trois zones:

- 1) Une zone à grande énergie où l'aube perce et traverse la paroi,
- 2) Une zone à basse énergie où l'aube est contenue et la paroi n'est pas perforée,
- 3) Une zone intermédiaire dans laquelle on trouve simultanément des tirs de l'un ou de l'autre des deux types précédents ainsi que des tirs pour lesquelles l'aube a été contenue mais la paroi perforée plus ou moins gravement.

L'ensemble de ces zones se trouve facilement limité par des droites dont la pente fournit la valeur de la constante ξ du schéma. L'éventail constitué par la zone intermédiaire représente la plage d'incertitude sur la validité du schéma et la valeur de ξ . Il y a lieu de noter que l'existence d'une telle plage d'incertitude nous semble bien naturelle du fait :

- 1) De la dispersion naturelle des phénomènes de perforation amplifiée ici par l'hétérogénéité de l'obstacle et la diversité des projectiles et des conditions de tir,
- 2) De la simplicité du schéma examiné qui ne peut naturellement prétendre tenir compte exactement de l'ensemble des phénomènes mis en jeu.

On observe ainsi entre les valeurs extrêmes de ξ recouvrant cette plage d'incertitude une variation de l'ordre de 1 à 2. Pour apprécier cette incertitude il convient de noter :

- 1) Que la variation due à l'effet d'incidence dans la plage explorée est de l'ordre de 1 à 6.
- 2) Que la variation due à l'effet de taille des projectiles est de l'ordre de 1 à 10.

Il en résulte qu'au moins en ce qui concerne ces deux effets fondamentaux le schéma proposé traduit de façon significative au moins l'ordre de grandeur de ces phénomènes.

Il a été procédé à une analyse similaire pour, séparément, les tirs sur le caisson de voilure et ceux sur les plaques simples. On observe le même résultat et les valeurs moyennes du coefficient ξ qui peuvent être déduites sont identiques à 1 hb près. Ceci nous permet de justifier en première approximation la schématisation que nous avons adoptée pour les structures complexes. De l'analyse détaillée de chacun de ces tirs on peut extraire par exemple les remarques suivantes particulièrement significatives :

- a) Effet d'incidence - Comparaison des tirs n° 46 et 50.
Le projectile est le même, aube de 7e étage lancée axialement talon en avant sur une plaque de 8mm d'AU2GN. L'énergie de ces projectiles est pratiquement identique 670 et 663 kgm. Par contre, l'incidence des tirs est différente respectivement 25 et 55°. Le premier perce la tôle et l'aube passe au travers alors que le second tir est arrêté.
- b) Effet de présentation - Comparaison des tirs 50 et 61.
Il s'agit toujours du même projectile et de la même cible. L'énergie est voisine : 634 kgm. L'incidence est la même 55°. Par contre l'aube est maintenant lancée lame en avant son axe faisant un angle de 30° avec la direction du tir. L'aube est arrêtée ne laissant qu'une légère empreinte dans la tôle.
- c) Effet dynamique - Cas du tir 48.
Il s'agit encore du même projectile et de la même cible. L'énergie est toujours du même ordre 615 kgm. L'incidence est de 25°. L'aube est présentée comme pour le tir 51. A l'impact l'aube ayant touché la plaque par le bout de la lame, elle s'est enroulée sur elle-même pour venir s'arrêter à plat sans la perforer. Ceci nous semble illustrer l'un des nombreux phénomènes annexes qui expliquent la dispersion naturelle des résultats observés.

L'ensemble de ces essais effectués avec le même projectile ayant une énergie pratiquement constante et sur la même cible démontre parfaitement par la diversité des résultats la complexité des phénomènes. Le schéma très simple considéré permet manifestement de faire rentrer l'ensemble de ces phénomènes dans un cadre suffisamment restreint pour être valablement utilisé à la détermination des objectifs que nous nous sommes proposés.

L'élaboration d'un schéma plus complexe pouvant réduire de façon significative la marge d'incertitude résiduelle nous paraît être une voie qui ne peut déboucher raisonnablement sur une méthode efficace. Ceci n'exclue pas naturellement de poursuivre les études fondamentales dans cette voie pour la compréhension des phénomènes et la recherche de meilleurs matériaux de blindage par exemple. Nous disons simplement que ceci sort du cadre de nos préoccupations techniques actuelles.

Pour déterminer le niveau de probabilité de perforation il convient de retenir la valeur moyenne de ξ . Ceci conduit à estimer la valeur moyenne de cette probabilité. C'est la valeur la plus probable, ou encore du point de vue statistique la meilleure estimation qui puisse être faite.

A ce stade il convient encore de rejeter le point de vue déterministe qui consisterait à prendre une valeur de ξ plus faible associée à un degré de confiance supérieure à 50 %. Ceci conduirait à évaluer un niveau de probabilité de perforation supérieur qui ne serait pas la meilleure estimation mais une borne supérieure associée à un degré de confiance sans signification du fait notamment de l'absence d'ailleurs bien compréhensible d'information analogue cohérente pour le modèle de base.

3.4 Observations complémentaires

Les essais effectués sur le caisson de voilure ont permis de faire un certain nombre d'observations complémentaires.

- a) En dépit des dégâts parfois importants imposés au caisson, sa résistance structurale intrinsèque ne paraît pas affectée compte tenu notamment du caractère fail-safe de la conception structurale. Ceci permet alors d'envisager et de réaliser la fixation de blindage de protection sur les points forts de la structure. Des essais ultérieurs ont permis de mettre au point et de justifier ces fixations.
- b) L'examen des perforations successives montre une déflexion négligeable des trajectoires. Ceci permet en particulier de justifier la notion de volume critique introduite a priori au § 1.4 et de simplifier notamment l'analyse ultérieure.
- c) A l'impact on observe généralement qu'une rotation assez rapide est communiquée au projectile. Pour la phase précédant la perforation ceci rend compte comme nous l'avons vu d'une part de la dispersion associée à ce phénomène. Pour la phase après perforation, on peut noter que l'énergie cinétique de rotation ainsi communiquée à l'aube est suffisamment faible pour être négligée devant celle de translation mais que ceci assure néanmoins une présentation aléatoire indépendante du projectile sur l'obstacle suivant.

4. UTILISATION DU SCHEMA

4.1 Détermination de l'énergie de perforation

Le schéma permet d'évaluer l'énergie nécessaire à la perforation pour un débris donné en fonction du périmètre de la section projetée. Cette valeur dépend de la présentation du projectile sur sa trajec-

toire. En accord avec les hypothèses du modèle et les constatations expérimentales précédentes nous avons admis que cette présentation est aléatoire. L'énergie de perforation se présente alors sous la forme d'une variable aléatoire dont nous allons déterminer la distribution de probabilité.

Les projectiles considérés ayant des formes relativement complexes, une représentation simple est obtenue par un découpage en faces triangulaires. La précision recherchée n'étant pas très élevée, un nombre relativement restreint de facettes suffit. Les Figures 6, 7 et 8 illustrent une telle représentation pour l'aube du 1er étage du compresseur basse pression vue par la pointe, sur le tranchant et à plat.

Une rotation des coordonnées permet alors de donner à ce projectile une présentation quelconque. L'ensemble des arêtes peut alors être projeté suivant la vitesse V sur la paroi. Un algorithme d'élimination permet ensuite de déterminer le contour extérieur et d'en déduire L .

On peut alors déterminer l'énergie de perforation et établir la statistique correspondante. On obtient ainsi :

- la probabilité p pour que l'énergie nécessaire à la perforation de la paroi soit au moins égale à une certaine valeur E .
- la densité de probabilité $\frac{dp}{dE}$ qui donne la probabilité dp pour que l'énergie nécessaire à la perforation du blindage soit comprise entre E et $E + dE$.

Les Figures 9 et 10 illustrent à titre d'exemple ce genre de résultat pour la perforation de la paroi d'intrados par une aube de 1er étage du compresseur basse pression issue du moteur 1 en direction de la nervure 12. Ceci permet de montrer que les projectiles de ce type ayant une énergie inférieure à environ 1 200 kgm pour ce tir ont une probabilité négligeable de traverser cette paroi. Il y a lieu de noter l'étalement considérable des énergies dans un rapport de 1 à 20 ce qui traduit outre l'effet de présentation de cette aube l'hétérogénéité importante de la structure de cette paroi. Il en résulte également que la déviation maximale des débris de ce type après perforation de cette paroi est réduite à 18°5 pour les débris à 100 % d'énergie et à 13°5 pour ceux à 55 % au lieu de 30°. Ceci réduit d'autant le volume critique au-delà de cette paroi et permet déjà d'éliminer la considération de certains risques.

4.2 Détermination de la probabilité de perforation

Soit $p_1(E)$ la distribution de probabilité en fonction de l'énergie des projectiles du faisceau incident considéré. La densité de probabilité $p_2(E)$ de l'énergie E des projectiles du faisceau émergent est fournie par le produit de convolution

$$p_2(E) = \int_{-\infty}^{+\infty} p_1(E+E') p'(E') dE'$$

Naturellement les bornes d'intégration sont réduites à celles de l'intersection des supports bornés des distributions p_1 et p' .

Les énergies E négatives correspondent à des projectiles arrêtés par l'obstacle et on a de ce fait dans le faisceau émergent :

$$p_2(E) = \int_0^E p_2'(E) dE$$

Pour E tendant vers l'infini, la probabilité $p_2(E)$ tend vers une valeur constante p_2 inférieure ou égale à 1 qui est la probabilité moyenne de passage des projectiles de l'ensemble du faisceau considéré à travers cet obstacle.

Nous pouvons distinguer trois cas suivant la nature de la distribution p_1 :

- 1) Tous les projectiles incidents ont la même énergie E_0 . La densité de probabilité p_1 se réduit à une distribution de Dirac concentrée en E_0 . On a alors :

$$p_2'(E) = \int_{-\infty}^{+\infty} \delta(E-E'-E_0) p'(E') dE' = p'(E-E_0)$$

Il y a lieu de noter que cette nouvelle répartition est largement étalée de $E_0 - E_{MAX}$ à $E_0 - E_{min}$ en désignant par E_{MAX} et E_{min} les énergies maximales et minimales de perforation.

Il en résulte que ce genre d'hypothèse introduite dans le modèle ne paraît pas cohérent avec les résultats de cette analyse. En fait, il s'agit d'une hypothèse trop déterministe pour recouvrir la multiplicité de la réalité.

- 2) Les projectiles ont une énergie supposée équirépartie entre deux limites E_1 et E_2 .

$$\text{On a alors } p_1 = \frac{1}{E_2 - E_1} \quad \text{et par la suite } p_2'(E) = \frac{1}{E_2 - E_1} [p(E_2 - E) - p(E_1 - E)]$$

Cette distribution est étalée de $E_1 - E_{MAX}$ à $E_2 - E_{min}$

- 3) La distribution p_1 est quelconque. C'est ce qui se présente après perforation d'un premier obstacle. Le produit de convolution est alors évalué numériquement de proche en proche.

A titre d'exemple, nous présentons les résultats suivants pour la détermination du risque de perforation de la nervure 12 par une aube de 1er étage issue du moteur 1 après traversée de l'intrados de voilure.

- Cas d'une aube à 100 % d'énergie - Figure 11. La probabilité de perforation est de 38 %.
- Cas d'une aube à énergie de 55 à 100 % - Figure 12. La probabilité de perforation est de 23 %. Il s'agit d'un tir sans déflexion. D'après le modèle l'énergie des débris de ce type décroît avec la déflexion comme nous l'avons indiqué - Figure 3.

On effectue donc ce calcul pour différente déflexion. Pour $\theta = 5^\circ$ la probabilité de perforation n'est plus que de 9 % - Figure 13.

Compte tenu de la probabilité de déflexion associée p_θ on peut alors déterminer la probabilité moyenne de perforation pour l'ensemble de ce type de débris.

$$\bar{p}_2 = \int_0^{\theta} p_2 p_\theta d\theta$$

Figure 14 - Cette probabilité est de 6 %.

On traite de même le cas de l'aube à 55 % d'énergie et celui de 0 à 55 %.

On obtient ainsi pour chaque type de débris :

- Fragment de disque ou aube à 100 %	38 %
- Aube de 55 à 100 %	6 %
- Aube à 55 %	0,7 %
- Aube de 0 à 55 %	0,1 %

On peut alors déterminer par simple sommation le risque de perforation associé à chaque type de panne :

- Type de panne 6 - 1 fragment de disque	
1 aube de 55 à 100 %	
2 aubes de 0 à 55 %	44 %
- Type de panne 7 - 1 aube de 55 à 100 %	
1 aube de 0 à 55 %	6 %
- Type de panne 8 - 1 aube à 55 %	0,7 %

La sommation pondérée de ces valeurs par la fréquence relative de ces types de panne détermine le risque global : $2,2 + 0,3 + 0,1 = 2,6 \%$.

L'examen de cette décomposition permet de se rendre compte que la quasi totalité des risques provient de l'éjection de fragment de disque. Le modèle proposé n'est donc pas homogène et pourrait être considérablement simplifié ce qui loin de nuire à l'analyse de sécurité permettrait de la clarifier notablement.

Pour continuer il faut tenir compte de la probabilité géométrique d'éjection dans la direction de la cible. On a ainsi par exemple $P_q = 3 \%$. Le risque associé est donc de $0,08 \%$.

En effectuant une détermination analogue pour l'ensemble des 4 moteurs et des 14 étages du compresseur il peut être établi que le risque de perforation des nervures 12 ou 21 est de l'ordre de 10^{-10} par heures de vol.

Un tel résultat permet alors d'étayer un jugement objectif sur l'intérêt d'un blindage de protection dans cette zone pour réduire de façon significative ce niveau de risque. Naturellement une telle analyse est à effectuer simultanément pour l'ensemble des risques de façon à faire ressortir les éléments essentiels pour pouvoir porter un jugement global.

5. PERSPECTIVES

Nous venons de voir comment le schéma proposé permet à partir du modèle d'éclatement fourni par le motoriste de déterminer le niveau des risques associés.

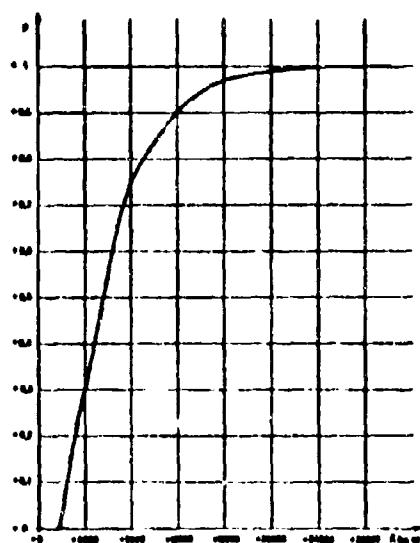
Ce schéma est volontairement aussi simple que possible. Compte tenu des objectifs visés il ne nous semble pas souhaitable de chercher à l'améliorer ce qui ne pourrait conduire qu'à des complications inutiles et rapidement inextricables. Par contre nous pensons que le type de modèle utilisé, bien que parfaitement convenable car il contient toutes les informations nécessaires, ce qui n'est certainement pas déjà un mince travail, gagnerait néanmoins à évoluer dans le sens d'une plus grande simplicité. L'analyse de sécurité associée y gagnerait en clarté sans perte de signification.

Incidemment il convient de suggérer l'utilisation du schéma proposé pour déterminer à partir de l'examen des dégâts provoqués lors de tels phénomènes l'ordre de grandeur de l'énergie des débris. Il y a là certainement une source d'informations des plus utiles pour étayer les hypothèses retenues sur ce point lors de l'élaboration de modèle de ce type.

Enfin il convient de noter que l'ensemble des protections de type actif, c'est-à-dire de blindages, représente pour CONCORDE une pénalité de masse de l'ordre de 600 Kg. En fait, compte tenu de toutes les protections passives également adoptées et bien qu'un bilan exact soit fort difficile à établir, c'est une pénalité globale de l'ordre d'une tonne qu'il faut considérer.

L'importance de ces chiffres qui traduit notre souci de la sécurité sur ce point nous impose de rechercher des améliorations à cette situation. Naturellement ceci conduit à poursuivre les recherches de matériaux et de conception de blindage plus efficaces. Mais simultanément ceci conduit également à revenir à l'origine de ces phénomènes et à se demander si des protections adéquates au niveau des moteurs ne seraient pas en définitive moins pénalisantes au niveau global de l'appareil.

Si de telles protections pouvaient être traduites par des modifications significatives du modèle d'éclatement, le schéma proposé devrait alors permettre d'établir sur des bases aussi rationnelles que possible un bilan global de la situation. Ce schéma devrait donc pouvoir se révéler être un instrument valable pour faire progresser nos conceptions dans le sens d'une plus grande efficacité et d'une meilleure sécurité. Je pense qu'alors il aurait pleinement atteint ses objectifs.



DISTRIBUTION DE LA DENSITE DE PROBABILITE DE L'ENERGIE POUR UN TON
D'UNE ANNE LPS DU MOTEUR 1 VERS LA MECANIQUE 10

Fig 8

A line graph showing the probability distribution of energy for a 1000 Hz tone. The y-axis is labeled 'P' and ranges from 0.0 to 1.0 in increments of 0.1. The x-axis is labeled 'E (J)' and ranges from 0 to 10000 in increments of 1000. The curve starts at (0,0), rises to a peak of approximately 0.9 at E = 1000, then drops sharply to near zero by E = 4000.

DISTRIBUTION DE LA DENSITE DE PROBABILITE DE L'ENERGIE DE PROBABILITE
DE L'ENTRANON POUR UN TON D'UNE ANNE LPS DU MOTEUR 1 VERS LA MECANIQUE 10

Fig 9

A line graph showing the probability distribution of energy for a 1000 Hz tone. The y-axis is labeled 'P' and ranges from 0.0 to 1.0 in increments of 0.1. The x-axis is labeled 'E (J)' and ranges from 0 to 10000 in increments of 1000. The curve starts at (0,0), rises to a peak of approximately 0.9 at E = 1000, then drops sharply to near zero by E = 4000.

PROBABILITE DE PROBABILITE DE LA MECANIQUE 10 PAR UN TON D'UNE ANNE LPS
(ANNE A 1000 Hz) POUR UN TON DU MOTEUR 1 A TRAVERS L'ENTRANON

Fig 11

A line graph showing the probability distribution of energy for a 1000 Hz tone. The y-axis is labeled 'P' and ranges from 0.0 to 1.0 in increments of 0.1. The x-axis is labeled 'E (J)' and ranges from 0 to 10000 in increments of 1000. The curve starts at (0,0), rises to a peak of approximately 0.9 at E = 1000, then drops sharply to near zero by E = 4000.

DEFLECTION 0 - 10°

PROBABILITE DE PROBABILITE DE LA MECANIQUE 10 PAR UN TON D'UNE ANNE LPS A 1000 Hz
D'ENERGIE POUR UN TON DU MOTEUR 1 A TRAVERS L'ENTRANON

Fig 12

A line graph showing the probability distribution of energy for a 1000 Hz tone. The y-axis is labeled 'P' and ranges from 0.0 to 1.0 in increments of 0.1. The x-axis is labeled 'E (J)' and ranges from 0 to 10000 in increments of 1000. The curve starts at (0,0), rises to a peak of approximately 0.9 at E = 1000, then drops sharply to near zero by E = 4000.

DEFLECTION 0 - 10°

PROBABILITE DE PROBABILITE DE LA MECANIQUE 10
PAR UN TON D'UNE ANNE LPS A 1000 Hz D'ENERGIE
POUR UN TON DU MOTEUR 1 A TRAVERS L'ENTRANON

Fig 13

A line graph showing the probability distribution of energy for a 1000 Hz tone. The y-axis is labeled 'P' and ranges from 0.0 to 1.0 in increments of 0.1. The x-axis is labeled 'E (J)' and ranges from 0 to 10000 in increments of 1000. The curve starts at (0,0), rises to a peak of approximately 0.9 at E = 1000, then drops sharply to near zero by E = 4000.

$\frac{1}{2} \cdot \frac{1}{\sqrt{2}} \cdot 10 \cdot 10$

PROBABILITE DE PROBABILITE DE LA MECANIQUE 10
PAR UN TON D'UNE ANNE LPS A 1000 Hz D'ENERGIE
POUR UN TON DU MOTEUR 1 A TRAVERS L'ENTRANON

Fig 14

STRUCTURAL EFFECTS OF ENGINE BURST NON CONTAINMENT

AUTHORS:- Dr. T.W. Coombe Ph.D., B.Sc., C.Eng., A.F.R.Ae.S.,
Head of Structural Development and Test.

British Aircraft Corporation Limited
Commercial Aircraft Division,
Filton House,
Bristol BS99 7AR,
UNITED KINGDOM.

D.F. Vowles, C.E., M.R.Ae.S.,
Research Stress Engineer.

British Aircraft Corporation Limited
Commercial Aircraft Division,
Filton House,
Bristol BS99 7AR,
UNITED KINGDOM.

SUMMARY :-

Structural impact damage by non-contained engine burst debris has become of increasing importance for the aircraft designer in view of the number of serious incidents to large transport aircraft recently experienced. This has occasioned the publication of the new British draft requirements on "Non-containment of Turbine Engine Debris". To date, the effect of and resistance to such damage has not yet become a part of the major design disciplines. The paper outlines the requirements and the specified acceptable levels of risk as applied to a large subsonic transport aircraft. The resultant damage forms are discussed and some test details given to illustrate the problems. Examples of engine fragment damage potentials are given with an empirically based equation relating fragment energy to target resistance for light alloy, titanium and steel targets.

Finally, two types of design solution are discussed as applied to a large subsonic jet transport.

1. British Draft Airworthiness Requirements

The problem of non-containment of engine burst debris became significant to the aircraft designer with the introduction of the gas turbine engine. Recent experience of an increasing number of serious incidents has led to the formulation by the CAA of paper No.513 "NON CONTAINMENT OF TURBINE ENGINE DEBRIS". This is now in its Draft Issue 2 form and sets out the proposed requirements aimed at alleviating the disastrous effects of the resultant damage. The essence of the paper is contained in the following extract :-

1.5. HIGH ENERGY ROTORS - NON CONTAINMENT OF DEBRIS

1.5.1. GASTURBINE PROPULSION ENGINES AND AUXILIARY POWER UNITS

Unless containment of debris is assured, design precautions shall be taken to minimise the probability of catastrophe being caused by non contained debris in the event of an engine rotor failure.

The requirements go on to emphasise the need for "maximum protection" and define, in rather broad terms, the acceptable levels of risk related to selected debris forms.

"Maximum protection" entails (a) an analysis of the complete A/C design, including all essential components and systems to establish the single and multiple failures resulting from non-containment which may have catastrophic consequences and (b) an interpretation of the analysis results to determine the chances of a catastrophe. The requirements list 3 levels of risk as follows :-

<u>Debris ejected</u>	<u>Acceptable risk of a resultant Catastrophe</u>	<u>Angular Spread (Areal)</u>	<u>Mass</u>
(i) <u>Single Fragment</u> 3rd disc.	Not more than a 1 in 30 chance	$\pm 3^\circ$	3rd of Bladed disc
(ii) <u>Multiple Fragments</u> 3 - 3rd discs.	Not more than a 1 in 10 chance	$\pm 3^\circ$	" each
(iii) <u>Pieces of Rim</u> <u>with Blades (2)</u>	Not more than a 1 in 100 chance	$\pm 5^\circ$	1/10th of bladed disc.

The angular ejection probability is taken as identical over the 360° arc of rotation and the debris trajectory is tangential to its C.G. radius. Figure 1 shows a simplified interpretation for one case - damage to the Fuselage.

The range of conditions to be covered by the analysis includes the following :-

- (a) Damage to Primary Structure and airframe surfaces (e.g. loss of structural strength including resultant deformation affecting aircraft control or operational range).
- (b) Damage to other Engines, Services and Equipment, i.e. flight and engine control systems, engine fuel supply isolation valves and their control.
- (c) Penetration of fuel tanks leading to fire.
- (d) Effect of release of large mass of fuel on aircraft handling characteristics and range.
- (e) Incapacitation of flight crew.

While this summary has covered requirements which are currently only in draft form it seems likely that it does give a good indication of the type of requirements with which the designer will be faced. It is apparent that some formidable new problems are being presented to the designer.

2. Damage Forms

The types of damage resulting from engine debris impact on normal aircraft structures at or near the penetration velocity involve significant and frequently extensive deformation, tearing and splitting of the structure. One major determinant of such effects is the debris impact velocity which can be related to the rotational velocities of the engine compressor or turbine.

Now the blade tip velocity will rarely exceed 460 m/s and consequently, a major fragment, such as a whole LP compressor blade, would have a CG translational velocity of approximately 300 m/s. A brief survey of the gas turbines in use would show that the impact velocities of such major fragments generally range between 150 and 300 m/s while smaller fragments such as turbine blades may reach 400 m/s. This suggests an inverse relationship between debris size and impact velocity.

Figure 2 illustrates this relationship.

Unfortunately, most of the test evidence to date is of a military origin, nevertheless it is significant that this velocity band is shown to produce the maximum damage levels.

Reference 1 indicates that the maximum lateral damage caused by 0.3" and 0.5" ball ammunition occurs between 270 and 540 m/s depending on the angle of impact.

Reference 2 indicates that the residual strength of a light alloy panel reaches a minimum at approximately 250 m/s impact velocity.

Debris at velocities below 150 m/s will also, of course, inflict significant damage. Recently, a test bed incident demonstrated the need to protect the engine intakes of a large supersonic transport aircraft against impact by debris which could be ejected forwards from the engine face at velocities of around 60 m/s. This debris was in the form of blades weighing up to 2½ Kg and, although the trajectory was less than 30° to the target plane, they penetrated up to 3 layers of 1.6mm fabricated light alloy structure emerging with sufficient residual velocity to damage structure outside of the intake altogether.

Figure 3 shows the type of damage experienced on a typical specimen from the resultant test program. The severe "petalling" and "splitting" are clearly seen.

As an example of the magnitude of the problem facing the designer, it is worth noting that the total number of test firings required to enable the above aircraft to meet the draft Issue 1 of the new requirements (rather less severe than the present Issue 2) exceeded 150.

It is conceivable that if an established analytical method had been available, a large proportion if not all of this test program could have been eliminated.

At present no generally applicable theoretical approach has been evolved and, in view of the many variables concerned, such a technique may well be impracticable. However, with increasing numbers of tests and actual incidents some derivation of empirical relationships should be possible, which equate damage form and extent to projectile size, orientation, velocity and target material, form, stiffness etc.

Figure 2 lists the variables about which data are required. It is unlikely that data collation alone would provide sufficient bases for such relationships. A program of specimen testing would doubtless be necessary to fill in the numerous gaps that must exist and to define the boundaries of the various equations.

One such an equation has already been derived from the test program mentioned earlier. This is described in the following section.

3. Fragment Damage Potentials

An impression of the destructive capacity of the debris forms referred to in the Paper is given by Figure 4. Here the fragment energy on impact is plotted against the weight of target material required to contain the fragment. The curves for 3 target metals and 2 angles of trajectory are drawn from the empirical relationship:-

$$E_k = \frac{L \cdot v \cdot t^2}{\cos^2 \theta}$$

- E_A - Energy absorbed by penetration of the target
- L - Periphery of the projected surface of the fragment at impact. (Assumed constant at 800 mm for 3rd discs and 1700 mm for rim pieces and blade).
- T - Dynamic shear strength of target material
- t - thickness of target (assuming the target is a flat plate).
- θ - Angle of Fragment Trajectory to the normal from the target plane.

Some test points are included indicating that the relationship is good up to an energy level of 10^4 KJ. Above this point the massive fragment energy involved in testing would entail a full order of increase in test rig complexity and cost. Also the problem of simply how and to what to attach the armour assumes considerable significance, the danger being that such impact energies may dislodge the armour and turn it into an ejected "fragment" in its own right. This could form a major part of such a test programme.

To emphasise the damage potential of the proposed fragments, typical weights of heavy wing and fuselage surfaces are indicated on the diagram giving some idea of their respective energy absorbing capabilities by reading across from the Light Alloy curves. The resulting energies are only approximate as both the curves and the test results are only concerned with flat plates. The stiffeners of the wing and fuselage (included in the weight shown) may offer appreciably increased energy absorption due to their depth. However, this does not alter the general inference of Figure 4 which is that even two or three layers of such structure is not capable of stopping the smallest of the three debris forms. Broadly speaking, the designer is faced with a choice or combination of two types of solution:-

- a) to avoid catastrophic results by design re-orientation or
- b) to contain or deflect the debris from critical areas by the use of armour.

Design solution (a)

If the aircraft is still in the initial design stages the designer has the ability to arrange the aircraft layout to locate critical volumes in safe areas and to ensure that the structures and systems are capable of absorbing damage resulting from a strike from a 3rd disc fragment to the standard demanded by the requirements.

A possible result of his efforts is shown on Figure 5. Here a hypothetical subsonic jet transport is shown with probably the widest range of impact problems likely to be encountered. For the sake of brevity we shall only consider threats from the wing mounted engines. First, the fuselage has been given an upper baggage hold with emergency pressure bulkheads fore and aft spanning the areas under threat from the fan and turbine discs. A walkway is required with pressure doors for communication between the two halves of the passenger cabin. To be effective the walkway has to be closed for the majority of pressurised flight thus cutting off the rear passengers from the forward cabin and cockpit. This assures that (a) the damage occurs when the fuselage is pressurised and (b) rapid decompression of the fuselage constitutes a catastrophe. Experience to date does indicate that most disc failures occur during take off in which case the fuselage is unpressurised. To what extent this order of probability (when statistically evaluated) will effect the requirements is not clear. However, the designer has also to show that the structure can support say, 60 to 85% of proof loads with a very large section destroyed in order to achieve a safe landing.

The fuselage case is as shown by the single fragment diagram (i) of Fig.1. Here the shell has to be able to contain damage inflicted anywhere in the shaded area. A typical effect of a strike is indicated on Figure 5. The solution can entail reinforcement of the shell for some distance fore and aft of the area under threat. The designer's existing "Fail-Safe" design practice goes a considerable way towards determining the required structure but the extent of damage possible far exceeds that expected by a fatigue damaged structure.

The behaviour of large structures under load suddenly inflicted with massive damage is not yet clearly understood. While analyses based upon fail safe experience can define static residual strengths, these do not include the effects of the dynamic load re-distributions that would occur. It is evident that a full scale research programme is needed to (a) determine the full extent of damage due to a large fragment including explosive de-compression if relevant and to (b) determine the most efficient structural solution.

The wing structure is normally multi spar, multi torque box construction and so present less of a problem to the designer. He must demonstrate, however, that any change in the wing aeroelastic properties do not place too severe restrictions on the aircraft speed and handling characteristics.

The fuel tanks and aircraft systems represent virtually the two extremes with regard to possible solutions.

On the one hand it is evident that fuel tanks outside of the accepted areas of risk cannot survive impact by any significant debris without some protection, because of the risk of fire or explosion. Therefore in the context of this design concept all bays under threat remain dry.

On the other hand, if one system (including all stand-by versions) were to be confined in the minimum area of acceptable risk, as indicated on Fig.1. Diagram (iii), then the letter of the requirements may be considered as having been met, that is assuming that loss of the complete system

is catastrophic. This, however, would contravene one of the basic tenets of system multiplication, i.e. dispersal of the standby systems remote from the primary system. In this case, the technique would be to locate the standby system remote from the primary system such that a complete 3rd disc whirling diameter could pass between the two areas.

It is quite possible that the majority of such solutions result in weight or performance penalties. These must be fully evaluated in order to determine the viability of the main alternative which is the use of armour.

5. Design Solution (b)

Containing the two debris forms of Fig.1 requires armour weights of between 140 and 220 Kg/m². If these can be located close to the ejection source their areas are kept to a minimum. Alternatively, they may be located further away but inclined so as to act more as deflectors than simply resisting penetration. Assuming the inclination is 60° reduces the armour weights to between 70 and 110 Kg/m². The re location may also provide a better anchorage for the armour as indicated in Figure 6 which shows the possible armour locations to cover the Single Fragment (i) and the Kin piece and Blade (iii). The threatened area related to the Multiple Fragments (ii) is also protected against strike by one of the 3rd discs while the probability of all three 3rd fragments striking this area must be regarded as virtually non-existent.

The problem of holding the armour suggests the use of rings around the nacelle or increased internal stiffening in the airframe. Either of these will increase the weight significantly thus requiring accurate analyses to evaluate each scheme thoroughly. Evidence exists to show that the dynamic strength of materials is often considerably better than their static strengths but specific data which to base such analyses is sparse. A research programme may be well justified to obtain such data.

There is little doubt that if a fully contained scheme can be proved viable then the end product could be a much more satisfactory aircraft from the operator view point. In this context, the armour performance becomes of paramount importance and it should be noted that very little research has yet been done to obtain essential data.

Most work to date has been concerned with military aircraft subject to gunfire damage which involves small mass, high velocity projectiles (e.g. Ref.3). While the results may give some indication of the effects of engine bursts, the necessary extrapolation is so considerable as to require experimental confirmation.

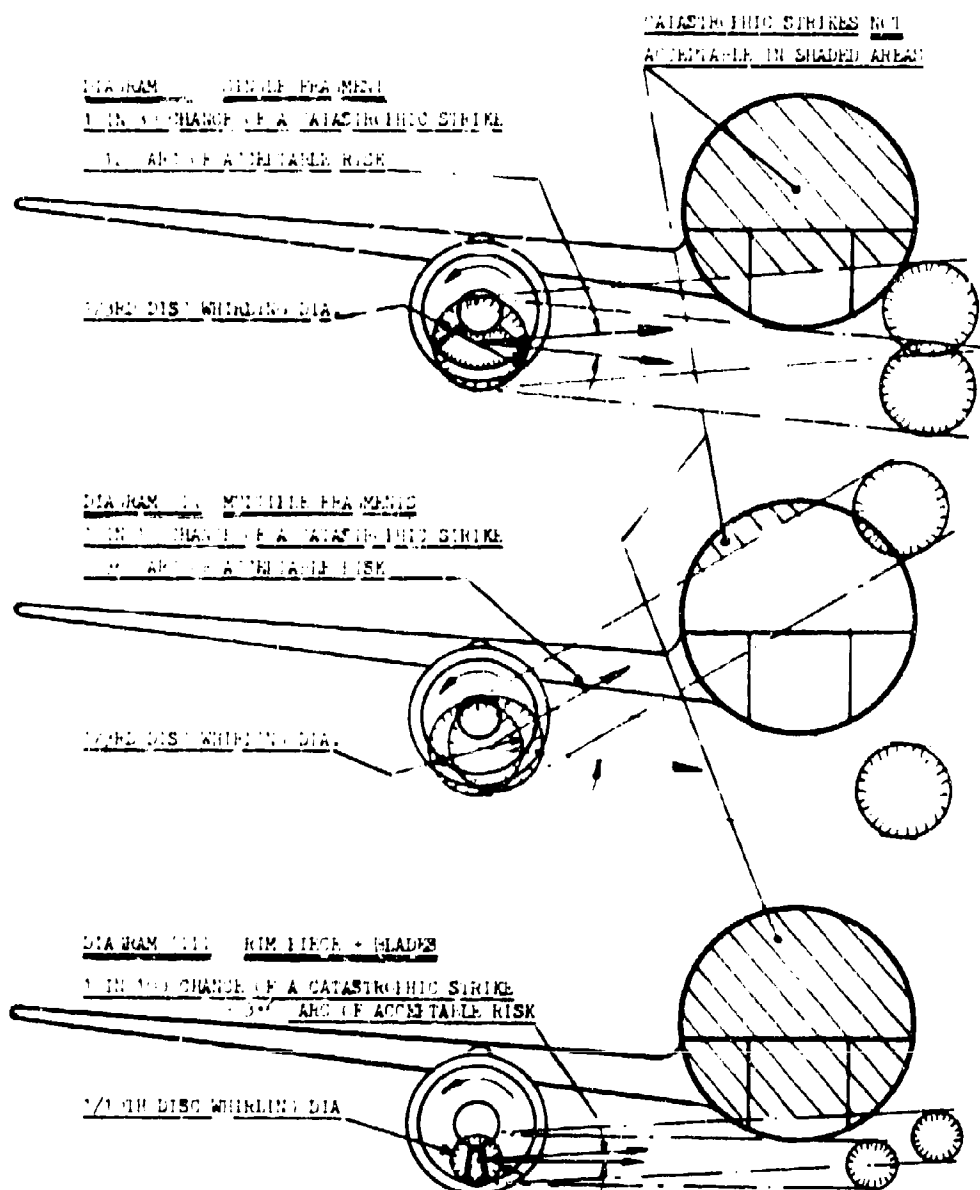
In conclusion, it can be seen that these brief and certainly not exhaustive notes outline a major extension of the designer's problems in the field of impact resistance.

References

1. Techniques for predicting the Structural Vulnerability of Combat A/c to Ballistic Impact x Jay Meisebran, G. Thomas Birch and John G. Avery - JARD Feb.1974.
2. A Parametric evaluation of the response of light weight metal and composite structure to gunfire x John G. Avery and Theodore R. Porter.
3. Fracture due to damage from projectile impact. John G. Avery. Engineering Fracture Mechanics, 1972 Vol 4 pp 749-763.

FIGURE 1

STRUCTURAL EFFECTS OF ENGINE FIRST FUEL CONTAINMENT
INTERPRETATION OF M.C.A.B. LATER 800, DRAFT ISSUE 1, ACCEPTABLE
LEVELS OF RISK OF A CATASTROPHIC STRIKE
CASE 1: FUSELAGE STRIKE BY ENGINE

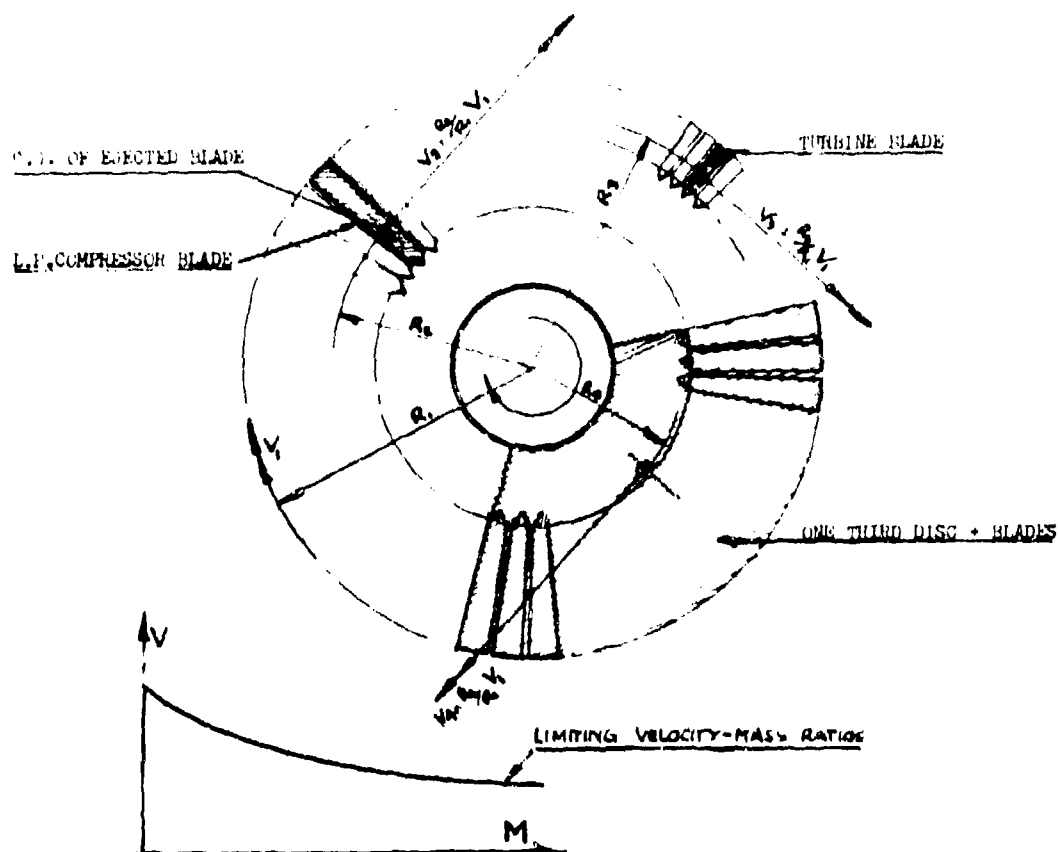


N.B. THE ARC OF ACCEPTABLE RISK ENCOMPASSES MINIMUM AREAS OF THE FUSELAGE.
 THE EXTENT OF A CATASTROPHIC STRIKE CAN BE CLEARLY DEFINED THEN THE
 ARCS MAY BE POSITIONED ACCORDINGLY.

FIGURE 2

STRUCTURAL EFFECTS OF ENGINE BURST NON-CONTAINMENT

DERRIS VELOCITY



DATA REQUIRED - SIMPLE VARIABLES

<u>PROJECTILE</u>	MASS - SIZE - IMPACT PROFILE - MATERIAL - VELOCITIES (BEFORE + AFTER PENETRATION) - TRAJECTORY (RELATIVE TO PLANE OF TARGET)
<u>TARGET</u>	TYPE - CONSTRUCTION - MATERIALS - DIMENSIONS (SKIN t + STIFFENER SIZES)
<u>DAMAGE</u>	TYPE - PENETRATION OR DENT - SHEARING OR PETALLING - MAXIMUM CRACK LENGTHS - AREA OF HOLE & DIMENSIONS

FIGURE 3

STRUCTURAL EFFECTS OF ENGINE BURST NON-CONTAINMENTTYPICAL LOW ENERGY TEST SPECIMEN DAMAGE← WITH BLADE STILL IN PLACE

<u>WT. OF BLADE</u>	1.73 KG
<u>IMPACT VELOCITY</u>	69.2 m/s
<u>K.E.</u>	421 KJM
<u>STRIKE ANGLE</u>	53°
<u>BLADE TIP FIRST</u>	
<u>TARGET SKIN</u>	1.8 mm CM001

WITH BLADE REMOVED →DETAILS AS ABOVE EXCEPT

K.E. 376 KJM
(V = 65.3 m/s)

N.B. THE TARGET IS A DOUBLE
SKINNED FOX WITH 10 mm DEEP
FRAMES. THE BACK FACE OF THE
INNER SKIN IS REINFORCED WITH
G.R.P. ARMOUR 0.5 mm THICK
WHICH WAS NOT PENETRATED.



FIGURE 4

STRUCTURAL EFFECTS OF ENGINE BURST NON-CONTAINMENT
FRAGMENT IMPACT ENERGY v. TARGET WEIGHT

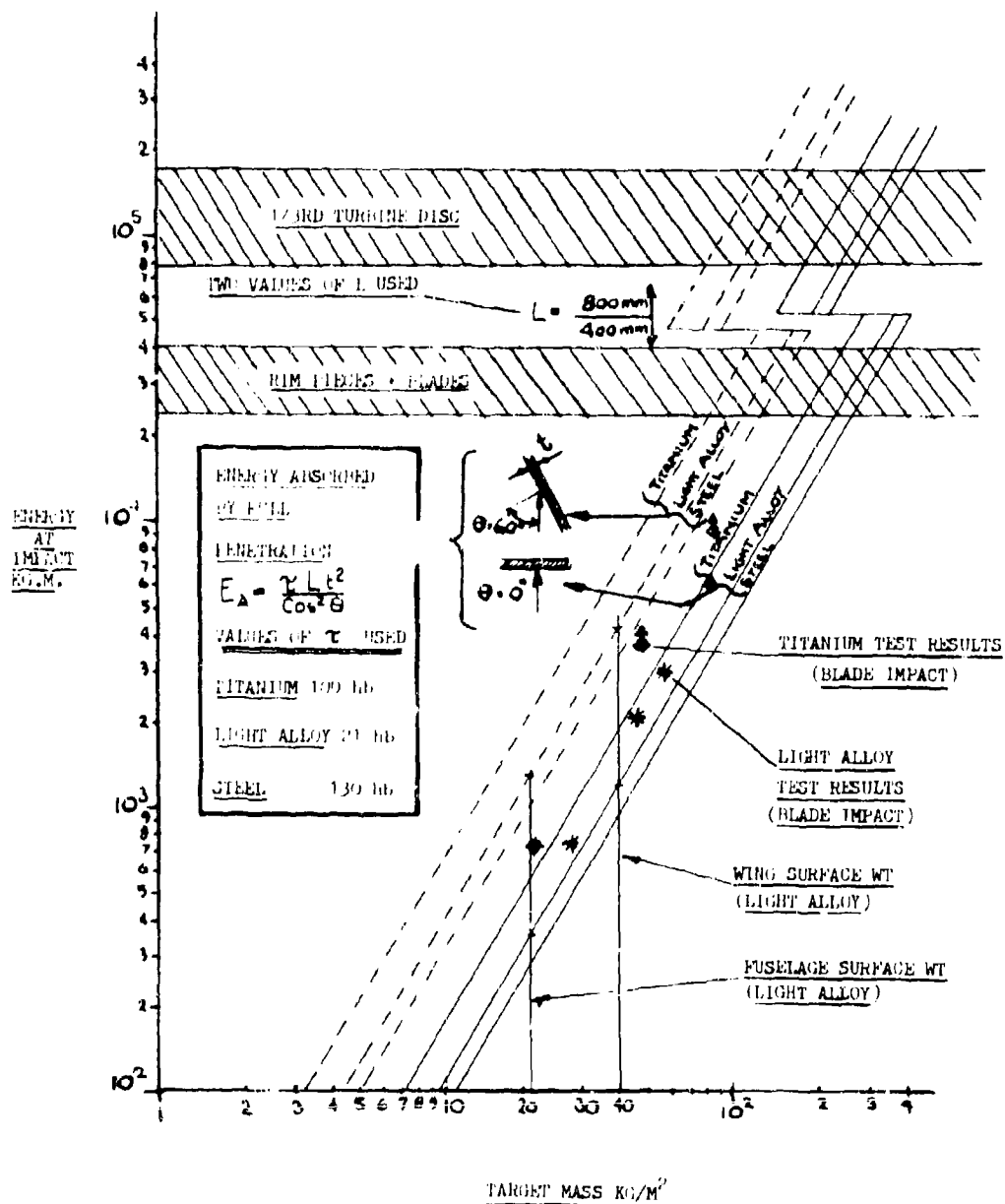


FIGURE 5

STRUCTURAL EFFECTS OF ENGINE BURST NON-CONTAINMENT
HYPOTHETICAL JET TRANSPORT LAYOUT OF DESIGN SOLUTION (a)

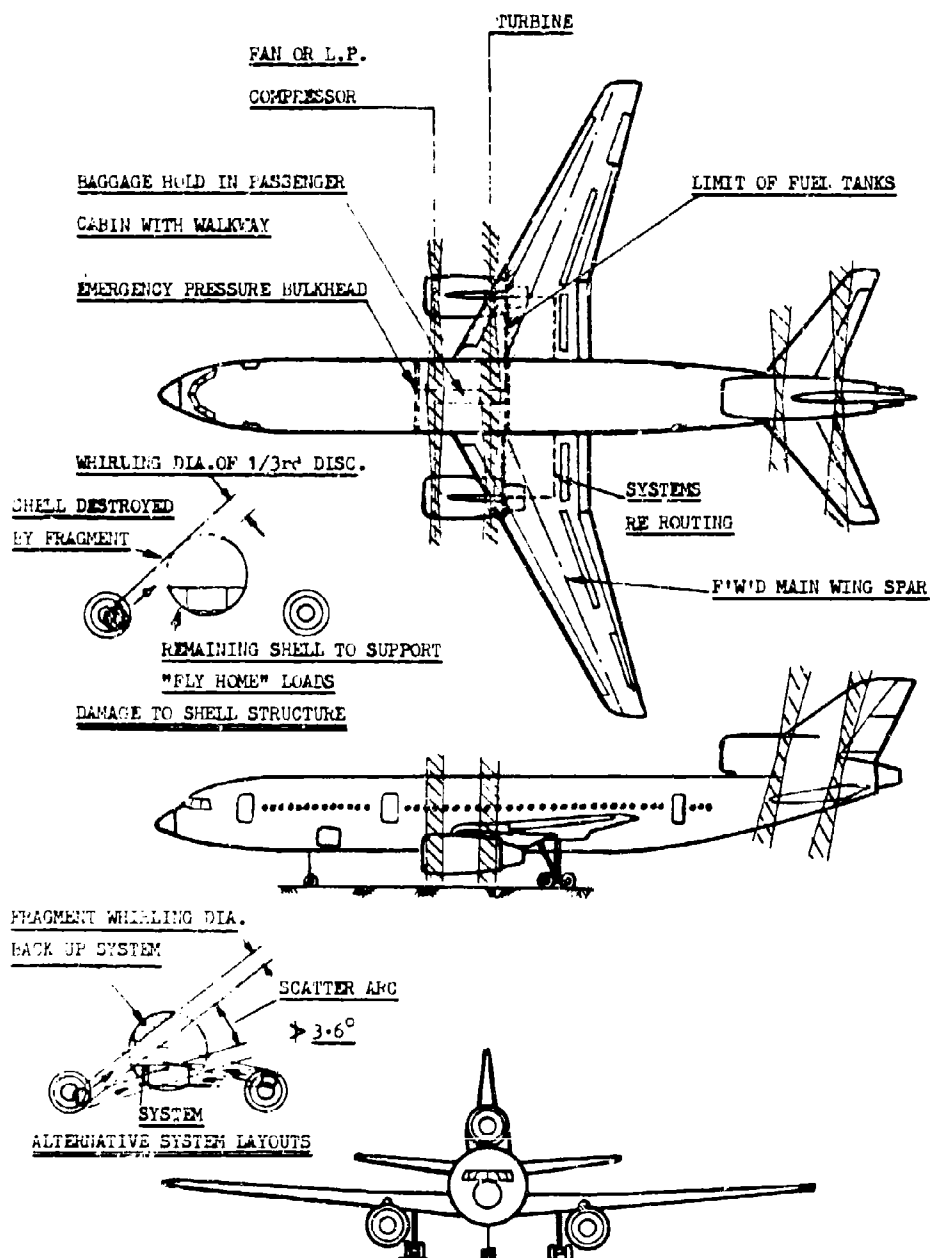
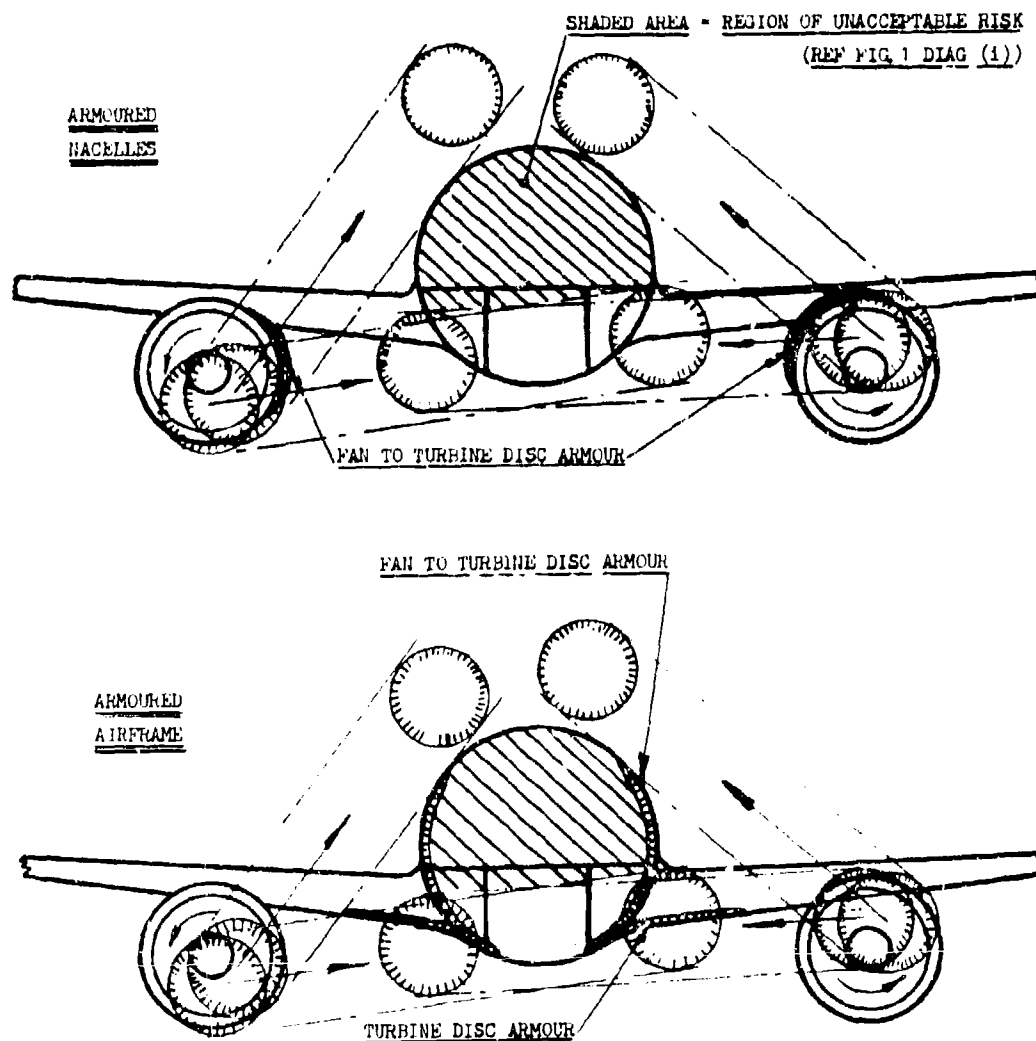


FIGURE 6

STRUCTURAL EFFECTS OF ENGINE BURST NON-CONTAINMENTUSE OF ARMOUR - DESIGN SOLUTION (L)PROTECTION AGAINST SINGLE FRAGMENT 1/3RD. DISC.(IN PRACTICE THESE SCHEMES ALSO AFFORD PROTECTION AGAINST MULTIPLE FRAGMENTS AND RIM PIECES + BLADES)

STUDIES OF ENGINE ROTOR FRAGMENT IMPACT ON PROTECTIVE STRUCTURE

by
G. J. Mangano
Naval Air Propulsion Test Center
Trenton, New Jersey
08628
USA

SUMMARY

Presented are: Data compilations on aircraft gas turbine engine rotor failures that occurred in U.S. commercial aviation in 1973; the results of exploratory and systematic experimentation conducted to provide design guidelines for turbine rotor burst fragment containment; an overview of the analytical effort directed toward rotor fragment containment by the Massachusetts Institute of Technology.

INTRODUCTION

A seemingly irreducible number of uncontained gas turbine engine rotor bursts occur each year in U.S. commercial aviation. The potential for catastrophe that can be associated with these events has prompted NASA to sponsor the Rotor Burst Protection Program. This program was developed and is being conducted by the Naval Air Propulsion Test Center in conjunction with the Massachusetts Institute of Technology. The basic goal of the program is to develop criteria and data for the design of optimum light-weight devices that can be used on aircraft to protect passengers and vital parts of the aircraft structure from the lethal and devastating fragments that are generated when a gas turbine engine rotor bursts.

The intent of this paper is to acquaint you with the RBPP by:

- Explaining what motivates us to pursue this effort.
- Describing the test facilities that were developed and are being used to implement the program.
- Presenting some of the experimental results that have been produced.
- Describing the MIT analytical effort.

Motivation for the RBPP

Impetus and motivation for the RBPP stems from the statistics of the rotor failure situation or problem in U.S. commercial aviation. The data that will be presented on this problem comes from analysis of Flight Standards Service Difficulty Reports (SDR) that are published daily by the Department of Transportation, Federal Aviation Administration (F.A.A.).

It has been stated that an irreducible number of uncontained rotor bursts occur each year. In fact, the data shown in figure 1 indicates that on the average 30 uncontained rotor bursts occur each year. A more detailed presentation of the statistics on rotor burst for the year 1973 are shown in figure 2. Here, the data is presented in terms of what part of the engine was affected, and how many rotor failures and bursts occurred. A rotor burst being defined as a failure that produced fragments. These data indicate that 170 rotor failures were experienced in 1973. These failures accounted for approximately 9% of the 2888 shutdowns that were experienced by the gas turbine powered U.S. commercial aircraft fleet. The data shown in figure 3 further characterizes the rotor burst problem by identifying: what types of fragments are being generated; where in the engine bursts occur; and what percentages of the bursts are uncontained. This type of data serves to establish where in the engine the burst problems exist and what type of fragment has the most potential for doing damage and therefore must be protected against. This in a sense directs our efforts so that the most critical aspects and locations of the rotor burst problem are addressed by the program. The conclusion that we've drawn from these and other more detailed data is that rotor burst in commercial aviation is a relatively sizeable problem with potentially serious consequences - at stake is the welfare and safety of literally thousands of airline passengers.

The question that we've addressed ourselves to is this: What can be done to minimize or eliminate the hazards and risks that are attendant to rotor burst? As we see it there are two basic alternatives: The level of safety that is needed can be achieved either through improved reliability or protection. We've chosen to pursue that goal which involves developing methods of providing lightweight protection. This position has been adopted, because the statistics of rotor burst show that some limit to reliability has been reached and we can expect to experience some minimum number of rotor failures each year. And, in order to ensure safety some measure of protection must be provided.

Test Facilities for the RBPP

From the outset, it was recognized that extensive experimentation and testing would be needed to meet the goals of the RBPP. Meeting these goals would involve:

- Characterizing the burst and fragment control processes.
- Conducting parametric studies to establish functional relationships between significant process variables.
- Evaluating the effectiveness of various rotor burst protection devices and configurations.

To accomplish these tasks a Rotor Spin Facility was designed and constructed at the NAPT. This facility is shown in figure 4. It consists of a control and data acquisition area which houses the controls and instrumentation used for test; and a test area which contains the spin chambers and auxiliary equipment such as the vacuum and lubrication pumps.

- The facility has two spin chambers. The smaller chamber can accommodate rotors up to 40 inches in diameter and has a working height of 32 inches. The large chamber, shown in figure 5, is comprised of a heavy walled (1 inch thick) vacuum vessel that is protected by a 5 inch thick laminated steel inner liner. The working space in this chamber is 10 feet in diameter with a height of 6 feet. It was designed to accommodate rotors from the largest aircraft engines that are made. This chamber has ports on its walls for instrumentation feed-thru and optical access. Typically the rotor to be burst is suspended vertically from an air turbine drive motor which mounts on the chamber lid as is shown. A family of air turbine motors are available to produce rotor speeds up to 15000 rpm. To minimize the power required to accelerate the rotors to failure, the chambers are evacuated to produce a vacuum of approximately 15 mm Hg. The main data acquisition systems used for test, aside from those used to monitor facility operational variables such as rotor speed, chamber pressure and the like, are the impact strain measuring and high-speed photo-instrumentation systems. The strain measuring system, which consists of balanced bridge millivolt signal conditioning equipment, two dual beam oscilloscopes, and a 14-channel magnetic tape recorder is used to measure and record the strains that are induced in the containment and deflection devices as a result of rotor fragment impact. The high-speed photo system is comprised of a continuous framing camera and photo lighting unit. The camera is capable of producing 225 pictures at a framing rate of 35000 frames per second. The lighting unit has an output of 12 million beam candlepower. These are just some of the salient features of the Spin Facility; more detailed information can be found in Appendix 2-16.

The Development of Design Guidelines

The experimental development of rotor fragment protection design guidelines, which is what this program is all about, has progressed through two distinct phases. The first phase involved the conduct of exploratory tests that were performed to determine what mechanisms were involved in the rotor fragment containment and deflection processes; and also to establish what variables significantly influenced these processes. The second and current phase involves the conduct of parametric experimentation to generate data for the design of fragment containment rings.

Exploratory Experimentation: During this phase of the program rotor and blade containment tests were conducted using rings made from a variety of materials. The purpose of these tests was to gain some insight into the processes and mechanisms that were involved in the containment process. High-speed photo-instrumentation was used to record the events that took place during containment. The photographs produced were analyzed to establish both fragment and ring behavior during the containment process.

1. Rotor Containment: In these experiments, turbine rotors were modified to burst into three equal pie sector fragments at a predicted speed and impact a freely supported ring that encircled the rotor. Figure 6 through 9 show selected frames from high-speed photographic sequences taken of several rings which are in the process of containing rotor fragments. The rings were made from a variety of materials: 4130 Steel; 2024-T4 Aluminum; Ballistic Nylon; and filament Wound Fiberglass. These photographic results show that the gross ring and fragment deformations are approximately the same for all the ring materials tested. The rotor fragments experienced deformations involving only the blades which were curled and bent while the disk portion of the fragment remained intact and suffered no apparent deformation. Frame-to-frame analysis of the fragment displacements recorded by the high-speed photographs revealed that the time that it took blade deformations to occur was approximately the same regardless of the ring material used, and varied only with burst speed. Blade deformation times became shorter as burst speed was increased.

The rings were displaced and deformed to generate the typical three lobed pattern associated with 3-fragment bursts; this is well illustrated in the high-speed photographs.

In all cases large displacements and deformations of the ring did not occur until fragment blade deformation was almost completed. This indicated that relatively small forces are generated by the blade deformation which occurs during the initial stages of containment. Based on these results some important observations were made:

- The rotor fragment blades in their deformation do not substantially absorb much of the fragment energy that must be dissipated during containment.

- The blades by virtue of their length and mass distribution serve only to prescribe the location of the fragment center of mass and the radial distance through which the non-deformable hub mass must travel during the initial stages of containment. These factors influence the trajectory and orientation of the fragment during the latter stages of containment when pronounced ring displacements and stresses are induced.

- Because the blades deform so readily, radial clearance effects are minimized. Differences in rotor-to-casing radial clearances between experiment and actual turbomachine construction are small compared to the blade length. Therefore, the ring and fragment behavior observed during experiments using radial clearances as large as 0.5 inches would be representative of the behavior that could be expected in an engine where rotor-to-casing clearances are measured in thousandths of an inch.

2. Rotor Blade Containment: In these experiments, blades from turbine rotors were modified to fail and impact containment rings made from 6061 (T6) and 2024 (T4) aluminum. Two types of rotor blade containment experiments of interest were conducted.

- Single blade bursts in which one blade mounted on a rotor disk was modified to fail and produce a blade fragment.

- Single blade bursts in which one blade in a fully bladed rotor was modified to fail.

These blade burst experiments were conducted to study the blade and ring interactions and deformations during the containment process.

The results of representative blade-fragment containment experiments, which are in the form of high-speed photographs, are shown in Figures 10 and 11.

Figure 10 depicts the sequence of events that occur when an isolated blade is contained by a freely supported ring whose thickness is representative of an engine casing. The ring deformation is seen to be local and extensive. The blade was deformed in a curling manner characteristic of turbine blades. Figure 11 shows the sequence of events that occur when a blade from a rotor fails, impacts a casing, and interacts with the blades remaining on the rotor. Initially ring deformation resembles that produced by the isolated blade burst. This is reasonable because the rings used and the burst speeds are the same for each experiment. But as time progresses, increasing interaction of the blade fragment with the other blades is observed and a failure of the ring occurs. This comparison provides evidence that greater forces and energy transfers are induced by blade interaction and clearly indicates that the momentum imparted to the blade fragment by other blades in the rotor adds measurably to its destructive potential. This imparted energy or momentum must be considered in any design analysis for blade containment rings or engine casings.

Rotor Fragment Deflection Devices

Protecting an aircraft from rotor fragment attack through the use of partial rings, which would serve to redirect fragment to less sensitive and vulnerable areas of the aircraft, is an attractive concept, since it promises considerable weight savings over complete ring systems which are designed to capture or contain the fragments. Two significant experiments have been conducted to examine the feasibility of this concept and to study the mechanics that are involved in the deflection process. For the first experiment, two half-rings of equal size and weight were installed around a turbine that was modified to burst in half. One half-ring was welded to a rigid mount at one end; the other end was free of any attachment (hinged section). The other half-ring was welded to rigid mounts at both ends (fixed). This arrangement made it possible to observe and evaluate the behavior of two different deflection ring configurations during one experiment.

The objectives of this experiment were to examine the feasibility of using a half-ring to control the trajectory of a rotor fragment and to establish what method of half-ring attachment would be most effective for fragment deflection purposes. Selected high-speed photographs taken during the experiment are presented in Figure 12. They show that the rotor fragments impacted the half-rings close to their points of attachment; this impact condition was considered to be the worst possible, and therefore, provided a rigorous test of how well the half-rings functioned as fragment deflection devices.

The fixed half-ring experienced failures near the points of attachment soon after impact. The fragment did not, as might be expected, enter the "protected region" as a result of these failures. Instead the fragment continued to interact with the free ring section and moved along what could be considered a safe trajectory.

The "hinged" half-ring behaved as anticipated: A plastic hinge formed close to the attachment point at impact. The half-ring pivoted about this point, while it guided the fragment over its inner surface along a safe, controlled trajectory away from the protected region.

The mounts for both half-rings failed during the fragment interaction. The results of this experiment demonstrate conclusively that half-rings can be used to provide suitable fragment trajectory control or deflection. However, the "hinged" half-ring appeared to function more effectively. In addition, it represented a lower weight and less complex configuration. The second experiment was similar to the first involving the same type of modified rotor and two steel half-rings. However, the half-rings were of different weight (one weighing approximately twice the other), and they were freely suspended rather than being fixed at one or both of their end points. The objective of this experiment was to determine if the inertia of a half-ring alone would provide the constraint needed to control the fragment trajectory. The half-ring weights were different to provide different inertial responses to impact. Selected high-speed photographs of this experiment are presented in Figure 13. They show that the fragments struck the half-rings at points considered to be optimal for the evaluation of their trajectory control capabilities.

The lighter or thinner of the two half-rings (both half-rings had the same internal diameter and axial length) deformed considerably during the impact process and offered almost negligible resistance to fragment translational motion. As a result the fragment moved with considerable energy into the region that was to be protected by the half-ring.

The heavier half-ring was also deformed during impact but not to the same extent as the thin half-ring. Fragment translational motion was somewhat arrested as a result of the interaction, but the course of the fragment was not controlled. Like the other fragment, it too moved into the region to be protected.

CONCLUSIONS

Regarding the Rotor Burst Fragment Containment Process:

- In a containment situation involving fragments from a typical axial flow turbomachine rotor, blade deformation constitutes almost all of the fragment deformation that occurs; the hub or disk portion of the fragment behaves as a rigid non-deformable body that causes distortion of the containment ring. The forces needed to deform the blades are relatively small, as are the energies absorbed by their deformation. Therefore, the blades on a rotor fragment do not significantly influence the distribution of the impact loads that are induced in a ring (provided the ring thickness approaches that required to effect containment and the fragment hub to blades mass ratio is large), nor do the blades absorb significant amounts of energy through their deformation during the containment process. The blades serve only to influence the fragment trajectory during the initial stages of impact. This also means that in cases where the rotor tip-to-ring clearance is small (test or operational clearances) the blade radial length becomes in effect the radial clearance that influences the orientation of the hub or disk portion of the fragment.

- The amount of blade deformation sustained by the rotor fragments during containment appears to

be independent of the hardness of the containment ring material. At equivalent burst speeds soft and hard materials alike cause the same type and degree of blade deformation.

- The general displacement and deformation characteristics of containment rings, optimally designed for weight reduction and subjected to rotor fragment attack, do not significantly vary for rings made from materials having a wide range of strengths and ductilities. The ring distorts to conform to the shape of the undeformed disk portion of the rotor fragment. The number of ring distortion sites is equal to twice the number of fragments attacking the containment ring. The magnitude of ring distortion, and the time it takes for these distortions to develop depends on the ring mass, material strength, thickness or stiffness, and the speed of the fragments at impact.

- The variables that appear to affect the containment process most significantly are:

- (1) The burst speed
- (2) The number of fragments
- (3) The blade tip-to-hub diameter ratio of the rotor fragments
- (4) The ring length-to-thickness ratio
- (5) The ring diameter
- (6) The ring material

Regarding the Rotor Burst Fragment Deflection:

- Rotor fragments can be effectively deflected (their trajectories controlled) through the use of partial rings of reasonable weight.

Parametric Experimentation: The parametric rotor fragment containment experimentation evolved from the exploratory testing, which provided an understanding of how certain variables significantly influenced the rotor fragment containment process. The goal of the parametric study is to experimentally derive data that will provide empirical guidelines for rotor fragment containment ring design. The approach taken is to establish a functional relationship between a measure of ring containment capability and the variables that characterize the rotor and ring, and significantly influence the containment process. These relationships, once established, will be the empirical guidelines needed for containment ring design.

The significant variables for fragment containment, as determined through experimental observation are:

Rotor:	Diameter	Speed
	Length	Material
	Tip-to-hub-ratio	Number and type of
	Weight/inertia	fragments
Ring:	Diameter	Axial length
	Radial thickness	Material

For purposes of developing the design guidelines and the test scheme needed to generate these guidelines, a dependent variable was formulated which measures the containment capability of the ring. This variable was called the specific contained fragment energy (SCFE) and is derived by dividing the rotor energy at burst by the weight of the ring required to contain this fragment energy. This variable is a combination of several of the significant variables, namely: The rotor mass inertia and speed; and a gross description of the ring in terms of its weight. The remaining significant variables become independent or experimental variables; that is, factors that are varied from test to test to determine what influence these variations have on the containment capability of a ring.

The four ring and rotor variables, which are being varied to determine how they affect the containment potential or characteristic of the ring (as measured by the SCFE), are:

- The ring inner diameter: Two diameters, one approximately twice as large as the other (31.64 and 15 inches), are being used for experimentation with rotors having correspondingly larger and smaller tip diameters (engine turbine rotors having tip diameters of 30.64 and 14 inches, respectively).

- The ring axial length: Three axial lengths are being used corresponding to 1/2, 1 and 2 times the axial lengths of the large and small diameter rotors (1.25 and 1 inch, respectively).

- The number of rotor fragments generated at failure: The rotors are modified to fail at their respective design speeds and produce pie-sector shaped fragments having included angles of 60°, 90°, 120° and 180°. These are designated as 6, 4, 3 and 2-fragment rotor failures, respectively.

- The ring radial thickness or outer diameter: The ring thickness is being varied until fragment containment is achieved for all combinations of ring (rotor) diameter, ring axial length, and the number of rotor fragments.

Other factors which will, in some way, influence the magnitude and orientation of the forces that are developed and the deformations and displacements that are sustained by the ring and rotor during containment interaction are:

- The mechanical properties of the rotor and ring materials.
- The fragment velocities.
- The rotor-to-ring radial clearance.
- The rotor-to-hub diameter ratio.

However, with the exception of the ring material, the variability of these factors is constrained within narrow limits by the dictates of good aerodynamic, thermodynamic and structural rotor design. For all practical purposes then, these factors are essentially constant from one turbomachine to another; therefore, there is no need to vary them in the experiments being conducted.

Although the mechanical properties of the materials used to make the containment rings can vary widely and are considered to be important factors in fragment containment design, the ring material being used for the experiments concurrently being conducted are purposely the same from one experiment to the other. Later, when the effects of the other variables have been established, the influence that the ring material mechanical properties has on the fragment containment process will be studied and incorporated into the main body of information that represents the guidelines for containment ring design.

Synopsis: The parametric study consists of a series of rotor burst containment experiments in which rotors of two different diameters are modified to burst at their respective design speeds into various numbers (2, 3, 4 and 6) of pie-sector fragments. These fragments impact rings made from 4130 cast steel that are freely supported and concentrically encircle the rotors at a radial clearance of 0.5 inches. The ring axial lengths are varied in three discrete steps of 1/2, 1 and 2 times the axial length of the rotors and their radial thicknesses are varied until fragment containment is achieved.

Conceptually the relationship and therefore the design guidelines developed through experiment could take the form shown in figure 14. Here the SCFE is plotted against the number of pie sector fragments generated at burst and the ring/rotor diameter. The rotor to ring axial length ratio is the parameter. The use of these functional relationship curves to design an optimum weight steel ring for a particular rotor application can be described as follows:

- Only two things must be known about the rotor prior to the design analysis:

- (1) The kinetic energy (KE_R) content at burst.
- (2) The size including tip diameter, axial length, and hub-to-tip diameter ratio.

The functional relationships between SCFE, the number of fragments and rotor diameter with the ratio of the ring axial length to the rotor axial length as the parameter, provide an indication of what the worst combination of burst conditions would be for the size rotor being considered; i.e., the lowest SCFE. Once the value of SCFE is obtained from the curves, it is divided into the total energy of the rotor at burst. The result of this division is the optimum weight of steel ring required to contain the rotor fragments.

$$(1) \quad W_t = \frac{KE_R}{SCFE}$$

This weight is used in equation (2) to calculate the radial thickness required to effect containment.

$$(2) \quad T = \left[r_i^2 + \frac{W_t}{LRG} \right]^{1/2} - r_i$$

Where:

- T = ring radial thickness.
- r_i = ring inner radius, which for practical purposes, equals the rotor radius: Rotor-to-casing operational clearances and considerations of minimum ring weight (the weight of a ring is directly proportional to the square of its inner radius) dictate that the ring and rotor radius be as equivalent as possible.
- LRG = ring axial length.
- KE_R = rotor energy at burst.
- SCFE = Specific Contained Fragment Energy factor: The value taken from the curve in Figure 14 for the size rotor being considered; the number of rotor fragments that result in the most adverse containment condition (the lowest SCFE value in the SCFE-MF plane); and the optimum ring-to-rotor axial length ratio (LRG/LRT) which is represented by the highest contour in Figure 14.

This general development and explanation of the data illustrates how the experimental results are to be used by designers to establish the weight and size of rings needed to contain rotor burst fragments.

Analytical Effort

As part of NASA's long range plan to provide design guidelines for rotor fragment containment and control, the Massachusetts Institute of Technology (MIT) has been developing models and methods that will be used to predict the transient response of rotor fragment containment and control devices. The MAPTC is providing experimental support for this activity. The objective of the MIT effort is to provide designers in industry with the analytical tools that are needed to develop optimum containment/control devices. The accomplishments of the MIT Aerodynamic and Structures Research Laboratory to date include:

- A computer program, JET 1 (NASA CR-107900) to predict the large deflection, elastic-plastic transient response of a single layer ring subjected to a prescribed distribution and time history of initial velocity and/or external forcing function that simulates roughly the forces applied to the "containment ring" from a single-blade impact.

- A similar program, JET 2 (NASA CR-72801), that treats multi-layer, multi-material, but isothermal rings. In this program, a more general description of prescribed externally applied mechanical forces is provided for the user.

- The JET 3 program, a more versatile program than those previously mentioned that permits predictions of large-deflection elastic-plastic transient responses of single layer, variable thickness complete and partial rings that are free or supported in various ways. This program takes into account various prescribed initial velocity distributions and/or transient externally applied loads.

- A collision imparted velocity method (CIVM) that is combined with one of the versions of the JET 3 program to produce the computer code CIVM-JET 4A (NASA CR-134494). This program permits the analyses of containment rings or deflector responses to impact attack from 1 to 6 fragments each having its own mass, mass moment of inertia, size, rotational velocity and translational velocity. Work is presently underway to modify this code with an improved impact subroutine, accommodation of ring support brackets and branches, and a more comprehensive strain-displacement description. This improved version is called the CIVM-JET 4B Code, and will be published in the fall of 1975.

The JET series computer programs have been and are being used by industry for material screening and in support of parametric studies concerning the fragment containment deflection problem. A detailed description of these codes is given in Appendix 1. A list of published technical reports and papers that have resulted from the analytical and experimental work is given in Appendix 2.

ACKNOWLEDGMENT

I would like to thank Messrs. S. Weiss, R. Siewert and A. Holmes of Aerospace Safety Research and Data Institute (ASRDI), NASA/Lewis, and Dr. E. Witmer of Massachusetts Institute of Technology for their help and direction in preparing this paper and for their support of the Rotor Burst Protection Program.

THE INCIDENCE OF UNCONTAINED ROTOR BURSTS IN U.S. COMMERCIAL AVIATION

1962 - 1973

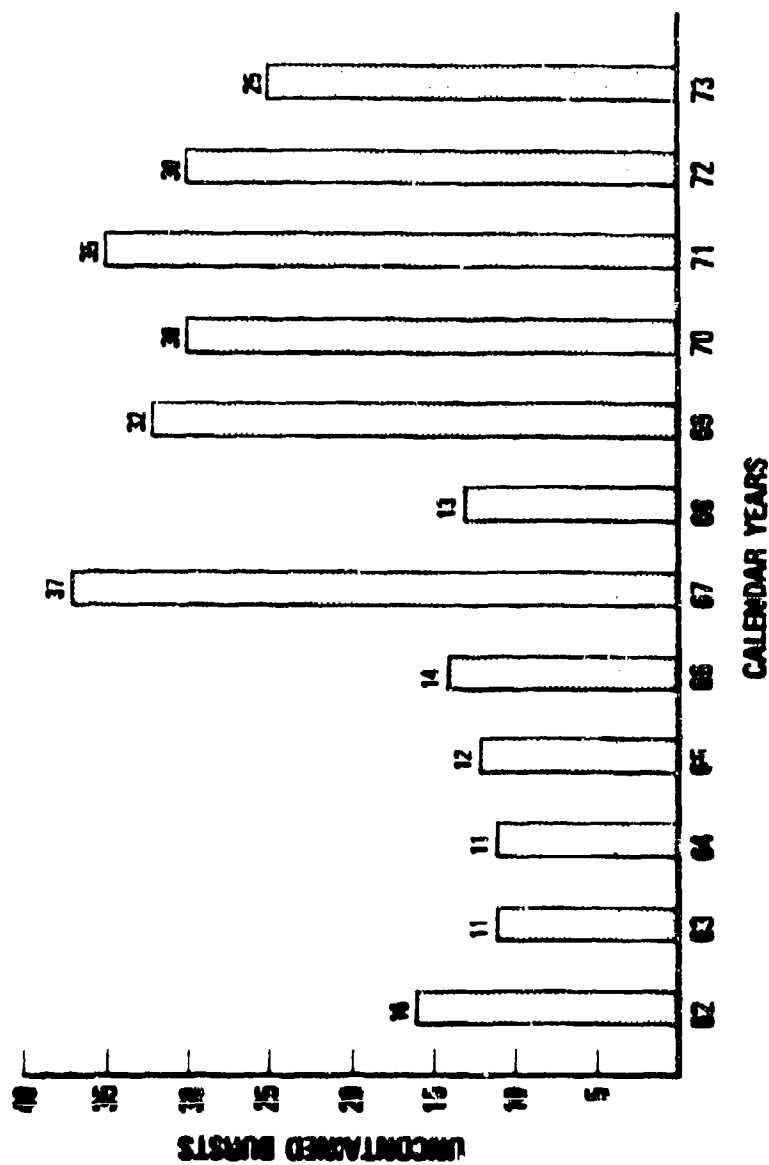


Figure 1

INCIDENCE OF ROTOR FAILURE/BURST IN U.S. COMMERCIAL AVIATION - 1973

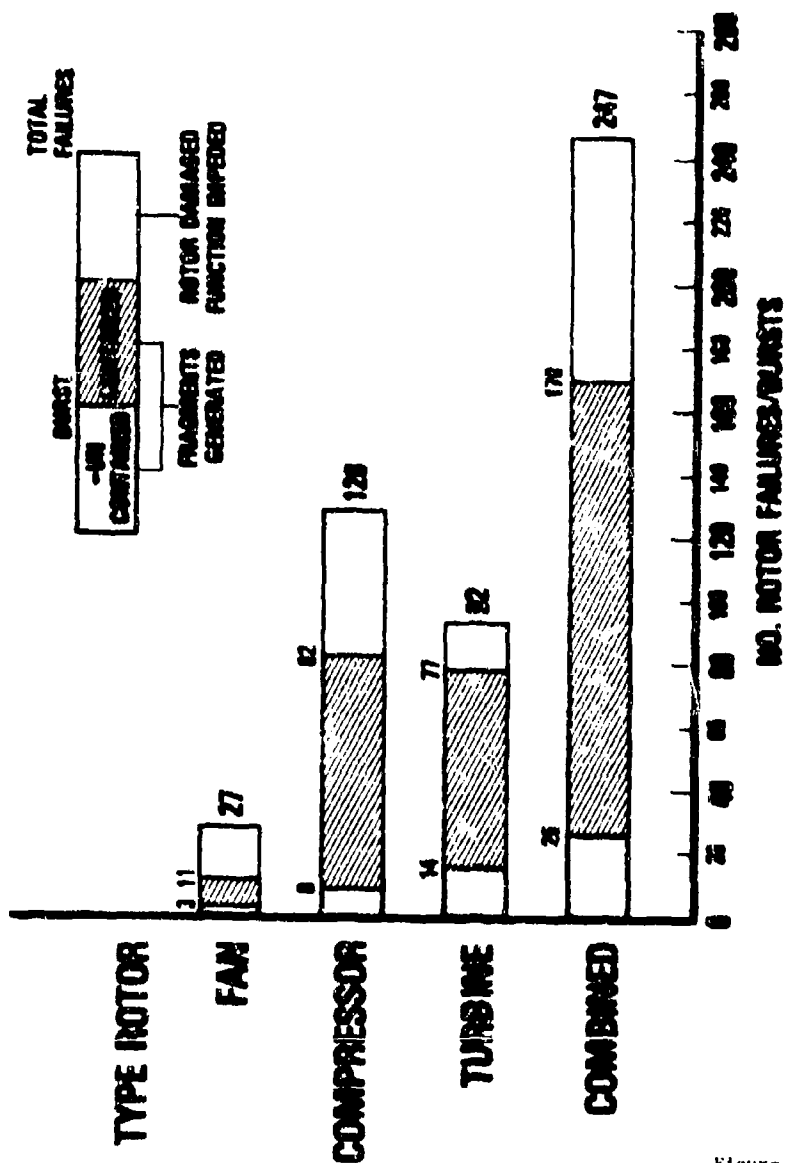


Figure 2

**COMPONENT AND FRAGMENT TYPE DISTRIBUTIONS
FOR CONTAINED AND UNCONTAINED ROTOR BURSTS⁽¹⁾
1973**

ENGINE ROTOR COMPONENT	TYPE OF FRAGMENT GENERATED						TOTALS	
	DISK		RIM		BLADE			
	TF	UCF	TF	UCF	TF	UCF	TF	UCF
FAN	0	0	0	0	11	3	11	3
COMPRESSOR	2	2	2	1	78	5	82	8
TURBINE	1	1	1	1	75	12	77	14
TOTALS	3	3	3	2	164	20	170	25

(1) FAILURES THAT PRODUCED FRAGMENTS

TF - TOTAL FAILURES
UCF - UNCONTAINED FAILURES

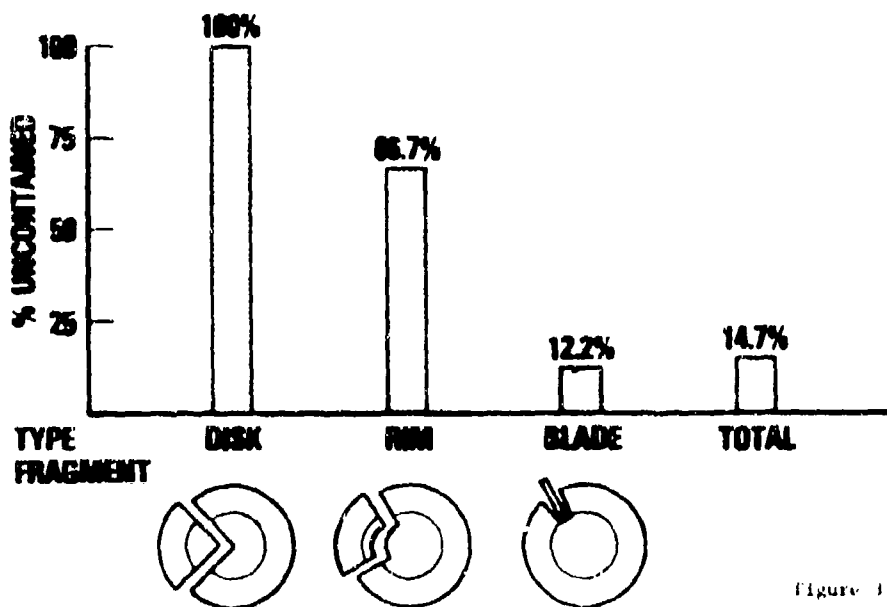
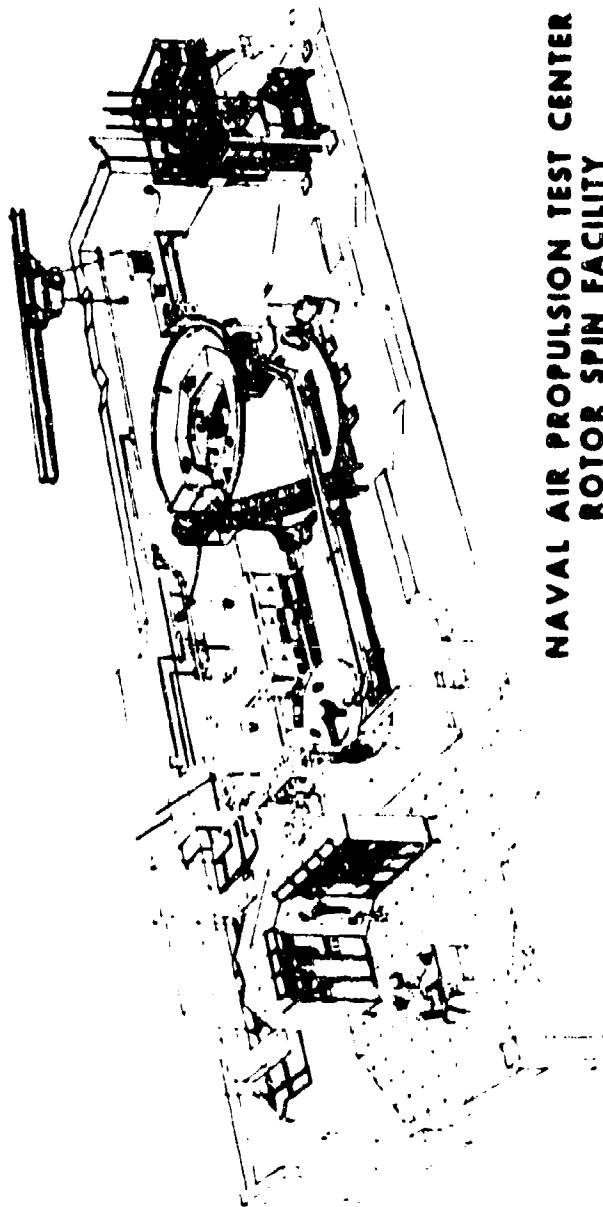


Figure 1



NAVAL AIR PROPULSION TEST CENTER
ROTOR SPIN FACILITY

Figure 4

EXPERIMENT 67 -

3 FRAGMENT ROTOR BURST INTO A 4130 STEEL RING

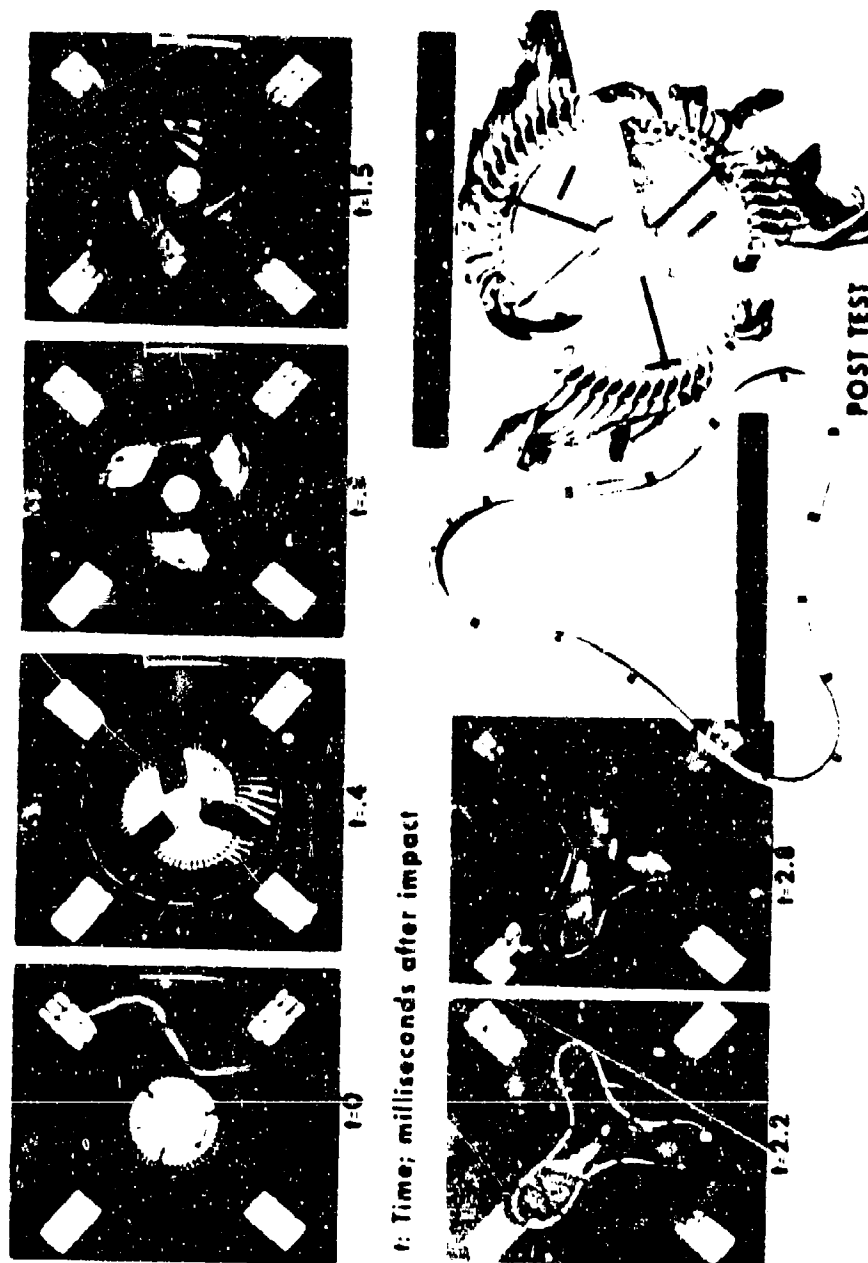
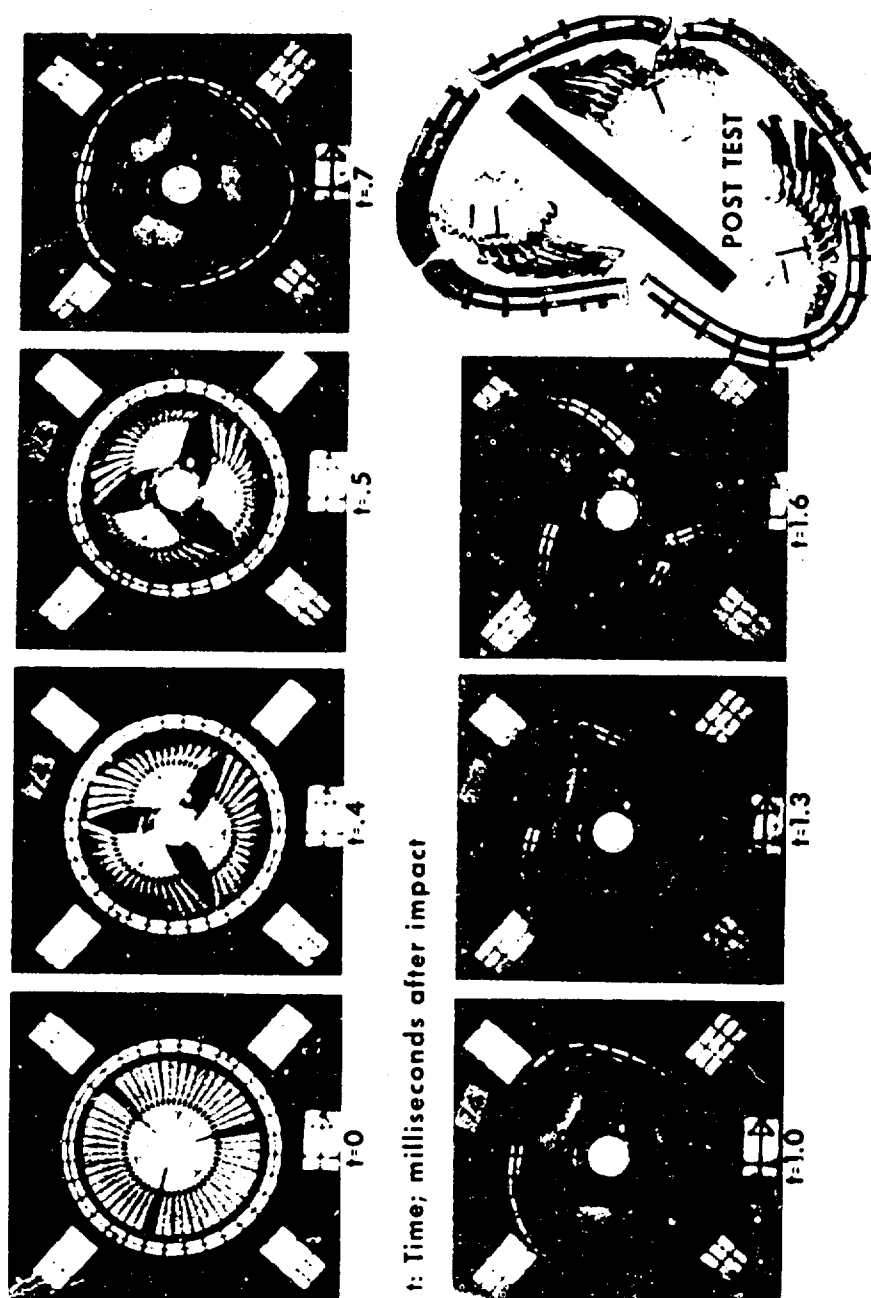


Figure 6

EXPERIMENT 74 -

3 FRAGMENT ROTOR BURST INTO A 2024-T4 ALUMINUM RING

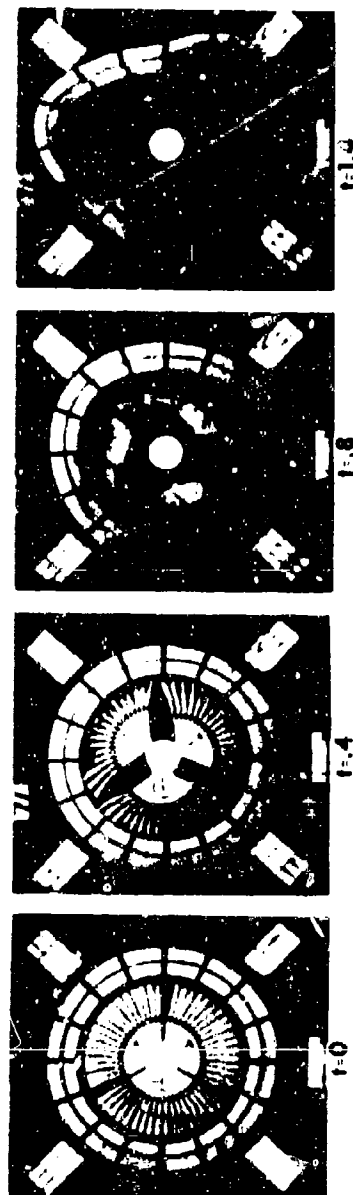


t: Time; milliseconds after impact

Figure 7

EXPERIMENT

3 FRAGMENT ROTOR BURST INTO A BALLISTIC NYLON WITH STEEL LINER RING



t: Time; milliseconds after impact

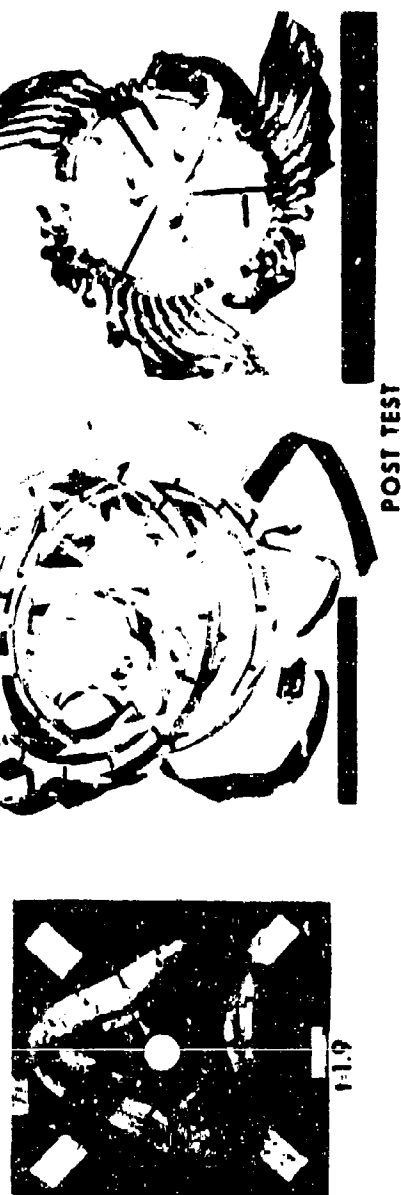


Figure 8

EXPERIMENT 86 -

3 FRAGMENT ROTOR BURST INTO A FILAMENT WOUND FIBERGLASS RING



Figure 9

EXPERIMENT 109 -

SINGLE BLADE BURST INTO A 6061-T6 ALUMINUM RING

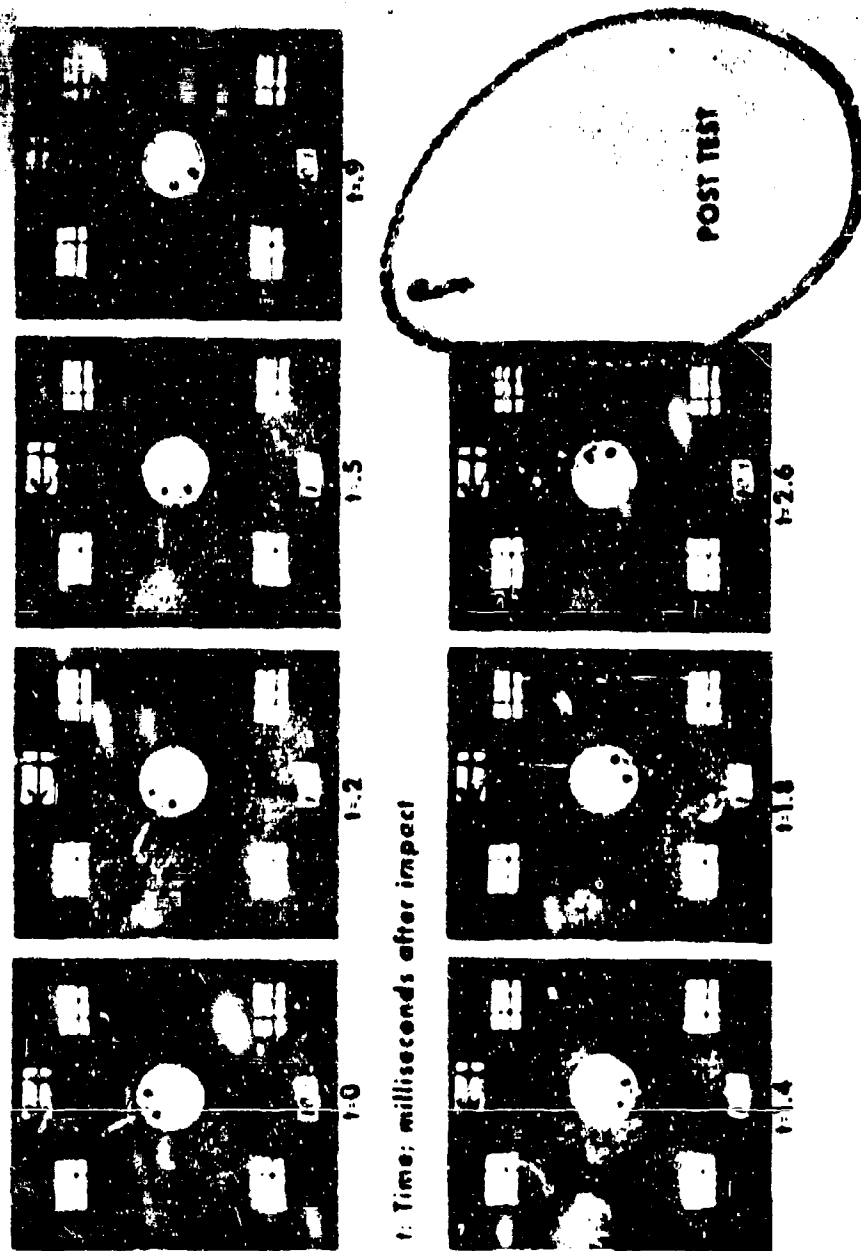
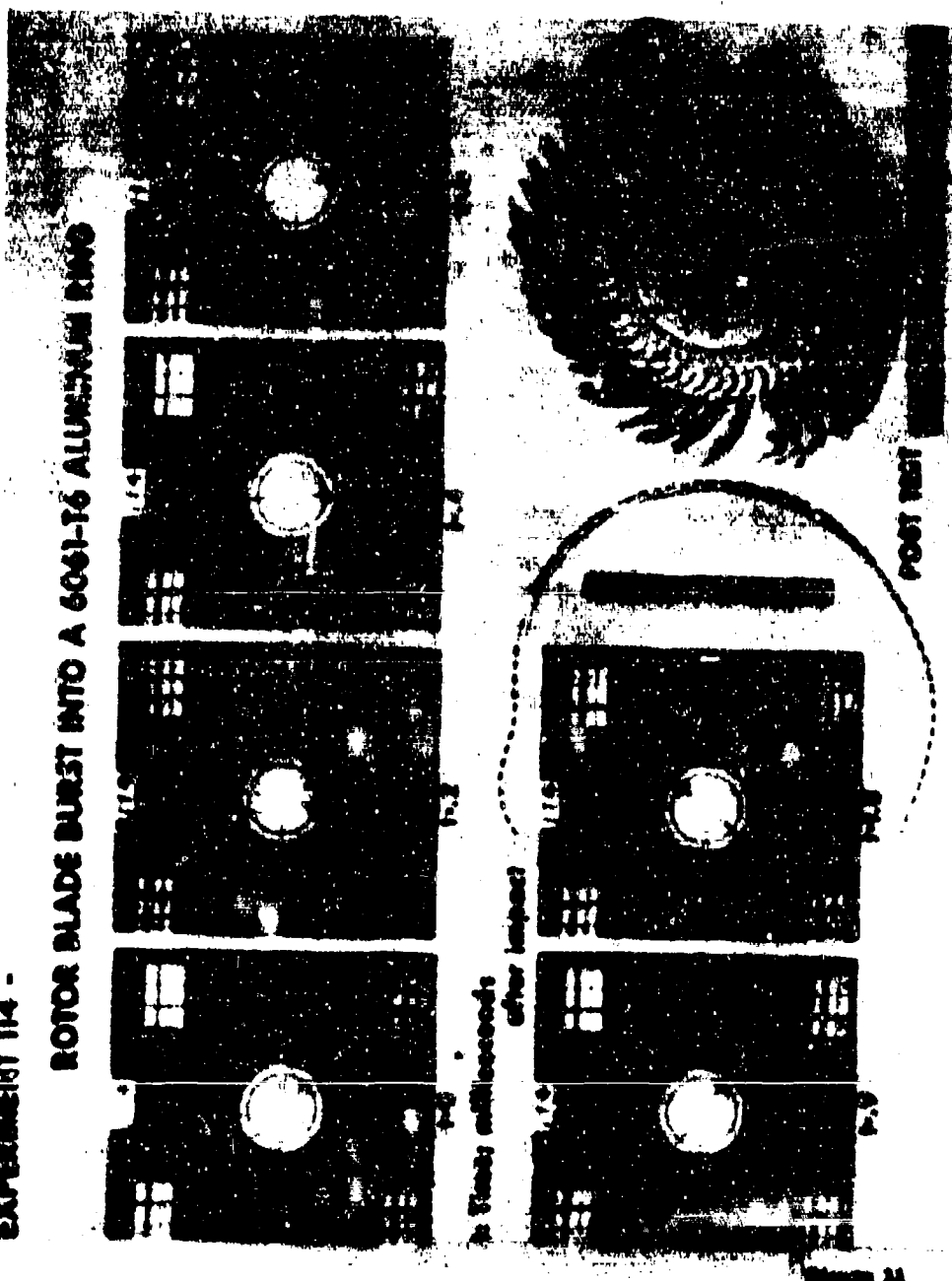


Figure 10

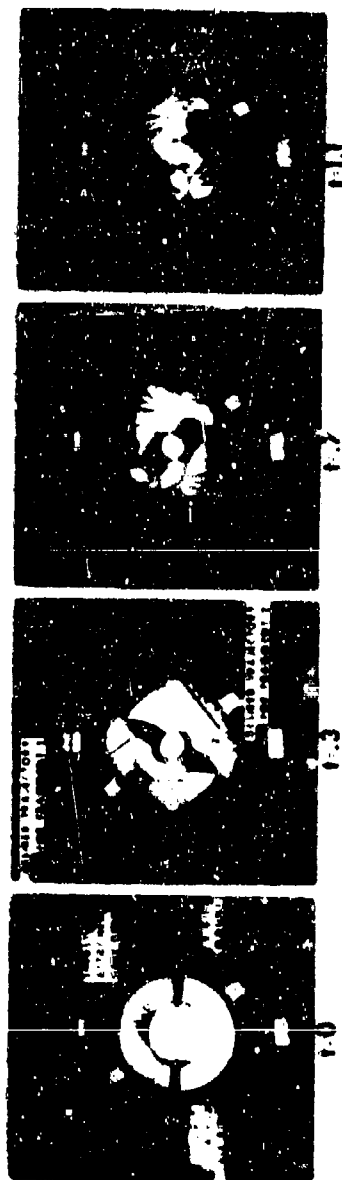
EXPERIMENT 114 -

ROTOR BLADE BURST INTO A 6061-T6 ALUMINUM RING



EXPERIMENT 120 -

2 FRAGMENT ROTOR BURST INTO RIGIDLY ATTACHED STEEL HALF RINGS



1. Time: milliseconds after impact

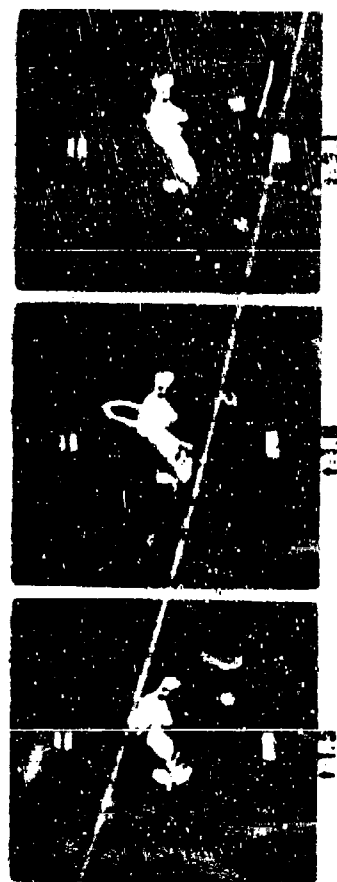


Figure 12

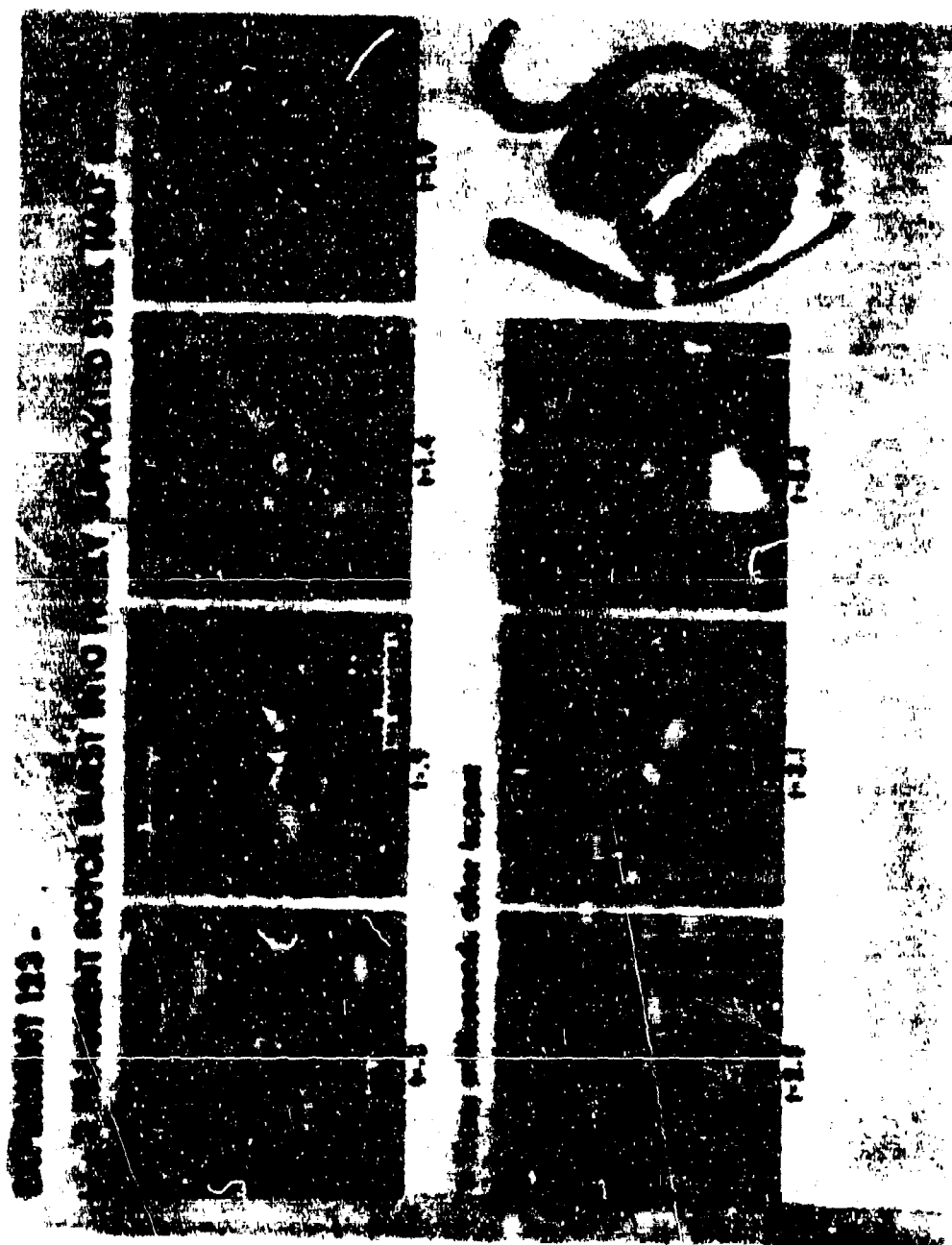
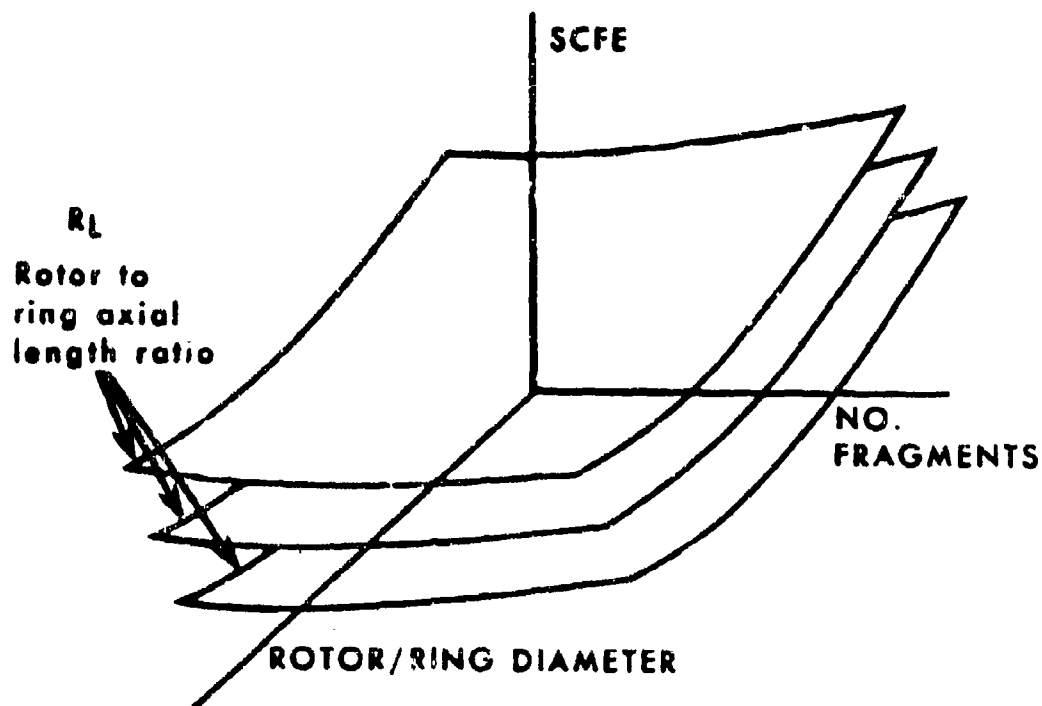


EXHIBIT 123 -

EXHIBIT 123 -

EXHIBIT 123 -

FUNCTIONAL RELATIONSHIP (CONCEPTUAL)



DERIVED EXPERIMENTALLY BY VARYING

- rotor diameter
- no. fragments
- ring axial length
- ring radial thickness

Figure 14

APPENDIX 1

SUMMARY OF THE CAPABILITIES OF THE COMPUTER CODES JET 1, JET 2, AND JET 3
FOR PREDICTING TWO-DIMENSIONAL TRANSIENT RESPONSES OF RING STRUCTURES

This appendix is intended to provide for the reader a convenient tabular summary of the principal features and capabilities of the two-dimensional transient large-deflection elastic-plastic structural response ring codes JET 1 (Ref. 15), JET 2 (Ref. 16), and JET 3A-3D (Ref. 24) developed under NASA MCR 22-0009-139. The present code CIVM-JET-4A has been developed by combining the CIVM procedure with a modified version of the JET 3C two-dimensional structural response code.

The JET 1 code of Ref. 15 pertains to single-layer complete, uniform-thickness, initially-circular rings of either temperature-independent or temperature-dependent material properties. These rings may be subjected to prescribed: (a) initial velocities, (b) transient mechanical loading, and/or (c) steady nonuniform temperatures. The finite-difference method employed in this code had been shown previously (Ref. 12) to provide reliable predictions for the case of temperature-independent material properties.

The JET 2 code was written in order to extend this finite-difference analysis capability to treat multilayer rings -- cases anticipated to be of future concern. In the interests of efficiency and the minimization of computer storage requirements, temperature-dependent material properties and thermal loading features were omitted from JET 2; if these omitted features should turn out to be needed urgently (but this, thus far, has not been the case), they could be added later.

Since the JET 1 and JET 2 codes pertained to initially-circular, complete rings of uniform thickness whereas there was interest also in variable-thickness, arbitrarily curved, partial as well as complete rings, the JET 3 series of codes was developed. To accommodate these latter features as well as a variety of types of (1) boundary conditions, (2) elastic-foundation supports, and (3) point elastic supports, the more versatile finite-element analysis procedure was developed and employed. For efficiency and user convenience, four versions of the JET 3 program were developed; each version accommodates both complete rings and partial rings. JET 3A and JET 3B pertain to uniform-thickness, initially-circular rings, and employ, respectively, the central-difference and the Houbolt finite-difference time operator; for certain cases, the latter finite-difference time operator may permit more economic converged transient response predictions than the former. The codes JET 3C and JET 3D are corresponding codes which accommodate variable-thickness, arbitrarily-curved rings.

In all of these codes (JET 1 through JET 3D), the stimuli: (1) initial velocity or impulse conditions and/or (2) transient mechanical loading must be prescribed by the user or analyst. The externally-applied forces experienced by a complete or a partial ring from fragment impact are not provided within these codes. The user must supply his own estimate of the distribution and time histories of these forces. However, in the CIVM-JET-4A code, fragment/ring interaction and response effects are handled internally automatically, for the idealized single-fragment and n-fragment cases provided and discussed in Appendix A.

In convenient tabular form, the principal features and capabilities of the codes JET 1, JET 2, and JET 3A-3D are given in the following:

Feature	JET 1 (Ref. 15)	JET 2 (Ref. 16)	JET 3A (Ref. 24)	JET 3B (Ref. 24)	JET 3C (Ref. 24)	JET 3D (Ref. 24)
Type of Spatial Analysis Formulation						
Finite Difference	x	x	-	-	-	-
Finite Element	-	-	x	x	x	x
Type of Finite-Difference Time Operator						
Central Difference	x	x	x	-	x	-
Houbolt (Backward Difference)	-	-	-	x	-	x
Ring Geometry						
Complete Ring	x	x	x	x	x	x
Partial Ring	-	-	x	x	x	x
Initial Configuration						
Circular	x	x	x	x	x	x
Arb. Curved	-	-	-	-	x	x
Constant Thickness	x	x	x	x	x	x
Variable Thickness	-	-	-	-	x	x
Single Layer	x	x	x	x	x	x
Multilayer Hard-Bonded (1 to 3 layers)	-	x	-	-	-	-
Boundary Conditions						
Ideally Clamped	-	-	x	x	x	x
Hinged Fixed	-	-	x	x	x	x
Symmetry	-	-	x	x	x	x
Free	-	-	x	x	x	x
Other Support Conditions						
Distributed Elastic Foundation	-	-	x	x	x	x
Point Elastic Springs	-	-	x	x	x	x

Feature	JET 1	JET 2	JET 3A	JET 3B	JET 3C	JET 3D
<u>Material</u>						
Single Material	x	-	x	x	x	x
Different for Each Layer	-	x	-	-	-	-
Homogeneous	x	x	x	x	x	x
Initially Isotropic	x	x	x	x	x	x
Temperature Independent	x	x	x	x	x	x
Temperature Dependent	x	-	-	-	-	-
EL	x	x	x	x	x	x
EL-PP	x	x	x	x	x	x
EL-LSH	x	x	x	x	x	x
EL-SH	x	x	x	x	x	x
EL-SH-SR	x	x	x	x	x	x
<u>Stimuli</u>						
Initial Velocity						
Arbitrary	x	x	x	x	x	x
Half-Sine over each of Selected Regions	x	x	x	x	x	x
Mechanical Loading						
Arbitrary Spatial Distribution with Arb. Time History	-	x	x	x	x	x
Half-Sine over each of Selected Regions	x	x	x	x	x	x
Triangular Time History	x	x	x	x	x	x
Arbitrary Time History	-	x	x	x	x	x
Thermal Loads (Temp. Distribution)						
Distribution Thru Thickness	x	-	-	-	-	-
Time-Independent Prescribed Circumferential Distribution	x	-	-	-	-	-
<u>Deformations: Kirchhoff</u>						
<u>Type Only</u>						
Small	x	x	x	x	x	x
Arbitrarily Large	x	x	x	x	x	x
<u>OUTPUT INFORMATION</u>						
<u>At Selected Times</u>						
Energy/Work Type and Amount	x	x	x	x	x	x
Nodal Station Data						
Locations Y, Z	x	x	x	x	x	x
Displacements	-	-	x	x	x	x
Moment Resultant	x	x	x	x	x	x
Circum. Force Resultant	x	x	x	x	x	x
Circumferential Strains						
Inner Surface	x	x	x	x	x	x
Outer Surface	x	x	x	x	x	x
Location where Prescribed Value is Exceeded	-	x	x	x	x	x
<u>At Certain Other Times</u>						
Time of First Yielding	x	x	-	-	-	-
Time when Strain First Exceeds a Prescribed Value	-	x	x	x	x	x
Time, Location, and Value of Largest Strain Reached During Run	-	-	x	x	x	x
<u>CAPACITY INFORMATION</u>						
Maximum No. of Finite-Difference Stations*	100	100	-	-	-	-
Maximum No. of Finite Elements*	-	-	50	50	50	50

* These limits can be circumvented by altering the dimensions of appropriate program variables (see each source reference).

APPENDIX 2

ROTOR BURST PROTECTION PROGRAM - REPORTS ISSUED

1. McCallum, R. B., Leech, J. W., and Witmer, E. A.: Progress in the Analysis of Jet Engine Burst-Rotor Containment Devices. ASRL TR 154-1, Aeroelastic and Structures Research Laboratory, Massachusetts Institute of Technology, August 1969. (Available as NASA CR-107900.)
2. McCallum, R. B.: Simplified Analysis of Trifragment Rotor Disk Interaction with a Containment Ring. AIAA Journal of Aircraft, Vol. 7, No. 3, May-June 1970, pp. 283-285.
3. McCallum, R. B., Leech, J. W., and Witmer, E. A.: On the Interaction Forces and Responses of Structural Rings Subjected to Fragment Impact. ASRL TR 154-2, Aeroelastic and Structures Research Laboratory, Massachusetts Institute of Technology, Sept. 1970. (Available as NASA CR-72801.)
4. Wu, R. W.-H. and Witmer, E. A.: Finite Element Analysis of Large Elastic-Plastic Transient Deformations of Simple Structures. AIAA Journal Vol. 9, No. 9, Sept. 1971, pp. 1719-1724.
5. Leech, J. W., Witmer, E. A., and Yeghiavan, R. P.: Dimensional Analysis Considerations in the Engine Rotor Fragment Containment/Deflection Problem. ASRL TR 154-3, Aeroelastic and Structures Research Laboratory, Massachusetts Institute of Technology, December 1971. (Available as NASA CR-72801.)
6. Wu, R. W.-H. and Witmer, E. A.: Finite-Element Analysis of Large Transient Elastic-Plastic Deformations of Simple Structures, with Application to the Engine Rotor Fragment Containment/Deflection Problem. ASRL TR 154-4, Aero-Technology, Jan. 1972. (Available as NASA CR-120886.)
7. Zirin, R. M. and Witmer, E. A.: Examination of the Collision Force Method for Analyzing the Responses of Simple Containment/Deflection Structures to Impact by One Engine Rotor Blade Fragment. ASRL TR 154-6, Aeroelastic and Structures Research Laboratory, Massachusetts Institute of Technology, May 1972. (Available as NASA CR-120952)
8. Wu, R. W.-H. and Witmer, E. A.: Computer Program - JET 3 to Calculate the Large Elastic-Plastic Dynamically-Induced Deformations of Free and Restrained, Partial and/or Complete Structural Rings. ASRL TR 154-7, Aeroelastic and Structures Research Laboratory, Massachusetts Institute of Technology, August 1972. (Available as NASA CR-120993.)
9. Wu, R. W.-H. and Witmer, E. A.: Approximate Analysis of Containment/Deflection Ring Responses to Engine Rotor Fragment Impact. AIAA Journal of Aircraft, Vol. 10, No. 1, January 1973, pp. 28-37.
10. Wu, R. W.-H. and Witmer, E. A.: Nonlinear Transient Responses of Structures by the Spatial Finite-Element Method. AIAA Journal, Vol. 11, No. 8, August 1973, pp. 1110-1117.
11. Collins, T. P. and Witmer, E. A.: Application of the Collision-Imparted Velocity Method for Analyzing the Responses of Containment and Deflector Structures to Engine Rotor Fragment Impact. MIT ASRL TR 154-8, August 1973. (Available as NASA CR-134494.)
12. Yeghiavan, R. P., Leech, J. W., and Witmer, E. A.: Experimental and Data Analysis Techniques for Deducing Collision-Induced Forces from Photographic Histories of Engine Rotor Fragment Impact/Interaction with a Containment Ring. MIT ASRL TR 154-5, October 1973. (Available as NASA CR-13548.)
13. Stagliano, T. R. and Witmer, E. A.: User's Guide to Computer Program CIVM-JET 4B to Calculate Large Nonlinear Transient Deformations of Single-Layer Partial and/or Complete Structural Rings to Engine Rotor Fragment Impact, MIT ASRL TR 154-9 (in preparation).
14. Wu, R. W.-H., Witmer, E. A., and Stagliano, T. R.: User's Guide to Computer Programs JET 5A and CIVM-JET 5B to Calculate the Large Elastic-Plastic Dynamically-Induced Deformations of Multilayer Partial and/or Complete Structural Rings, MIT ASRL TR 154-10 (in preparation).
15. "Turbine Disk Burst Protection Study" Phase I Final Report on Problem Assignment NASA DPR #R-105 - NAEC-AEL-1793 of 31 Mar 1965 - AD No. not yet assigned.
16. "Turbine Disk Burst Protection Study" Final Phase II-III Report on Problem Assignment NASA DPR #R-105 - NAPTIC-AEL-1848 of 28 Feb 1967 - AD No. 820894
17. "Rotor Burst Protection Program Initial Test Results" Phase IV Final Report on Problem Assignment NASA DPR #R-105 - NAPTIC-AED-1869 of 5 Apr 1968 - AD No. 850921
18. "Rotor Burst Protection Program" Phase V Final Report on Problem Assignment NASA DPR #R-105 - NAPTIC-AED-1901 of May 1969 - AD No. 693446.
19. "Rotor Burst Protection Program - Phases VI and VII: Exploratory Experimentation to Provide Data for the Design of Rotor Burst Fragment Containment Rings" - NAPTIC-AED-1968 of March 1972 - AD No. not yet assigned.
20. "Rotor Burst Protection Program": Statistics on Aircraft Gas Turbine Engine Rotor Failures that Occurred in Commercial Aviation During 1971, Report on NASA DPR C-41581-B, MOD 4 - Report No. NAPTIC-PE-12 of Feb 1973.
21. "Rotor Burst Protection Program": Statistics on Aircraft Gas Turbine Engine Rotor Failures that Occurred in U. S. Commercial Aviation During 1972, Report on NASA DPR C-41581-B, MOD 5 - Report No. NAPTIC-PE40 of Mar 1974.

22. "Rotor Burst Protection Program": Statistics on Aircraft Gas Turbine Engine Rotor Failures that Occurred in U. S. Commercial Aviation During 1973, ASME Paper No. 75-GT-12, Mar 1975.

TENUE DES CARTERS MOTEURS LORS DES RUPTURES D'AUBES

par

J. IMILRY

D.A.E.C.M.A.

Centre d'EVRY - CORBEIL

Laboratoire de la Direction Technique

B.P. N° 81

91100 EVRY CEDEX

RÉSUMÉ

Cette étude analyse la manière dont les aubes rompues viennent frapper le carter moteur puis décrit une installation d'essais très simple permettant d'envoyer des projectiles à vitesse variable sur des cibles représentant le carter.

Les essais effectués montrent le comportement aux impacts à froid et à chaud d'un assez grand nombre de matériaux, qu'il s'agisse de matières corroyées ou coulées aussi bien pour des alliages d'aluminium et de titane que pour des aciers et des alliages de nickel ou de cobalt. Ils mettent également en évidence l'influence de la rigidité, de l'épaisseur et de la masse de la cible. Ils sont comparés à quelques essais à plus grande dimension afin de juger de l'influence de l'échelle et de mieux analyser les déformations de la cible en vue de rechercher une corrélation entre le comportement aux impacts et les résultats des essais mécaniques classiques.

Cet ensemble d'essais permet enfin de dégager un certain nombre de règles qui peuvent servir de guide au responsable chargé de dessiner un carter devant contenir les aubes.

SUMMARY

An analysis has been carried out of the way in which a ruptured blade impacts an engine case. Then a simple test bench, which allows to project bullets at a variable speed on a small target representative of a case, is described.

Tests on various materials such as aluminum, titanium, iron, nickel and cobalt base alloys in wrought or cast form have been conducted at room as well as at elevated temperatures. This test is also able to show the influence of the stiffness, thickness and mass of the target.

A few experiments with larger projectiles and larger plates are currently being performed. They will allow to study the scale effect and to analyse more accurately the strain distribution in the target, thus giving elements for some correlation of the impact behaviour of materials with their classical mechanical properties.

Finally our test allows to draw a few guide-rules for the design of a blade containing case.

-00000-

Il est demandé aux constructeurs de turboréacteurs de garantir que les carters soient capables de contenir les aubes de compresseur ou de turbine qui pourraient pour une cause quelconque se rompre. Il s'agit aussi bien de ruptures de la pale ou de l'attache sous l'effet d'excitations vibratoires ou de ruptures par fatigue à partir de blessures provoquées par l'absorption de corps étrangers, que de ruptures produites par l'ingestion d'oiseaux.

En général, les carters des étages de compresseurs haute pression ainsi que les carters des étages moyenne pression sont capables de retenir les aubes qui sont de plus petite dimension et seuls les carters des premiers étages de compresseurs doivent être renforcés. Le problème le plus difficile se pose avec les grandes aubes de soufflantes à talons intermédiaires mais des renforcements de carters sont quand même nécessaires pour contenir les aubes des premiers étages des réacteurs à simple flux. Du côté turbine ce sont les aubes les plus longues et à talons au sommet qui sont également les plus difficiles à contenir mais certaines aubes à grande corde et avec pied à échasse de la turbine haute pression peuvent nécessiter des renforcements de carters.

D'une manière générale la difficulté majeure vient des grandes aubes de soufflante dont les dimensions s'approchent de celles des hélices et qui comportent des talons intermédiaires (voir planche 1). Bien que le constructeur prenne le maximum de précautions pour que des ruptures ne puissent pas se produire dans le pied, les règlements imposent de considérer le cas de la séparation complète de l'aube muni de son attache.

L'examen cinématographique des ruptures de pale sous l'effet d'une charge explosive dans l'attache ou d'un tir d'oiseau montre que l'aube en se séparant du disque prend un mouvement de rotation autour de son centre de gravité et vient frapper le carter par la partie massive de son pied. La vitesse d'impact peut dépasser nettement la vitesse d'entraînement tangentielle de son centre de gravité. Ainsi le premier impact est un impact à incidence proche de la normale avec une vitesse de l'ordre de grandeur des vitesses

circonférentielles des aubes, par exemple de 200 à 400 m/s. On peut donc en déduire que les carters de compresseur doivent résister à des projectiles présentant des arêtes anguleuses et de mêmes caractéristiques mécaniques que les aubes, c'est-à-dire environ 1000 MPa de charge de rupture, envoyés à incidence normale à des vitesses de l'ordre de 300 m/s.

Il s'agit alors pour le motoriste de choisir le matériau le mieux adapté pour la fabrication des carters et de déterminer la technologie et l'épaisseur qui permettent avec la masse la plus faible de contenir les projectiles.

Dans ce but, nous avons entrepris une campagne d'essais métallurgiques afin de comparer le comportement d'un grand nombre de matériaux sous l'effet d'impacts à grande vitesse.

INSTALLATION D'ESSAI

A partir de ces données, nous avons utilisé une installation d'essai très simple permettant d'envoyer des projectiles à vitesse et inclinaison variable sur des plaques. Cette installation comporte un dispositif de chauffage de la cible pour étudier le comportement des matériaux pour carter turbine.

L'installation (planche 2) comprend un pistolet de scellement normalement utilisé pour fixer des pièces d'acier dans le béton, une cabine de tir avec les dispositifs de sécurité empêchant le tir quand la cabine n'est pas fermée, un socle orientable pour la fixation de la cible ainsi qu'un chalumeau pour chauffage éventuel de la cible jusqu'à 1000°C. Une chaîne de mesure (planche 3) constituée de deux cellules photo-électriques et d'un chronomètre Kocher donne la vitesse du projectile pour chaque tir car, malgré les précautions prises, il n'a pas été possible d'obtenir une relation assez précise entre la quantité de poudre de la cartouche et la vitesse du projectile.

CHOIX DU PROJECTILE

Le projectile utilisé est un cylindre de 8 mm de diamètre terminé par un tronc de cône à 90°. Il est réalisé dans un acier à 1000 MPa de charge de rupture et sa masse est de 1 gramme. Avant de retenir cette forme avec tronc de cône représentée planche 4, nous avons comparé sur une même cible les effets des deux autres formes de projectile de même masse, l'un terminé par une calotte sphérique, l'autre par une face droite chanfreinée. Contrairement à notre attente, la perforation d'une cible en matériau à faible fragilité a eu lieu pour la vitesse la plus faible avec le projectile à calotte sphérique tandis que le projectile pointu ne perforait la cible que pour une vitesse très supérieure. On constate en effet que la forme sphérique donne la plus faible déformation à la cible et perce uniquement par cisaillement tandis que la forme pointue déforme très nettement la cible avant de la perforer. Lorsque le matériau de la cible a une faible capacité de déformation, le projectile pointu provoque des criques radiales en mettant en évidence le comportement fragile du matériau. Le projectile sphérique au contraire conduit à un essai de résistance à la perforation par cisaillement. Le projectile à front droit entraîne de légères déformations et a un effet proche de celui du projectile sphérique.

Nous n'avons pas retenu la forme sphérique estimant que la rupture par cisaillement pouvait facilement se déduire des caractéristiques mécaniques classiques des matériaux et nous nous sommes intéressés plus particulièrement, à l'aide du projectile pointu, au comportement fragile à grande vitesse de déformation.

FORME DE LA CIBLE

Pour une même épaisseur de 2,5 mm, trois formes de cibles ont été comparées (planche 5) :

- une plaque fortement bridée laissant libre une surface circulaire de diamètre double de celui du projectile,
- une plaque carrée fixée sur ses côtés laissant libre une surface carrée de 90 mm x 90 mm,
- une plaque rectangulaire encastrée seulement sur un petit côté et laissant libre un rectangle de 30 mm x 90 mm.

La planche 6 montre les résultats obtenus avec huit matériaux différents allant des alliages d'aluminium et de magnésium aux alliages de titane et aux aciers. On constate que plus la cible est rigide, plus la perforation est facile. On s'approche plus loin qu'avec la cible très rigide la vitesse de perforation s'approche par excès de la vitesse de perforation par cisaillement pur.

INFLUENCE DE LA VITESSE DU PROJECTILE

La planche 7 montre la déformation de la cible en fonction de la vitesse, pour une cible en alliage très ductile (alliage Al - 5 Mg) peu encastrée. Aux très grandes vitesses, on a une perforation par cisaillement pur sans absorption d'énergie à distance : c'est le cas d'une balle perforant une vitre en laissant un trou bien rond. Aux vitesses plus faibles il y a des déformations près de l'impact et à distance.

INFLUENCE DES CARACTÉRISTIQUES MÉCANIQUES DE LA CIBLE

Pour un acier martensitique au chrome molybdène vanadium, nous avons fait varier les caractéristiques mécaniques en jouant sur le traitement thermique de revenu. On constate (planche 8) que pour cet acier

40 CDV 20 (Vescojet 1000), le meilleur comportement a lieu pour une charge de rupture d'au moins 1200 MPa et que le comportement fragile n'est net qu'à 1400 MPa. Ces essais obtenus avec le projectile pointu et une cible peu encastrée, c'est-à-dire dans des conditions où la fragilité a le plus de facilité de se manifester, montrent qu'on peut obtenir une bonne résistance aux impacts avec un matériau traité à un haut niveau de caractéristiques mécaniques, pourvu que sa ductilité reste supérieure à 8%.

INFLUENCE DE L'ÉPAISSEUR

Les essais sur des cibles d'épaisseur variable ont été effectués sur des alliages d'aluminium et de magnésium car nous voulions voir dans quelle mesure on pouvait remplacer des carters minces en acier par des carters plus épais en alliages légers forgés ou coulés. On constate (planche 9) que la vitesse de perforation augmente à peu près proportionnellement à la racine carrée de l'épaisseur ou encore que l'énergie cinétique $1/2 mv^2$ entraînant la perforation est proportionnelle à l'épaisseur de la cible.

S'il s'agit de cisaillement pur, l'énergie de rupture par perforation aurait pu s'exprimer sous la forme approchée :

$$0,66 R \times \pi d e \times v$$

- R représentant la contrainte de rupture en traction

- $\pi d e$ la surface cisailée par le projectile de diamètre d sur une cible d'épaisseur e.

Cette formule simplifiée admet que la contrainte de rupture par cisaillement à grande vitesse est égale à 66% de la contrainte de rupture par traction et que cette contrainte de rupture se conserve pendant tout le déplacement de cisaillement qui est voisin de l'épaisseur. Cette formule donne une vitesse de perforation proportionnelle à l'épaisseur.

Sur la planche 9 nous avons porté cette vitesse de perforation par cisaillement pur. Elle correspond au cas où toute l'énergie cinétique du projectile est utilisée pour tondre la cible par cisaillement. Chaque fois qu'il y aura absorption d'énergie en dehors de ce cisaillement, en particulier pour déformer la cible près de l'impact ou à distance au droit de l'encastrement, la vitesse de perforation sera plus élevée. Par contre, lorsque la cible sera fragile, elle pourra "voler en éclats" en absorbant moins d'énergie que pour la perforation par cisaillement.

On voit sur la planche 9 que la vitesse pratique de perforation ne descend en dessous de la vitesse théorique de perforation que dans le cas des cibles rompues avec un faciès fragile. Les écarts sont les plus grands lorsque les cibles ont une faible épaisseur car elles peuvent alors se déformer fortement par flexion ; dans ce cas, l'énergie absorbée peut au total être 3 à 6 fois supérieure à l'énergie théorique de cisaillement. Ainsi l'augmentation d'épaisseur est moins payante que ne la laisserait prévoir la loi de vitesse proportionnelle à l'épaisseur e qui repose sur la théorie du cisaillement maximum alors que c'est précisément avec les fortes épaisseurs que la plus grande part de l'énergie est absorbée par cisaillement ; lorsque l'on double l'épaisseur, la vitesse de perforation est multipliée par un facteur plus proche de 1,1 que de 2. Nous insistons sur ce point car de nombreux auteurs en présentant des lois où la vitesse est proportionnelle à l'épaisseur, ne soulignent pas assez le fait qu'aux faibles épaisseurs et aux faibles vitesses les cibles peuvent absorber beaucoup plus d'énergie que par le seul cisaillement ; ces lois sont par contre très utiles pour évaluer le risque de perforation. De la même façon, on peut penser que si une cible est constituée de deux tôles au lieu d'une seule d'épaisseur double, les deux tôles, grâce à leur plus grande souplesse, pourront absorber davantage d'énergie mais il faut être très prudent dans cette voie, compte tenu de la faible résistance au déchirement des éléments minces.

COMPARAISON DES MATÉRIAUX À ÉPAISSEUR CONSTANTE

La planche 10 rassemble un grand nombre de résultats obtenus avec une cible de 2,5 mm d'épaisseur encastrée sur un petit côté ; quelques résultats avec une cible fortement bridée ont été ajoutés.

Nous avons classé les matériaux en tenant compte à la fois de la vitesse de perforation mesurée, de la vitesse théorique de perforation par cisaillement et des critères de fragilité. Les meilleurs résultats sont obtenus avec l'acier Vescojet 1000 traité à 1200 MPa et avec l'alliage base cobalt Hb 25. L'alliage base nickel Waspaloy se place bien malgré une légère fragilité intergranulaire n'entraînant pas de criques radiales.

Quelques essais ont été effectués sur une cible durcie superficiellement par une nitruration de 0,15 mm d'épaisseur sur la face recevant le projectile. Aucun avantage et même plutôt une certaine baisse de résistance a été observée par suite de la fragilité du revêtement un peu à l'extérieur de l'impact, là où les déformations ont lieu par extension. On peut penser qu'en tir oblique la nitruration aurait apporté un avantage.

COMPARAISON À MASSES ÉGALES

Le classement présenté planche 11 permet une comparaison des matériaux de masse spécifique différente.

La première famille, basée à la fois à l'essai de tir sur plaquette faiblement encastrée et à la perforation par cisaillement, ne comprend que des matériaux à faible masse spécifique. On voit l'avantage que l'on peut tirer des alliages d'aluminium et de magnésium forgés ou coulés et des alliages de titane à condition

de s'écarter d'une légère fragilité. Bien que les fortes épaisseurs écartent les possibilités de déformation à distance, ces matériaux semblent supérieurs aux aciers et surtout aux aciers inoxydables austénitiques non durcis qui se trouvent très mal placés par suite de leur faible tenue au cisaillement.

Les alliages d'aluminium ont l'avantage d'être économiques et de bien "contenir" les projectiles mais ils risquent d'être fortement blessés à cause de leur très bonne usinabilité et de leur faible dureté ; leur ductilité médiocre pourrait être un inconvénient lorsqu'il y a des variations de rigidité ou d'épaisseur.

Cette comparaison à même masse désavantage l'alliage base cobalt HS 25 dont la densité est 10% plus élevée que celle des aciers. Par contre cet alliage trouve son intérêt au niveau de la turbine par suite de sa bonne tenue à chaud.

ESSAIS D'IMPACT A CHAUD

Des tirs ont été exécutés sur des cibles chauffées par un chalumeau en vue d'étudier le comportement des carters mais aussi des aubes mobiles forgées ou coulées. La planche 12 confirme ainsi le bon comportement du HS 25 à 700° et 800°C. Les essais sur matériaux pour aubes mobiles montrent que la fragilité à température ambiante de l'Udimet 700 forcé s'atténue très fortement à chaud. L'Inconel 713 coulé est fragile à toute température ; malgré cette fragilité, l'énergie absorbée par le projectile est très supérieure à celle que l'on déduit du calcul de cisaillement.

ESSAIS SUR MATERIAUX COMPOSITES

Des tirs ont été effectués sur des plaques de 300 mm x 300 mm, réalisées en composites de différentes épaisseurs constitués de couches de tissu de verre imprégnées de résines époxydes.

On constate (planche 13) comme pour les aciers et alliages que la vitesse du projectile entraînant la perforation n'augmente pas aussi vite que l'épaisseur de la cible ainsi qu'il résulterait d'une perforation par cisaillement pur. Ici encore, aux faibles épaisseurs qui correspondent à de faibles vitesses du projectile, on observe d'importantes détériorations du matériau loin du point d'impact mais sous forme de délamination entre les différentes couches de tissu. Aux grandes vitesses, la détérioration est plus localisée et l'on peut penser que l'énergie absorbée se rapproche du travail de perforation par cisaillement. Les essais montrent également que la résistance de la cible augmente lorsque pour la même épaisseur totale on passe de une à deux, puis à trois plaques superposées. Il apparaît aussi que les composites considérés réalisés avec des fibres de verre se présentent aussi bien que les meilleurs matériaux métalliques et dépassent même légèrement l'alliage de titane Ti-6Al-4V. Il est vraisemblable qu'en faisant varier la qualité des fibres et de la résine ainsi que la nature et le nombre des couches de tissu, on pourrait obtenir des résultats supérieurs. Il semble qu'il faille rechercher à la fois des fibres plus résistantes tout en conservant une certaine aptitude au délamination des couches. Une solution intéressante pourrait être obtenue en renforçant une plaque de métal de faible épaisseur par du composite.

INTERET D'ESSAIS DE TRACTION A GRANDE VITESSE

Il nous a paru intéressant afin de mieux comprendre le comportement aux impacts des cibles, d'étudier l'effet de la vitesse de déformation sur les caractéristiques mécaniques de la matière. Dans ce but, nous avons entrepris sur des éprouvettes cylindriques des essais de traction à grande vitesse à l'aide d'un dispositif à arbalète ; les vitesses de déformation étaient comprises entre 10-4/s et 103/s, la vitesse appliquée dans l'essai classique de traction étant voisine de 10-3/s. L'exploitation a été effectuée à partir de la cinématographie à grande vitesse. On constate que pour la plupart des matériaux, la charge de rupture a tendance à augmenter aux grandes vitesses alors que l'allongement réparti diminue ou augmente suivant les matériaux (voir planches 14 et 15). Cette exploitation a été décevante car elle n'a pas permis d'expliquer le plus ou moins bon comportement des matériaux constituant les cibles. Il est toutefois à signaler que les déformations ne sont pas uniformes tout le long de l'éprouvette, la mise en déplacement se faisant progressivement avec propagation d'une onde plastique ; d'autre part le mode de déformation unidirectionnelle est très différent de celui des cibles qui est biaxial voire même triaxial au droit du contact du projectile.

CONCLUSION DES POSSIBILITES D'ESSAIS

Les essais présentés concernent le tir de projectiles de 1 gramme et de 8 mm de diamètre sur des plaques plus ou moins encastrees de 2,5 mm d'épaisseur en acier ou de plus forte épaisseur lorsqu'il s'agit de matériaux de plus faible masse spécifique. Les perforations ont alors lieu pour des vitesses comprises entre 300 et 500 m/s. Nous avons montré que plus la vitesse du projectile augmente moins la cible absorbe d'énergie à distance et que si la cible n'est pas trop fragile, l'énergie absorbée correspond alors au travail de perforation par cisaillement en poinçonnage. D'autres conditions d'essais conduiraient à une énergie absorbée d'autant plus grande que la cible pourrait se déformer à distance ; le problème se complique car les facultés de déformation d'une cible dépendent non seulement de sa ductilité et de sa rigidité en flexion, mais aussi de la vitesse du projectile. En effet, les forces d'inertie de la cible s'opposent aux déplacements à grande vitesse que voudrait lui imposer le projectile. En plus de l'énergie absorbée par déformation, intervient alors la notion d'énergie de mise en mouvement de la cible. Aux grandes vitesses cette énergie devient très importante et tout se passe comme si la rigidité de la cible augmentait. La flexion de la cible présentée planche 1 illustre ce phénomène.

L'analyse des conditions d'essais est simple lorsque l'on considère la perforation par cisaillement ; en effet la vitesse de perforation se déduit de la formule :

$$1/2 mV^2 = 0,66 R \cdot W \cdot d \cdot e^2$$

Si on considère des projectiles de dimension variable mais homothétiques, leur masse varie avec le cube des dimensions. La vitesse de perforation prend alors la forme :

$$V^2 = k \cdot \frac{e^2}{d^2} \quad \text{ou encore} \quad V \text{ proportionnel à } \frac{e}{d}$$

d représentant le diamètre du projectile ou simplement une dimension linéaire. Il suffit ainsi d'augmenter l'épaisseur de la cible dans le même rapport que les dimensions du projectile pour conserver la même vitesse de perforation par cisaillement. Comme dans ce cas la cible devient plus rigide on peut s'attendre en pratique à une plus faible énergie absorbée par déformation ; pour éviter la perforation il est donc nécessaire d'augmenter l'épaisseur de la cible un peu plus fortement que les dimensions du projectile.

Lorsque l'on veut comparer des cibles de même masse mais de masse spécifique ρ différents, il faut dans la formule précédente noter que l'épaisseur e varie comme $1/\rho$. L'énergie absorbée par cisaillement est alors proportionnelle à R/ρ^2 , grandeur particulièrement élevée pour les matériaux à faible densité.

Sur la planche II, l'expression R_e qui varie comme R/ρ^2 montre l'évolution de cette grandeur pour les matériaux considérés. Signalons à ce propos que les alliages magnésium lithium encore plus légers donneraient des valeurs de résistance au cisaillement très supérieures.

Pour une meilleure précision dans le calcul de l'énergie absorbée par cisaillement, il serait nécessaire d'effectuer ces essais de poinçonnage à grande vitesse mais nous pensons que pour des matériaux suffisamment ductiles notre estimation $0,66 R$ pour la contrainte de rupture par cisaillement reste acceptable.

L'estimation de l'énergie absorbée par déformation à distance semble difficile à atteindre par le calcul et nous avons vu qu'elle peut être 4 fois plus élevée que l'énergie de poinçonnage dans le cas des cibles de faible épaisseur. La qualité à rechercher pour une cible est une charge de rupture élevée allée à un bon allongement réparti, l'allongement localisé au droit de la striction ayant peu d'intérêt.

Nous avons peu parlé des ruptures fragiles qui viennent limiter l'énergie absorbée par la cible car les tirs avec projectile pointu sont particulièrement aptes à mettre en évidence cette fragilité ; grâce à ces essais il est très facile d'écarter les matériaux fragiles à l'impact et il n'est pas nécessaire de rechercher une corrélation entre cette fragilité et des caractéristiques mécaniques telles que la résilience sur éprouvette lisse et la ductilité dans un essai de traction biaxiale.

RECOMMANDATION POUR LA CONCEPTION D'UN CARTER DEVANT CONTENIR LES AUBES

L'ensemble des essais présentés et leur analyse permettent de dégager quelques idées simples pour la conception des carter. On a vu combien il est important de rechercher par tous les moyens, à retarder la perforation par cisaillement en favorisant au maximum l'absorption d'énergie par déformation ou, dans le cas de matériaux composites, par délamination.

Pour "retenir" les aubes avec un carter de masse minimale, il est nécessaire de rendre le carter le plus souple possible à la manière d'un filet, en évitant au maximum tout ce qui peut apporter de la rigidité. L'idéal consisterait en un cylindre d'épaisseur constante ou évoluant lentement, relié de façon souple ou flottante à la structure mais la technologie s'oppose généralement à cette configuration. Les brides devront être conçues avec le minimum de rigidité, par exemple grâce à des festonnages, et avec un raccordement très progressif à la partie cylindrique car toute zone rigide favorise la perforation par poinçonnage.

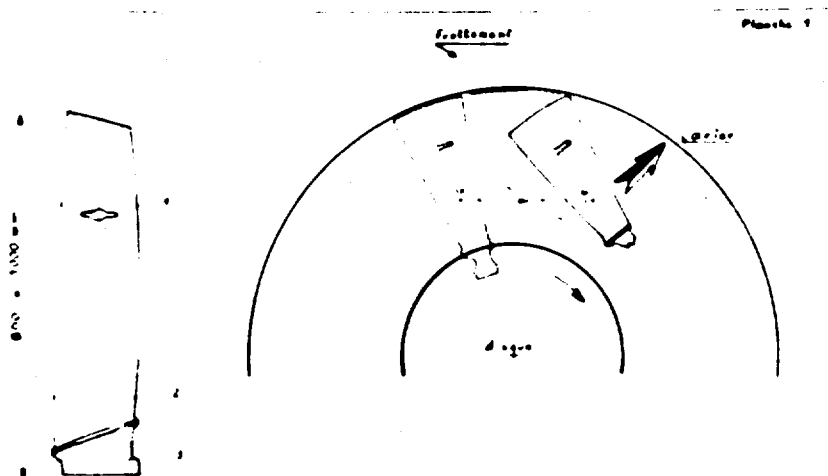
Lorsque des renforcements d'épaisseur sont à prévoir sur un carter pour contenir les aubes, la répartition de cette masse doit être utilisée afin de niveler au mieux les épaisseurs en vue d'aboutir à une rigidité plus uniforme. Bien souvent, il sera préférable de concevoir un carter d'épaisseur minimale assurant juste les fonctions technologiques et aérodynamiques et de prévoir à l'extérieur un deuxième carter d'épaisseur constante à suspension souple constituant un véritable bouclier. Cette solution apparemment lourde car deux tôles séparées absorbent moins d'énergie par cisaillement qu'une tôle unique d'épaisseur double, présente l'avantage de favoriser le "piégeage" des projectiles dans l'enceinte comprise entre les deux parois au lieu de les conserver dans la veine avec le risque de provoquer la rupture de tout l'aubage ; en outre cette solution permet une très bonne absorption d'énergie par déformation du bouclier.

Le cas d'un carter en deux parois montre qu'il ne suffit pas de contenir les projectiles par un carter unique parfaitement résistant sans se préoccuper de l'évacuation des projectiles. Le problème doit être examiné sur un plan plus général qui dépasse de notre étude ; en prenant en compte les phénomènes de détérioration en cascade et de bourrage ainsi que les possibilités d'orienter les projectiles dans une enceinte ou dans une direction où ils ne seraient pas dangereux.

CONCLUSION

La suite d'essais technologiques très simples de modèles vérifiés mais effectués sur une grande diversité de matériaux nous avons pu d'une manière très pratique dégager un certain nombre d'idées

« simple » pour juger de l'aptitude des matériaux à bien résister aux impacts dans le domaine des vitesses comprises entre 200 et 1500 m/s et de l'importance des effets de rigidité et d'inertie de la cible. Ces quelques notions doivent servir de guide à l'ingénieur chargé de choisir les matériaux, et les conceptions technologiques les mieux adaptées pour les carter devant contenir les aubes.



Plaque 1

Installation d'essai d'impacts

Plaque 2

Vue d'ensemble

Coffret électrique électro-vanne



Arrivée d'air
comprime
pour
commande
de la
sécurité

dispositif de fixation

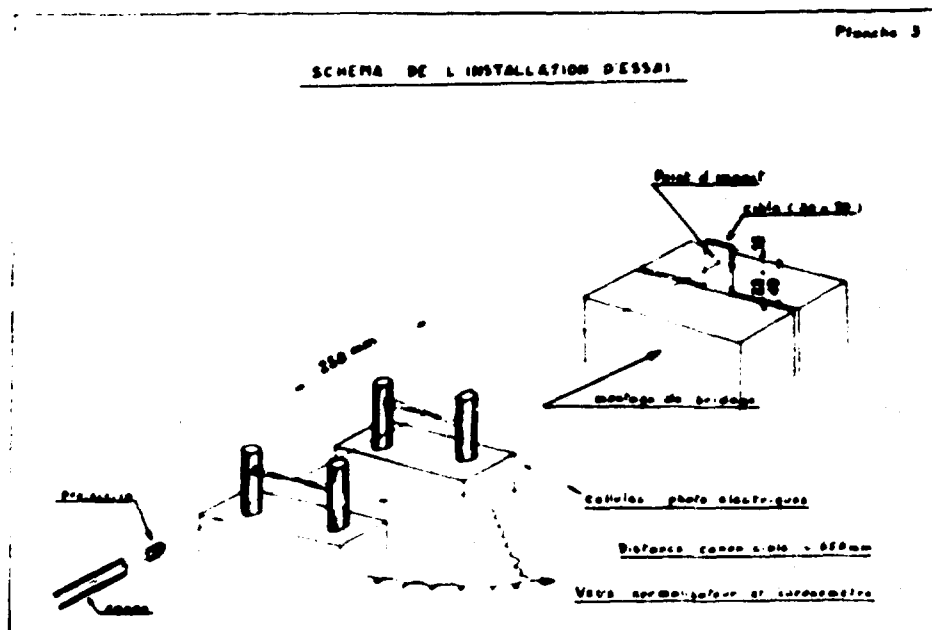
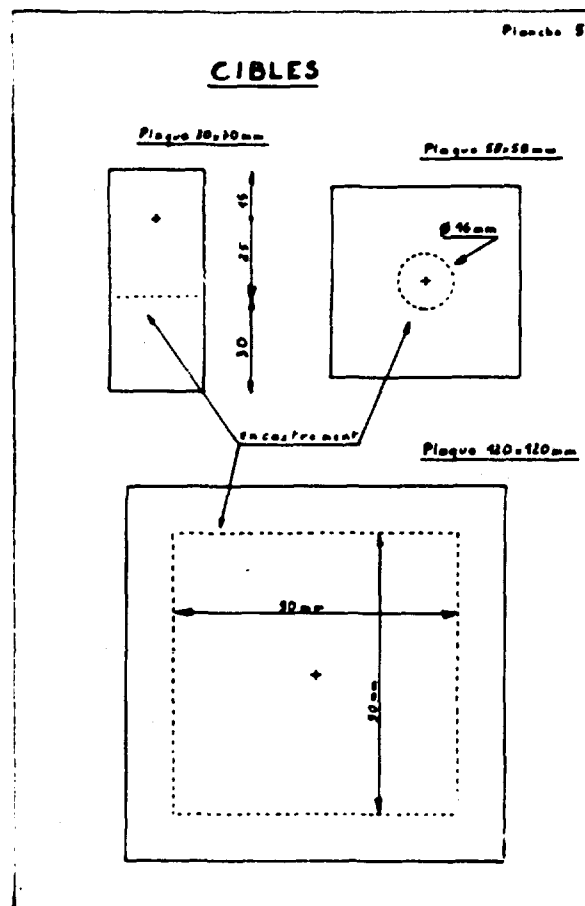


Planche 4

INFLUENCE DE LA FORME DU PROJECTILE

projectile acier R=1000 MPa
cible acier à 18% Cr R=120 MPa - épaisseur 2.5mm (classe 40)

PROJECTILE	VITESSE DE PERFORATION
<p>m=3g</p>	300 m/s
<p>m=3g</p>	345 m/s
<p>m=3g</p>	410 m/s



INFLUENCE ENCASTREMENT

épaisseur 2,5mm

MATIERE	R MPa	VITESSE DE PERFORATION (mm/s)		
		encastree sur acier 45	encastree sur acier 45	encastree sur acier 45
Z12C13				
Classe 610	1010	280	310	330
Z12C13				
Classe 610	740	320	350	360
HS 25				
base Cobalt	1000	390		470
TAGV				
T. 6A - V	1060	310	380	405
TU2				
T. 25C	685	320	340	360
AUSGN				
Al 25C - 12M - 12M	420	210	240	250
AG 5				
Al 5Mg	510	260	260	300
ZT1				
Mg 37% 22 Zn	195	120		180



1 - 100 m/s 2 - 150 m/s 3 - 210 m/s 4 - 280 m/s 5 - 330 m/s

Influence des caractéristiques mécaniques de la cible

cible 30x70 encastree sur la petite cible
épaisseur 2,5mm

Acier	R MPa	Vitesse de perforation m/s	Type de rupture
	940	400	ductile
	1230	420	ductile
40CDV20	1420	390	fragile écaillement
Acier	1620	440	fragile écaillement
Vaccorjet 1000	1830	240	fragile écaillement

Influence de l'épaisseur

Cible rectangulaire 30x70mm encastree sur une petite cible

MATIERE	R MPa A%	Epaisseur mm	Vitesse de perforation m/s	Type de rupture	Vitesse théorique cisaillement (Loi 68)
ZT1	195	2,5	180		110
Mg 37%	34	5	255	Fragile	220
		7	280		310
		2,5	300		435
AG 5	300	5	390	Ductile	270
Al 5Mg	21	6	430		330
Foie		8	510		460
		2,5	240		145
AUSGT	330	5	355	Fragile	290
Al 5C - 12M - 12M	55	7	400 - 490		400
		2,5	360	Ductile	205
TU2	680	5	300		410
T. 25C	465				

Vitesse théorique cisaillement

$$V_s = 0,66 R \cdot E$$

$$V_s = 400 \cdot E_{max} \cdot V_{max}$$

CLASSEMENT A EPAISSEUR CONSTANCE 2.5mm

MATIERE	R MPa	VITESSE DE PERFORATION m/s		VITESSE DE PERFORATION m/s	TYPE DE RUPTURE
		à 100 mm	à 100 mm		
40 CDV20 (acier doux)	1230	420	360	280	Ductile
MS 23 (acier doux)	1000	470	390	250	Ductile
TAGV (acier doux)	1080	485	310	265	Très légère fragile
WASPALOY (acier doux)	1250	450		280	légère fragile
A 286 (acier inoxydable)	1080	330	280	250	légère fragile
Classe 450	740	360	320	215	Ductile
A 286 (acier inoxydable)	1080	340		270	Ductile
TU2 (C 25Cu)	680	360	320	205	Ductile
C 286 (acier inoxydable)	1000	380		250	légère fragile
Classe 450	640	400		160	Ductile
AUTON (acier doux)	460	240	210	165	légère fragile
AGS (acier doux)	300	500	230	140	Ductile
AUTON (acier doux)	350	240		145	Fragile
ZT1 (acier doux)	190	180	120	110	fragile moussu

* à 100 mm de diamètre, l'épaisseur de la plaque est de 2.5 mm.

CLASSEMENT A MEME MASSE

cible 30x70 mm encastree sur la plaque

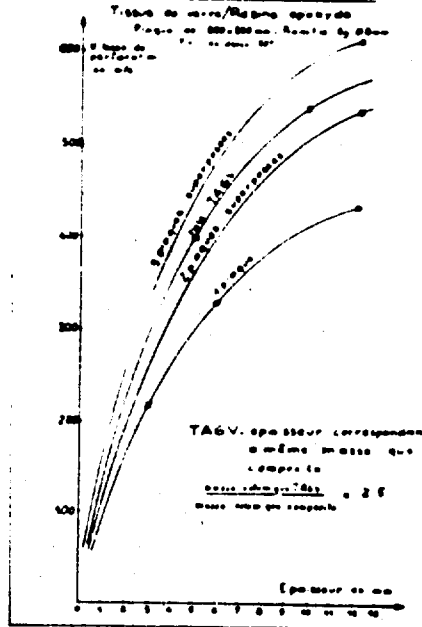
Matériau	R MPa	a mm	Re daN	Re daN	Vitesse de perforation m/s	Type de rupture	Vitesse de perforation m/s
TAGV (acier doux)	1080	45	490	2200	520	Très légère fragile	70
ZT1 (acier doux)	190	41	210	2200	400	Fragile moyenne	80
AU2GN.421Cu (acier inoxydable)	440	7	310	2200	380	légère fragile	60
AGS (acier doux)	300	7	240	1500	475	ductile	380
TU2 (C 25Cu)	680	45	310	1400	460	ductile	370
40 CDV20 (acier doux)	1230	25	340	770	480	ductile	280
WASPALOY (acier doux)	1250	25	310	780	450	légère fragile	280
A 286 (acier inoxydable)	1080	25	270	680	340	ductile	260
MS 23 (acier doux)	1000	225	225		430	ductile	230
18/8 (acier inoxydable)	500	25	425	310	400	ductile	200

ESSAIS A HAUTE

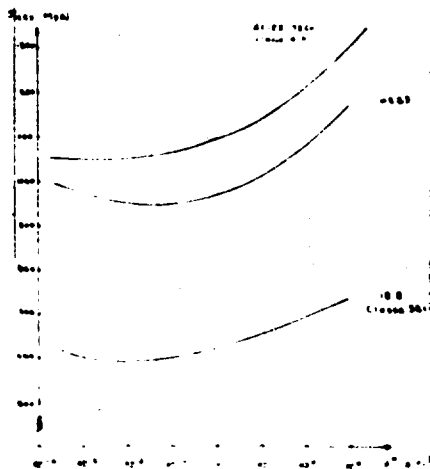
Page 19

Matériau	σ_{10}	R	A ₁₀	Temps de perforation	Type de rupture	Temps de rupture
C263	20	920	16	930		260
	100	780	39	930	éclate	220
	100	810	22	930	fragile	220
MS25	20	1000	20	470		250
	100	750	50	370	éclate	180
	100	320	39	380		180
Métal 700	10	1100	45	340	fragile	170
	100	980		320		150
	100	850		290	éclate	150
Inox 713	20	780	5	910		220
	100	810	5	900	fragile	180
	100	140	4	310	éclate	240
Acier	1000	160	14	290		150

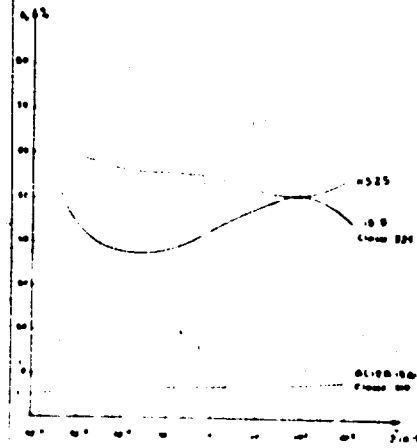
TESTS SUR PLAQUES EN COMPOSITE



Planché 4
CONTRAINTES DE RUPTURE EN FONCTION
DE LA VITESSE DE DEFORMATION



Planché 5
ALLONGEMENT REPARTI EN FONCTION DE LA
VITESSE DE DEFORMATION



DISCUSSION SUMMARY

by

J.G. Avery

Prior to the start of the discussions, the meeting was privileged to view a US Navy film on the impact damage to aircraft wings, kindly loaned by Mr. T. F. Kearns, Chairman of the Structures and Materials Panel. This film showed the kind of battle damage which had been sustained on the older type of aircraft wings with light skins stiffened by riveted stringers over a sub-structure of ribs and spars. This could be compared with the damage sustained on more modern wings, with heavier skins on a lighter sub-structure, as demonstrated on a test wing which was loaded and then impacted by representative projectiles. These tests showed clearly that catastrophic failures could occur if the initially applied stress level was high enough, so as to reduce the corresponding critical crack length below that produced by the projectile impact.

DISCUSSION FOLLOWING SESSION I

Avery (Boeing): I would like to start the discussion period by reviewing some of the things we heard in today's presentations. The importance of establishing a design methodology for design of impact damaged structure was emphasized and it was pointed out that this should be done within existing structural integrity procedures. It was also mentioned that verified analytical models must be made available for use in design. These models include damage prediction and residual strength prediction. It is important that these models be formulated in terms of the parameters used in design, for example material selection and geometric definition. We heard some good examples today of models which reflect this. But the models must also reflect the threat parameters as this is the other side of the problem. These parameters include threat type and conditions of engagement.

In the presentation today, we heard descriptions of several analytical models that can be used in design, including:

- (1) hydraulic ram pressures,
- (2) structural damage due to blast and fragments,
- (3) finite element applications,
- (4) overall vulnerability assessment

All of these are the very things that must be addressed in impact damage tolerant design.

There are several interesting things that we did not discuss this morning and I would like to mention some of these for your contemplation. One is criteria for impact damage tolerant design. For example, operation in a hostile environment will generally be determined by a procuring agency rather than the designer. But assuming that such operation has been specified, how do you formulate this in terms that a designer can use? How should the criteria be formatted and what should be specified? It's clear from today's presentations that the threat is important and this must obviously be specified. Also the conditions of engagement, i.e., projectile velocity and obliquity, affect the damage size. Consequently, criteria must address engagement conditions. The load acting at the time of damage imposition is a factor that must be specified, as well as the residual strength required after damage. There are interesting and timely questions that can be asked concerning the appropriate way of specifying these criteria. Should they be specified in probabilistic form, for example, or should worst case conditions be used? Should you require survival against worst case damage and worst case loading acting simultaneously, or should one back-off from this?

Another area not discussed was repair of structural damage. The airframe is always damaged to some extent and the question of repair criteria becomes very important. When a damaged aircraft returns to base in an all-out war situation, under what conditions can it be returned to service and what conditions dictate repair? How does the structural design affect the capability to repair damage?

We did not discuss penetration capability but we will hear a good deal about this during tomorrow's session on engine debris. The question of whether or not a projectile penetrates an element of structure is an extremely important aspect both of structural vulnerability and of vulnerability in general. However, there is substantial data available for predicting penetration in aircraft materials by bullets, at least, so I think it was appropriate to concentrate on other areas today.

And finally, I would appreciate any comment you might have concerning the content and format of the AWARD Design Manual on Impact Damage Tolerance of Structures, which is currently being prepared.

Haskell (BRL): Regarding the threat, this depends on the project manager's view of the usage intended for the airplane. At BRL, we have taken typical battle field scenarios and used these to develop criteria that the aircraft must meet. For example, if the attacking weapons were a certain distance away we would know the slant range and therefore the velocity. So we have required a certain degree of invulnerability to projectiles at a specific slant range and we have selected a variety of attack orientations for which the aircraft is evaluated.

Avery (Boeing): Then I think an important consideration is, having done that, how does one formulate this into a criteria that a designer can utilize.

Haskell (BRL): Well, damage can be estimated analytically or from test firings, once the engagement conditions are specified. We require knowledge of the loads in the stringers, longerons and skin, and we compare these loads with stresses calculated from our analytical methods and require that the aircraft avoid catastrophic failure. It's fairly easy to follow this procedure.

Avery (Boeing): I've had some experience with a criteria specification of this nature. An H- projectile threat was specified. It was also specified that the damage location and size was to be the most severe case. In addition, damage was to be inflicted during a 4-g maneuver, and limit load residual strength capability was required. Finally, a 2-hr return-to-base criteria was imposed. This criteria is specific enough so that it allows a designer to produce an airframe that will comply, provided he has sufficient data on weapon terminal effects and structural response to ballistic impact. In this particular case, the criteria specified imposed a 30% weight penalty.

The point that I'm driving at is that all design is driven by criteria, that are hopefully specified initially. If impact damage tolerance considerations are ever to be incorporated into aircraft design, criteria must be effectively formulated and transmitted to the designer. I think there are many questions that must still be resolved concerning the development and implementation of criteria. Probably what must be done is to initiate studies to establish the effect of impact damage criteria on aircraft weight, cost and reparability.

Harpur (BAC): Of course, we have a similar situation regarding other types of damage. I'm thinking of the fail safe criteria for aircraft. Rather simple criteria have been formulated saying that the aircraft shall sustain loss of a single primary structural element and then sustain 80% or 100% limit load (depending upon which side of the Atlantic you happen to reside!). I don't know whether such simple criteria can be applied to damage from projectiles. I have a rather unpleasant feeling that one could have very complicated criteria indeed because of the variety of possible threats. It's likely that, if one attempts to cover these in an overall manner, the designer will be faced with an almost impossible task. I wonder if any one has any ideas toward developing simple criteria, that might at least say that aircraft A was as good as aircraft B?

Squadron Leader Perry (RAF): My interest is mainly in the repair of battle-damaged aircraft and we have tried to establish some simple criteria to assist us. Here we have to take a returned aircraft that has been damaged and determine whether it is fit to fly. My concern is not with the vulnerability of the aircraft. What we hope to do is to produce a Manual for the aircraft maintenance engineer to use. We have decided for the European war situation we will only require a maximum of 20 sorties and we will accept a degradation in airworthiness such that we have an ultimate factor of 1.0 rather than 1.5. We assume typical damage and we aim to specify the maximum amount of damage that the aircraft can sustain without having to be repaired, using simple repair techniques that we plan to develop. We have three categories:

- (1) Aircraft will be permitted to fly with a reduced safety factor up to its full operational envelope, say 7-g for a ground attack aircraft.
- (2) Aircraft can just release its load, say 3.5-g.
- (3) The final category, that would just permit the aircraft to fly back to a rear repair base.

So we feel that those are rather simple criteria and we hope to produce a Design Manual in about a year's time.

Avery (Boeing): This work on repair would be of value for inclusion in the AGARD Design Manual and we would be very appreciative of any information that you could provide.

Shaw (RAE): I think the most important reason for including repair in the AGARD study is that it's not just a matter of repairing damage, rather the important consideration is to reduce the repair problem. Therefore reducing the extent of the damage if possible.

Avery (Boeing): That is a very important point.

Squadron Leader Perry (RAF): Another point that I would like to make is that we don't want slightly more damage tolerant aircraft that are much more difficult to repair. Honeycomb, for example, is nearly impossible to repair. Another thing that we would like to see re-adopted is the transport joint. We saw the skin/stringer configuration in the film and those aircraft were all constructed with transport joints and structural elements were easily replaced. Unfortunately, it seems that today all aircraft are made in one piece and this makes repair difficult. If we look at something like the Harrier, which is operating away from the main base, the amount of available facilities is extremely limited and we see cannibalization as an efficient means of repair. The Harrier wing can be removed in a matter of hours. This was not the result of battle damage considerations, it was done to change the engine. But if it can be done on a weight conscious airplane like the Harrier, then it should be possible on all aircraft to change all major structural elements and we see this as an important consideration in repair.

Avery (Boeing): While we are on the subject of repair, is there any comment on fiber composite structure concerning its ease of repair relative to metal structure? As far as bullet impact is concerned, composites tend to show localized damage, as opposed to the response of a material like 7075-T6 that often shows substantial cracking well beyond the impact point. I would suspect that this one factor might be an advantage, i.e., smaller damage size. But damage size is not the whole story by any means, because one must consider the technique of repair and even the question of whether repair is even feasible in fiber composite primary structure. There has been some research in composite repair, even including the development of a field repair kit.

Squadron Leader Perry (RAF): This is certainly the thing we are looking for. We are looking at the possibility of using composites to repair metal structure. How practical it is we don't know.

Haskell (BRL): Do you think there is enough data available on repair of composites to include treatment in your Design Manual? Consider blast damage, for example, that might rip off an entire panel.

Avery (Boeing): I agree. At best, all we could do is mention what work has been done. Actually, in all these areas, we're trying to put available data into a Design Manual that will get wide distribution and will hopefully be placed on the designer's bookshelf. If there's lack of data I think it will be quite evident and making this lack visible is another objective of the manual.

Harpur (BAC): I would like to add to that, in that I think the AGARD Manual activity should be a progressive thing, so that subsequent information can be added as it becomes available. As of today, we don't know everything about this subject, by any means.

Avery (Boeing): I had a question for Mr Massmann, concerning the relative performance of honeycomb structure versus skin stringer structure under blast attack. As I recall, as far as panel deflection was concerned, the differences between the two was insignificant. Do you feel there might be a difference with regard to failure at the attachments to spars and ribs? Would the stiffer configuration transmit more load to the attachments and induce a failure there?

Massmann (IABG): I think the stiffness of the panels is not important as far as the loads transmitted to the ribs and spars is concerned. You must carry the entire load, so perhaps you may have an altered distribution, but the average value will be approximately the same. Another point is that the load distribution can be different between honeycomb panels and the stiffened panels. For example, the ends of the honeycomb panel can be attached differently than possible for the stiffened panel. Stiffened panels can be riveted separately, a practice not feasible with honeycomb panels. For damage tolerance, it is best to have many panels and this principle cannot be applied with honeycomb.

Avery (Boeing): So you feel that other factors being equal, the most damage tolerant approach is to use stiffened skin rather than honeycomb, in regard to blast response?

Massmann (IABG): I think so. There are additional effects with honeycomb. For example, with a time delay such that the overpressure occurs between the honeycomb facesheets, very large damage results. This doesn't occur in stiffened panel designs.

Perhaps I may make some other comments regarding the structural design. In wing structures, for example, it is most important to investigate damage tolerant configurations. A two spar wing with one spar destroyed has very little structural capability. If you increase the number of spars you can obtain improved damage tolerance. However, if the additional spars result in spacing that is too close it is possible that all the spars can break. So there is an optimum value and I think these values should be in the design manual.

Avery (Boeing): I agree. I've done studies of this sort, and this can be a big factor. It also involves considering the size of damage that can be imposed by the given threat and superimposing this on the proposed configuration to determine how much of the substructure will be damaged. Now, when you mentioned inclusion of this in the Design Manual, did you have in mind actual numerical results from studies that you are aware of, that could be made available, or were you thinking of a more general treatment describing how such studies might be conducted?

Masemann (IABG): I believe there are some existing results that could be made available. This might be supplemented by new calculations.

Avery (Boeing): We did a brief study once on the effect of number of spars versus the weight penalty associated with making a specific wing configuration invulnerable to a high-explosive projectile threat. The weight penalty was reduced substantially in going from two spars to four spars. However, the weight penalty began to increase beyond four spars, i.e., the penalty was larger for the 5-spar configuration than for the 4-spar configuration. The reason for this was the fact that the threat could severely damage two spars in the 5-spar configuration, because of the reduced separation. As we mentioned this morning, there are at least three design techniques that can be used to improve structural survivability, namely: reduce the probability of hitting critical structure, improve damage resistance, and improve damage tolerance. I think the example that I've just discussed is an application of the first technique, i.e., reducing the chance of damaging critical structure.

Haskell (BRL): I have two questions, one for Mr Avery and one for Mr Kardels. In your paper, Mr Avery, you referred to damage resistance and damage tolerance. Are these exclusive of one another, or is damage resistance or damage tolerance ultimately the more important? It may be possible to get an unfair picture by attempting to assess damage resistance relative to damage tolerance. Is this what you were trying to point out, that the end product was really the damage tolerance and not only the damage resistance?

Avery (Boeing): No doubt about that. With regard to strength, the key factor is the tolerance, as this is the strength of the structure when it contains a specified amount of damage. For example, a classical method of improving damage tolerance is to increase the number of load paths. The first priority is probably the improvement of damage tolerance. However, you can also improve survivability by improving damage resistance, because this reduces the size of the damage. The other area where damage resistance is important, as opposed to damage tolerance, is the consideration of repair, because a large factor in repair time and technique is the size of the damage.

Haskell (BRL): My second question is for Mr Kardels. In your paper on vulnerability analysis, have you performed a sensitivity analysis of the relative effect of the various aircraft components on total vulnerability and can you say anything about the importance of structural vulnerability relative to other systems such as fuel, crew and so on?

Kardels (IABG): In general, I can provide you with these results. In my paper today I only considered the wing area. It is possible to say, in general, that out of maybe 30 percent of all the simulations that we have made, we have failure within the cockpit area or the engine area. That's possible. We have incorporated in our model over 3,000 components, where a component is, for example, an actuator, a hydraulic line, a fuel tank. These are included in the functional diagrams, such as I showed for the hydraulic system. From these analyses you can get an overview about what happens if any component fails. But today I have no specific results to show you.

Shaw (RAE): Analysis of all available combat data from UK experience shows that structural damage has traditionally been a minor cause of loss, something less than 5%. The majority of aircraft types considered in these statistics were constructed of the old 'Dural' alloys, but a large number were constructed of high strength alloys and there was no indication that the loss rate was going to increase due to the use of these low toughness alloys. But, we've got to recognize that there are a number of circumstances that could result in a higher loss rate due to structural damage. The first is the use of low fracture toughness materials, the second is inappropriate designs that fail to inhibit the consequences of brittleness, and the third is more frequent exposure to high-energy weapons effects.

Squadron Leader Perry (RAF): I'd like to take that a little further. In your summary, Mr Avery, you said a significant portion of losses were attributed to structural failure. Would you care to elaborate on this?

Avery (Boeing): In that regard, data are normally reported in terms of major systems, such as structure, fuel system, flight controls, and so forth. Typically, no single system accounts for more than 20% or 30% of the losses, so this places things in perspective. I'm not sure how one determines these things. Hydraulic ram, for example, is that a fuel system failure or a structural failure? It's both, there's a big interaction between them. If hydraulic ram damage is reduced, the probability of fire or fuel starvation becomes much less. In another sense, almost anytime a projectile penetrates the airframe, whether it involves a hydraulic line or a control line or a pump, there are some aspects of the type of technology that we have discussed under the topic of structural damage. In other words, there's an impact, a penetration, some damage, so in that sense there's a great deal of interaction that may not show up in statistics.

Massmann (IABG): I think these values depend on the combat situation, the amount of damage imposed by the threat, and other factors. Mr Shaw mentioned the figure of 5%. Can you describe which kind of wing design, threat and combat situation corresponds to your figure of 5%? I think it's highly dependant on these parameters, and it's important to know which inputs you have used.

Shaw (RAE): These analyses were conducted on all available combat data. They took in all types of aircraft that are on record. Both copper and zinc alloys of aluminium were included, as well as two-spar wings and multi-spar wings. The reason why many aircraft constructed of aluminium-zinc alloys didn't prove to be structurally vulnerable was because they were multi-spar. It was purely fortuitous that they didn't suffer, since they hadn't been designed for that particular reason.

Avery (Boeing): I think that's a good point. Another comment is that more stringent design criteria concerning weapon threats are being imposed. Previously, design criteria might require resistance to a 0.50 caliber bullet, whereas now the high-explosive projectile is considered. From the design standpoint this makes a big difference and will enhance the importance of structural vulnerability.

Squadron Leader Perry (RAF): We're very much concerned with trends in aircraft design. The biggest factor is the change from the concentrated spar design to the distributed end-load design and none of Mr Shaw's statistics would include any of the latter kind. Virtually all military aircraft today are built of one top skin and one bottom skin, and as we saw from the movie a single projectile can cause this to unzip from side to side. We are concerned that we should get away from this kind of design.

Avery (Boeing): This leads us back to a discussion of fiber composite applications and I would like to clarify some statements that I made earlier. The fiber composites, i.e., boron and graphite, have generally poor fracture toughness characteristics. They are comparable to a material like 7075-T6. So in using these materials, a lot of consideration has to be given to configuration. You would probably never use a monolithic configuration when battle damage is important, simply because of the low toughness. The fracture toughness of the composites depends on the orientation of the fibers, i.e., the lay-up. A balanced lay-up has fibers in the 0, 45, and 90-degree directions, where the 0-degree direction would correspond to the span of a wing. The ± 45 -degree fibers carry the shear loads in the skin, and the 90-degree fibers assist with the internal pressure loads. The 0-degree fibers, of course, carry the wing bending loads. There is substantial evidence indicating that the presence of the 0 and 90-degree fibers reduces the fracture toughness of the laminate. Consequently, in applications involving battle damage criteria, it might be best to separate the 0-degree fibers from the skin material by concentrating them into the spar caps. This parallels, somewhat, Squadron Leader Perry's comment on design approach.

Taig (BAC): I'm very glad to hear this comment, which is an approach I have advocated, i.e., the use of composites in this sort of old-fashioned mode, of splitting up the longitudinal and shear load capability of the material. I agree with this so much. In fact, I'm convinced that, if Squadron Leader Perry is going to convince the requirements people that a return to the type of design where bending material is concentrated in spar caps is warranted, then he is actually making quite a strong case for composite materials. Because, within the other constraints that we have in designing modern aircraft, we just haven't the space to go back to that type of design. We've been forced that way because of performance requirements, in many cases against our better judgement and the one way of reversing this is through the use of fiber composites.

Squadron Leader Perry (RAF): I think that we mustn't forget the political aspects of all this. It was only in 1967, when NATO adopted this policy of flexible response, that we in the RAF had a need for consideration of battle

damage repair. The big need was always to deliver the weapon, while now we have to operate on the battle field. And I think that vulnerability and repair will take a higher place in the order of things that have to be balanced in an aircraft design. So while designers may have been forced a certain way in the past, it may be that things will change, so that we consider vulnerability to be even more important than performance.

Petiau (Dassault): I have a question, which has been partially answered. Does the case of the impact of projectiles on aircraft under high load factors exist in reality? We have studied this in particular on the Mirage F1 and have found one part that might be partially destroyed by modern projectiles ignoring of course large shells.

It seems to me that, if one wishes to destroy the structure, the effects of blast are more effective, not by the destruction of small elements, but rather an overall effect caused by an explosion a long way off, such that the blast would affect the whole wing or fin. Is there any information on response to such explosions?

Haskell (BRL): In order to destroy aircraft at a distance by blast, there has to be a rather large explosion. Greater than these small or medium size anti-aircraft projectiles. These would have to detonate within several meters. A nuclear blast can do this, of course. But to use blast to completely destroy the structure one must have a very large quantity of explosive. Surface to air missiles can do this, if close enough. But you need a large amount of explosive to destroy an entire wing, for example.

Petiau (Dassault): Do you think a charge of several tens of kilograms would be sufficient?

Haskell (BRL): Well, it depends on where it's detonated and on the structure and the material. For tens of kilos the critical distance could be, say, of the order of 25 feet. Does anyone else have any information on this?

Massmann (IABG): I have no further comment. I agree with Dr Haskell.

Taig (BAC): I wanted to go back to a slightly different aspect of the same problem. Mr Haskell indicated that many small panels, particularly longitudinally divided, seemed to be the answer. But does there come a point where it is, in fact, the longitudinal stiffener that becomes a risk rather than the individual panel? I should think that this must be so. So is it possible that it is actually an optimum spacing that we are seeking, rather than a minimum spacing?

Haskell (BRL): Certainly there is an optimum and this depends on the individual design specifications. There are some designs now that are quite good and quite light weight that have many stringers rather than massive longerons. These appear to have good damage tolerance. When you ask if there is an optimum, I agree that there is and my calculations favor an aspect ratio of 4 to 6. This is apparently what structural designers have determined, based on structural integrity requirements in general. So a good aircraft designer appears to automatically achieve good blast damage tolerance.

Massmann (IABG): If you have an outside explosion, the pressure amplitude is the same whether you have very large panels or very small panels. But if you have an internal explosion, the overpressure is governed by the volume. If you have an increase in volume you have a decrease in overpressure, so I think this is an optimum for internal explosion.

Harpur (BAC): I was not too clear from Mr Massmann's paper this morning about his mention of venting areas. I believe he showed that the internal overpressure was affected considerably by the venting area. Was he suggesting that this was an area of the structure that might blow-off allowing a pressure decay? I'm not too clear on the definition of venting area.

Massmann (IABG): When a projectile goes inside a volume a hole is created at the surface. This is the venting area. But this venting area is larger than the projectile.

Harpur (BAC): Is this an example where it would be a good idea to have low damage resistance initially, so that you get a large venting area, provided the structure holds together?

Haskell (BRL): We have found in most of the general structures that we've tested, that there is sufficient volume to absorb the blast products and that it is not necessary to artificially vent. We've found in helicopter tail booms that the quasi-static pressures caused by the residual gases was not as significant as the blast waves, since there was sufficient volume to allow the products to expand without adding to the blast wave damage. Of course, this was true for a specific case. Obviously the structure can be over-matched.

Harpur (BAC): This suggests that designers should avoid the use of solid diaphragms, and use open-braced ribs instead.

Coombe (BAC): One must remember that once the projectile gets inside the structure there are many other things besides the structure that can be damaged leading to adverse effects on the airplane. It's really survivability that we're talking about. It's no good dealing with larger amounts of damage in the structure if there are other things about that will lead to catastrophic failure of the airplane.

Avery (Boeing): That's a very good point. I think the thought there is that if we do have larger threats and larger damages, then not only structural vulnerability increases in importance, but also the vulnerability of every thing else in the airplane. Perhaps in direct proportion.

There's another aspect to the impact damage problem that hasn't been mentioned today. That is the loss of stiffness due to material removal and the effect this may have on the flutter performance of the aircraft. Not only do we have the possibility of strength degradation but also the possibility of stiffness degradation. A structural vulnerability assessment must examine this failure mode as well.

Another topic concerns the use of finite element techniques in battle damage applications. The basic problem, of course, is to find out where all the loads go after elements have been damaged. The finite element technique is used in structural design, it is an available tool, and it's readily adapted to the analysis of damaged structure. In addition, it offers the opportunity to model damage in ways that can lead to accurate results. Programs such as NASTRAN are readily available, and every airframe manufacturer has programs of their own to apply. So I think that finite element applications in damage analysis will increase. This brings up questions concerning techniques. What are the best ways to model the damage? What are the best ways to represent the structure? What simplifications can be employed? What kind of elements are best for damage analysis, and what type of programs should be used? For example, should one use programs capable of dynamic elastic-plastic response, or should such programs be used for local analysis only, and combined with a general purpose program for load redistribution away from the damaged area? There are many questions of this type that must be answered. Does anyone care to comment on finite element techniques?

Petiau (Dassault): As outlined in my paper we, at A.M.D., have studied the problem in detail and have come to treat it in a manner similar to that for fatigue cracks. An overall idealisation is used to get the boundary conditions correct followed by a very fine idealisation using 2- or 3-dimensional finite elements as appropriate.

This is very expensive and it would be preferable to demonstrate that the sensitivity of structures to projectile damage is not a big problem.

Avery (Boeing): Perhaps something that would be useful in this area would be a research effort that proceeds in conjunction with testing. One could impose various types of damage in a representative full-scale test article and then conduct tests to establish load redistribution experimentally. At the same time a finite element analysis would be conducted, wherein various techniques are explored which might lead to basic ground rules for subsequent use. In this connection, Mr Massmann in his paper presented an application where he used a very sophisticated finite element program (MARC), to verify a simpler model which he developed. Having verified the simpler model, he can then proceed to use it in subsequent calculations. I think this is a very significant application.

Haskell (BRL): It happens that we are carrying on a study of this sort now, in regard to lightweight helicopter structure. We will perform tests where we cut out parts of the structure, and we will compare measured strains and deflections with calculated values obtained using the NASTRAN and hand analysis methods, so that we will have two extremes among analysis tools.

Harpur (BAC): In Mr Haskell's paper he showed a picture of the effects of material strength on the safety factor. From what I could understand of it, he was plotting a curve through a number of discrete points for different materials. I wonder what that would look like if you took one material at a time and varied the heat-treat, for

example? I have a feeling that it must be a rather oversimplified result to show that the stronger a material the better it is.

Haskell (BRL): I'm sure that's the case. If you increase the strength you're bound to get a more damage tolerant structure. I used the materials I did because of practical limitations upon the availability of different materials, and I did not include high-strength composites. So to answer your question, I'm sure that if we kept everything constant and just increase strength, that you will get higher damage tolerance. However, if you take everything into account, the possible maximum strength that is available and its other attendant properties, the damage tolerance does not always continue upwards, because with increased strength you get lower ductility, which then decreases damage tolerance.

Harpur (BAC): Yes, this is what I was thinking. With regard to fracture mechanics we know that 2024-T3 is a very good material but when we go to 2024-1851 we get very bad fracture toughness, possibly worse than 7075-T6. So one has a variety of process conditions for each material and this may be even more important than composition. Some elaboration would be useful.

Petiau (Dassault): I should like to ask Mr Haskell a question on the extrapolation of his method to fibrous materials, which have a plastic behaviour a lot different from that of classical materials, in that the plastic phase is much reduced. However in the degradation of the panels the plastic phase is important. Will this not cause some difficulty in extrapolation?

Haskell (BRL): This is true. However, we are attempting to use this model, within the next several months, for a preliminary study of the effects on composites, assuming isotropy and using material properties from tensile tests directly in the model. Certainly, I realize that the composite characteristics are much more complex than this. It's just an attempt to utilize an existing simple model and apply it to something more complicated. We could be amiss in this, but we are trying to do as best we can.

Avery (Boeing): There's another factor in regard to the blast response of fiber composites and that is the fact that the interlaminar shear strength of fiber composites is low and pressure loads can have disastrous results due to inducing delaminations. In other words, the failure mode may be much different than in metals. Another fact is that in many fiber composites the response will be virtually elastic to failure. Graphite, for example, has a very low strain to failure as does boron.

Shaw (RAE): I'd like to show a picture of some significant structural damage (Fig.1). This was tested over 20 years ago. The wing was impacted under 3-g conditions, with a 30 mm high explosive round. It was constructed in an alloy roughly equivalent to the old 75 ST. This configuration had very few ribs. I don't think one need say more!

Avery (Boeing): Thank you for showing us the picture which I recognize. That data was made available to the AGARD study and will be represented in the Design Manual.

Harpur (BAC): One final question directed at Mr Kardels, which may link us into tomorrow's discussion. I wonder if in his vulnerability analysis he is able to consider the secondary effects of a projectile hit into an engine. In other words, if the engine breaks up does he consider where the engine projectiles go?

Kardels (IABG): Yes, we do consider this.

The meeting was then adjourned until the following day.

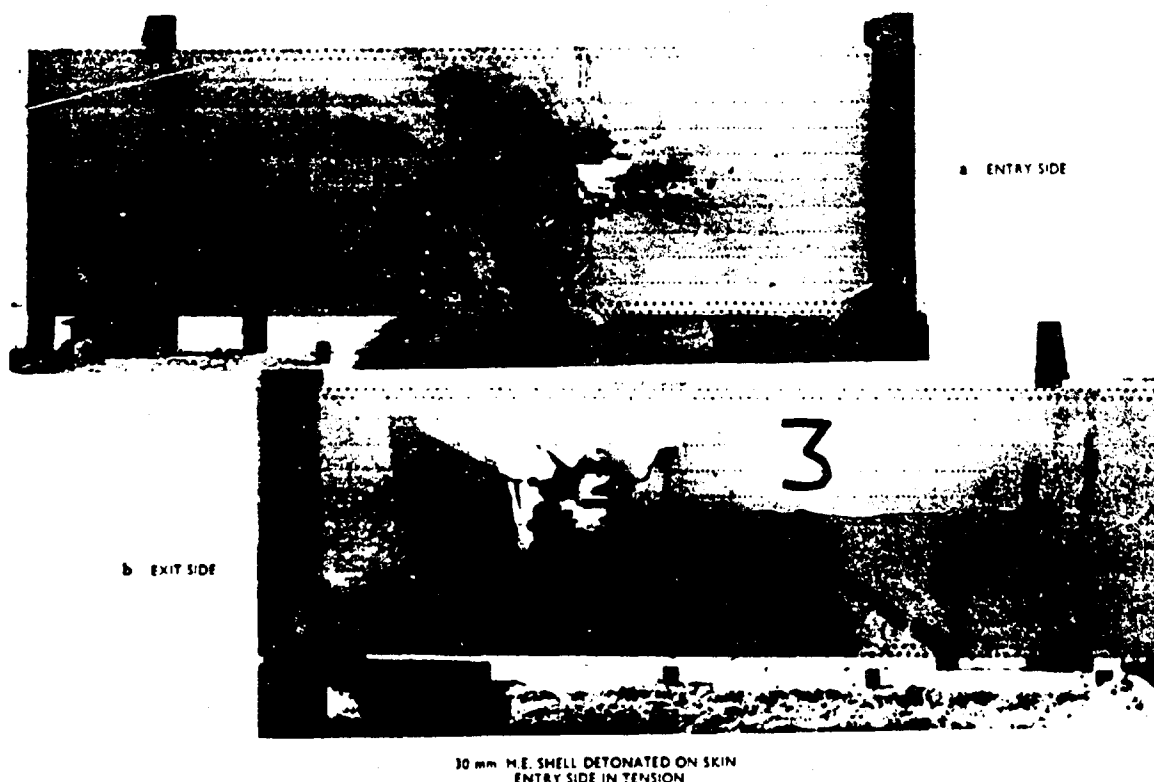


Fig.1 Damage to a D.T.D.687-box beam

DISCUSSION FOLLOWING SESSION II

Harpur (BAC): Today we have seen that, in engine containment, we have a problem similar to that of military projectiles but for the military case the projectile comes from the enemy whereas in the engine debris case the engine manufacturer and the airframe manufacturers are more friendly and not deliberately trying to upset each other. So for the engine debris case, there is at least a possibility of preventing the generation of the projectile, as well as trying to improve the resistance of the structure that is hit. There are differences also, for example, in that the possibility of having an impact from an engine failure is far more remote than in the case of the projectile impact on military aircraft, since in the latter case we must expect that it will be shot at. However, there is in the engine debris problem, the possibility of preventing projectiles from leaving the engine carcass and this provides for trade-offs between engine design and airframe design. This sort of option is not available in the case of military projectiles, i.e., we cannot persuade the enemy to make his projectiles smaller and less damaging. Further, of course, the engine debris does not explode when it penetrates the airframe, as does an HE military projectile. In addition, the engine debris is more predictable in its direction of attack and velocity. But it is probably less well-defined in terms of its shape, as the geometry of engine fragments can be quite peculiar. The residual strength capability after damage is also somewhat different. The military aircraft may be required to perform evasive maneuvers and may not be able to land immediately because of operations over hostile territory. In contrast, after an engine burst, the aircraft will try to get down as quickly as possible, although we must bear in mind, of course, that this might involve strenuous maneuvers.

Additionally, we discussed yesterday the problem of repair and the need that the military have to repair as quickly as possible so that the aircraft can return to battle. However, this is less important for the engine burst problem, as it is a very rare event and one can accept more time and expense before returning the aircraft to service. In summary, we have similarities and in some instances a change in emphasis. Clearly, however, projectile impacts from both military projectiles and engine debris projectiles present a similar problem to the aircraft designer.

To start our discussions, I noted in Mr McCarthy's paper that the total containment of engine debris would add about 50% to the basic engine weight. On one of his figures, however, he showed that one need only stop about 10% of the bladed disk weight to reduce the number of incidents by 72%. What is the weight penalty associated with this? How does the weight penalty vary with debris size?

McCarthy: We've related the results to the situation where the engine cases have flanges (casings are bolted together) and where the restriction of the flanges affects the deformation of the cases. From this we arrived at our figure of 50% increase in weight. We have done tests on fragments up to four blades on a piece of disk which is about 6.5% of a bladed disk. This required double the casing thickness. We've not tested fragments larger than that, so I'm not sure how the weight trade comes out. We are planning tests with larger fragments, up to one-third segments in fact.

Jubé (Aerospatiale): I was surprised in the two papers this morning that nothing was said of the improvement brought about by the use of new composite materials. I mean Kevlar fiber, for instance. In my opinion, protection against engine debris is not fundamentally different than protection against bullets, which is now in many cases solved by the use of Kevlar, sometimes using no resin, i.e. only layers of cloth. This has been proven effective for low speed bullets up to 500 meters/second. Over this the efficiency is less but this range of speed seems to cover the range of engine debris. I guess this development work is already in progress among civil manufacturers. I wonder if anyone could provide additional information? We intend to push for this development in France, because it provides a means of obtaining protection without a big weight penalty.

McCarthy (Rolls-Royce): The effect of impact from a high velocity bullet is quite different from that of a low velocity piece of engine. Armor plating designed for bullets is often not effective for the debris. The change-over occurs at approximately 1,000 feet per second. We tested fiber glass and carbon fiber as containment rings and found them to be far less effective than steel or titanium. Some tests have been done in America with Kevlar without resin and the results appear to be good. One has to think how this would be applied, it would be like putting a bag around the engine I suppose and it has severe limitations concerning temperature. We're proposing to do some tests with Kevlar, we've already done some with resin and the results were not good. We shall be following on with tests without resin.

Avery (Boeing): I should make some comment regarding the application of Kevlar to the engine debris problem, as we have done some of that work. I have no data to release, but perhaps this can be done at a future meeting. However, we are optimistic about Kevlar applications. It also agrees with our results that efficiency is improved without the resin. The Kevlar 29 has been more effective than fiberglass, ballistic nylon, woven roving and other materials of this sort. And its efficiency is very high as a light-weight armor concept. I do agree about the attachment and application problems. This is an area that must be looked into. Another facet is that it does require a certain amount of space and this can pose an application problem. The key feature in the penetration resistance of this material depends on its capability to move at impact, so that energy is absorbed in membrane action. When used without the resin this action is enhanced but this requires space. Perhaps quantitative support for my statements can be provided at a later time.

Harpur (BAC): Pursuing this theme, I wonder if anybody has looked into other forms of woven material? Would a woven metal mesh be effective? This seems to be one of the areas we must consider in the Design Manual. Although there is a difference between debris and military projectiles, it would seem that a somewhat similar situation concerning armoring does exist. Would someone like to say anything from the military armor point of view that might be of benefit as far as engine debris is concerned?

Avery (Boeing): I think what Mr McCarthy was getting at a moment ago, is that one effective form of armor for military projectiles is a hard ceramic material backed up by a fiber composite material. The hard surface tends to break up the projectile and change its shape. This is especially effective against armor piercing projectiles as these rely to some extent upon their shape to effect penetration. The softer back-up material absorbs the energy. However, for engine debris projectiles, as we said before you have diverse shaped projectiles not designed as penetrators. I'm sure that deforming or breaking-up these projectiles by the use of ceramic tile armor would not be as effective as it is for the military projectiles. I wonder if anyone agrees with me on this?

Shaw (RAE): It's been mentioned that the main difference between debris and military projectiles is the velocity regime. The response of all materials is different because of these velocity effects. The ceramic armor, as mentioned, is primarily effective in breaking up projectiles and this is not applicable to engine debris. It has also been found that military armour can be effective against fragments but this is mainly at high velocities. It's doubtful that the very high cost of these materials could be justified in view of the very small potential for improvement.

Avery (Boeing): I would like to address a question to Mr Thiery, in order to increase my understanding of his work. Did you show some test results with E-glass that indicated rather good resistance to penetration? Is that correct?

Thiery (SNECMA): Test results for epoxy glass, presented this morning, were for several thicknesses and for different numbers of layers for a given thickness. They have been compared with a sheet of solid titanium of the same weight and the resistance against thickness behaves in the same way; epoxy glass has the same order of strength as titanium.

Avery (Boeing): So that would indicate that E-glass is a fairly efficient penetration resistant material?

Thiery (SNECMA): I have the impression that it has a fairly good resistance but have not done comparative tests with other fibres. These tests are in hand.

Avery (Boeing): If it were established that fiberglass was efficient in resisting penetration, would the application be to fabricate engine cases from fiberglass?

Thiery (SNECMA): An engine casing with blades fixed to it would be difficult in composites alone. More interesting would be a casing in fairly thin metal reinforced with a layer of composite. The problem is to choose the fibre and number of layers for maximum containment.

McCarthy (Rolls-Royce): We've done some tests on fan blade containment using a carbon-fiber containment ring. The blade easily penetrated the ring with little loss of energy. We followed this up with tests of a carbon fiber containment ring lined with metal. Because of the amount of stretch in the carbon fiber, the metal inner casing tore, moved outwards as the carbon fiber stretched, and the fiber then catapulted the metal back into the blades with disastrous results.

Massmann (IABG): We've heard about what happens when the fragment gets outside the engine but what happens to the operation of the engine and what is the effect of fragments inside the engine?

McCarthy (Rolls-Royce): If the fragment is inside the engine, the effect depends on the surroundings. A fan blade, for example, is likely to go down the by-pass duct and avoid the core engine. A blade at the front of the compressor is likely to do considerable damage. At the turbine end, if the turbine blades are between two rows of nozzle guide vanes at close spacing, then the release of a turbine blade is likely to damage a large number of other blades in the same row. That is the case for forged blades. For cast blades, more widely used nowadays, release of a blade in a space like that can cause failure of all blades in a row and probably failure of a number of blades downstream. On the other hand, if axial space is provided between the row of blades and the next row of nozzle guide vanes, then the amount of damage can be considerably reduced. So, the effect depends very much on the design of the engine. In some engines you can lose a turbine blade without even knowing about it. In other engines, shut down is certain.

Shaw (RAF): While we're on this subject, has the effect of engine vibration after debris ejection been investigated? Some RAF tests have indicated that the engine can divest itself of the fuel system, for example, before it can be shut down. It seems to us that failure of these components due to engine vibration can be just as serious as the debris impact on the structure.

Coombe (BAC): I was going to follow Mr Shaw's question with another question to the engine manufacturers. In the situation described by Mr Shaw, is there any evidence that these vibrations can lead to massive engine failures? Going back to the vibration, blades have come off in flight leading to exactly the consequences you described, Mr Shaw. It is a thing that has to be taken account of, not only during run-down but also during the subsequent windmilling that may occur for a long time during subsequent flight. On the other hand, I know of one blade release on a test stand that solved the problem quite readily, because it broke the front bearing and the engine stopped, quite violently. So there are a whole range of conditions that are difficult to quantify and difficult for both the engine and airframe manufacturers to deal with. But it is a problem that people are thinking of.

McCarthy (Rolls-Royce): When a blade comes off, the vibration in most cases will increase to the extent that it will exceed an acceptable level. In engines, for civil use anyway, we have vibration level indicators and when an acceptable level is exceeded the engine is simply shut down. I think in most cases the engine would be shut down anyway because, for a fan blade, the forces are so enormous that the engine will shut down of its own accord. I remember a case where an engine lost an LP turbine blade over the Atlantic and this went unnoticed as there were no monitoring equipment in use at the time. The flight was completed but it shook loose practically every nut and bolt in the engine. So it can happen, of course, but with vibration monitoring equipment it is very unlikely to be a problem.

Harpur (BAC): While we're still on the first event, i.e., the engine failure itself, and before we get on to the interaction with the structure, I would like to ask another question obviously directed at Mr McCarthy. In the work he described to improve the situation, I noted that in all cases it was anticipated that something will come off, although the objective is to make this debris as small as possible and to contain them within the engine. Nevertheless, that's going to be an expensive engine repair, even though you prevent damage to the airframe. I wonder what were the possibilities of preventing anything from coming off at all? Could one make a fail-safe engine, in the sense of finding the defect before it gets to catastrophic size? What are the possibilities of devising inspection techniques or of altering engine design so as to remove the possibility of engine break-up entirely?

McCarthy (Rolls-Royce): I can't see us ever getting to the position of ever eliminating engine failures altogether. We have looked at the way engines have failed and try to prevent these failures in the future. Design is constantly being modified to achieve that end. But engines continue to find new ways to fail and we never quite catch up with it. With regard to detection of incipient failures, we have made significant advances. We have the vibration monitoring equipment, we have magnetic chip detectors in the oil system and the use of the intrascope has proved to be invaluable. It was treated with scant respect a few years ago but is now widely used, allowing observation of the blade and combustion components of the core engine to spot incipient failures. As far as spotting incipient failure in a disk, this is a much more difficult problem and we don't know any way at present of detecting a crack in a rotating disk during engine service. This presents a problem because in modern disk materials the fracture toughness is such that very small cracks can go critical. So we rely heavily on cyclic testing of disks to establish disk life and service limits.

Harpur (BAC): I was afraid you would answer in that manner. We must face the fact that we have safe-life rather than fail-safe engines but that we try to get a fail safe airplane in the end, by controlling the debris in an orderly way. I wonder if this problem of inspection could be put to our NDI colleagues who might think of some clever solution. I think there is a need to continue to seek a method of finding the cracks before they get too large. This also entails making the critical crack length as long as possible. I don't know whether there is a compromise that could be reached. Certainly it is difficult enough to design an engine to perform its own function. Whether it's possible to use materials with higher fracture toughness, or even use crack stoppers, I don't know.

Perhaps we should move on to other subjects, unless someone has further comments.

Coombe (BAC): I have a question on statistics. Mr McCarthy presented a case on the basis of UK statistics only. While one major release in 8.5 million hours sounds quite a lot, if you do the sum and assume that there are four engines fitted in each of 100 airplanes, I think you get a major release once every 20,000 hours in every airplane. This is twice in the lifetime of every single airplane in the fleet. That's not negligible in those terms. So we should ask for world statistics, because with those sort of numbers it's not a "way-out" problem that you're talking about.

McCarthy (Rolls-Royce): "Major release" is probably not the right word. I was talking about debris that would cause penetration of a wing or fuselage. This could be just part of a blade, resulting in a very small hole. I don't think that's a major release. The number of releases involving *major pieces* has been very small indeed, I believe 5 or 6 in 124 million hours.

Harpur (BAC): It's not very frequent, but it's still there, so we must do everything possible to reduce it. In terms of the consequences of the failure, I wanted to ask Mr Huret about conditions under which the structure is damaged. It seems there are three levels of damage that one needs to establish in determining the safety of the airplane, depending on the part one is considering. If the part involves structural integrity only, then it may be perfectly permissible to allow penetration, providing adequate strength remains. But if system components or people are behind the structure, then we might allow some perforation but not complete penetration. In the third case, for example a fuel tank, no perforation at all could be tolerated. I wasn't too clear from Mr Huret's presentation whether he could distinguish between these three cases using his analysis approach. Could Mr Huret clarify this?

Huret (SNIAS): The test results show a zone of high energy where the fragments pass through the engine casing, a zone of low energy where they do not pass and an intermediate zone where there is a bit of everything, due to the uncertainty of all the highly complex phenomena which occur. It is not our object to discriminate accurately between a casing which is punctured and one which is punctured but stops the blade. The probability will be marginally greater for one than for the others but insignificant for an order of magnitude comparison with certain other risks.

Harpur (BAC): Yes, I can understand the difficulty. It's probably more difficult than with military projectiles because of the irregular shape of the projectile. It's possible that the projectile has sharp corners. Also, of course, the blade itself may be damaged, and curl up into some peculiar shape that would not cause damage to the structure.

Has the effect of the impact on the projectile been studied to any extent? Can one design blades or structure so as to bend the blade enough so it won't penetrate?

McCarthy (Rolls-Royce): In working on the deflector plate we were concerned about the shape of the missile, so we made a study of the various pieces of blades and disks coming out of engines. Invariably the blades are bent over above the platform, more or less tangentially and the most penetrating fragment has been the broken off disk diaphragm, or disk web area, having a fairly thin edge capable of slicing through. So we developed a fragment reproducing this, and even put saw teeth on it. We also gave it the proper spin so that the rotational energy represented a realistic projectile. So we covered this aspect in designing and developing the deflectors.

Petiau (Dassault): I should like to ask about deflector plates, because it seems to me more efficient from a weight point of view to protect the sensitive parts of aircraft by deflecting fragments rather than stopping them. For the Falcon 50 we have been studying V-shaped deflectors to protect the rear end but have almost no data on which to base a design and would welcome any suggestions.

McCarthy (Rolls-Royce): We've developed deflectors. The purpose, of course, is to protect vital parts of the aircraft, so it has a limited dimension. It must be positioned and angled so as to deflect the missile. We've tried aluminum, steel, hardened steel, stiffened plates, titanium plates. We find the best to be titanium plate mounted on honeycomb of NOMEX. We've investigated scaling effects and have established some scaling laws from tests of deflectors from 1 to 4 square feet, using missiles from 3 to 25 pounds at 600 fps. The outcome was that $MV^3 \sim t^3$, where t is the thickness of the material.

Harpur (BAC): On the subject of deflectors, I'm sure the same type of thing must be considered on the military side, i.e., establishing the conditions under which projectiles will ricochet. Does anyone wish to comment on this? Has there been detailed study of ricochet of bullets?

Avery (Boeing): Yes there have been, in the sense that many studies have been conducted to determine the ballistic penetration limits of aircraft structural materials. In most applications the angle of impact is not zero degrees, so that the penetration models developed from this work have been formulated in terms of projectile obliquity as well as velocity. So one can find a fair amount of data on conditions of ricochet for specific projectile/target interactions and the physical principles involved might well be of some value for the engine debris case. As far as specific armor design configurations are concerned, it must be recognized that there is limited use of armor in military aircraft, although certain vehicles have substantial armor in the cockpit area and in some cases this is designed to take advantage of projectile deflection. I think the general answer is that correlations have been made between impact conditions and ricochet probability and this probably could be of some use in designing debris deflectors.

Shaw (RAE): There have been a lot of tests on the ricochet of projectiles but the shape of the projectile has a significant influence. Most military projectiles will ricochet readily because of the ogive shape. But others have been designed specifically to prevent ricochet and a blunt projectile, such as encountered in debris, is least likely to ricochet.

Harpur (BAC): I wonder if we might discuss design criteria aspects. Dr Coombe mentioned this in his paper and gave details of a proposed CAA regulation that requires that certain conditions of engine failure must be sustained by the aircraft with a specified probability of survival, this probability being lower for very large failures. The requirement doesn't take into account the actual probability of failure for the specific engine being considered. It would seem that there is a gap here and I wonder if there was some way to determine these engine failure probabilities quantitatively, so that we might arrive at an overall risk level of both engine failure and resulting aircraft risk. We cannot calculate this overall probability at present because we don't have engine failure probabilities and the requirement seems, at the moment, to be avoiding this issue.

McCarthy (Rolls-Royce): We have been quite anxious to show the airworthiness authorities that the probability of non-contained failures has been diminishing as we advance in the art. We've been unable to satisfy them because they argue that, although we have eliminated past failures, the use of new materials and new designs is likely to offset the improvements made. Therefore, they feel that the probability of failure is the same as it has been over the years. We've been trying to demonstrate that the probability of non-containment has been eliminated entirely in some instances. I feel that the statistics are misleading in some respects, in that it has often been said that the rate of non-containment has not been diminishing with the introduction of the latest fan engines. But, if you look at the data, you see that it is the old engines that continue to fail, not the new engines. The new engines cannot be properly assessed yet, because they don't have millions of service hours.

Harpur (BAC): Are there any comments on the type of criteria defined by the CAA, that is, taking three typical types of engine debris and relating them to a probability of catastrophe? In fact, these criteria accept the fact that an overall catastrophe could occur with each type of debris but ensure that the probability of catastrophe is sufficiently low so as to be acceptable, for example, one in thirty for the disks.

Avery (Boeing): I wouldn't care to comment on the severity of the CAA proposed regulation, or the penalties associated with meeting it, but, in terms of providing a designer with a criteria that he could work with, I felt it's quite good. I have another question. I first heard of the regulation over a year ago, and it was in draft form then. I note that it is still in draft form, so I would like to ask what is the status of adoption?

McCarthy (Rolls-Royce): The regulation is following a normal adoption cycle, i.e., a draft is circulated for comment, in order to arrive at a compromise regulation. This exercise is currently being completed.

Coombe (BAC): I would just like to add one thing. Just because it's in draft form don't imagine you're not going to be asked to meet something like it.

Shaw (RAE): It occurred to me during Dr Coombe's paper that it may be useful to study some of the test data available on penetration tests involving continuous rod warhead fragments. The cuts produced by the continuous rods are much cleaner and much narrower than that produced by engine fragments but it may be that some results might be useful relative to the effect of long cuts produced by tangential impacts.

Avery (Boeing): I have a question, but I'm not sure who would like to answer it. In hearing the engine debris papers, it was made clear that there is a definite need to solve the problem, especially in view of the regulation. Much work has been done toward finding an appropriate solution. These approaches have included reducing engine failures but, for the airframe, we have discussed containment concepts, involving either the case, per se, or a reinforced case, and also supplementary protection such as shielding and deflector concepts. In addition, we heard of some very substantial configurational concepts, involving the location of critical components on the aircraft. So, it would appear that a number of different approaches are being investigated in order to meet the requirements and is there any resolution at this point as to what approach or combination of approaches will evolve? Have we reached the stage yet where a path to follow has been revealed? Where do we stand toward developing a design approach?

McCarthy (Rolls-Royce): The tests that we've been doing are designed to provide the data required to establish the feasibility of various options. Clearly, the aircraft lay-out is critical as far as local thickening of cases is concerned. A three engine aircraft requires thickening of three parts of the casing and this may be unattractive. We've covered the deflector option as well, and have generally attacked the problem of large pieces coming out, to try and avoid the worst cases, and this work is going ahead as is our work to reduce engine failures in general. But thickened cases versus deflectors is still an open question depending on aircraft layout.

Harpur (BAC): Yes, I can see the engine manufacturers dilemma concerning case thickening. Obviously, he would like to sell his engines for a variety of vehicles and if he tries to cover all possible configurations he may end up with casings thickened all the way around. It is possible to develop a special shield separate but close to the engine. This could be part of the airframe, in a way, and would not require a different engine case for every application.

McCarthy (Rolls-Royce): This is very attractive in some respects but the problem is weight increase. We try to include the extra weight required for containment into the engine casing in order to take advantage of the additional strength, rather than carrying weight which does nothing.

Coombe (BAC): I think that since the requirement has been around for such a short time that no general design guidelines have been established regarding layout. There are some simple rules. For example, if you have a four engine aircraft with little wing sweep-back, the engines must be a long way apart to prevent one engine from knocking out the others. This makes for a funny looking airplane. Also, there are different layouts for different tasks. For example, a military transport aircraft (such as a C-130) may require a high wing and this is quite different than a civil layout. The problems are different. Another factor, as can be seen from Mr Huret's paper is that there is much work in studying the statistics of this problem and the time and money invested can be substantial. The designers will have to employ simple design layout procedures in order to avoid making too many of these expensive calculations.

REPORT DOCUMENTATION PAGE			
1. Recipient's Reference	2. Originator's Reference AGARD-CP-186	3. Further Reference ISBN 92-835-0154-3	4. Security Classification of Document UNCLASSIFIED
5. Originator	Advisory Group for Aerospace Research and Development North Atlantic Treaty Organization 7 rue Ancelle, 92200 Neuilly sur Seine, France		
6. Title	IMPACT DAMAGE TOLERANCE OF STRUCTURES		
7. Presented at	the 41st Meeting of the Structures and Materials Panel in Ankara, Turkey, 28 September - 3 October 1975.		
8. Author(s)	Various		9. Date January 1976
10. Author's Address	Various		11. Pages 202
12. Distribution Statement	This document is distributed in accordance with AGARD policies and regulations, which are outlined on the Outside Back Covers of all AGARD publications.		
13. Keywords/Descriptors	Aircraft Vulnerability Structures Damage Projectiles Proceedings		14. UDC 629.73.02:539.537
15. Abstract <p>A Specialists Meeting was held by AGARD in September 1975 to stimulate collection of data for a manual, expected to be completed in late 1977, on the subject of the resistance of aircraft structure to the impact of projectiles. There is a great need to extend past AGARD work on the subject (AGARD Advisory Report AR-47 on "Physical Vulnerability of Aircraft") to include design methodology and the proposed manual is intended to do this. Among the subjects covered in this exploratory conference were: blast effects; the types of damage produced by different projectiles; the failure characteristics of the structure under load and its residual strength and life after damage; the relationship between spread of damage, materials used, and detail design features; the degree of projectile penetration and the related hydraulic ram effect in fuel tanks; and distribution of size, velocity and direction of engine debris fragments and their effect on structure. The relationship to improved aircraft damage tolerance of such factors as: the use of armor and deflectors; the employment of modified engine design (to cause blade failure to be more likely than disc failure and to contain a large portion of the resultant debris); the effectiveness of analysis of damaged structures; and the utilization of methods of improvement of overall aircraft layout are also considered.</p>			